Effect of Extended Exposure Topotecan on Drug Resistance Using a Novel 3D Spheroidal Model of Castrate-Resistant Prostate Cancer

By

Joshua Therman Davis

A dissertation submitted to the Graduate Faculty of
Auburn University
in partial fulfilment of the
requirements for the degree of
Doctor of Philosophy

Auburn, Alabama
May 6, 2023

Keywords: cancer, spheroid, tumor microenvironment,
resistance, transcriptomics, heterogeneity

Approved by

Robert Arnold, Chair, Professor of Drug Discovery and Development
Peter Panizzi, Professor of Drug Discovery and Development
Jayachandra Ramapuram, Professor of Drug Discovery and Development
Daniel Parsons, Professor Emeritus of Drug Discovery and Development
William Ravis, Professor Emeritus of Drug Discovery and Development

Abstract

Cancer consistently commands the highest number of therapeutic drug approvals each year, however, this has yet to yield significant clinical benefits for metastatic disease. Instead, most drugs are likely to increase survival a few months before quickly succumbing to resistance. A major reason for these poor results is the absence of resistance as an early drug screening criterion, which is due in part to lacking *in vitro* models capable of assessing long-term potency. In this project, we developed a novel 3D spheroidal model system of castrate-resistant prostate cancer to assess the long-term potency of maximum tolerable dosed (MTD) topotecan, extended exposure (EE) topotecan, and docetaxel to assess whether this model system could accurately predict previous clinical results and whether alternative treatment schedules could impact drug resistance. We found that MTD topotecan led to a 40-fold reduction in potency over a 3-month study duration, while EE topotecan and docetaxel maintained similar potency throughout the study. These results suggest that MTD topotecan likely has a low barrier to drug resistance and is likely to generate rapid resistance clinically, while EE topotecan and docetaxel likely have higher barriers to drug resistance. Using transcriptomic approaches, we found that MTD treated cells displayed increased heterogeneity and rapidly underwent epithelial-mesenchymal transition, leading to increased production of efflux pumps and altered production of topoisomerases. Interestingly, EE treated cells were less heterogeneous and did not undergo these changes. Importantly, docetaxel is the gold standard for prostate cancer and MTD topotecan failed clinically. EE topotecan was successful in previous *in vivo* trials but has not been assessed clinically. Thus, our model correctly predicted poor clinical results from MTD topotecan and excellent clinical results from docetaxel. It also supports the need for further evaluation of EE topotecan for use in metastatic castrate-resistant prostate cancer. Overall, this project proposes that stable long-term potency is an excellent predictor of clinical outcomes and should be implemented early in the drug screening process and suggests that treatment scheduling can have a profound effect on the underlying cancer cell population and impacts clinical efficacy more than previously expected.

Acknowledgments

I am extremely grateful to my advisor and chair of my committee, Dr. Robert Arnold, for his invaluable support, feedback, and guidance. I also could not have completed this endeavor without my committee (Dr. Jay Ramapuram, Dr. William Ravis, Dr. Peter Panizzi, and Dr. Daniel Parsons), who generously provided their time, knowledge, and expertise. I am also thankful of Dr. Spencer Durham for sharing his time, expertise, guidance, and support, which enabled me to become a better educator.

I am also grateful to my lab mates (Taraswi Mitra Ghosh, Lani Jasper, Ahmed Alnaim, Matthew Eggert, and Chu Zhang) for their moral support and kindness, which helped me through the most stressful days of the program. I also am extremely thankful of Jenny Johnston for her kindness and for keeping me on track throughout my doctoral program.

Finally, I am especially grateful for my parents (Melanie Davis, Gary Davis, Bill Lake, and Lakeeta Davis), sister (Megan Schneider), and wife (Charlotte Muse), who have continuously encouraged and supported me. Their belief in me kept me motivated throughout this journey.

Table of Contents

List of Tables

List of Figures or Illustrations

List of Abbreviations or Symbols

OS	Overall survival
PFS	Progression-free survival
SD	Standard deviation
ECM	Extracellular matrix
VEGF	Vascular endothelial growth factor
GMP	Glomeruloid microvascular proliferations
EPR	Enhanced permeability and retention
αSMA	Alpha smooth muscle actin
CAF	Cancer associated fibroblasts
EGF	Epidermal growth factor
PDGF	Platelet derived growth factor
FGF2	Fibroblast growth factor 2
SHH	Sonic hedgehog
HGF	Hepatocyte growth factor
IGF1	Insulin-like growth factor 1
TGF-β	Transforming growth factor beta
MMP2/9	Matrix metallopeptidase 2/9
IFN-γ	Interferon gamma
GM-CSF	Granulocyte-macrophage colony stimulating factor

TNF	Tumor necrosis factor
G-CSF1	Granulocyte colony stimulating factor 1
TAM	Tumor associated macrophages
ICAM1	Intercellular adhesion molecule
VCAM	Vascular cell adhesion protein
TEC	Tumor endothelial cells
PD-L1	Programmed death ligand 1
HB-EGF	Heparin binding EGF like growth factor
SDF-1	Stromal cell derived factor 1
Ang-1	Angiopoietin 1
MSC	Mesenchymal stem cells
TSG-6	TNF-stimulated G6 protein
IL-1RA	Interleukin-1 receptor antagonist
PGE2	Prostaglandin E2
IDO	Indoleamine 2,3 dioxygenase
TLR4	Toll-like receptor 4
TLR3	Toll-like receptor 3
HDGF	Hepatoma derived growth factor
MCP-1	Monocyte chemotactic protein 1
T-MSC	Tumor associated mesenchymal stem cells
TAN	Tumor associated neutrophils

TRAIL	TNF related apoptosis inducing ligand
NK	Natural killer
ROS	Reactive oxygen species
NOS	Nitric oxide synthase
ARG-1	Arginase 1
G-MDSCs	Granulocyte-like myeloid derived suppressor cells
NET	Neutrophil extracellular traps
PD-1	Programmed cell death protein 1
LAG-3	Lymphocyte activation gene 3
TIGIT	T cell immunoreceptor with IG and ITIM domains
NCR	Natural cytotoxicity receptor
NKG2D	Natural killer group 2D receptor
ULBP	UL16 binding protein 1
MICA	MHC class I polypeptide related sequence A
MICB	MHC class I polypeptide related sequence B
BAG6	Bag cochaperone 6
DC	Dendritic cells
cDC	Conventional DC
MHC	Major histocompatibility complexes
PAMP	Pathogen associated molecular patterns

DAMP	Damage associated molecular patterns
TIDC	Tumor infiltrating dendritic cells
M-CSF	Macrophage colony stimulating factor
TCR	T cell receptor
APC	Antigen-presenting cell
Tregs	Regulatory T cells
CTLA-4	Cytotoxic T-lymphocyte associated protein 4
TME	Tumor microenvironment
TAM	Tumor associated macrophages
MDSC	Myeloid derived suppressor cells
CAF	Cancer associated fibroblasts
LPS	Lipopolysaccharide
CpG	Unmethylated bacterial DNA
HCC	Hepatocellular carcinoma
BCR	B cell receptor
Bregs	Regulatory B cells
STAT3	Signal transducer and activator of transcription 3
ATP	Adenosine triphosphate
ADP	Adenosine diphosphate
COX-1	Cyclooxygenase-1
12-LOX	12-lipooxygenase

CAA	Cancer-associated adipocytes
PAI-1	Plasminogen activator inhibitor-1
MMP	Matrix metalloproteinases
MRP-1	Multidrug resistance associated protein 1
BCRP-1	Breast cancer resistance protein 1
ETS	Early tumor shrinkage
NSCLC	Non-small cell lung cancer
IC50	Half maximal inhibitory concentration
HER-2	Human epidermal growth factor receptor 2
MTD	Maximum tolerated dose
PSA	Prostate specific antigen
PR	Partial response
BMDC	Bone marrow-derived cells
EPC	Endothelial progenitor cells
HIF-1α	Hypoxia inducible factor 1 α
MTT	Thiazolyl blue tetrazolium bromide
SRB	Sulforhodamine B
ROS	Reactive oxygen species
NOC	N-nitroso compounds
TDP1	Tyrosyl DNA phosphodiesterase 1

CPD	Cyclobutene pyrimidine dimers
PP	Pyrimidone phosphoproducts
BER	Base excision repair
NER	Nucleotide excision repair
MMR	Mismatch repair
HR	homologous recombination
NHEJ	Non-homologous end joining
TLS	Translesion synthesis
APE1	Apurinic/apyrimidinic endonuclease 1
Pol β/δ/ε	Polymerase β/δ/ε
LIG1	DNA ligase 1
XRCC	X-ray repair cross contaminating protein
FEN1	Flap endonuclease 1
GGR	Global genomic repair
TCR	Transcription coupled repair
XPA/B/C/D/F/G	Xeroderma pigmentosum complementation group A/B/C/D/F/G
CETN2	Centrin 2
UV DDB	Ultraviolet DNA damage binding
CSA	Cockayne syndrome group A
CSB	Cockayne syndrome group B
TFIIH	Transcription initiation factor II H

RPA   Replication protein A

ERCC1   DNA excision repair protein 1

PCNA   Proliferating cell nuclear antigen

AGT/MGMT O^6 alkylguanine DNA alkyltranserase

AlkBH1-8/FTO AlkB related α-ketoglutarate-dependent dioxygenase

DSB   Double strand break

DNA-PKcs   DNA-dependent protein kinases

PNKP   Polynucleotide kinase

APLF   Aprataxin and PNKP like factor

AMP   Adenosine monophosphate

MRE11   Meiotic recombination 11

NBS1   Nijmegen breakage syndrome 1

ATM   Ataxia-telangiectasia mutated

TIP60   Lysin acetyltransferase 5

H2AX   H2AX variant histone

MDC1   Mediator of DNA damage checkpoint 1

RNF   Ring finger protein

TP53BP1   Tumor protein P53 binding protein 1

BRCA1   Breast cancer gene 1

EXO1   Exonuclease 1

DNA2   DNA replication helicase/nuclease 2

BLM   BLM RecQ like helicase

ATR   ATR Serine/threonine kinase

ATRIP   ATR interacting protein

PALB2   Partner and localizer of BRCA2

BARD1   BRCA1 associated RING domain 1

RMI1/2   RecQ mediated genome instability ½

GEN1   GEN1 holliday junction 5' flap endonuclease

Mus81   MUS81 structure specific endonuclease subunit

EME1   Essential meiotic structure specific endonuclease

SLX1/4   SLX1 Homolog A, Structure-Specific Endonuclease Subunit

GEMM   Genetically engineered mouse models

FBS   Fetal bovine serum

eGFP   enhanced green fluorescent protein

PBS   Phosphate buffered saline

DMSO   Dimethyl sulfoxide

CV   Coefficient of variability

PCA   Principal components analysis

MDS   Multidimensional scaling

tSNE   t-distributed stochastic neighbor embedding

ABC   ATP binding cassette

MDR	Multidrug resistance
EE	Extended exposure
EPCAM	Epithelial cell adhesion molecule
MET	Mesenchymal-epithelial transition
TWIST 1/2	Twist related protein ½
Zeb 1/2	Zinc finger E-box binding homobox 1
QC	Quality control
GEP	Global gene expression profile
DEG	Differentially expressed genes
IPA	Ingenuity pathway analysis
NP40	Nonionic polyoxyethylene
EDTA	Ethylenediaminetetraacetic acid
DTT	Dithiothreitol
TGX	Tris-glycine-extended
PVDF	Polyvinylidene difluoride
TBS	Tris-buffered saline
HRP	Horseradish peroxidase
CLDN	Claudin
CDH1	E-Cadherin
LAMB	Laminin beta 3
MUC	Mucin

KRT	Keratin
PATJ	PATJ crumbs cell polarity complex component
ESRP1/2	Epithelial splicing regulatory protein 1/2
GRHL2	Grainyhead like transcription factor 2
OVOL1	Ovo like transcriptional repressor 1
QKI	Quaking homolog KD domain RNA binding
RBFOX2	RNA binding motif protein 9
SRSF1	Serine/arginine rich splicing factor 1
TCF3	Transcription factor 3
YAP1	Yes1 Associated Transcription regulator
CDH2	N-Cadherin
CTNNB1	Beta catenin
S100A4	A100 calcium binding protein A 4
CDH11	OB-Cadherin
FN1	Fibronectin
ITGA5	Integrin α5
LAMA5	Laminin 5
VIM	Vimentin
TOP1/2/3	Topoisomerase 1/2/3
CEACAM5	CEA cell adhesion molecule 5
GJB3	Gap junction protein beta 3

TJP3	Tight junction protein 3
LAD1	Ladinin 1
MPZL2	Myelin protein zero like 2
LSR	Lipolysis stimulated lipoprotein receptor
EPHA1	EPH receptor A1
ERBB3	ERB-B2 Receptor tyrosine kinase 3
MYO5B	Myosin VB
PRSS8	Serine protease 8
LCN2	Lipocalin 2
TRIM29	Tripartite motif-containing protein 29
FXYD3	FXYD domain containing ion transport regulator 3
PROM2	Prominin 2
SPINT1	Serine peptidase inhibitor kunitz type 1
ST14	ST14 transmembrane serine protease matriptase
SSB	Single strand breaks
DSB	Double strand breaks
SNP	Single nucleotide polymorphism
SSA	Single strand annealing
Alt-EJ	Alternate end joining
ZIP	Zero interaction potency

The Tumor Microenvironment: An overlapping network of complex interactions and its impact on drug resistance

1. Introduction: potency does not yield survival

Cancer is responsible for over 600,000 deaths each year in the United States alone.[1] It is an insidious disease that grows inconspicuously until, often, a cure is untenable. To make matters worse, the aberrant cell is not an external invader, but rather a corrupted self. This familiarity leads to a complex therapeutic problem that has yet to be resolved. How can a drug potently kill cancer cells while simultaneously sparing healthy cells? Researchers have spent decades attempting to develop a malignancy-targeting, healthy-sparing, oncologic silver bullet. A drug that targets an indispensable cancer protein found ubiquitously in all cancers. However, despite developing extremely potent drugs, a reliable cure for metastatic solid tumors has yet to be found. Instead, most treatments reduce tumor burden initially, but fail within months as patients develop regimen crippling resistance.

An analysis of 192 unique clinical studies between 2007 and 2017 comparing biologic and targeted medications to the treatment standard for different cancer types demonstrated an average post progression free survival of 9.7 months with a biologic/targeted medication and 9.8 months without a biologic/targeted medication.[2] The addition of a biologic/targeted agent increased overall survival (**OS**) and progression-free survival (**PFS**) by 1.2 months (+/- 3.8 (OS SD) and +/- 2.5 (PFS SD)). **Treating patients with a novel targeted/biologic agent in 192 unique clinical trials only**

increased progression free survival by 1.2 months on average.[2] Although the preclinical

in vitro and *in vivo* data is not publicly available, based on the FDA requirements to

initiate clinical trials, it's expected that each of these drugs demonstrated sufficient

potency, adequate target specificity, significant tumor reduction, adequate

pharmacokinetic parameters, and reasonable toxicity. While there are obvious

limitations to analyzing multiple drugs and cancer types simultaneously, only 2 studies

reported an increase in OS by 25 months. The remaining 190 studies increased OS less

than 12 months. Some even showed decreased survival. Conventional chemotherapy

yielded similar results. (Meta-analyses of patients with advanced disease: colorectal: OS

increased by 6 months,[4] glioma: OS increased by 2 months,[5] gastric: OS increased by

0.75 months,[6] breast: OS survival increased by 9.9 months,[7] non-small cell lung cancer:

OS increased by 2.8 months)[8] Between 1941 and 2014, the FDA has approved 96

different cytotoxic and targeted oncologic medications with varied mechanisms of

action, yet prolonging life significantly remains elusive. Each of these agents is capable

of killing cancer cells and shrinking tumors, but few cure patients.

WHY DO SO MANY POTENT CHEMOTHERAPEUTIC AGENTS FAIL TO PROLONG LIFE?

2. Resistance is impacted by the cancer and the drug

Prior to drug exposure, cellular sensitivity most likely resembles a normal distribution with a mean and standard deviation determined by the inherent resistance and heterogeneity of the patient's cancer, respectively. A chemotherapeutic eliminates cancer cells when a sufficient drug concentration is achieved at the drug target of a sufficiently sensitive cell during a given time frame (exposure-response). It should be stressed that the malignant cells play a role at least as important as the therapeutic agent in determining whether a drug is successful in eliminating the cancer cell. It should also be noted that numerous barriers exist between drug uptake and the target-drug interaction that impede drug exposure and result in an extremely variable drug exposure profile. Drug exposure variability in combination with cell sensitivity variability leads to reduced exposure-sensitivity overlap and fewer dead cancer cells. To illustrate these concepts, we will review the complexities of tumor microenvironment, provide insights into how these concepts affect drug resistance, and discuss potential mechanisms to overcome and prevent treatment failure.

2.1. Normal Vascular Organization

Vasculature within healthy tissue contains a well-defined hierarchical organization structure generally proceeding from arteries to arterioles to capillaries to postcapillary venules and finally to veins. These vessels are usually coated with a single layer of endothelial cells in varying continuity depending on the tissue and with varying elastic membrane and smooth muscle thickness. The vessel wall is typically thinnest and

most permeable at the capillaries to allow adequate oxygen, nutrient, and waste exchange. Typically, capillaries are spaced at intervals between approximately 100 to 200 μm, which corresponds to the effective diffusion range of oxygen.[12,16] In conjunction with endothelial cells, healthy capillaries are also enveloped by a basement membrane and surrounded by pericytes, which function as regulators of angiogenesis and blood flow. As indicated above, the endothelial layer can exist in varying degrees of continuity. [12,13]

Continuous endothelium is the most restrictive and is found in organs such as the brain, lungs and muscle. As the name suggests, continuous endothelium lacks significant gaps between endothelial cells. Continuous endothelium usually contains tight junctions capable of restricting macromolecules over 2 nm.[12,13]

Fenestrated endothelium is found in the renal glomerulus and endocrine tissues and allows more rapid convective exchange of molecules. They consist of 70 nm gaps covered by a thinner diaphragm that increases water and small solute exchange with minimal exchange of macromolecules.[12,13]

Discontinuous endothelium is found in organs such as the liver, bone marrow, or spleen and consist of 100 nm to 200 nm gaps between endothelial cells that are permeable to most molecules, including drugs and drug carriers or nanomedicines, but not cells.[12,13]

Each of these endothelial structures ensures proper organ function, but as discussed below, they also play a significant role in tumor drug delivery.

2.2. Tumor Vascular Disorganization and Consequences

In contrast to the highly organized structure of normal vasculature, tumor vasculature is chaotic and irregular. The well differentiated hierarchy found in normal tissues is lost in tumor vasculature. Tumor growth usually leads to rapid and disorganized angiogenesis. The vessels branch erratically consisting of excessive loops, arteriovenous shunts, and dead ends. Tumor vessels also tend to be larger, exhibit discontinuous endothelium, and lack adequate pericyte involvement. These abnormalities are a byproduct of fundamental developmental deficiencies induced by excessive release of proangiogenic factors without tapering and subsequent release of antiangiogenic factors. Consequently, tumor vessels are immature and excessively leaky, causing the blood to become increasingly viscous as it moves throughout the tumor. The uncontrolled proliferation and hyperproduction of extracellular matrix (**ECM**) molecules found in tumors compress blood vessels and increase geometric resistance.[10,13,14,15,17]

Blood flow within these tortuous vessels is erratic and discontinuous, leading to variable perfusion patterns. Blood flow is also not unidirectional and can flow backward or stagnate. Blood flow is a function of blood pressure across the vascular bed, blood viscosity, and geometric resistance. Blood pressure entering the tumor from the arterial side is usually similar to normal tissue, but the microvascular blood pressures within the tumor are elevated due to venous compression, which leads to an impaired pressure gradient. As the hematocrit increases from vessel leakiness, blood viscosity increases, and blood flow is reduced. The tortuous branching of the tumor vessel structure and vessel compression from solid stress increase the geometric resistance and further

reduces blood flow to the tumor. The abnormal tumor vascular network and altered

blood flow tend to reduce drug uptake, however, as shown below, these characteristics

are not uniform, and temporal and spatial variabilities can exists within an individual

tumor.[10,13,14,15,17]

2.2.1. Tumor Vascular Variability

In addition to the structural malformations described above, tumor blood vessels

are also highly heterogeneous. As early as the 1970s, eight distinct types of blood

vessels were identified in tumors according to their structural, functional, and

anatomical properties.[13,14,15,19] Currently, tumor blood vessels are classified into 6

distinct categories: mother vessels, glomeruloid microvascular proliferations, capillaries,

vascular malformations, feeder arteries and draining veins, and vascular mimicry.[13,14,15]

Tumors have been found to use multiple mechanisms of blood vessel formation that

result in variable permeability and sensitivity to antiangiogenic (vascular endothelial

growth factor (**VEGF**) based therapies.

Sprouting angiogenesis

The most prominently associated vessel formation mechanism of tumors is

sprouting angiogenesis. This mechanism is also heavily represented in pre-clinical tumor

models. Sprouting angiogenesis occurs when endothelial cells from existing vasculature

proliferate and migrate to form new blood vessels. These blood vessels, commonly

called mother vessels, are formed from excessive VEGF stimulation and exhibit

discontinuous endothelium, poorly developed basement membranes, and loose

pericyte contact. Mother vessels are typically transient structures that mature into daughter vessels (glomeruloid microvascular proliferations, vascular malformations, and capillaries) with differing permeability characteristics and VEGF dependence.[12,13,14,15]

Mother vessels

Mother vessels resemble the highly fenestrated, enlarged, and leaky vasculature that predominates the preconceived notions of "normal" tumor vasculature. Mother vessels can form from pre-existing venules and capillaries within hours of a tumor cell injection. Mother vessels develop after degradation of the basement membrane and inhibition of pericyte attachment, which enlarges the blood vessel. Mother vessels are sustained using a high concentration of VEGF and may collapse or form clots due to their thin walls and sluggish blood flow. Because of these issues, mother vessels are usually transient structures that eventually transition into more stable daughter vessels.[12,13,14,15,20,21]

Daughter vessels: glomeruloid microvascular proliferations, vascular malformations, and capillaries

Glomeruloid microvascular proliferations (**GMP**) are found in many VEGF expressing tumors and are associated with poor prognosis. Glomeruloid microvascular proliferations depend on VEGF for continued maintenance. They are hyperpermeable but appear somewhat less leaky than mother vessels and more closely resemble renal fenestrations. Glomeruloid microvascular proliferations are formed from mother vessels

when the lumen is separated, pericytes are recruited, and excessive abnormal basement membrane is secreted.

Vascular malformations are formed from mother vessels when smooth muscle cells are recruited to the mother vessel and the large lumen remains intact. These vessel formations are not permeable to plasma proteins. They are also less dependent on VEGF for initiation and don't require excessive VEGF for maintenance and stability.

Capillaries can develop from mother vessels when endothelial cells grow within the lumen and divide the lumen into smaller subsections. These smaller subsections eventually separate and mature into relatively normal capillaries that are not hyperpermeable.[13,14,15,20]

Feeder arteries and draining veins

In contrast to angiogenesis, which typically refers to increasing capillary density, arteriogenesis and venogenesis refers to formation of new or remodeled arteries and veins. Usually, these vessels are derived from pre-existing arteries and veins. These tortuous vessels tend to be larger than vascular malformations and are capable of existing in a low VEGF environment. As the name suggest, these vessels function to supply and drain the microvasculature of the tumor. [13,14,15]

Vessel coercion

Tumors do not rely solely on sprouting angiogenesis for vessel construction. Instead, some tumor lesions commandeer existing vasculature by growing alongside

these vascular networks. These coerced vessels provide the nutrient and oxygen concentrations necessary for tumor growth. The coerced vessels are not hyperpermeable and possess normal vessel characteristics, which may cause resistance to anti-VEGF therapies. These vessels may also diminish drug delivery mechanisms that rely on hyperpermeability such as the enhanced permeability and retention (**EPR**) effect with nanoparticles.[12]

Vascular mimicry

In some tumors, malignant cells can obtain molecular characteristics similar to endothelial cells and have been found to line red blood cell-filled spaces. These interactions have been labeled as vascular mimicry; however, this characteristic is still highly debated. It is uncertain whether the fluid-filled sacs found in tumors are due to trauma or if they represent functioning vasculature. If functional, it would suggest that vascular mimicry may provide another route for cancer to evade antiangiogenic therapies.[13,14]

Intussusception

New vasculature can also form by splitting apart existing blood vessels. This is thought to occur initially by the formation of an endothelial pillar within the existing blood vessel that slowly begins to extend outward until it splits the vessel in two. These vessels do not rely on VEGF and have normal vessel properties, including normal permeability, normal basement membrane properties, and normal pericyte involvement. These vessels are also not thought to be susceptible to VEGF therapies.[12]

Vasculogenesis

Finally, tumor vasculogenesis occurs when circulating endothelial precursors merge to form a new branching vascular network of capillaries. This network will eventually combine with existing vasculature and will mature after recruiting additional perivascular cells. These networks behave similarly to normal capillary beds and lack significant hyperpermeability or dependence on VEGF.[12]

Spatial heterogeneity in tumor vasculature

As stated above, the vasculature of normal tissues is highly organized and precise, ensuring the distance between cells and the nearest capillary is less than 100 μm (usually 50-100 μm), which is below the diffusional limitations of oxygen and other nutritional molecules. The cell to capillary distances in tumors significantly exceeds 100 μm due in part to the chaotic and disorganized structure of parts of the tumor vasculature as well as the limitations that these abnormalities place on blood flow and blood pressure. The growth rate of malignant cells also plays a significant role on the vascular density of the tumor. When the tumor rapidly grows, it outpaces its vascular infrastructure and results in reduced vascular density relative to a slower growing tumor. Additionally, limitations of certain subpopulations with the tumor as well as high interstitial pressure may limit angiogenesis in some regions. [12,13,22]

Effects of Solid Stress on Vascular Networks

The force generated from cell-cell, cell-matrix, and matrix-matrix interactions is known as solid stress. Solid stress is elevated in tumor tissue. Tumors accumulate solid

stress from the uncontrolled proliferation of malignant cells and from excessive matrix

production. Solid stress can compress blood and lymphatic vessels, which can block drug

entry into the tumor, can limit nutritional access, and can decrease waste elimination.

These effects cause the tumor microenvironment to be hypoxic, acidic, necrotic, and

resistant. These microenvironment characteristics can significantly alter cell

proliferation regionally and can lead to altered drug responses. Collapsed lymphatic

vessels impede the lymphatic system surrounding the tumor causing a buildup of fluid

and tissue macromolecules that increases the interstitial fluid pressure of the

tumor.[10,11,12,24,25] This is further exacerbated by the excessive vessel leakiness present in

some tumor regions. In normal tissues, the transcapillary pressure gradients are slightly

negative resulting in capillary outflows; however, this force is nonexistent in some

tumor regions, which decreases drug uptake. Transient increases in tumor interstitial

fluid pressures can also efflux drugs away from the tumor, further limiting drug

distribution.[10,26]

Summary of vascular variability

Overall, these issues lead to spatial heterogeneity of the tumor vascular bed and

variable nutrient, oxygen, waste clearance, and drug delivery and waste clearance.

When viewing each component of vascular variability together, the complexity of the

tumor vasculature is increased exponentially. Diffusion distance variability occurring

from spatial heterogeneity is overlayed with tumor vessel structure heterogeneity,

which is overlayed with heterogeneity derived from the impact of solid stress on vessel

integrity and fluid pressure. To illustrate this idea, imagine two malignant cells each

positioned 100 μm away from the nearest vessel. One cell is positioned near a GMP while the other is positioned near a normal capillary. Although these cells are equally close to a blood vessel, differing vessel properties will alter drug, nutrient, and oxygen exposures. If the interstitial fluid pressure in these regions is also variable, then drug distribution would be impacted further. The scale for each of these variables is also most likely a gradient and could potentially have an infinite number of possible values, however, based on cellular physiology, each variable most likely affects cells in a manner consistent with a series thresholds instead of a true gradient.

2.3. Tumor stromal cells with known variability

Direct-acting anti-cancer agents receive the most developmental support, however, interactions between cancer and stromal cells within the tumor microenvironment may play a more significant role in determining patient outcomes. A tumor is more appropriately viewed as an aberrant organ with malignant cells as the core drivers, but with participation by local and recruited stromal cells. Stromal cells act on cancer cells in a few different ways. Stromal cells can interact directly with cancer cells. This type of interaction is usually mediated by surface receptors such as those found on CD8^{+} T cells. Stromal cells can also interact with cancer cells more indirectly through paracrine signaling such as the release of growth factors and cytokines. Another possible interaction of stromal cells is through structural changes to the tumor microenvironment. This can include secretion of extracellular matrix proteins or production of large structures such as blood vessels. Lastly, stromal cells can interact with other stromal cells, which can influence their stromal-tumor interactions. The

major stromal cells that are known to significantly influence the tumor

microenvironment are: fibroblasts, macrophages, endothelial cells, pericytes, platelets,

natural killer cells, lymphocytes (B and T), mesenchymal stem cells, dendritic cells,

neutrophils, and adipocytes. These cell types and their tumor interactions will be

discussed below. [27,28,29,30,31,32,33,34,35]

Fibroblasts

The main function of fibroblasts is to maintain and regulate the extracellular

matrix (**ECM**) components of tissues. Fibroblasts enrich the ECM through secretion of

macromolecules such as collagens, glycoproteins, and proteoglycans. They also degrade

the ECM by secreting proteolytic enzymes such as metalloproteinases (**MMPs**), lysyl

oxidases, tissue inhibitors of MMPs, and cathepsins. In this way, fibroblasts can remodel

the ECM as necessary to provide structural and physiological support for tissues. While

the ECM may seem simple, a "matrisome" of over 300 ECM components has been

detected using mass spectrometry.[28,36] In addition to its role in maintaining the

structural integrity of tissues, the ECM can also communicate with cells though ligand

binding. These cell-matrix interactions can alter cellular functions such as proliferation,

survival, morphology, adhesion, and motility. Matrix proteins can also sequester growth

factors and can act as a reservoir to promote tissue homeostasis and wound repair.[28,36]

It is thought that the ECM initially displays anti-tumorigenic properties during early

tumorigenesis, but these effects eventually become pro-tumorigenic over time.

Under normal circumstances, many fibroblast functions can occur in a quiescent state where they can migrate, secrete ECM components, and degrade the ECM when necessary. However, in some normal instances, such as wound healing, or in pathological conditions, such as cancer or fibrotic illness, fibroblasts may become activated, proliferate, and secrete higher levels of ECM components. When under sustained stress or during wound healing, resident fibroblasts can differentiate into myofibroblasts. Myofibroblasts are identified (though not exclusively) by their expression of α smooth muscle actin (**αSMA**), which binds to actomyosin fibers to contract and stiffen the ECM permanently. Myofibroblasts are also extensive producers of ECM components. After sufficient wound healing, in normal tissues, myofibroblasts should undergo apoptosis or should dedifferentiate into quiescent fibroblasts. However, in the tumor microenvironment, fibroblasts become corrupted. The most important inducers of cancer-associated fibroblast (**CAF**) activation are transforming growth factor beta (**TGF-β**), epidermal growth factor (**EGF**), platelet derived growth factor (**PDGF**), fibroblast growth factor 2 (**FGF2**), sonic hedgehog (**SHH**), and IL-1β. CAFs are unable to undergo apoptosis or dedifferentiate into quiescent fibroblasts. CAFs are proliferative, mobile, and excessively secretory.

Although CAFs can appear similar, they are a heterogeneous population of cells with different pathways of origination. In a thorough review of CAFs by Walter et al,[33] 15 unique subpopulations of CAFs were identified based on unique markers and functions. CAFs can be recruited from resident fibroblasts in a similar fashion to myofibroblasts. In addition to the growth factors listed above, hypoxia and oxidative stress can also

activate these fibroblasts. Additionally, some CAFs can differentiate from other cell lineages such as epithelial cells (epithelial to mesenchymal transition), endothelial cells (endothelial to mesenchymal transition), adipocytes, pericytes, and smooth muscle cells. Mesenchymal stem cells (**MSC**) derived from the bone marrow may also differentiate into CAFs. Because the total CAF population can be derived from multiple methods of recruitment, the overall CAF population is heterogeneous. While it's easier to summarize CAFs based on clear cut functions, the physiological reality is much more complex.

In contrast to normal fibroblasts, CAFs secrete abnormal and excessive ECM components, creating a denser and stiffer ECM. These changes can impede adequate drug delivery, especially for high molecular weight drugs. CAFs also secrete excessive cytokines (CXCL12, IL-6), growth factors (EGF, hepatocyte growth factor (**HGF**), FGF, insulin-like growth factor 1 (**IGF1**), TGF-β), and matrix metallopeptidases (**MMP2, MMP9**) relative to normal fibroblasts. These components can increase the proliferation rate and metastasis of tumor cells. Dysregulation of the ECM can inhibit apoptosis and increase tumor stem cells. Although these functions are found broadly in CAFs, it's important to stress the heterogeneity of these cell populations. Some CAFs can have a tumor-suppressive role through suppression of regulatory T cells. Other CAFs can improve drug sensitivity of tumors. Some CAFs specialize in ECM remodeling, while others specialize in immunosuppression or angiogenesis.

Macrophages

Macrophages have a significant role in immunity and in tissue homeostasis. Macrophages originally differentiate from circulating monocytes and function to clear away cell debris, tumor cells, and toxic substances through phagocytosis. They also stimulate the innate immune system through cytokine release or complement activation and the adaptive immune system through antigen presentation.[60] Macrophages are diverse and can become highly specialized as demonstrated by the Kupffer cells in the liver, alveolar macrophages in the lung, microglia in the central nervous system, or splenic macrophages in the spleen. These macrophages function as detoxifiers, scavengers, and recyclers.[59] Currently, there are two main classes of macrophages: M1 and M2. Exposure to interferon gamma (**IFN-γ**), granulocyte-macrophage colony stimulating factor (**GM-CSF**), or tumor necrosis factor (**TNF**) will cause macrophages to differentiate into the classical M1 phenotype, which are responsible for fighting infections, degrading damaged tissues, and activating inflammatory pathways. The M1 macrophages are excellent antigen presenting cells. They are high expressors of IL-12, IL-23, and IRF-5 and low expressors of IL-10. The M1 macrophages also stimulate TH1 helper cells, which are important mediators of the adaptive immune response. Alternatively, macrophages exposed to granulocyte colony stimulating factor 1 (**G-CSF-1**), IL-4, IL-10, IL-13, IL-33, or TGF-β may differentiate into an alternative M2 macrophage that functions in parasitic infections, tissue remodeling, allergic disease, or angiogenesis. M2 macrophages can be further subdivided based on the specific activating mechanism into M2a, M2b, and M2c macrophages. In general, all M2 macrophages, except for M2b, are identified by high IL-10 expression, low IL-12

expression, and low production of pro-inflammatory cytokines such as IL1, TNF, and IL-6.[58,60]

Like CAFs, tumor associated macrophages (**TAMs**) are a highly heterogeneous population. TAMs are recruited from circulating monocytes derived from the bone marrow or spleen or activated from resident macrophages within tissue.[58] Circulating monocytes are recruited to the tumor site by characteristics such as hypoxia (**HIF-1^α**), inflammation, and high lactic acid levels. These conditions stimulate the release of stimulatory and chemotactic chemokines.[60] TAMs are subdivided into anti-tumorigenic M1-like TAMs (IL-12^{high}, IL-10^{low}, MHC-II^{high}) and pro-tumorigenic M2-like TAMs (IL-12^{low}, IL-10^{high}, MHC-II^{high}). M1-like TAMs produce pro inflammatory cytokines such as IL-1β IL-6, IL-12, IL-23, CXCL-9, CXCL10, and TNF-α, stimulate CD8$^+$ T cells, and appear to have a tumor suppressive effect. On the other hand, M2-like TAMs mainly secrete anti-inflammatory cytokines such as IL-10, TGF-β, CCL17, CCL18, CCL22, and CCL24. M2-like TAMs promote tumor invasion and metastasis, epithelial-mesenchymal transition, angiogenesis, and immunosuppression.[58] Although not fully evaluated, there is some evidence that BM derived macrophages have a more significant role in antigen presentation and immune stimulation, while tissue derived macrophages are more likely to play a more significant role in ECM remodeling.[58] Hypoxia appears to play a major role in subdividing the TAM populations. M1-like TAMs are found predominately in areas of relatively high oxygen saturation while M2-like TAMs can be found in hypoxic areas. Hypoxia can cause TAMs to express genes in a more similar fashion to M2-like TAMs, suggesting that the regionality of TAMs is more likely based on environmental

influences rather than a macrophage phenotype preferring a specific environment. M2-like TAM localization in hypoxic regions is consistent with its function as a mediator of angiogenesis and accomplishes this role through matrix remodeling through MMP secretion and vascular stimulation through VEGF secretion. TAMs are also highly plastic and can exist in phenotypes lying somewhere in between the M1-like and M2-like polarizations depending on signaling from the tumor microenvironment. For instance, CD169^{+} and TCR^{+} macrophages are distinct subpopulations that exist within the M1 and M2 classification. Some cells can also simultaneously express M1-like and M2-like characteristics. These TAM phenotypes are also reversible, allowing cells to continually adapt to a new environment.[58,60]

TAMs exhibit significant heterogeneity, which can drastically affect their function and role within the tumor microenvironment. TAMs play a significant role in tumor progression and treatment resistance and influence the diversity of the tumor cell population. These characteristics are not steadfast as TAMs are adaptable and will respond to environmental ques. Thus, it is important to clarify that while the M1 and M2 classifications allow for easier functional organization and comprehension, the true phenotypic complexity of macrophages is much more complicated.

Endothelial cells

Endothelial cells coat the inner lumen of blood vessels and regulate the exchange of nutrients, oxygen, and macromolecules from the capillaries to the interstitial space. During angiogenesis, endothelial cells are usually recruited from pre-

existing vessels and during vasculogenesis, endothelial cells are usually recruited from bone marrow-derived progenitor cells. Endothelial cells also play a significant role in inflammatory processes by controlling leukocyte recruitment through the production of adhesion molecules (E-selectin, P-selectin, intercellular adhesion molecule (**ICAM-1**), vascular cell adhesion protein (**VCAM**), etc.) and regulation of leukocyte extravasation. Endothelial cells are intrinsically antithrombotic to prevent local thrombotic events from inducing systemic events. They accomplish this through the binding of antithrombin produced by the liver, which inhibits thrombin, and through the production of thrombomodulin, which alters thrombin, preventing fibrinogen activation and promoting protein C activation. However, in highly inflammatory environments, endothelial cells are less antithrombotic, which likely plays a significant role in platelet recruitment and activation in oncologic diseases.[61]

As described above, tumor endothelial cells (**TECs**) form heterogeneous and abnormal structural networks that are sometimes excessively leaky. In this abnormal tumor environment, TECs can be highly proliferative and more drug-resistant than normal endothelial cells. TECs also respond abnormally to EGF, VEGF, and adrenomedullin and are resistant to serum starvation.[63] TECs are heterogeneous and respond to the microenvironment. TECs within a high metastatic environment have shown increased proliferation, migration, and invasion relative to TECs originating from low metastatic tumors. TECs originating from highly metastatic tumors also display increased stemness and a wider differentiation potential. Tumor cell signaling, hypoxia, and nutrient deprivation help drive the phenotypic changes of TECs and a variable

tumor microenvironment drives TEC heterogeneity.[63,65] Kida et al. has reported

aneuploidy and genomic instability within TEC populations, which suggests that tumor

cells may have a substantial and far more enduring impact on stromal cells and that

stromal cells may be even more corruptible than previously expected.[62,63,64]

Importantly, they evaluated human cancer cells in a xenograft mouse model, which

allowed the separation of human tumor cells from mouse TECs. In this study, after the

separation of human and mouse cells, they demonstrated that mouse endothelial cells

within the tumor possessed aneuploidy, but endothelial cells outside of the tumor did

not. Additionally, they screened twenty human renal cell carcinoma patients and

determined ~30% of patients' endothelial cells demonstrated aneuploidy.[62] However,

it's not yet understood whether the tumor cells or tumor microenvironment directly

causes genomic instability or whether the microenvironment better tolerates abnormal

cells and allows increased accumulation of detrimental mutations.

TECs also have important functions in tumor metastasis and tumor cell

proliferation. TECs provide vascular access for tumor cells and help drive metastasis

through the secretion of adhesion molecules, which function to stimulate extravasation.

Elevated expression of Notch1 and biglycan in TECs also helps promote tumor cell

migration and metastasis.[63] TECs secrete a number of stimulatory factors such as

endothelin-1, FGF, TGF-β, IL-6, IL-8, IL-3, IL-1, PDGF, G-CSF, and GM-CSF.[63] Many of

these factors are produced by other cell lines, highlighting the interconnected nature of

the tumor microenvironment and how expression abnormalities can feed off each

other, leading to amplification of these abnormalities. TECs also downregulate their

tumor suppressive functions relative to normal endothelial cells, which increases tumor

cell survival. Moreover, in contrast to normal endothelial cells, TECs decrease the

expression of cellular adhesion molecules such as E-selectin, P-selectin, ICAM-1, and

VCAM-1, which causes inefficient recruitment of leukocytes and creates an overall

immunosuppressive microenvironment.[61,63] Release of proangiogenic factors also

causes TECs to express CD95 and programmed death ligand 1 (**PD-L1**), which induces

apoptosis in CD8^{+} T cells, but spares regulatory T cells.[63] Similar to other stromal cells,

it's important to emphasize that TECs are heterogeneous and each subpopulation may

possess all or none of these characteristics, depending on microenvironmental

influences. It's also important to highlight the significant number of cell types that are

influenced by TECs through direct signaling, paracrine signaling, and through structural

changes to the tumor microenvironment.[63,65]

Pericytes

As discussed in the vasculature section, pericytes maintain the structure,

integrity, and permeability of the vasculature and have a supportive role in maintaining

healthy endothelial cells. They also regulate angiogenesis, blood flow, and immunity.

High density pericytes form the restrictive barriers found in the brain and retina and

help remove toxic substances from these privileged sites. In a similar role, pericytes in

the liver and kidney alter the arrangement of endothelial cells in the capillary beds of

these organs, which is vital for organ function. Additionally, specialized pericytes located

in the glomeruli of the kidneys help filter toxic substances out of the blood. [66,67,69]

Conventionally, pericytes are known exclusively for their vascular supportive role, which may suggest that these cells have a rigid and narrow phenotype, however, recent work has demonstrated an increased capacity for pericytes to differentiate into mesenchymal cells such as osteoblasts, chondrocytes, fibroblasts, and adipocytes.[68] The multipotent capabilities of pericytes suggests that these cells may share similarities to mesenchymal stem cells and most likely possess significant population heterogeneity within the tumor microenvironment. In fact, pericytes are known to dynamically express different markers depending on their tissue location, which indicates that distinct subpopulations of pericytes can be produced from different microenvironments. A few specific factors that are known to influence pericytes are platelet derived growth factor receptor beta, CD13, CD146, and alpha smooth muscle actin.[66,68,69] Some even classify pericytes as perivascular stem cells due to their multipotency.[66]

Specifically, within the tumor microenvironment, pericytes have been shown to regulate angiogenesis, metastasis, and cancer stem cell maintenence.[66,69] During angiogenesis, PDGF-β, heparin binding EGF like growth factor (**HB-EGF**), and Stromal cell derived factor 1 (**SDF-1**) are secreted from endothelial cells to stimulate pericyte recruitment and activation. Pericytes then secrete VEGF and Angiopoietin 1 (**Ang-1**) to support the surrounding endothelial cells.[66,69] As described above, the tumor microenvironment possesses significant vessel heterogeneity consisting of some normal vessels and some abnormal vessels. Many of these abnormal vessels lack significant pericyte involvement, leading to increased vessel leakiness and increased metastatic potential for tumor cells.[66] Additionally, pericytes can stimulate tumorigenesis through

growth factor secretion, but may also possess some antitumor effects. It has been shown that high pericyte density is associated with lower metastatic potential but increased primary tumor growth. This may suggest that pericytes function as a barrier to tumor cell extravasation but can also stabilize blood vessels, increasing oxygen and nutrient delivery to the tumor. In contrast, low pericyte density has been associated with increased tumor invasion and metastasis.[66] Pericytes can impede the immune system by inhibiting lymphocyte activation (RGS5, IL-6), however, possessing too few pericytes has also been shown to increase the proportion of myeloid-derived suppressor cells within the tumor. This demonstrates that pericyte inhibition may stimulate or suppress a tumor depending on the current function of tumor adjacent pericytes. Additionally, pericytes can recruit TAMs through the secretion of SDF-1, and, reciprocally, M2-like TAMs can recruit pericytes, indicating a possible positive feedback loop between these two cell types. Pericytes may also play a role in drug resistance by protecting endothelial cells from anti-angiogenic therapy through the secretion of pro-angiogenic factors and by creating a physical endothelial-pericyte barrier.[69]

Mesenchymal stem cells (aka mesenchymal stromal cells)

In contrast to many of the cell types discussed so far, MSCs are identified by their multipotent ability to differentiate into many different types of cells such as fibroblasts, osteoblasts, adipocytes, chondrocytes, epithelial cells, hepatocytes, and neuronal cells under appropriate conditions.[71,73,74] MSCs were originally thought to originate exclusively from the bone marrow, however, resident MSCs are now known to exist in many different types of tissues including adipose, synovial, muscle, ligament,

salivary gland, skin, and lung.[71,72,73,74] Importantly, MSCs derived from different

microenvironments have demonstrated differing proliferation rates, differing

differentiation capabilities and tendencies, and differing transcriptome and secretome

patterns, highlighting the population heterogeneity of MSCs.[72,73] While still debatable,

the International Society for Cellular Therapy identifies MSCs using a few phenotypic

characteristics: MSCs must adhere to plastic surfaces in standard culture conditions,

MSCs must possess a multipotent ability to differentiate into adipocytes, chondrocytes,

and osteoblasts, MSCs must express CD105, CD73, and CD90, and MSCs must not

express CD45, CD34, CD14, CD19, CD79a, CDq1b, or HLA-DR. However, since these

recommendations debuted in 2006, a few additional characteristics have been included

by other investigators such as expressing CD29, CD44, CD49, CD106, CD140b, CD166,

and STRO-1, and not expressing CD11b, CD31, and CD133.[72,73,74] Also, MSCs may

sometimes display differentiation heterogeneity with only a fraction of cells

differentiating when exposed to appropriate culture conditions. One possible

explanation for these results maybe a loss of differentiation potential due to excessive

proliferation. The microenvironment also significantly impacts the heterogeneity of

MSCs. MSCs originating from different tissues display phenotypic and functional

heterogeneity, emphasizing how difficult characterizing this particular cell can be. MSCs

can display inter and intra-clonal heterogeneity. Not only can differences be identified

between MSCs isolated from adipose tissue and bone marrow, but even between MSCs

derived from the same progenitor. [73] A wide range of potential markers are currently

being assessed to help differentiate MSCs from different tissues, but a conclusive list has not been finalized.

The most well-known role of mesenchymal stem cells (**MSCs**) is in injury related tissue repair. Inflammatory mediators released following an injury such as TNF-α, IL-1, and INF-γ stimulate tissue remodeling, which activates MSCs to differentiate and replace damaged stromal cells. During injury, MSCs will also release their own mediators such as EGF, FGF, PDGF, TGF-β, VEGF, HGF, IGF-1, angiopoietin-1 (**Ang-1**), keratinocyte growth factor (**KGF**), TNF-stimulated G6 protein (**TSG-6**), interleukin-1 receptor antagonist (**IL-1RA**), prostaglandin E2 (**PGE2**), indoleamine 2,3 dioxygenase (**IDO**), and stromal derived factor 1 (**SDF-1**). As can be expected, these mediators have wide-ranging effects, including stimulation of angiogenesis, stimulation of resident stromal cells such as fibroblasts, osteoblasts, and chondrocytes, and stimulation of ECM deposition and tissue repair. MSCs can also have inhibitory effects on cancer cells by inhibiting angiogenesis or by inducing tumor cell apoptosis.[72,74] Determining whether MSCs are harmful or beneficial for cancer cells appears to depend on the specific tumor microenvironment.

MSCs significantly affect immune modulation, but may be both pro and anti-inflammatory, depending on environmental cues, an effect somewhat similar to macrophage polarization discussed above. MSCs tend to be more proinflammatory in the initial stages of an inflammatory cycle and more anti-inflammatory in the later stages of an inflammatory cycle. When exposed to an environment with low levels of TNF-α and INF-γ or with high levels of toll-like receptor 4 (**TLR4**), MSCs will display a pro-

inflammatory phenotype, known as MSC1. MSC1s can secrete high levels of cytokines to inhibit tumor growth and can inhibit the activity of MMPs to reduce invasion and metastasis. On the other hand, if MSCs are exposed to high levels of TNF-α or INF-γ or if MSCs are stimulated through toll-like receptor 3 (**TLR3**), they will display an anti-inflammatory phenotype known as MSC2. In normal wound healing, it is thought that high levels of TNF-α and INF-γ signal an end to an inflammatory cycle, the effects of which may be mediated by MSC2 cells. MSCs can exert an immunosuppressive effect on many immune cells. They can upregulate TH2 polarization and downregulate TH1 polarization of CD4^{+} T cells. MSC2 can inhibit the activity and proliferation of CD8^{+} T cells, B cells, and NK cells. Also, MSC2 can activate regulatory T cells and M2 macrophages and inhibit M1 macrophage differentiation. Lastly, MSC2 can decrease antigen presentation of DCs, further reducing the efficacy of the adaptive immune system.[71,74] Because MSC cells are undifferentiated, they are capable of producing a wide range of immunosuppressive mediators, however, these mediators are not yet finalized, and significant variability exists in the expression patterns of both MSC1 and MSC2 phenotypes. In fact, some investigators report many alternative expression patterns and significant overlap for each of the MSC phenotypes. This most likely reflects that characterizing a highly heterogeneous cell type like MSCs in many different microenvironments can be difficult. Rather than memorizing every potential molecule that can by expressed by MSCs, it's important to remember that these cells are multipotent and extremely responsive to environmental cues with expression patterns that will most likely be highly dependent on the model system and tumor type.

MSCs can be recruited to tumor sites by similar factors responsible for recruitment of stem cells such as FGF, hepatoma derived growth factor (**HDGF**), IL-6, monocyte chemotactic protein 1 (**MCP-1**), SDF-1, urokinase plasminogen activator, and VEGF. After exposure to the tumor microenvironment, some MSCs will gain abnormal characteristics and will become tumor associated MSCs (**T-MSCs**). T-MSCs are more proliferative and immunosuppressive than normal MSCs and can have both pro-tumorigenic and antitumorigenic effects depending on the microenvironment. Instead of polarizing into either MSC1 or MSC2 phenotypes, T-MSCs usually fall somewhere within the spectrum and are highly heterogeneous. Some studies have demonstrated differential expression patterns of T-MSCs from exposure to different growth factors and cytokines, indicating that T-MSCs have a high potential for population heterogeneity. Interestingly, gene expression analysis comparing T-MSCs from a primary mammary tumor to T-MSCs from its associated lung metastasis revealed tissue-specific transcriptomic changes. This highlights that stromal cell heterogeneity increases exponentially with each additional metastatic site. Through direct, indirect, or structural interactions, T-MSCs can stimulate angiogenesis, ECM remodeling, cancer proliferation, EMT, invasion, and metastasis. T-MSCs can also exert effects by differentiating into different cell types. Similar to fibroblasts, T-MSCs can secrete factors such as IL-6 and TGF-β, but T-MSCs can also fully differentiate into a CAF-like phenotype.[74]

Neutrophils

Known mainly for their role as a first line defender against microbial pathogens, neutrophils often go unnoticed in oncologic diseases. However, as will be discussed

below, neutrophils can have a substantial impact on tumor growth and drug response. Neutrophils the most abundant white blood cell in circulation with an estimated 100,000,000,000 cells produced daily.[76] Neutrophils surveil the body in search of invading organisms and are highly recruited to injured tissues. Neutrophils can phagocytize microbes, can release antimicrobial granules containing myeloperoxidase, cathelicidins, defensins, and MMPs, can release a microbicidal respiratory burst, or can release neutrophil extracellular traps to ensnare the microbe.[75,77] Neutrophils also regulate inflammatory and immune processes and can influence neighboring cells through the release of cytokines.[75,77,78,79,80] A less commonly known function of neutrophils is their supportive role in maintaining hematopoietic stem cell populations. Neutrophils encourage hematopoietic stem cells to become quiescent, which prevents proliferative stress and DNA damage and ensures that a reserve of stem cells is maintained in the underlying tissue.[79]

Consistent with the theme of this review, neutrophils possess heterogeneity, even with their limited circulation half-life. Neutrophils are able to adapt and respond differentially to environmental cues like surface receptors or cytokines. Environmental heterogeneity causes neutrophils to express heterogeneous surface receptors and to possess a heterogeneous transcriptome. [75,76,79,80] One unique mechanism that is highlighted in neutrophil heterogeneity is a process known as neutrophil ageing. Neutrophils are known to alter phenotypic characteristics and functions as they circulate in the bloodstream. However, ageing is not uniform, which creates a diverse group of neutrophils that can be exposed to different microenvironments, enhancing

heterogeneity. Aging neutrophils have been shown to lose L-selectin expression and gain CD11b and CXCR4 expression after a short circulation time.[77,80] Neutrophils may also exit bone marrow in a more immature state and can slowly become more mature as they circulate. Immature neutrophils have blunted responsivity, neutrophil extracellular traps (**NET**) secretions, ROS production, and phagocytosis. These changes are caused by toll-like receptor, CXCR2, and CXCR4 signaling and are largely controlled by the internal molecular clock of neutrophils, the circadian rhythm, and external interactions.[75,77,78,79,80]

Neutrophil heterogeneity of cancer patients is even more pronounced. For example, one study analyzed the neutrophils of a cohort of melanoma patients and found at least seven distinct neutrophil subtypes.[80] This substantial heterogeneity is caused by interactions between the natural circadian, molecular, and external actions of neutrophils and the heterogeneity of the tumor microenvironment. These tumor associated neutrophils (**TANs**) can have both protumor and antitumor effects depending on the neutrophil subclone and the tumor environment. Some investigators use nomenclature similar to TAMs in which antitumoral neutrophils are labeled N1 and protumoral neutrophils are labeled N2. N1 neutrophils secrete high levels of TNFα, CCL3, ICAM-1, and low levels of arginase axis and N2 neutrophils secrete high levels of CCL2, CCL3, CCL4, CCL8, CCL12, CCL17, CXCL1, CXCL2, CXCL8, and CXCL16.[78] High TGF-β exposure induces N2 neutrophils and low exposure induces N1 neutrophils. An important antitumor mechanism active in some TANs is the expression of TNF related apoptosis inducing ligand (**TRAIL**), which allows TANs to induce apoptosis in tumor cells.

In another unique antitumor mechanism, TANs can ingest pieces of the tumor cell's plasma membrane. TANs can also form neutrophil-dendritic hybrids with enhanced antigen presentation capabilities to activate CD8+ T cells. Similarly, TANs also possess the ability to activate B cells and Natural killer (**NK**) cells.[75,76,77,78,79]

During initial tumorigenesis, TANs can contribute to the oxidative tumor environment through release of reactive oxygen species (**ROS**), which causes DNA damage and further destabilizes the genomes of cancer cells. While this can initially inhibit tumor growth, over time, genetic instability will produce more resistant and aggressive cancer cells.[75,80] TANs also have the ability to stimulate tumor growth through release of factors such as PGE2 or IL-1RA. Additionally, neutrophils are capable of altering the tumor microenvironment through release of proangiogenic factors and MMPs in response to hypoxia.[75,78] Neutrophils suppress the immune system through release of anti-inflammatory mediators such as ROS, nitric oxide synthase (**NOS**), and arginase 1 (**ARG-1**). They can also directly inhibit immune cells through expression of immune checkpoint ligands, and by preventing immune cells from invading the tumor.[75,78,80] Immunosuppressive neutrophils bear a striking resemblance to granulocytic myeloid derived suppressor cells, a subset of myeloid derived suppressor cells. In fact, a panel of six surface markers (CD11b, CD14, CD15, CD33, CD66b, HLA-DR) was unable to differentiate the two cell types, and currently, no method exists to differentiate these cell types.[77] Some investigators have concluded that granulocyte-like myeloid derived suppressor cells (**G-MDSCs**) are a subset of neutrophils, while others believe that each cell type is unique. On another note, NETs secreted form neutrophils

can influence the extracellular matrix of tumors, increasing the tumor cell proliferation rate, influencing stromal cells, and acting as a barrier to cytotoxic immune cells. Clinically, TANs are associated with a poorer response to chemotherapy and radiotherapy. Furthermore, TANs can enhance the metastatic potential of a tumor by forming cell clusters around circulating tumor cells and supporting these cells throughout circulation, which increases their proliferative and metastatic potential. Neutrophils can also form clusters at distant metastatic sites to prime these sites to respond more favorable to tumor cells.[75,78,80]

Natural killer cells

In contrast to many of the cells discussed in this overview without mechanisms related to malignancies, one of the main roles of natural killer (**NK**) cells is controlling tumor growth. The other major role of NK cells is fighting intracellular infections.[87,88,89,90] NK cells use a complex combination of inhibitory and stimulatory surface signaling to identify and target distressed host cells. NK cell receptors can recognize altered expression of target cell surface antigens when they undergo cell stress, viral infection, or tumor transformation. They also have built in protection mechanisms utilizing the MHC class I receptors for identification of self. NK cells receive simultaneous inputs from each surface receptor. If the inhibitory inputs exceed the stimulatory inputs, then natural killer cells will identify the cell as unstressed self and the cell will be spared. If the stimulatory inputs exceed the inhibitory inputs, then the cell will be identified as either stressed self or missing self, which will stimulate the natural killer cell to release its granules.[87,88,89,90,91] These granules contain perforin, which forms pores in the cell

membrane of target cells, granzymes, which stimulate apoptosis in the target cells, and cytokines such as INF-γ and TNF-α, which further activate the immune system.[88,89,91] While a complete list of the NK cell receptors and their complementary ligands is out of the scope of this overview, a great review of this information has been conducted by Sivori et. al (2019).[89]

The major inhibitory receptors present on NK cells include receptors capable of recognizing the major histocompatibility complex such as HLA-A, HLA-B, HLA-C, HLA-E, and HLA-G.[89,90,91] Interestingly, some NK cells possess receptors that are activated in response to the major histocompatibility complex, however, the purpose of these receptors is not currently known. Generally, the major histocompatibility complex acts as a sign of self and can stave off an attack from NK cells, provided the cell is not overtly producing stimulatory ligands. Other inhibitory receptors produced by NK cells include programmed cell death protein (**PD-1**), lymphocyte activation gene 3 (**LAG-3**), or T cell immunoreceptor with Ig and ITIM domains (**TIGIT**). PD-1 and LAG-3 are extremely important targets for monoclonal antibodies, which improve immune activation against tumor cells by inhibiting the interaction between the ligand and receptor. TIGIT has been found to be upregulated in tumor associated NK cells, indicating a role in immunosuppression.[88,89,91]

The natural cytotoxicity receptor (**NCR**) receptor is an important stimulatory receptor that can recognize intracellularly localized proteins that become localized on the cell surface in response to stress. NCR receptors can also detect expression of some ligands that are not expressed in healthy cells, but are expressed in tumor cells and are

associated with upregulated oncogenic pathways such as Myc. The natural killer group

2D (**NKG2D**) receptor is another important stimulatory receptor that detects stress

induced self-ligands such as UL16 binding protein (**ULBP**s) and MHC class I polypeptide

related sequence A (**MICA**)/MHC class I polypeptide related sequence B (**MICB**), which

are structural homologs to HLA receptors and are upregulated by infected, stressed, or

malignant cells.[87,90,91] Natural killer cells also express the CD16 (FCγRIII) receptor, which

binds to antibodies such as IgG and functions in conjunction with B cells to induce

antibody dependent cell mediated cytotoxicity. Distressed cells presenting antigens that

can be bound by antibodies alter the balance of inhibitory and stimulatory signals

present on natural killer cells, causing granule release. NK cells also play a major role in

tumor surveillance by identifying and eliminating tumor cells that downregulate MHC

class I receptors. Downregulation of MHC class I receptors protects these tumor cells

from CD8^{+} T cell cytotoxicity. NK cells are also capable of detecting distressed or

infected cells and can target their destruction, though not in an adaptable

manner.[87,88,89,90,91]

In contrast to many of the cell types discussed so far that are highly

heterogeneous, NK cells appear to be more uniform. While NK cells do display some

heterogeneity, overall literary evidence does not currently reveal a wide range of

phenotypes and the phenotypes that are known appear to be more distinct and

consistent.[87] In humans, NK cells are separated into two major subsets according to

CD56 expression. CD56^{bright} cells are found predominantly in tissues and represent only

a small fraction of circulating NK cells. These cells are poorly cytolytic but can secrete

cytokines such as IFN-γ, TNF-β, and GM-CSF and will proliferate rapidly in response to IL-2 or IL-15. CD56^{dim} cells are found predominately in circulation and less commonly in tissues. These subtypes can express cytokines and can initiate a strong cytotoxic effect in response to stimulatory signals. As CD56^{dim} cells mature, they progressively lose proliferating capacity and progressively gain cytotoxic capabilities. The expression patterns of the surface receptors on CD56^{dim} cells change as the cells mature, which increases the cytotoxic potential of these cells.[87,88,89,90,91] IFN-γ, TNF-α, IL-2, IL-12, IL-15, IL-18, and IL-21 are known to activate NK cells to increase proliferation, cytotoxicity, and cytokine secretion. On the other hand, TGF-β is a well-known inhibitor of NK cell function and is secreted by regulatory T cells, a cell with a significant role in immune escape.[90]

The tumor microenvironment significantly alters the function and activity of NK cells. Environmental characteristics such as hypoxia or acidosis, or the release of factors such as IDO, TGF-β, PGE2, bag cochaperone 6 (**BAG6**), or B7-H6 can reduce the expression of activating receptors and impair NK cell function. NCR^{low} NK cells have been detected more frequently in patients with tumors, highlighting the immunosuppressive capabilities of the tumor microenvironment. This may be partially due to TGF-β, which favors the recruitment of CD56^{bright} cells and decreases the recruitment of CD56^{dim} cells. Hypoxia and nutrient deprivation also cause NK cell dysfunction. Hypoxia decreases the production of cytotoxic granules, which decreases the cytotoxic capabilities of NK cells. Additionally, the tumor microenvironment strongly prefers more immature NK cells with lower levels of activating receptors, perforin, and granzymes.[88,89,91]

Tumor cells can evade NK cell-mediated cytotoxicity through a few mechanisms. Tumor cells can secrete activating ligands into the microenvironment, which act as decoys for the surface receptors of NK cells and can cause internalization and loss of activity of the surface receptor. Loss of ULBPs, MICA/MICB, or other types of stimulatory ligands through selective pressure can also reduce NK mediated cell killing.[88] Some tumor cells instead rely on overstimulation of inhibitory signals on NK cells to prevent cytotoxicity. This can occur through overexpression of MHC class I molecules or overexpression of immune checkpoint ligands such as PD1/2. While the tumor microenvironment has a substantial effect on NK cell function, corrupted NK cells do not appear to become as protumorigenic as some other cell types mentioned in this overview. Instead, the tumor microenvironment appears to place NK cells in a more neutral state. Whether this means NK cells can be restored more easily to an antitumorigenic phenotype remains to be seen.[88,89,91]

Dendritic cells

Dendritic cells (**DCs**) are a highly heterogeneous cell type known mainly for their role as a professional antigen presenting and immune regulating cell.[92,93,94] Dendritic cells can be found in circulation, lymphoid tissue, and non-lymphoid tissue. Many different subsets of dendritic cells have been identified with unique morphology and functionality such as Langerhans cells, myeloid derived dendritic (conventional DCs (**cDC1, cDC2**)) cells, monocyte derived dendritic cells (inflammatory DCs), and plasmacytoid dendritic cells.[92,93,94,95,96,97] However, newer techniques such as scRNA-seq allow more precise delineation of DC subtypes, revealing heterogeneity even among

cells from the same subtype.[91] DCs ingest, degrade, process, and present antigens using major histocompatibility complexes (**MHC**), co-stimulatory molecules (CD40, CD80, CD86), and adhesive molecules (CD11a, CD15s, CD18, CD29, CD44, CD49d, CD50, CD54) to effector cells such as T cells, B cells, neutrophils, and natural killer cells.[91,93] MHC receptors are identified as class I and class II based on function and cell type. MHC class I receptors are found on all nucleated cells and function to present endogenous peptides as a measure of cellular health. MHC class II receptors are found only on antigen-presenting cells and present exogenous peptides such as antigens from a pathogen to active other immune cells. Myeloid-derived dendritic cells are thought to play a major role in the activation of CD4$^+$ and CD8$^+$ T cells. Plasmacytoid DCs are thought to release interferon during viral infections, and monocyte-derived DCs are activated during inflammation, but play a smaller role in maintaining immune homeostasis. [94,95,97] Dendritic cells found in the thymus also play an important role in maintaining immunologic homeostasis by inducing tolerance in thymocytes through negative selection.[92] Importantly, although each subpopulation of DCs is thought to have a specific role, the phenotype and function of DCs are heavily influenced by the microenvironment. For example, while plasmacytoid DCs can be highly immunosuppressive and tolerogenic, they have also demonstrated capacity to activate cytotoxic lymphocytes, depending on the microenvironment.[93,94]

Professional antigen-producing cells such as dendritic cells, macrophages, and B cells are more efficient activators of effector cells because of their expression of MHC molecules, costimulatory molecules, and adhesive molecules. The simultaneous

expression of these molecules activates effector cells more robustly relative to non-professional antigen-presenting cells, which do not express these accessory molecules.[92,94] However, dendritic cells are also thought to exist in two main functional states: immature and mature. Immature DCs express fewer MHC molecules, costimulatory molecules, and pro inflammatory cytokines. Immature DCs also have increased phagocytic activity, which enhances their ability to ingest stimulatory molecules such as pathogen associated molecular patterns (**PAMPs**) or damage associated molecular patterns (**DAMPs**). These molecules convert immature DCs to mature DCs. Mature DCs have reduced phagocytic activity and increased MHC, costimulatory molecule, and adherence molecule expression. Thus, immature DCs function to detect aberrations and mature DCs function to propagate this signal.[92,94,]

During activation, mature dendritic cells also release inflammatory cytokines such as IL-1β, IL-6, TNF-α, IL-12, and IL-23 to further stimulate effector cells, recruit additional immune cells, and initiate an inflammatory response within the tissue.[92,93,94] Activated dendritic cells have increased motility and may relocate to secondary lymphoid organs to further recruit T-cells.[93] Although DC maturity is an important factor influencing the DC phenotype, the process of DC maturation is not always straightforward and is heavily influenced by the microenvironment, which can reverse DC maturation and can create a tolerogenic and immunosuppressive phenotype.[94] DC maturity has also been found to exist as a range of maturities instead of as two discrete phenotypes. Additionally, the net antitumor effect resulting from dendritic cell maturity is complex and is dependent

on the variability that occurs from tumor cells, the tumor microenvironment, and the effector cells.[92,94,95,96,97]

Tumor infiltrating dendritic cells (**TIDCs**) are notoriously difficult to characterize due to their relatively low quantity, inherent heterogeneity, and inconsistent identity markers. Depending on the cancer type and other unknown variables, elevated TIDCs can either increase overall survival or decrease overall survival, which illustrates the limitation of using simple surrogate markers such as the degree of dendritic infiltration as a predictor of patient outcomes.[94,97] Although the true phenotype of TIDCs is extremely complex, TIDCs are typically characterized as immunosuppressive with reduced costimulatory molecule expression, reduced antigen processing and presentation, and elevated regulatory molecule expression.[96,97] Factors found within the TME such as IL6, IL10, macrophage colony stimulating factor (**M-CSF**), GM-CSF, TGF-β1, VEGF-A, IDO, gangliosides, and arginase have been found to induce an immunosuppressive phenotype.[95] Although many genetic pathways are important, PD1 and TIM3 have demonstrated special significance in altering DC phenotypes. Stimulation of PD1 through PDL1 and PDL2 leads to impairment of effector cell activation through reduced immunostimulatory cytokine production, reduced costimulatory factor expression, and ineffective antigen presentation. TIM3 inhibits Th1 type T cells and leads to the release of immunosuppressive factors from DCs. TIM3 has been studied extensively in autoimmune diseases. Its inhibition exacerbates autoimmune diseases, which suggests that it plays a role in self-tolerance.[96,97] While this is a common portrayal of TIDCs, phenotypic heterogeneity combined with the variability of the tumor

microenvironment should dissuade investigators from accepting this singular view of

TIDCs wholeheartedly. Additionally, temporal variability can occur, which affects the

TIDC phenotype, the quantity of TIDCs present in the tumor, and the overall effect of

TIDCs on tumor growth. Temporal variability also highlights the potential drawbacks of a

TIDC-based oncologic treatment. If TIDCs are helpful at an earlier cancer stage and

harmful at a later stage, a TIDC-based regimen could help or harm a patient, depending

on the progression of the disease and the timing of therapy. Additionally, metastatic site

variability further increases complexity. If TIDCs have a more immunostimulatory role

during the initial growth of a cancer lesion and a more immunosuppressive role for a

larger lesion, then a TIDC-based therapeutic could lead to the reduction of larger

tumors, but stimulation of microtumors.

T cells

T cells have many important functions in the adaptive immune system, including,

direct killing of abnormal cells, activation of immune cells, stimulation of the

inflammatory response through cytokine release, and regulation of the immune system.

T cells originate in the bone marrow and migrate to the thymus where maturation and

clonal selection occur. This is necessary to eliminate aberrant T cells that would mount

an immune response against healthy cells and eventually lead to autoimmune reactions.

T cells are easily differentiated from other cells in the immune system by their

expression of T cell receptors (**TCR**), which identify and selectively bind foreign

antigens.[100,107] The TCR is alternatively spliced through a complex series of mechanisms

that allow a theoretical 10^{15} to 10^{20} unique TCR receptors.[108] This allows T cells to

recognize an incredibly high number of unique antigens without prior exposure. After exposure to an appropriate antigen fragment by an antigen-presenting cell (**APC**) and after receiving additional costimulatory signals, a T cell clone will rapidly proliferate and will mount an immune response against the specific pathogen or infected/malignant cell. T cells can differentiate into several different subtypes, depending on inputs from the antigen presenting cell and the microenvironment.[99,100,107]

The most well-known subtypes are CD8+ cytotoxic T cells, CD4+ helper T cells, and regulatory T cells. Cytotoxic T cells recognize antigens from the MHC class I receptors on the target cells and use cytotoxic granules to directly kill the infected or malignant cells. T helper cells can differentiate into many different subtypes with unique functions. Th1, Th2, Th9, Th17, Th22, and follicular Th cells are the most well-known.[99,100,107] Each Th subtype expresses unique cytokines and has unique functions. Th1 expresses IL-12, IL-2, interferon gamma, and TNF and functions to enhance antiviral immunity, activates the bactericidal activity of macrophages, and stimulates B cell antibody production. Th2 releases IL-4, IL-5, and IL-13 and functions to encourage B cell survival and production of IgE antibodies and stimulates eosinophils and mast cells. Th2 cells are mainly engaged in mounting responses against parasitic organisms but may also inadvertently cause inflammatory diseases such as asthma.[99,107] Th9 produces IL-9, IL-10, and IL-21 and is thought to be related to Th2 and thus also functions in parasitic immunity, but also has a role in anticancer immunity.[99,101] Th17 expresses IL-17, IL-21, IL-22, IL-25, and IL-26 and is associated with prolonged inflammatory responses such as with chronic infection or cancer.[99,107] Th22 produces IL-22 and is a tissue homing cell

that plays a role in wound healing and anti-inflammatory, antibacterial, and antiviral activities.[99,102] Follicular Th cells produce IL-4, IL-10, and IL-21 and function mainly in B cell isotype switching and differentiation of B cells to plasma cells for long-term immunity.[99] Regulatory T cells (**Tregs**) are another subset of T cells that produce TGF-β, IL-10, and cytotoxic T-lymphocyte associated protein 4 (**CTLA-4**) and function to suppress other immune cell responses, especially other T cells. When functioning properly, Tregs prevent inappropriate autoimmune diseases and help resolve immune reactions after an infection has been eliminated. Unfortunately, Tregs do not always function appropriately and can cause immune tolerance in diseases such as cancer.[99,100,105] After encountering an infection, activated T cells can also differentiate into long-lived memory T cells to help mount a more rapid response during reinfection.[99,100] T cells can differentiate into many different cell types, each capable of releasing unique cytokines and completing unique functions, which highlights the plasticity and heterogeneity of T-cells.

When entering the tumor microenvironment, T cells encounter a heterogeneous and variable combination of signals that cause T cell dysfunction, lead to impaired T cell activity, and prevent adequate clearance of tumor cells. Exhausted T cells lose proliferative capacity and reduce cytokine production. Dysfunctional T cells can also arise from improper stimulation, leading to anergic T cells that are unable to adequately eliminate tumor cells. Typically, T cell dysfunction is more significant in chronic infections and diseases such as cancer. The severity of dysfunction has been associated with the level of antigen stimulation as well as the duration of exposure to that

antigen.[103,104,106] A few well-known inhibitory receptors expressed by dysfunctional T

cells include PD-1, CTLA-4, Tim-3, LAG-3, and TIGIT. PD-1 and CTLA-4 act as targets for

the immune checkpoint inhibitors, which are currently the most influential inhibitory

receptors in oncology. T cell dysfunction severity is correlated with the quantity and

degree of inhibitory receptor expression. T cells with the greatest dysfunction also

express the greatest variety and quantity of inhibitory receptors.[104,106] However, if the

tumor microenvironment (**TME**) is not producing sufficient inhibitory ligands, then T cell

dysfunction may be ameliorated as both the receptor and ligands are required for

activation of the inhibitory pathways within T cells.[103,104,106] Interestingly, regulatory T

cells are important immunosuppressive cells within the TME and can lead to inhibition

of effector T cells through production of immunosuppressive molecules such as TGFβ

and IL10. Other important cell types within the TME that influence effector T cells have

been noted throughout this review, but include tumor associated macrophages (**TAMs**),

myeloid derived suppressor cells (**MDSCs**), cancer associated fibroblasts (**CAFs**),

adipocytes, and endothelial cells. A few of the most important immunosuppressive

molecules that can cause T cell dysfunction include IL10, IFN, IDO, adenosine, VEGF-A,

TGFβ, and IL35. [103,104,105] Importantly, because many different immunosuppressive

molecules can influence T cells, the manner of T cell dysfunction is quite heterogeneous.

B cells

    B cells are bone-marrow derived lymphocytes that are commonly known for

producing circulating antibodies. Antibodies are known for their nearly unlimited

capacity to adapt in response to novel antigens. This capacity is maintained through the

combinatorial rearrangement of the V, D, and J gene segments in the heavy chain and

the V and J gene segments in the light chain. These rearrangements can potentially yield

an estimated one quintillion unique antibodies. Although many B cells are produced

each day, not all B cells will become activated. Instead, B cells stay dormant until they

encounter a stimulatory antigen. Type I T-cell independent antigens such as

lipopolysaccharide (**LPS**) or unmethylated bacterial DNA (**CpG**) can stimulate B cells

through toll like receptors. Type II antigens such as polysaccharides engage the B cell

receptor and can induce an antigen specific immune response. Proteins are usually T cell

dependent and require helper CD4$^+$ T cells for full activation. In this process, B cells will

bind to a protein antigen, internalize the antigen-receptor complex, and process the

protein into small fragments presented on the MHC class II receptor. CD4$^+$ T Cells will

become activated after binding to this MHC Class II receptor and will stimulate B cell

cytokine release, proliferation, immunoglobulin production, and potentially isotype

switching. After activation, B cells differentiate into plasma cells, which are specialized

to produce significantly higher levels of immunoglobulins. In addition to antibody

production, B cells also function in antigen presentation and immune regulation. B cells

are important for CD4 T cell function and priming. B cells release cytokines that can

influence other cells of the immune system such as T cells, dendritic cells, and

macrophages. These cytokines can also influence the development of lymphoid tissue or

Peyer patches and can affect wound healing.[110,113]

As described above, B cells have many distinct roles, however, broadly, they can

be summarized into three main functions: antigen presentation, antibody production,

and immune regulation. B cells are not widely known for their antigen-presenting

capabilities but are in fact more sensitive to antigens than dendritic cells. This is due to

increased binding affinity between B cells and the target antigen. B cells also far

outnumber dendritic cells in the tumor microenvironment and may actually stimulate

$CD4^+$ T cells more significantly than dendritic cells inside the tumor. Confirming this

ability, B cells can internalize and express tumor specific antigens via MHC surface

receptors. However, many tumor environments have deficient antigen-presenting

machinery, suggesting that B cell antigen presentation may be impaired in these

environments.[111,113]

Antibody-producing B cells (plasma cells) were previously viewed as a strictly

beneficial cell that inhibits malignancy, however, new evidence suggests that infiltrating

plasma cells can cause a variable response that dependent on the cancer type. In

particular, isotype switching appears to have a major role in the phenotypic

characteristics of the plasma cell. [111,112,114] In some cancers, plasma cells switch to an

IgG^+ producing state, which is known to preferentially recruit cytotoxic T cells. These

plasma cells are more likely found in tumors with greater inflammation and are

generally associated with a more positive outcome. However, even this is not universally

true for all cancer types. For instance, in some hepatocellular carcinomas (**HCCs**), B cells

produce IgG4, which does not activate effector cells as aggressively and can interfere

with IgG1, which elicits a much stronger response. Thus, $IgG4^+$ B cells can produce

immune privilege within the tumor site. In these sites, macrophages can become

polarized to the immunosuppressive M2 phenotype and can enhance tumor

progression. Importantly, stimulation of IgG4 is the result of environmental cytokines and thus appears to be a response to the tumor microenvironment. IgA$^+$ plasma cells, on the other hand, are known to preferentially recruit regulatory T cells and secrete immunosuppressive markers such as IL-10 and PD-L1. IgA$^+$ plasma cells are usually associated with poorer prognosis and therapeutic resistance. The tumor microenvironment also activates B cell receptor (**BCR**) clones inconsistently, leading to decreased amplification of neo-antigen specific B cell clones and inconsistent humoral defense against the tumor cells and eventual immune escape.[111]

Another potential subpopulation of B cells that can influence the tumor microenvironment is regulatory B cells (**Bregs**). Most Bregs have immunosuppressive capabilities that can reduce immune mediated cytotoxicity against tumor cells, however, some Bregs can also become immunostimulatory in some cases. At this time, Bregs do not appear to have a single defining set of surface receptors, but do appear to consistently express IL-10 and sometimes express PD-L1.[109,112] Thus, the Breg population is heterogeneous, but utilizes a similar mechanism to elicit immunosuppression. Bregs can also produce other immunomodulatory effectors such as TNF-α, lymphotoxin, signal transducer and activator of transcription 3 (**STAT3**), CD49b, CD73, and erbin.[112] However, these effectors are usually not expressed uniformly, further increasing the complexity of the Breg population. Additionally, a B-cell response that may sometimes appear like an immunosuppressive effect initially, such as the inhibition of a T cell response, can sometimes lead to a more durable antitumor response. This occurs when Bregs prevent the overactivation and apoptosis of anti-tumor T cells.[111] Like many cell

responses, the environment in which the cell is acting dictates whether the cell is behaving beneficially or detrimentally. Most cellular responses have an appropriate function in a healthy environment but may have a negative effect in the context of the tumor microenvironment.

Platelets

Platelets are terminally differentiated anucleated cell fragments produced from large megakaryocytes. Platelets perform critical functions in hemostasis, thrombosis, and wound healing. Platelets assist in maintaining vascular integrity by quickly adhering to sites of injury and by secreting granules to recruit additional circulating platelets to form a dense clot. The most prominent activators of platelets are thrombin, ADP, von Willenbrand factor (**vWF**), and collagen. Platelets contain three types of granules. Dense granules contain over 200 small molecules including calcium, adenosine triphosphate (**ATP**), adenosine diphosphate (**ADP**), serotonin, and epinephrine. Alpha granules release larger molecules such as P-selectin, fibrinogen, VWF, EGF, VEGF, and PDGF. These molecules function in cell adhesion, coagulation, inflammation, proliferation, and immune activation. Lysosomal granules contain enzymes such as cathepsins, elastases, collagenases, and glucosidases that degrade debris, which is important for the repair and remodeling of the vasculature. Platelets can also produce bioactive lipids through cyclooxygenase-1 (**COX-1**) and 12-lipoxygenase (**12-LOX**), which activate other platelets and influence other stromal cells.[116,117]

Tumors are sometimes described as wounds that never heal. which suggests that platelets may have a significant impact on tumorigenesis. Indeed, platelets affect many different aspects of tumorigenesis including tumor growth, angiogenesis, and metastasis. In response to signals from the tumor microenvironment, the platelet proteome is significantly altered relative to platelets from healthy patients, highlighting the reciprocal influence of the tumor microenvironment. It is well documented that cancer patients have increased thrombotic risk, which is caused by platelet activation by cancer cells. This phenomenon, known as tumor-cell induced platelet aggregation, occurs because tumors can express many of the same activating factors expressed by platelets, including thrombin, ADP, tissue factor, and vWF. As depicted above, activation of platelets in response to injury releases granules, which function to further stimulate and recruit platelets and to stimulate wound healing. Wound healing includes both tissue repair and vascular repair. Thus, granules released from platelets stimulate tissue growth and angiogenesis. In a tumor, these mechanisms are commandeered to stimulate tumor cell proliferation and to overstimulate angiogenesis. α-granules containing TGF-β, VEGF, and PDGF are the most important stimulators of tumorigenesis and angiogenesis. Additionally, platelets can further destabilize the inflammatory environment of tumors through the release of chemokines and interleukins such as CXCL1, CXCL4, CXCL5, CXCL7, CXCL12, and IL8. Platelets can also directly suppress the immune system through secretion of TGF-β. Platelets also have a major role in metastasis. The platelet's lysosomal granules contain degrading enzymes like MMPs, which can help degrade the ECM and can encourage metastatic spread. Platelets can

also mediate cancer-endothelial interactions to encourage cancer cell extravasation.

After extravasation, platelets can form barriers around circulating tumor cells,

protecting them from sheer stress and from the immune system. Activated platelets

also help form pre-metastatic niches through granule release, increasing the chances of

successful metastatic seeding.[115,117]

Adipocytes

Adipose tissue functions primarily to store energy from excess caloric intake. In

periods of abundance, energy is stored as high energy lipids that can undergo lipolysis in

periods of scarcity to provide energy for critical organ function. In contrast to white

adipose tissue, which is the primary high energy storage vehicle, brown adipose tissue

regulates thermogenesis through lipid oxidation. Brown adipose tissue appears darker

because of high concentrations of mitochondria: the oxidative machinery responsible

for thermogenesis. Adipose tissue regulates energy homeostasis through the release of

adipokines. One of most studied adipokines is leptin, which is released during food

uptake and can suppress apatite and promote lipid oxidation. Adiponectin is another

important adipokine that functions to stimulate lipid oxidation, inhibit inflammation,

and reduce diabetes risk and obesity. Resistin, on the other hand, reduces glucose

tolerance and insulin activity. Omentin enhances the insulin response and reduces blood

glucose. Interestingly, adipose tissue can be heterogeneous depending on the tissue

location. Heterogeneous adipose tissue varies based on proliferation potential,

adipokine and cytokine release, and response to external stimulation.[119,120]

It is well documented that obesity can increase the risk of acquiring some types of cancer. In obese patients, adipose tissue is usually in a state of mild inflammation, which is characterized by excessive release of adipokines and cytokines. These molecules can create an environment that is more receptive to cancer cells. Specifically, adipose tissue is known to be important in breast, prostate, colon, and ovarian cancers. Additionally, the risk of estrogen-dependent cancers such as endometrial or breast cancer increases because excessive adipose tissue converts androgens to estrogens. Adipocytes in close proximity to tumors can become influenced by the tumor microenvironment and are known as cancer-associated adipocytes (**CAA**). CAAs can influence tumor growth and metastasis through adipokine secretion. CAAs may share similarities to CAFs as they share a similar upstream mesenchymal lineage. CAAs also tend to be less mature, which can alter the phenotypic and secretory profile of the adipocyte. In some cancers such as breast cancer, adipocytes appear to play a larger role in the tumor microenvironment and overall tumorigenesis. Adipose tissue *in vitro* produces greater survival benefits than even fibroblasts for some breast cancer cell lines. Over time, adipose tissue near a growing tumor has been found to shrink and be replaced by fibroblast-like cells, which suggests that mature adipocytes are converting to immature preadipocytes. This conversion can lead to increased expression of cytokines such as IL-6 and plasminogen activator inhibitor-1 (**PAI-1**), factors such as TGF-β and TNF-α, and matrix metalloproteinases (**MMPs**). CAAs can also influence the ECM of the TME through the secretion of collagen VI, which has been shown to increase the

survival of breast cancer cells. In all, CAAs can influence proliferation, metastasis, immune function, angiogenesis, and the ECM.[118,120]

Tumor cell variability

Centuries of study have uncovered many advantageous characteristics of cancer cells that make treatment notoriously difficult. The so-called hallmarks of cancer include characteristics such as induction of vascular networks, activation of metastatic capacity, replicative immortality, excessive proliferation, resistance to apoptosis, immune evasion, and genomic instability. Additionally, newer characteristics are being evaluated such as phenotypic plasticity, epigenetic reprograming, induction of senescence, and alteration of microbiomes. Importantly, these cancer hallmarks can be thought of as milestones necessary for a tumor to progress from a single cell to an aggressive metastatic disease.[122,123,127] Immortality, unyielding proliferation, and resistance to apoptosis are necessary to form microtumors as cell proliferation must exceed cell death to sustain tumor growth. Progression from microtumor to tumor requires access to the vasculature to achieve the necessary nutrient and oxygen capacity to sustain growth. Then, after the tumor has reached maximal capacity, metastasis is necessary to maintain growth. Additionally, inhibition of the immune system is necessary to prevent tumor regression and to allow access to the circulatory system. From a clinical viewpoint, these characteristics are gained sequentially, which explains why a stage-based treatment approach is usually used. However, linear gain of function mutations in this fashion are unlikely.

While each cancer hallmark is undeniably important in describing the development and progression of the oncologic disease state, phenotypic plasticity, epigenetic reprogramming, and genetic instability are the fundamental causes of treatment failure.[123,124,127] If a cancer cell were merely a genetically stable mutant with the gain of function characteristics listed above, an effective treatment could be achieved easily. Or said differently, the adaptability of cancer is its most dangerous attribute. To add context, Werner, et al. (2018) found an average of 1.14 mutations per division during normal hematopoiesis and a 4-to-100-fold increase in mutations per division from colorectal, lung, and renal cancers.[121] The combination of increased mutational capacity with excessive proliferation provides cancer cells with a massive competitive advantage relative to healthy cells. Each cancer hallmark alone would produce an easily treatable disease with the exception of an excessively adaptable cell. Excessively adaptable cells can quickly gain each of the other cancer hallmarks. Indeed, it is well established that genetic mutation is the direct cause of oncologic disease with a simple point mutation being sufficient to cause excessive proliferation.[124,130,131] However, while a single hallmark is not concerning alone, they can exponentially increase cancer adaptability. Any hallmark that prolongs cell survival allows mutational activity to build within a single cell, creating a more aggressive cell over time as demonstrated in **figure 1**.[121,124] **Figure 1** arranges cancer types in ascending order based on the mutation frequency and neoantigen load of the cancer. As can be expected, cancers that arise from excessive carcinogenic exposure such as melanoma from sunlight, lung and bladder cancers from smoking, or stomach, esophageal or colorectal

cancers from ingesting carcinogens led to a higher mutation frequency and a higher

neoantigen load. These cancers also tend to be more aggressive with rapid growth and

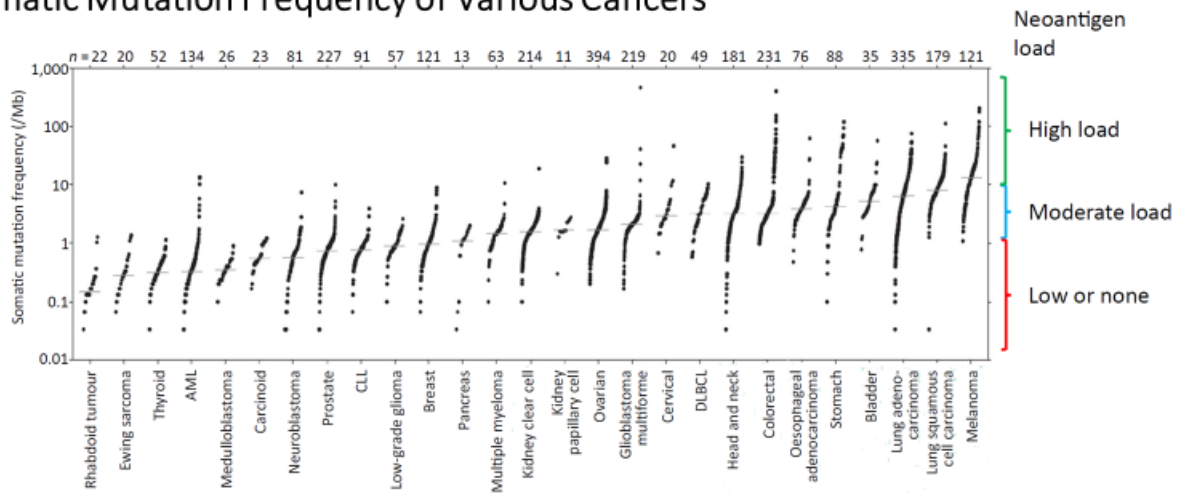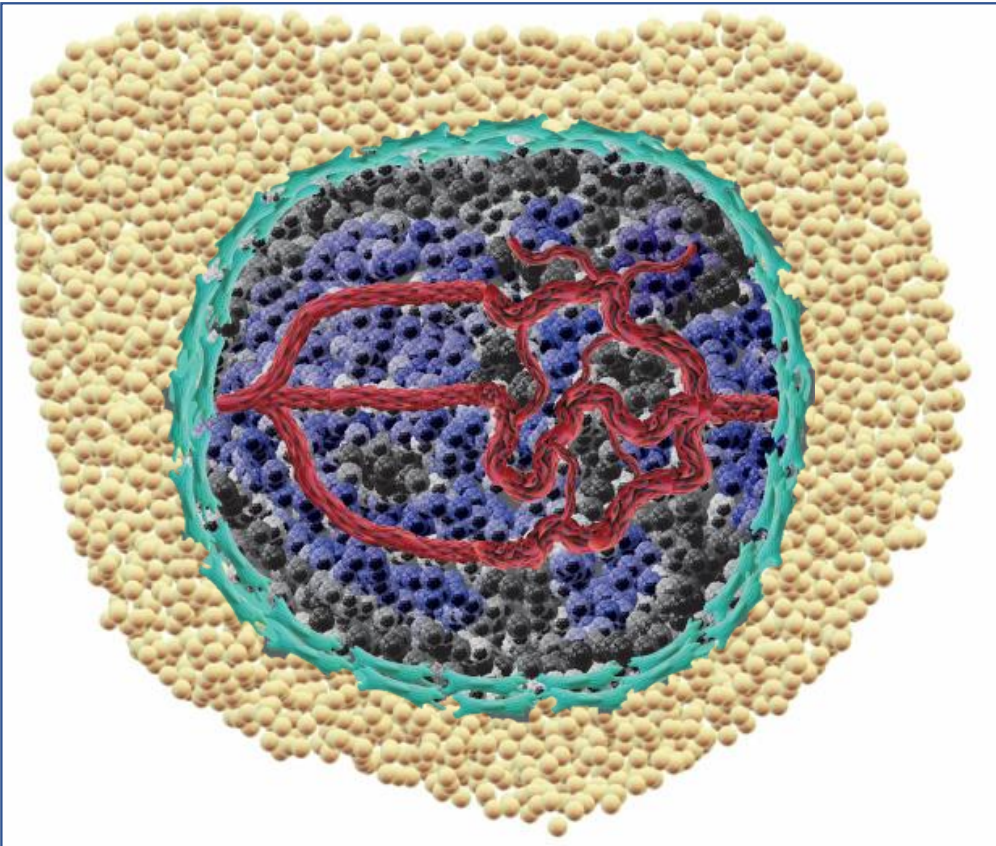rapid metastatic spread and have poorer survival statistics.

Figure 1. Demonstrates the somatic mutation frequency of multiple cancer types. Cancer types are arranged based on their mean mutation frequency from left to right. The number of samples included in the analysis are shown on the top of the graph. The anticipated neoantigen load is also included on the right side of the graph.[121]

In conjunction with genomic instability, phenotypic plasticity and epigenetic reprogramming provide cancer cells with greater flexibility to adapt to a heterogeneous environment. Phenotypic plasticity and epigenetic reprogramming let cancer cells adapt without requiring genomic mutations and thus allow more rapid adaptation within the limits of the human genome. As described in painstaking detail above, the tumor microenvironment is extraordinarily complex. In summary, the vasculature of the tumor microenvironment is highly heterogeneous and uses many different mechanisms to access the body's blood supply. This can range from the typical large, tortuous, and leaky mother vessels to normal coerced vessels to vascular mimicry. Not only do these vessels respond heterogeneously to antiangiogenic therapy, but they also expose the surrounding cancer cells to varying nutrient, oxygen, and drug levels. The extracellular matrix of the tumor is also highly heterogeneous, which is a consequence of stromal cells and cancer cells releasing a heterogeneous combination of effector molecules. The physical barriers[10,12,24] of the tumor causes variable drug exposure, which protects sensitive cells long enough to develop protective mutations.[51] Stromal cell variability also creates unique microenvironments through combinatorial influences. For instance, a microenvironment created by platelets, T-cells, and macrophages will be different from a microenvironment created by natural killer cells, fibroblasts, and endothelial cells. Additionally, the heterogeneity of these stromal cells greatly increases the number of potential unique microenvironments. Complexity from each environmental factor within the tumor microenvironment overlaps and further delineates the tumor into smaller and smaller unique microenvironments. Each unique microenvironment within

the tumor could then theoretically have an optimal cancer mutant that would outcompete other cancer mutants in a Darwinian fashion.[44,45,46,47] Thus, the combination of a highly plastic and amorphous cancer cell with a highly heterogeneous microenvironment yields a tumor with significant phenotypic and genotypic heterogeneity. However, it is conceivable that constraints exist that prevent extremely fine heterogeneity. The degree of selective pressure necessary to encourage distinct mutant subclones is currently unknown. If multiple cells were needed to achieve a critical threshold in a ligand-receptor interaction in order to apply selective pressure to a cancer population, then the theoretical maximum heterogeneity of the population would be lower. Examples of these concepts are shown in **figure 2**, **figure 3a**, and **figure 3b**.

Figure 2. Influence of Vasculature Heterogeneity on Tumor Heterogeneity

Normal Vessel   Leaky Vessel

Cancer Cell   Hypoxic Cancer Cell   Oxygenated/Nutrient Rich Cell

Figure 3a. Influence of Stromal Cells on Tumor Heterogeneity

Red Blood	Platelet	Neutrophil	B Cell
Adipocyte	Macrophage	Dendritic Cell	T Cell
Natural Killer	Cancer Cell	Fibroblast	Prostate
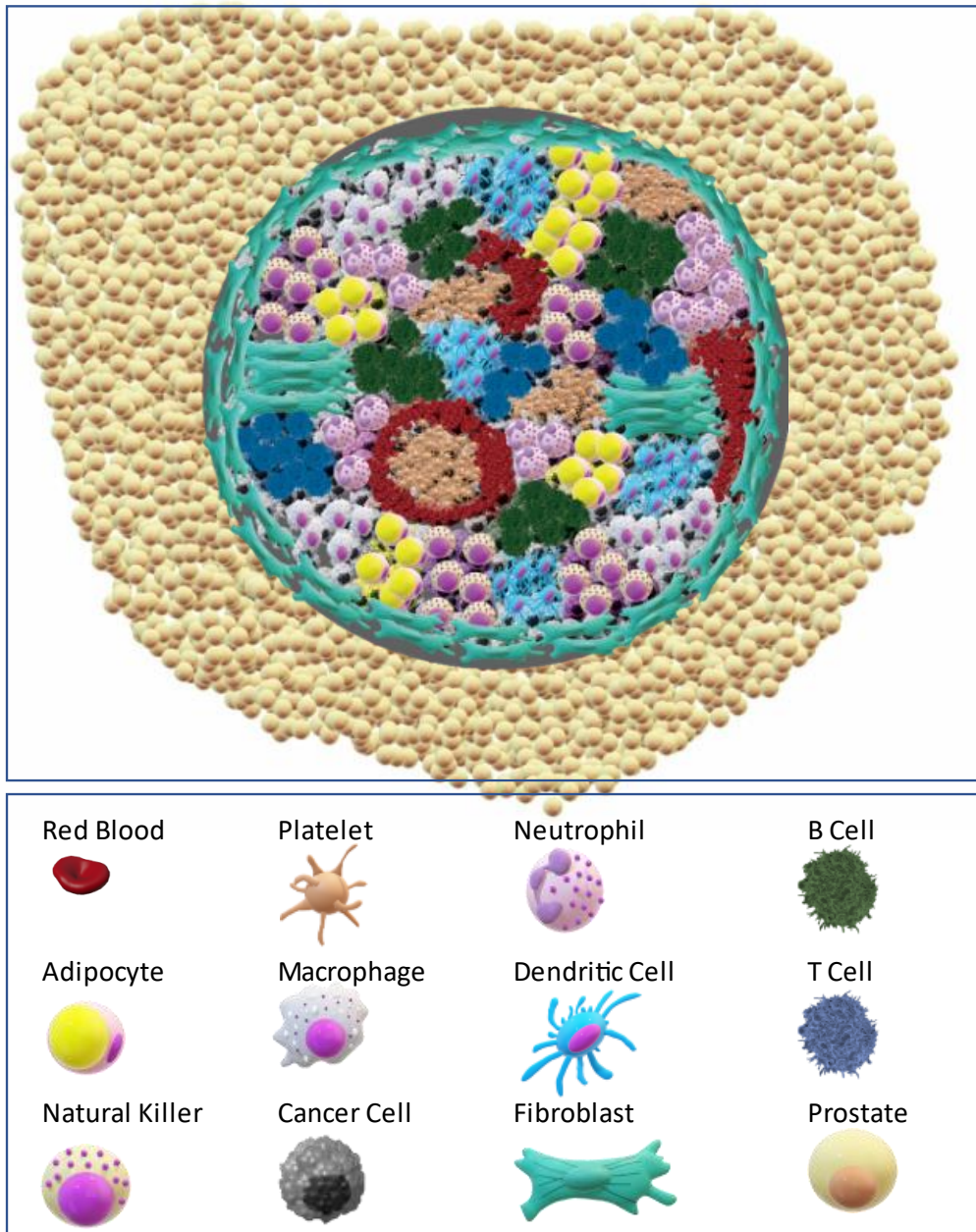
Figure 3b. Influence of Stromal Cells on Tumor Heterogeneity

Red Blood Cell   Platelet   Neutrophil   B Cell

Adipocyte   Macrophage   Dendritic Cell   T Cell

Natural Killer Cell   Cancer Cell   Fibroblast   Prostate
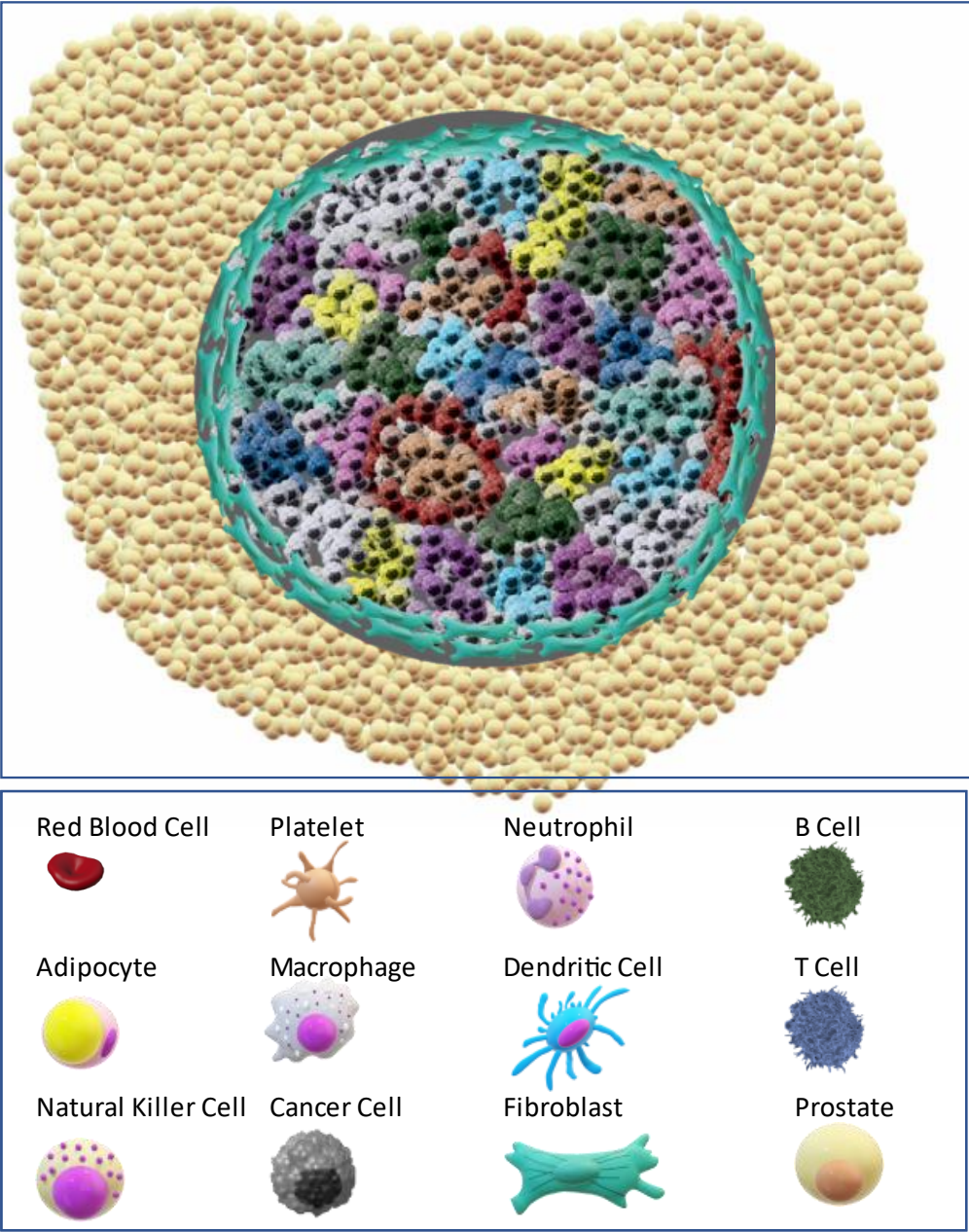
2.4. Tumor metastatic variability

The heterogeneous complexity of the cancer population is then increased exponentially when tumors begin to form at distant sites during metastatic spread.[122,125] The same Darwinian principles in combination with the unique microenvironments found at distant metastatic sites increase the theoretical maximum number of unique cancer subclones achievable within a single patient. The microenvironment of the lung is very different from the brain which is very different from the liver. These microenvironments contain specialized cells such as alveolar macrophages, microglia, and Kupffer cells that are unique to these microenvironments and would influence the cancer cell in a novel way. In essence, the theoretical maximum number of cancer subclones is directly proportional to the number of unique microenvironments accessible by the cancer cells.[48,49] This is illustrated in **figure 4**.

Figure 4. Influence of Metastatic Spread on Tumor Heterogeneity
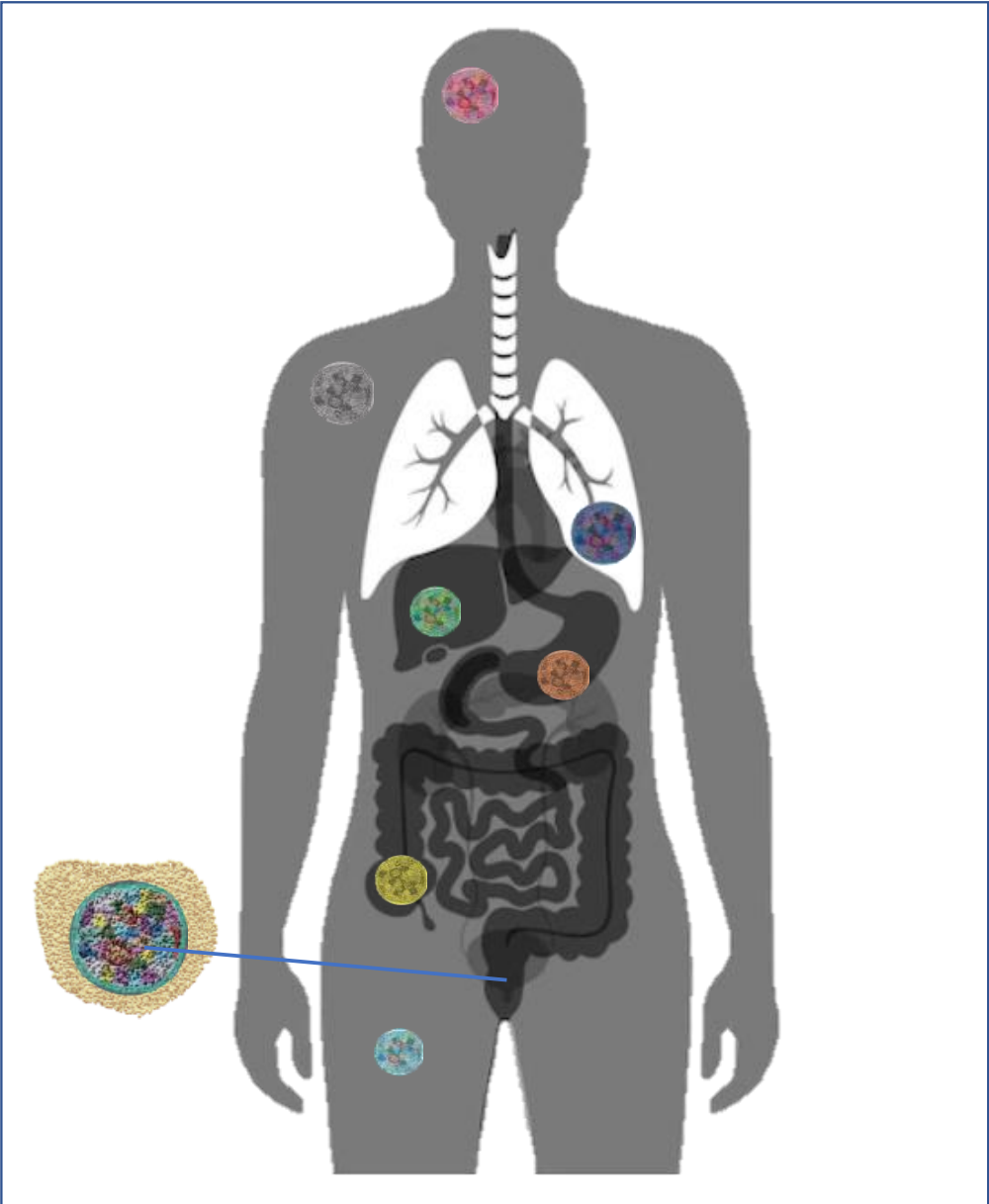
2.5. Fate of mutations and their impact on resistance

Cancer mutations do not flow in a specific direction to intentionally produce more effective cells, but instead occur randomly based on the inherent genetic instability of the cancer cell. Truthfully, this is not entirely true as mutations are more likely to occur in vulnerable regions of the genome. Thus, highly condensed and unused regions of DNA are less likely to be damaged and less condensed regions of DNA are more likely to be damaged. This will lead to some regional clustering of mutations in different tissues. Also, environmental factors may cause specific types of DNA damage to predominate within a specific tissue such as red meat, sunlight, or smoking. However, broadly it holds true that chance plays a role in generating cellular mutations. Each novel mutation can fall within a range between highly detrimental and highly beneficial outcomes. Although highly detrimental mutations can occur quite frequently, they will rarely be retained by the cancer population as the downstream impact of the mutation reduces the cell's competitiveness, quickly eliminating the mutation. It's important to highlight that because many harmful mutations may lead to cell death, the overall mutation rate of a given population may be understated based on comparisons between population genomes. This is because only neutral or beneficial mutations will be retained. A mutation that is highly beneficial will most likely spread throughout the cancer population as it allows cells possessing the mutation to outcompete wild-type cells. This would only hold true, however, if the trait is beneficial in each specific microenvironment within the tumor. The degree of benefit affects the rate of uptake by the tumor population. Neutral mutations would most likely only take hold in a growing

tumor in a cell population simultaneously expressing a beneficial mutation. It would be unlikely for a neutral mutation to grow market share within a tumor as it does not make a cell more fit. Neutral mutations, however, may impact resistance as mutations are only neutral in the context of the current tumor microenvironment and may provide benefit when exposed to novel selective pressure. To illustrate these ideas, I designed a computer program to simulate a tumor population experiencing a novel mutation. This simulation uses an assumed cell turnover or death rate of 0.153846, which has been estimated as a reasonable ratio for a confined tumor, however, this is not intended to be used for clinical estimates as the turnover ratio is most likely highly tumor specific.[128,129] The purpose of these figures is to provide context for how rapidly a mutation can take hold based on its growth benefits and based on the selective pressure experienced by the wild-type cells.

Methods: The simulation is based on an initial 100,000 cell microtumor, which would equate to a roughly 770μm^3 cube of PC3 cells based on an average diameter of 16.6μm.[126] This is similar to the size of 3D spheroids which have a diameter of roughly 1000μm. For the purpose of the simulation, the tumor was assumed to have no net growth, which is more appropriate to assess Darwinian competition as it more accurately simulates a scarce microenvironment. Each simulation includes parameters for growth rate and death rate, which are used to calculate a probability of death and a probability of growth for a single cell. The full microtumor is assumed to undergo a daily cell turnover of approximately 15384 cells from cited turnover rate above. Death is assumed to occur randomly and not catastrophically, meaning death occurs at an

individual cell level. The specific type of cell (wild or mutant) that dies is selected based on probabilities from the parameters discussed above. Then, the replacement cell is also selected based on probabilities from each populations' growth rate. This occurs for each of the 15385 cells on a daily basis for 1000 days. If a cell population reaches 0, then the simulation is ended. Each simulation is executed 10 times and the number of "successes" (when a mutant overtakes the population) and "failures" (when a mutant dies out) is displayed. The overall run time is approximately 10 minutes for 10 simulations. Although 10 simulations may not produce the most accurate mean, the overall trend should provide an interesting perspective. For context, a 10-simulation run of a 10% positive mutation produced 1 success and a 100-simulation run produced 12 successes. Additionally, a graph representing the overall curve is shown for a successful run and for the average of 10 runs. The individual population characteristics are adjusted, and these parameters are listed for each simulation. A copy of the code used in the simulations is provided as an appendix.

The first 4 simulations (**Fig. 5. a-d**) shown below assess the growth trajectory and success frequency of a novel positive mutation that impacts the growth rate of a cell. As the benefit of the mutation increases, the probability that the mutation will eventually dominate the population increases. Additionally, the time to success decreases as the benefit of the mutation increases (~900 days, 10% vs ~140 days, 100%). This can occur with mutation benefits even as low as 10%. However, interestingly, a novel positive mutation does not guarantee that the mutation will overtake the wild population. Instead, the incumbent population has probability benefits due to the sheer magnitude

of the population difference. Even positive mutations can die out due to random chance. Overall, this may not change what will eventually occur for a cancer population as the reasons for the mutation may be consistent such as transcription leading to a more vulnerable section of the genome. Instead, it may simply require additional time for the mutation to be repeated with genomic stability and proliferation rate also playing a role. I.e. eventually someone will hit the lottery, given enough tickets sold. Although not shown, a 100 simulation of 1000 total cells (to decrease runtime) with a novel neutral mutation led to a single successful run, indicating that random chance can even lead to additional diversity that isn't strictly Darwinian. This can become problematic as neutral mutations are only relatively neutral based on the selective pressure of the environment. Lastly, a 10000-simulation run of 1000 total cells with a novel negative mutation (-10%) was conducted which resulted in zero successes. The next two simulations (e-f) assess for the growth trajectory, success frequency, and time to success of an inherent mutation that provides some growth benefit. A 1% cell population or 1000 cells were used to simulate an inherent population. The time to success is decreased from ~900 days to ~550 days for the 10% positive mutation and from ~500 to ~320 for the 20% positive mutation. More important was the probability of success, which increased drastically from 10% to 100% success for the 10% positive mutation and from 30% to 100% success for the 20% positive mutation. This indicates that the most significant hurdle for a novel mutation was the first few days in which the population was being established. After the population reached a critical threshold, the chances of a failing mutation were significantly reduced. This was the least likely

scenario encountered in an unchanging microenvironment because an inherent

population was not likely to remain at 1% for a long time according to the simulations,

however, it does provide context for what might occur when exposing a tumor with

inherent resistance to a drug that turns a neutral mutation to a positive mutation.

Essentially, it's almost a certainty that the mutation will overtake the population.

Figure 5a.

Wild Type vs Novel Mutant with Positive Mutation Increasing Growth by 10%
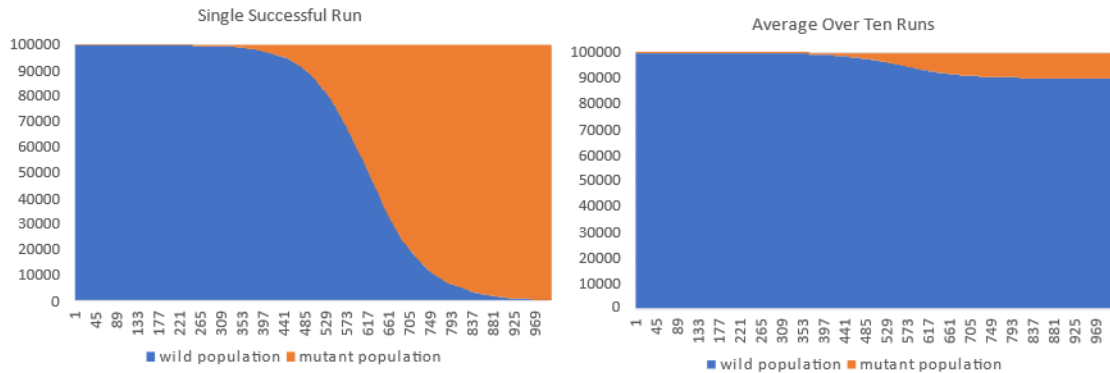
- Number of Runs: 10
- Death rate: 0.153846 Wild starting pop: 99999 Wild replication rate: 1 Wild death adj: 1
- Mutant starting pop: 1 Mutant replication Rate: 1.1 Mutant death adj: 1
- Fails: 9   Successes: 1

Figure 5b.

Wild Type vs Novel Mutant with Positive Mutation Increasing Growth by 20%

- Number of Runs: 10
- Death rate: 0.153846 Wild starting pop: 99999 Wild replication rate: 1 Wild death adj: 1
- Mutant starting pop: 1 Mutant replication Rate: 1.2 Mutant death adj: 1
- Fails: 7   Successes: 3

Figure 5c.

Wild Type vs Novel Mutant with Positive Mutation Increasing Growth by 50%
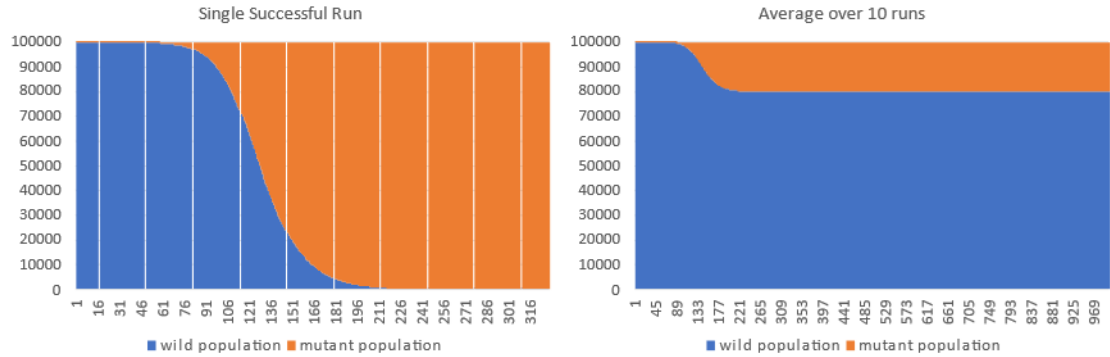
- Number of Runs: 10
- Death rate: 0.153846 Wild starting pop: 99999 Wild replication rate: 1 Wild death adj: 1
- Mutant starting pop: 1 Mutant replication Rate: 1.5 Mutant death adj: 1
- Fails: 8   Successes: 2

Figure 5d.

Wild Type vs Novel Mutant with Positive Mutation Increasing Growth by 100%
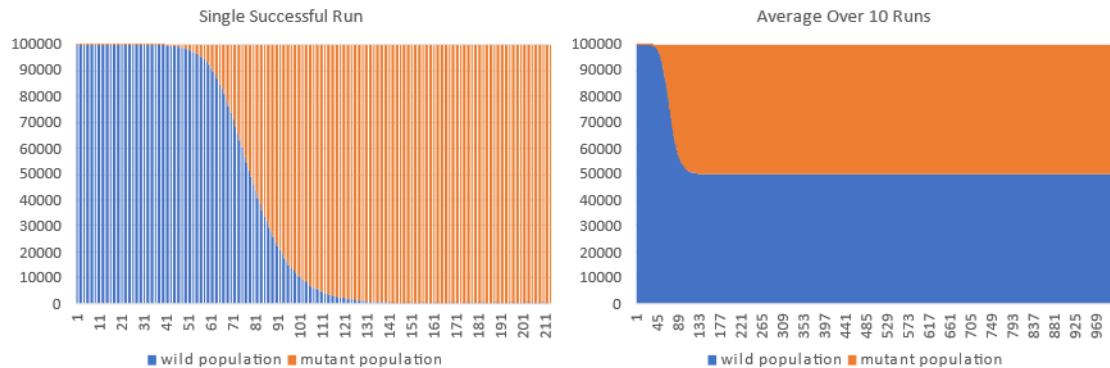
- Number of Runs: 10
- Death rate: 0.153846 Wild starting pop: 99999 Wild replication rate: 1 Wild death adj: 1
- Mutant starting pop: 1 Mutant replication Rate: 2 Mutant death adj: 1
- Fails: 5   Successes: 5

Figure 5e.

Wild Type vs Inherent Mutant (1%) with Positive Mutation Increasing Growth by 10%

- Number of Runs: 10
- Death rate: 0.153846 Wild starting pop: 99000 Wild replication rate: 1 Wild death adj: 1
- Mutant starting pop: 1000 Mutant replication Rate: 1.1 Mutant death adj: 1
- Fails: 0   Successes: 10

Figure 5f.
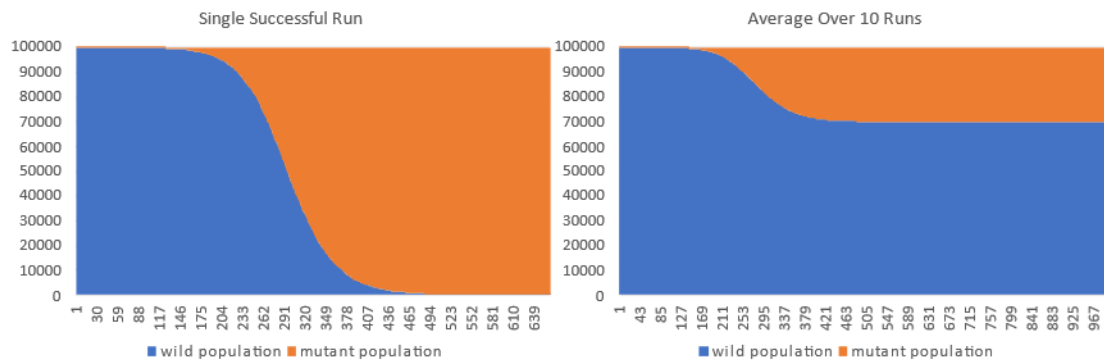
Wild Type vs Inherent Mutant (1%) with Positive Mutation Increasing Growth by 20%

- Number of Runs: 10
- Death rate: 0.153846 Wild starting pop: 99000 Wild replication rate: 1 Wild death adj: 1
- Mutant starting pop: 1000 Mutant replication Rate: 1.2 Mutant death adj: 1
- Fails: 0   Successes: 10

The next 4 simulations (**figure 5 g-j**) assesses how a cytotoxic and cytostatic

agent affects the growth trajectory, success frequency, and time to success of a 10%

beneficial unsusceptible mutant. The success frequency increased from 10% to 50% and

the time to success decreased from ~900 days to ~80 days after exposure to a cytotoxic

agent that increases the death rate of the wild population by 100% to 0.307692 (**figure 5**

g). The success frequency increased from 10% to 100% and the time to success

decreased from ~900 days to ~110 days after exposure to a cytostatic agent that

decreases the growth of the wild population by 50% (**figure 5 i**). Additionally, as

expected, an inherent population greatly increased the success frequency and

decreased the time to success for both a cytotoxic and cytostatic agent (**figure 5 h, j**).

Though not shown, for a susceptible mutant with a 10% positive benefit exposed to a

cytotoxic agent, the time to success decreased from ~900 days to ~420 days for a novel

mutation and from ~500 days to ~280 days for an inherent mutation. The probability of

success increased from ~10% to ~30% for a novel mutation and was unchanged for an

inherent mutation (100%). An important assumption was made that the increase in

growth rate for these cells did not subsequently increase susceptibility to the agent. The

major take away from these simulations is that the addition of an oncologic drug that

alters the selective pressure of the microenvironment and weakens the wild population

will significantly increase the probability and decrease the time for a novel or inherently

unsusceptible mutant to overtake the population. Exposure to a chemotherapeutic also

decreased the time to success of susceptible novel mutants. This indicated that

exposure to a chemotherapeutic resulted in more rapid cell turnover and was likely to lead to a more aggressive phenotype more quickly than would occur naturally.

These simulations also provide some perspective on how rapidly a mutation can become the dominant phenotype of the cancer population. Due to the doubling time, a single cancer cell can quickly repopulate the tumor. While this phenomenon is helpful during fetal development and wound healing, it makes treating oncologic diseases extremely difficult. Even when competing against the larger wild type cell line, a novel mutant can overtake the tumor in a matter of months, depending on the context. Using some simple math and assuming an uninterupted series of doublings, a tightly spaced tumor (1 μm^3) could be created by a single cell in 6 days, a 1 mm^3 tumor in 26 days, a 1 cm^3 tumor in 36 days, and a 10 cm^3 tumor in 46 days. Even if a patient were given a blockbuster drug that lead to a 99.9999999% kill rate and left a single cell alive out of billions, that single cell has the potential to repopulate the tumor within months.

Figure 5g.

Wild Type vs Unsusceptible Novel Mutant with Positive Mutation Increasing Growth by 10% after exposure to a Cytotoxic Agent (100%)

- Number of Runs: 10
- Death rate: 0.153846 Wild starting pop: 99999 Wild replication rate: 1 Wild death adj: 2
- Mutant starting pop: 1 Mutant replication Rate: 1.1 Mutant death adj: 1
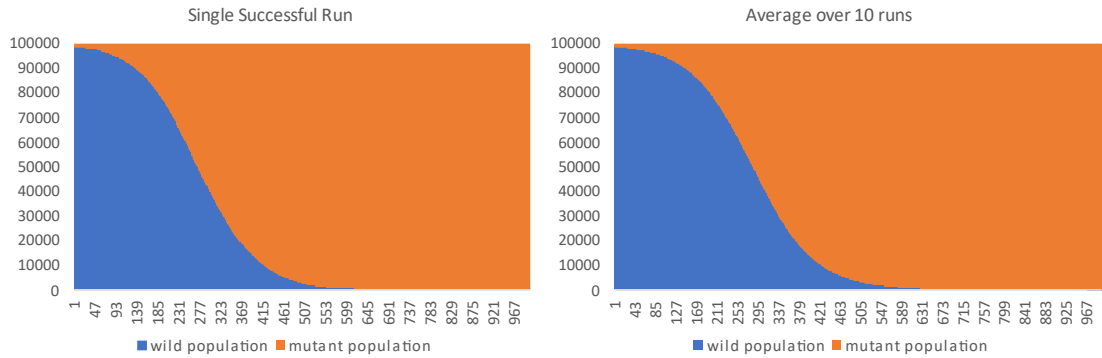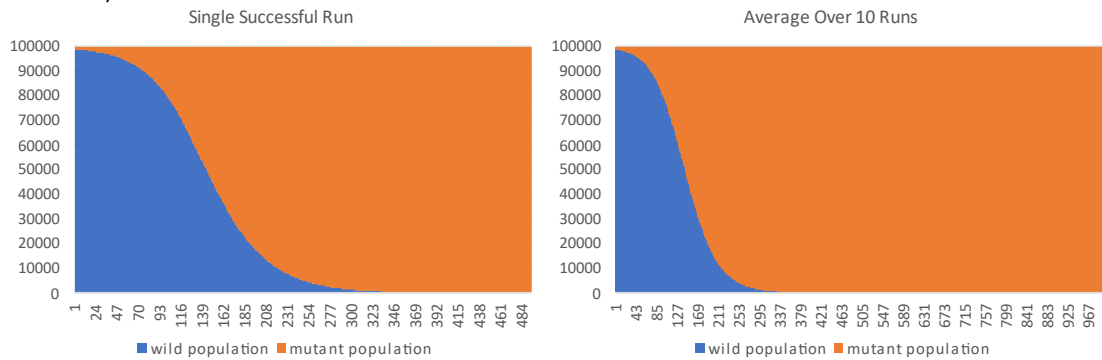- Fails: 5   Successes: 5

Figure 5h.

Wild Type vs Unsusceptible Inherent(1%) Mutant with Positive Mutation Increasing Growth by 10% after exposure to a Cytotoxic Agent (100%)
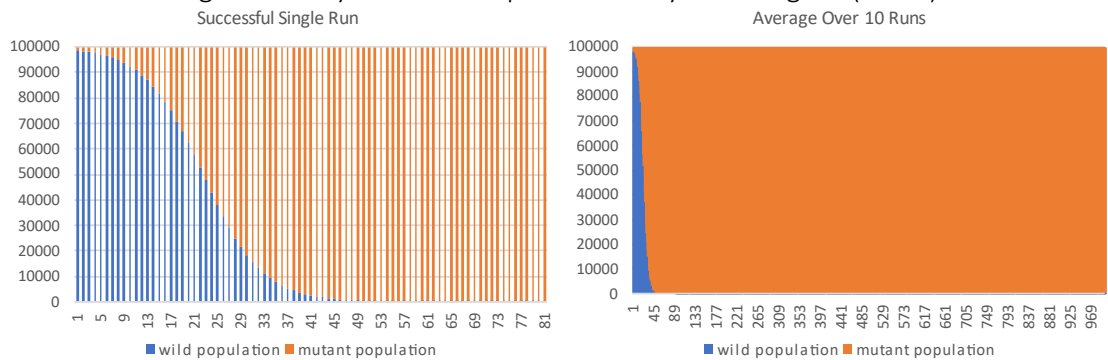
- Number of Runs: 10
- Death rate: 0.153846 Wild starting pop: 99000 Wild replication rate: 1 Wild death adj: 2
- Mutant starting pop: 1000 Mutant replication Rate: 1.1 Mutant death adj: 1
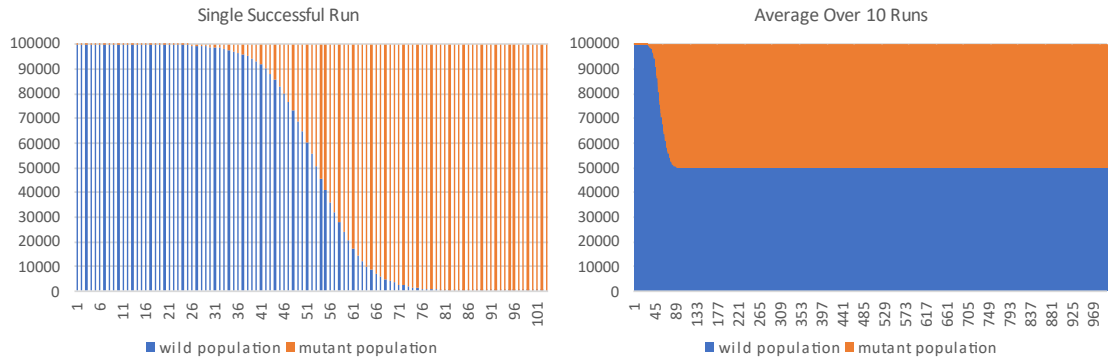- Fails: 0   Successes: 10

Figure 5i.

Wild Type vs Unsusceptible Novel Mutant with Positive Mutation Increasing Growth by 10% after exposure to a Cytostatic Agent (50%)

Successful Single Run — Average Over 10 Runs
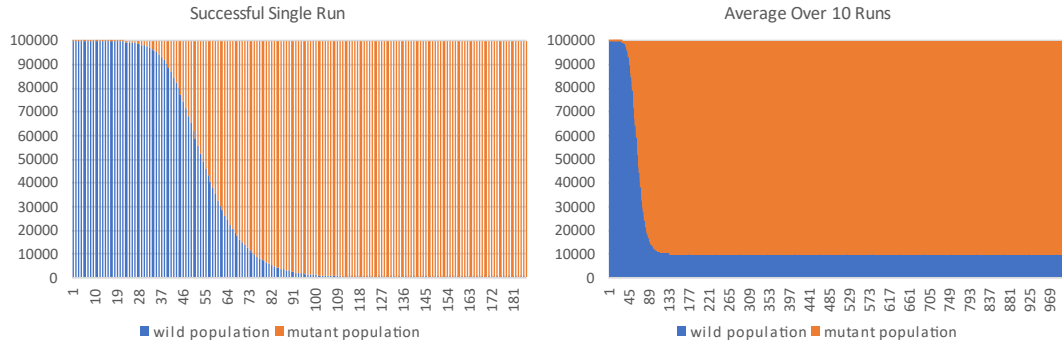
- Number of Runs: 10
- Death rate: 0.153846 Wild starting pop: 99999 Wild replication rate: 0.5 Wild death adj: 1
- Mutant starting pop: 1 Mutant replication Rate: 1.1 Mutant death adj: 1
- Fails: 1   Successes: 9

Figure 5j.

Wild Type vs Unsusceptible Inherent Mutant(1%) with Positive Mutation Increasing Growth by 10% after exposure to a Cytostatic Agent (50%)

Single Successful Run — Chart Title
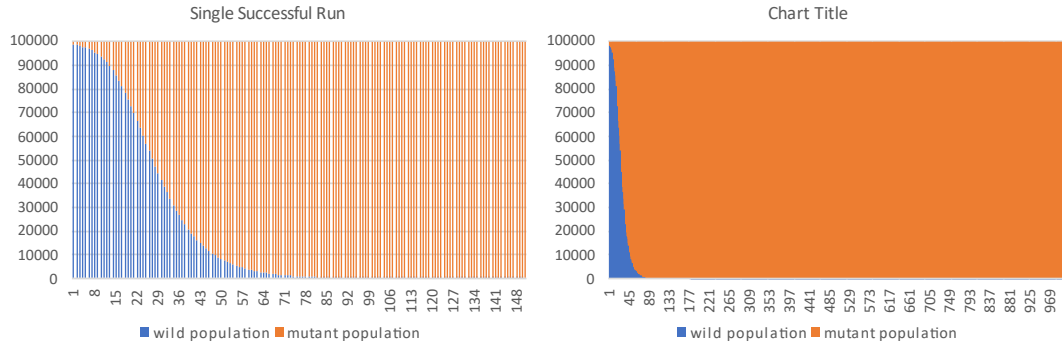
- Number of Runs: 10
- Death rate: 0.153846 Wild starting pop: 99000 Wild replication rate: 0.5 Wild death adj: 1
- Mutant starting pop: 1000 Mutant replication Rate: 1.1 Mutant death adj: 1
- Fails: 0   Successes: 10

3. **Summary - Bringing it all together**

Cancer cells are genetically unstable with some cancers producing 100-fold additional mutations per division. It's estimated that a 2 cm^3 tumor contains 2 x 10^9 cells. If 80% of a 2 cm^3 tumor are tumor cells, then there are approximately 1.6 x 10^9 cancer cells. After each of these cells replicates, 1.6 x 10^{11} mutations are possible. The diploid human genome is only 6.4 x 10^9 bases, meaning the entire genome could be mutated in a single replication cycle for a relatively small tumor without metastatic sites. As easy as this math sounds, the real-world scenario is much more complicated with senescent or dormant cells potentially contributing fewer mutations, with duplicate mutations reducing the total number of unique mutants, or with more complicated translocations impacting multiple genes simultaneously. It's important to understand that while beneficial mutations are extremely rare and while the probability of resistance may be 1 in 6.4 billion, or even higher for high barrier drugs requiring multiple simultaneous mutations, given sufficient time, the mutation frequency of a malignant cell combined with a large cell count significantly increases the odds in favor of cancer cells developing resistance. After reviewing the simulations, the time for a novel mutation to supplant the incumbent population is most likely relatively short and dependent on the degree of benefit as well as the selective pressure against the incumbent population. If an inherent population is present, this time decreases significantly. Additionally, the microenvironment of the tumor is segmented based on overlaying gradients produced from variability in the tumor vasculature, from variability in the extracellular matrix, and from variability in the number and types of stromal cells

present. Stromal cells are also highly heterogeneous, which increases the number of potential microenvironments exponentially. The addition of metastatic sites increases this number even further. As the diversity of microenvironments increases, due to Darwinian-based evolutionary principles, the diversity of the cancer population increases. Greater cancer diversity increases the probability that an inherently resistant cell is present prior to drug therapy. Drug therapy applies selective pressure to the cancer population and reveals this inherently resistant population, which quickly becomes the dominant phenotype and leads to therapeutic resistance within months of initiating therapy.

Based on the extraordinarily large pool of cancer cells, the diversity of the tumor microenvironment, and the variable drug exposure profile, it is almost certain that resistance is either present prior to therapy or will develop in protected compartments relatively rapidly. This is evident in the introductory statistics describing the clinical effects of ~200 clinical trials of targeted/biologic drugs as well as the effects of chemotherapeutic agents, which broadly improve overall survival by only a few months.

4. **Possible solutions**

One aspect that is hindering our ability to adequately deal with the cancer problem is our current drug development framework. Drug approval focuses on a single drug with a clear mechanism of action that has well-defined benefits and risks. This framework has worked well when designing drugs for ailments such as hypertension or diabetes because our cells are stable and generally respond as expected to therapy.

They work well when targeting pathogens with unique proteins that can be selectively targeted using high concentrations as toxicity is low and resistance can be prevented. However, the heterogeneity of the tumor and its complexity are not easily countered by a single drug mechanism with a narrow therapeutic index and low barrier to resistance. The mutational capacity of cancer cells even counters our immune system, which is far more complex and can target an almost infinite number of antigens. Thousands of drugs with unique drug targets to combat cancer have already been designed, yet every drug eventually fails, regardless of the drug target and regardless of the drug potency. One day we may finally discover cancer's Achille's heel and develop a drug with high potency, low toxicity, and minimal resistance, however, at the moment, that bar seems incredibly high.

Our current focus as investigators is identifying novel mechanisms using potency as the standard of success. An oncologic drug is selected when it successfully eliminates cancer cells or shrinks tumors. Yet, as we have seen, a drug that eliminates 80%, 90%, or 99% of cancer cells will still be unsuccessful over the long term. So, why is potency the drug characteristic that is desired? It is estimated that more than 90% of all cancer-related deaths occur due to drug resistance.[37] Cancer drug resistance can take many different forms. Cancer cells can develop specific mutations in gene sequences of target proteins, which can alter the binding affinity of the compound and lead to reduced potency. Malignant cells can also reduce the activity of a cancer agent by downregulating enzymes that are important for the activation of a prodrug-type molecule. Cancer cells can upregulate detoxifying enzymes such as glutathione

transferases or cytochrome P450 enzymes. Drugs can be subjected to extensive efflux through P-glycoprotein, multidrug resistance associated protein 1 (**MRP-1**), breast cancer resistance protein 1 (**BCRP-1**), or another transporter within the ATP binding cassette family. Although chemotherapeutic agents have many different mechanisms of action, most initiate cell death through apoptotic mechanisms. Cancer cells exhibit downregulation of proapoptotic molecules and upregulation of antiapoptotic molecules, which limits the overall efficacy of many chemotherapeutic agents. DNA damage is a major target for many oncologic medications. In response, many cancers can upregulate DNA repair enzymes to overcome stalled replication forks and prevent apoptotic signaling. Many targeted therapeutics inhibit upregulated growth receptor pathways to achieve selectivity. These pathways utilize a cascade of enzyme reactions to transmit external signals internally. Inhibition of these pathways can be mitigated through the production of a constitutively active enzyme downstream from the drug target. Also, the growth kinetics within tumors can be altered, which provides inherent resistance against chemotherapies that target rapidly dividing cells.[11,38,39] By illustrating the numerous potential mechanisms of resistance, it's easy to see that chemotherapeutics are at a significant disadvantage when treating malignant cells. Chemotherapeutics possess a single drug mechanism, but cancer cells employ many different mechanisms to nullify the therapeutic. Chemotherapeutics are also static, meaning their mechanism never changes, while malignant cells are dynamic and adapt constantly.

When viewed comprehensively, evidence from multiple clinical trials over the past century suggests that while a single mechanism can be quite potent initially, over

time, most therapies progressively lose potency. It's extremely likely that a drug will achieve its greatest response after the first dose and will progressively lose potency as the malignant cell population adjusts to the medication. Importantly, a comprehensive analysis on the ability of early tumor shrinkage (**ETS**), which is defined as a reduction of tumor size by at least 20-30% in the first 8 weeks, to predict overall survival in metastatic colorectal patients did not find a significant correlation (R=0.37; 95% CI – 0.31-0.78; P=0.28).[52] Additionally, while analysis on early tumor shrinkage in advanced non-small cell lung cancer (**NSCLC**)[53,54], advanced biliary tract cancer[55], and metastatic pancreatic cancer[56] demonstrate some separation in the survival curves (median survival difference of 10.93 months[53], 6 months[54], 4.9 month[55], and 3.2 months[56]) between patients with ETS and patients without ETS, the number of patients achieving cures did not significantly change. Instead, as depicted in **figure 6**,[53] the survival curve was merely shifted, representing a delay in survival outcomes rather than a cure. However, the long-term success of therapy is influenced by the resistance potential of the patient's tumor cells. The development of novel cytotoxic agents theoretically increases the number of potentially treatable (as opposed to curable) tumors, but the mutational threshold required for resistance impacts overall survival to a much higher degree. Therefore, based on decades of previous data and numerous prohibitive physical and biological mechanisms, the continued effort to focus on cytotoxic potency is likely to result in marginal improvements to patient survival as more influential drug characteristics are largely ignored during drug development.

Kaplan Meier curve demonstrating the effects of early tumor shrinkage
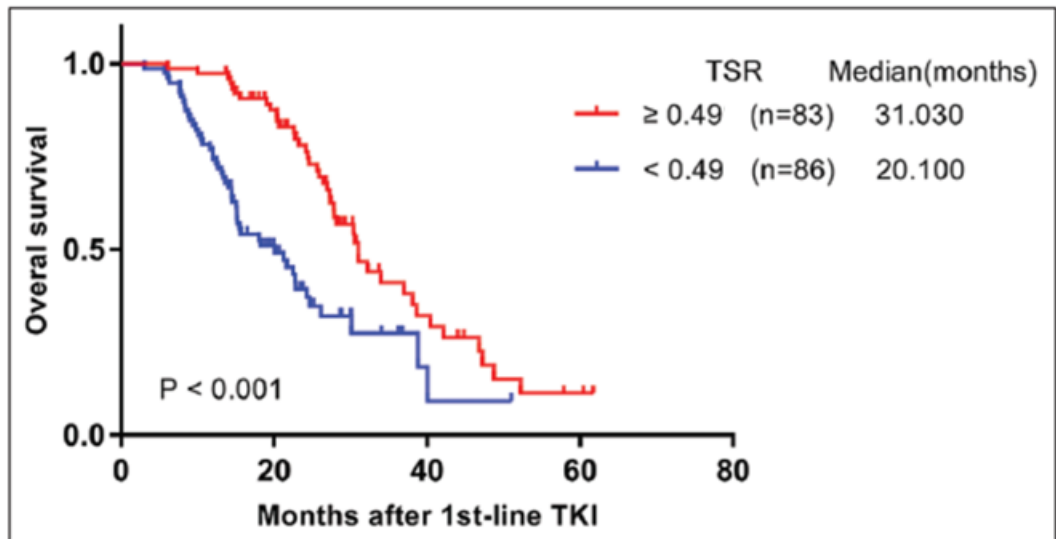
Figure 6: Kaplan Meier curve depicting overall survival in non-small cell lung cancer patients with (red) and without (blue) early tumor shrinkage.[53]

Although early tumor shrinkage is a mixed surrogate marker at best, most methods used to screen for novel chemotherapeutics rely on high throughput half maximal inhibitory concentration (**IC50**) assays. The drugs that show adequate potency are then fine-tuned through chemical approaches to ensure adequate pharmacokinetic properties at which time the drug will be tested using animal models of the target cancer type. If the drug shrinks the tumor and has adequate toxicity properties, it may be selected for further processing. Throughout the entire drug development process, we focus on short-term potency as a surrogate for clinical efficacy when most evidence suggests that long-term potency is a much more important factor in clinical outcomes. The most important property impacting clinical outcomes is the drug's barrier to resistance. Instead of screening for drugs utilizing short 72-hour IC50 assays, we have developed a long-term multi-week assay that utilizes successive IC50 data to assess how stable the drug's potency is over time. If drugs were selected based on potency stability over time, then drugs with higher barriers to resistance would be emphasized and the probability of resistance would be far lower. Many low potency drugs may be ignored in the current developmental process that have high barriers to resistance and have a higher therapeutic index. As an example, a drug that kills 60% of cancer cells after the first treatment, 20% after the second, and 5% after the third would have a progressively worse therapeutic index. Although this is undeniably true, it is rarely considered. However, a drug that stably kills 5% of cancer cells would have a stable therapeutic index and could be rationally combined with other agents and produce predictable

outcomes with predictable toxicity. Instead, the initial outcome of many of our current drugs is reasonably well estimated, but the subsequent doses are not.

Focusing on drug potency instead of drug resistance also limits our understanding of the potential resistance mechanisms for the novel therapeutic. If an antiangiogenic therapy could be inhibited using any one of a thousand different potential resistance pathways, then it might be more prudent to target another pathway. Quantifying the number of potential resistance mechanisms and quantifying the number of mutations required to achieve each mechanism could allow us to better predict the most likely pathway of drug resistance and could help us design drugs to counter this resistance to preserve drug efficacy. Even simply encountering drug resistance earlier in the drug development process could allow more rapid identification of possible pitfalls in the drug mechanism, reducing overall development costs.

Focusing on drug resistance also enables investigators to identify novel drug mechanisms that are not cytotoxic and should have much more advantageous toxicity profiles. As an example, research into the genetic stability of cancer cells may identify a druggable target that regulates DNA repair. Upon administration, the cancer cell could upregulate DNA repair enzymes, reduce the frequency of mutations, and improve genetic instability. Improved genetic instability would not only potentially delay drug resistance but may also reduce aggressiveness over time and improve the competitiveness of our immune system. This mechanism should have limited toxicity and may actually reduce cancer prevalence over time.

Another potential approach to limit the competitiveness of cancer cells could be targeting the diversity of the cancer population through population engineering. In this method, a novel gene could be introduced into the cancer population through a gene editing approach that targets a specific gene only found in the cancer population. This gene would provide cancer cells with a protective mechanism against a chemotherapeutic that would be given to the patient for a short period of time. Due to the selective pressure of the chemotherapeutic, the cells that incorporated the new genetic code would have a greater survival benefit and would quickly become the dominant phenotype within the cancer population. This would reduce genetic diversity. The new genetic code would also contain a second gene that would make these cells significantly more sensitive to a different chemotherapeutic. This should improve the treatment efficacy compared to treating a population of unknown diversity. Although these are just two examples of novel mechanisms that could be used to target cancer adaptability, many more could be identified if more focus were allocated to overcoming this challenge.

A different approach to combating the adaptability of cancer cells could be through the design of drug platforms instead of individual drugs. In this scenario, the drug platform would be designed in two separate parts. One section would be designated for identifying and targeting the cancer cell and the other would be designed as the payload. The drug platform could use a targeting mechanism such as novel DNA mutations or novel cancer antigens. The payload could be anything that has demonstrated efficacy in killing the cancer cells, and if designed properly, could be more

toxic than what is possible with a free drug. What would make this approach unique from targeted therapies such as nanoparticles or liposomes is the ability to adapt the drug platform based on individual cancer characteristics and the treatment changes that occur over time. Instead of relying on a human epidermal growth factor receptor 2 (**HER2**)-targeted liposome of doxorubicin, which quickly becomes ineffective as cancer cells stop producing HER2, the drug platform would be approved using a variable targeting approach. The patient's cancer would initially be screened for unique genetic mutations that are present in most of the population. The top 5 mutations could be chosen, and 5 separate targeting molecules could be made. Then, after the initial treatment, the tumor can be biopsied again and a new set of targeting molecules could be selected. In this way, the treatment can adapt as the cancer adapts, which may prolong treatment efficacy.

5. **Final Thoughts**

Cancer is an extraordinarily diverse disease with heterogeneity arising from the vasculature, extracellular matrix, stroma, and metastatic sites. Each of these factors converge into overlapping gradients that increase the complexity of the microenvironment. Microenvironment complexity in conjunction with an unstable cancer cell genome drives tumoral heterogeneity. Genomic instability and tumoral heterogeneity drastically reduce the probability that each cancer cell is sufficiently sensitive to an oncologic agent and increases the probability that a resistant mutant will emerge and become the dominate phenotype. Although significant time and effort is used to identify novel oncologic agents based on initial drug potency, initial drug

potency rarely predicts clinical outcomes. Instead, clinical outcomes are controlled by

drug resistance. To more effectively identify and design novel oncologic drug therapies,

more emphasis should be placed on selecting drugs with high barriers to resistance.

Additionally, more effort should be placed on developing novel methods to reduce

genetic instability as well as in designing more sophisticated treatment modalities

capable of countering cancer's adaptability.

References

1. Heron, M. (2019). Deaths: Leading causes for 2017. National Vital Statistics Reports, 68(6).

2. Hess, L. M., Brnabic, A., Mason, O., Lee, P., & Barker, S. (2019). Relationship between progression-free survival and overall survival in randomized clinical trials of targeted and biologic agents in oncology. Journal of Cancer, 10(16), 3717–3727. https://doi.org/10.7150/jca.32205

3. Houts, P. S., Lenhard, R. E., & Varricchio, C. (2000). ACS cancer facts and figures. Cancer Practice, 8(3), 105–108. https://doi.org/10.1046/j.1523-5394.2000.83001.x

4. Jonker, D. J., Maroun, J. A., & Kocha, W. (2000). Survival benefit of chemotherapy in metastatic colorectal cancer: A meta-analysis of randomized controlled trials. British Journal of Cancer, 82(11), 1789–1794. https://doi.org/10.1054/bjoc.1999.1254

5. Stewart, L. A. (2002). Chemotherapy in adult high-grade glioma: A systematic review and meta-analysis of individual patient data from 12 randomised trials. Lancet, 359(9311), 1011–1018. https://doi.org/10.1016/S0140-6736(02)08091-1

6. Oba, K., Yamamoto, S., Nakamura, K., Bang, Y. J., Bleiberg, H., Burzykowski, T., … Yamamura, Y. (2010). Role of chemotherapy for advanced/recurrent gastric cancer: An individual-patient-data meta-analysis. JAMA - Journal of the American Medical Association, 49(7), 1565–1577. https://doi.org/10.1016/j.ejca.2012.12.016

7. Cole, B. F., Gelber, R. D., & Aron Goldhirsch. (1995). A quality-adjusted survival meta-analysis of adjuvant chemotherapy for premenopausal breast cancer. Statistics in Medicine, 14(16), 1771–1784. https://doi.org/10.1002/sim.4780141606

8. Marino, P., Pampallona, S., Preatoni, A., Cantoni, A., & Invernizzi, F. (1994). Chemotherapy vs supportive care in advanced non-small-cell lung cancer: Results of a meta-analysis of the literature. Chest, 106(3), 861–865. https://doi.org/10.1378/chest.106.3.861

9. Sun, J., Wei, Q., Zhou, Y., Wang, J., Liu, Q., & Xu, H. (2017). A systematic analysis of FDA-approved anticancer drugs. BMC Systems Biology, 11(Suppl 5). https://doi.org/10.1186/s12918-017-0464-7

10. Chauhan, V. P., Stylianopoulos, T., Boucher, Y., & Jain, R. K. (2011). Delivery of Molecular and Nanoscale Medicine to Tumors: Transport Barriers and Strategies. Annual Review of Chemical and Biomolecular Engineering, 2(1), 281–298. https://doi.org/10.1146/annurev-chembioeng-061010-114300

11. Mansoori, B., Mohammadi, A., Davudian, S., Shirjang, S., & Baradaran, B. (2017). The different mechanisms of cancer drug resistance: A brief review. Advanced Pharmaceutical Bulletin, 7(3), 339–348. https://doi.org/10.15171/apb.2017.041

12. Kim, S. M., Faix, P. H., & Schnitzer, J. E. (2017). Overcoming key biological barriers to cancer drug delivery and efficacy. Journal of Controlled Release, 267(September), 15–30. https://doi.org/10.1016/j.jconrel.2017.09.016

13. Nagy, Janice., Husain, Amjad., Jaminet, S., Dvorak, A., Dvorak, H. (2016). Tumor Vasculature: Structure and Function. 1–9. Retrieved from https://radiologykey.com/knee-10/

14. Nagy, J. A., Chang, S. H., Dvorak, A. M., & Dvorak, H. F. (2009). Why are tumour blood vessels abnormal and why is it important to know? British Journal of Cancer, 100(6), 865–869. https://doi.org/10.1038/sj.bjc.6604929

15. Nagy, J. A., Chang, S. H., Shih, S. C., Dvorak, A. M., & Dvorak, H. F. (2010).

    Heterogeneity of the tumor vasculature. Seminars in Thrombosis and Hemostasis,

    36(3), 321–331. https://doi.org/10.1055/s-0030-1253454

16. Cai, Y., Zhang, J., Wu, J., & Li, Z. Y. (2015). Oxygen transport in a three-dimensional

    microvascular network incorporated with early tumour growth and preexisting

    vessel cooption: Numerical simulation study. BioMed Research International, 2015.

    https://doi.org/10.1155/2015/476964

17. Jang, S. H., Wientjes, M. G., Lu, D., & Au, J. L. S. (2003). Drug delivery and transport

    to solid tumors. Pharmaceutical Research, 20(9), 1337–1350.

    https://doi.org/10.1023/A:1025785505977

18. Oba, K., Yamamoto, S., Nakamura, K., Bang, Y. J., Bleiberg, H., Burzykowski, T., …

    Yamamura, Y. (2010). Role of chemotherapy for advanced/recurrent gastric cancer:

    An individual-patient-data meta-analysis. JAMA - Journal of the American Medical

    Association, 49(7), 1565–1577. https://doi.org/10.1016/j.ejca.2012.12.016

19. Warren BA.The vascular morphology of tumors Tumor Blood Circulation:

    Angiogenesis, Vascular Morphology and Blood Flow of Experimental and Human

    Tumors 1979CRC Press Inc.: Boca Raton, FL; 1–47.Peterson, H-I (ed) pp [Google

    Scholar]

20. Nagy, J. A., Feng, D., Vasile, E., Wong, W. H., Shih, S. C., Dvorak, A. M., & Dvorak, H.

    F. (2006). Permeability properties of tumor surrogate blood vessels induced by

    VEGF-A. Laboratory Investigation, 86(8), 767–780.

    https://doi.org/10.1038/labinvest.3700436

21. Pettersson, A., Nagy, J. A., Brown, L. F., Sundberg, C., Morgan, E., Jungles, S., … Dvorak, H. F. (2000). Heterogeneity of the angiogenic response induced in different normal adult tissues by vascular permeability factor/vascular endothelial growth factor. Laboratory Investigation, 80(1), 99–115. https://doi.org/10.1038/labinvest.3780013

22. Baish, J. W., Stylianopoulos, T., Lanning, R. M., Kamoun, W. S., Fukumura, D., Munn, L. L., & Jain, R. K. (2011). Scaling rules for diffusive drug delivery in tumor and normal tissues. Proceedings of the National Academy of Sciences of the United States of America, 108(5), 1799–1803. https://doi.org/10.1073/pnas.1018154108

23. Prasetyanti, P. R., & Medema, J. P. (2017). Intra-tumor heterogeneity from a cancer stem cell perspective. Molecular Cancer, 16(1), 1–9. https://doi.org/10.1186/s12943-017-0600-4

24. Mitchell, M. J., Jain, R. K., & Langer, R. (2017). Engineering and physical sciences in oncology: Challenges and opportunities. Nature Reviews Cancer, 17(11), 659–675. https://doi.org/10.1038/nrc.2017.83

25. Stylianopoulos, T., Martin, J. D., Chauhan, V. P., Jain, S. R., Diop-Frimpong, B., Bardeesy, N., … Jain, R. K. (2012). Causes, consequences, and remedies for growth-induced solid stress in murine and human tumors. Proceedings of the National Academy of Sciences of the United States of America, 109(38), 15101–15108. https://doi.org/10.1073/pnas.1213353109

26. Heldin, C. H., Rubin, K., Pietras, K., & Östman, A. (2004). High interstitial fluid pressure - An obstacle in cancer therapy. Nature Reviews Cancer, 4(10), 806–813. https://doi.org/10.1038/nrc1456

27. Senthebane, D. A., Rowe, A., Thomford, N. E., Shipanga, H., Munro, D., Al Mazeedi, M. A. M., … Dzobo, K. (2017). The role of tumor microenvironment in chemoresistance: To survive, keep your enemies closer. International Journal of Molecular Sciences, 18(7). https://doi.org/10.3390/ijms18071586

28. Valkenburg, K. C., De Groot, A. E., & Pienta, K. J. (2018). Targeting the tumour stroma to improve cancer therapy. Nature Reviews Clinical Oncology, 15(6), 366–381. https://doi.org/10.1038/s41571-018-0007-1

29. Balkwill, F. R., Capasso, M., & Hagemann, T. (2012). The tumor microenvironment at a glance. Journal of Cell Science, 125(23), 5591–5596. https://doi.org/10.1242/jcs.116392

30. Hirata, E., & Sahai, E. (2017). Tumor microenvironment and differential responses to therapy. Cold Spring Harbor Perspectives in Medicine, 7(7), 1–14. https://doi.org/10.1101/cshperspect.a026781

31. Quail, D. F., & Joyce, J. A. (2013). Microenvironmental regulation of tumor progression and metastasis. Nature Medicine, 19(11), 1423–1437. https://doi.org/10.1038/nm.3394

32. Hinshaw, D. C., & Shevde, L. A. (2019). The tumor microenvironment innately modulates cancer progression. Cancer Research, 79(18), 4557–4567. https://doi.org/10.1158/0008-5472.CAN-18-3962

33. Walter, S. G., Scheidt, S., Nißler, R., Gaisendrees, C., Zarghooni, K., & Schildberg, F. A. (2021). In-depth characterization of stromal cells within the tumor microenvironment yields novel therapeutic targets. Cancers, 13(6), 1–19. https://doi.org/10.3390/cancers13061466

34. Bussard, K. M., Mutkus, L., Stumpf, K., Gomez-Manzano, C., & Marini, F. C. (2016). Tumor-associated stromal cells as key contributors to the tumor microenvironment. Breast Cancer Research, 18(1), 1–11. https://doi.org/10.1186/s13058-016-0740-2

35. Galland, S., & Stamenkovic, I. (2020). Mesenchymal stromal cells in cancer: a review of their immunomodulatory functions and dual effects on tumor progression. Journal of Pathology, 250(5), 555–572. https://doi.org/10.1002/path.5357

36. Belhabib, I., Zaghdoudi, S., Lac, C., Bousquet, C., & Jean, C. (2021). Extracellular matrices and cancer-associated fibroblasts: Targets for cancer diagnosis and therapy? Cancers, 13(14). https://doi.org/10.3390/cancers13143466

37. Goldie, J. H., & Coldman, A. J. (2009). Drug Resistance in Cancer: Mechanisms and Models, 256. Retrieved from http://books.google.com/books?id=nAR0deuqpyAC&pgis=1

38. Wang, X., Zhang, H., & Chen, X. (2019). Drug resistance and combating drug resistance in cancer. Cancer Drug Resistance. https://doi.org/10.20517/cdr.2019.10

39. Housman, G., Byler, S., Heerboth, S., Lapinska, K., Longacre, M., Snyder, N., & Sarkar, S. (2014). Drug resistance in cancer: An overview. Cancers, 6(3), 1769–1792. https://doi.org/10.3390/cancers6031769

40. Jain, R. K. (1994). Barriers to drug delivery in solid tumors. Scientific American, 271(1), 58–65. https://doi.org/10.1038/scientificamerican0794-58

41. Foo, J., & Michor, F. (2014). Evolution of acquired resistance to anti-cancer therapy. Journal of Theoretical Biology, 355(2), 10–20. https://doi.org/10.1016/j.jtbi.2014.02.025

42. Hanahan, D., & Weinberg, R. A. (2011). Review Hallmarks of Cancer : The Next Generation. Cell, 144(5), 646–674. https://doi.org/10.1016/j.cell.2011.02.013

43. Vasan, N., Baselga, J., & Hyman, D. M. (2019). A view on drug resistance in cancer. Nature, 575(7782), 299–309. https://doi.org/10.1038/s41586-019-1730-1

44. De Lartigue, J. (2018). Tumor heterogeneity: A central foe in the war on cancer. Journal of Community and Supportive Oncology, 16(3), e167–e174. https://doi.org/10.12788/jcso.0407

45. Fisher, R., Pusztai, L., & Swanton, C. (2013). Cancer heterogeneity: Implications for targeted therapeutics. British Journal of Cancer, 108(3), 479–485. https://doi.org/10.1038/bjc.2012.581

46. Balkwill, F. R., Capasso, M., & Hagemann, T. (2012). The tumor microenvironment at a glance. Journal of Cell Science, 125(23), 5591–5596. https://doi.org/10.1242/jcs.116392

47. Oudin, M. J., & Weaver, V. M. (2016). Physical and chemical gradients in the tumor microenvironment regulate tumor cell invasion, migration, and metastasis. Cold Spring Harbor Symposia on Quantitative Biology, 81(1), 189–205. https://doi.org/10.1101/sqb.2016.81.030817

48. Frame, F. M., Noble, A. R., Klein, S., Walker, H. F., Suman, R., Kasprowicz, R., … Maitland, N. J. (2017). Tumor heterogeneity and therapy resistance - implications for future treatments of prostate cancer. Journal of Cancer Metastasis and Treatment, 3(12), 302. https://doi.org/10.20517/2394-4722.2017.34

49. Liu, J., Dang, H., & Wang, X. W. (2018). The significance of intertumor and intratumor heterogeneity in liver cancer. Experimental and Molecular Medicine, 50(1), e416-8. https://doi.org/10.1038/emm.2017.165

50. Raynaud, F., Mina, M., Tavernari, D., & Ciriello, G. (2018). Pan-cancer inference of intra-tumor heterogeneity reveals associations with different forms of genomic instability. PLoS Genetics, 14(9), 1–18. https://doi.org/10.1371/journal.pgen.1007669

51. Pribluda, A., De La Cruz, C. C., & Jackson, E. L. (2015). Intratumoral heterogeneity: From diversity comes resistance. Clinical Cancer Research, 21(13), 2916–2923. https://doi.org/10.1158/1078-0432.CCR-14-1213

52. Petrelli, F., Pietrantonio, F., Cremolini, C., Di, M., Coinu, A., Lonati, V., … Barni, S. (2015). Early tumour shrinkage as a prognostic factor and surrogate end-point in colorectal cancer : A systematic review and pooled-analysis. European Journal of Cancer, 51(7), 800–807. https://doi.org/10.1016/j.ejca.2015.02.011

53. Yu, S., Wang, X., Wang, X., Wu, X., Xu, R., Wang, X., … Wenfeng, L. (2019). Tumor shrinkage rate as a potential marker for the prediction of long-term outcome in advanced non-small cell lung cancer treated with first-line tyrosine kinase inhibitors.

Journal of Cancer Research and Therapeutics, 15(7), 1574–1580.

https://doi.org/10.4103/jcrt.JCRT_481_19

54. Wei, M., Ye, Q., Wang, X., Wang, M., Hu, Y., Yang, Y., … Cai, J. (2018). Early tumor

shrinkage served as a prognostic factor for patients with stage III non-small cell lung

cancer treated with concurrent chemoradiotherapy. Medicine (United States),

97(19), 1–6. https://doi.org/10.1097/MD.0000000000010632

55. Kim, S. T., Jang, K. T., Lee, S. J., Jang, H. L., Lee, J., Park, S. H., … Park, J. O. (2015).

Tumour shrinkage at 6 weeks predicts favorable clinical outcomes in a phase III study

of gemcitabine and oxaliplatin with or without erlotinib for advanced biliary tract

cancer. BMC Cancer, 15(1), 1–8. https://doi.org/10.1186/s12885-015-1552-y

56. Vivaldi, C., Fornaro, L., Cappelli, C., Pecora, I., Catanese, S., Salani, F., … Vasile, E.

(2019). Early tumor shrinkage and depth of response evaluation in metastatic

pancreatic cancer treated with first line chemotherapy: An observational

retrospective cohort study. Cancers, 11(7), 1–12.

https://doi.org/10.3390/cancers11070939

57. Nagy, Janice., Husain, Amjad., Jaminet, S., Dvorak, A., Dvorak, H. (2016). Tumor

Vasculature: Structure and Function. 1–9. Retrieved from

https://radiologykey.com/knee-10/

Macrophages

58. Wu, K., Lin, K., Li, X., Yuan, X., Xu, P., Ni, P., & Xu, D. (2020). Redefining Tumor-

Associated Macrophage Subpopulations and Functions in the Tumor

Microenvironment. Frontiers in Immunology, 11(August), 1731.

https://doi.org/10.3389/fimmu.2020.01731

59. Saldana, J. I. (n.d.). Macrophage Fact Sheet. British Society for Immunology.

Retrieved from https://www.immunology.org/public-information/bitesized-

immunology/cells/macrophages

60. Zhou, J., Tang, Z., Gao, S., Li, C., Feng, Y., & Zhou, X. (2020). Tumor-Associated

Macrophages: Recent Insights and Therapies. Frontiers in Oncology, 10(February),

1–13. https://doi.org/10.3389/fonc.2020.00188

Endothelial Cells

61. Pearson, JD. (2000). Normal endothelial cell function. Lupus, 9, 183-188.

62. Hida, K., & Klagsbrun, M. (2005). A New Perspective on Tumor Endothelial Cells:

Unexpected Chromosome and Centrosome Abnormalities: Figure 1. Cancer

Research, 65(7), 2507–2510. https://doi.org/10.1158/0008-5472.CAN-05-0002

63. Akino, T., Hida, K., Hida, Y., Tsuchiya, K., Freedman, D., Muraki, C., … Shindoh,

M. (2009). Cytogenetic abnormalities of tumor-associated endothelial cells in human

malignant tumors. American Journal of Pathology, 175(6), 2657–2667.

https://doi.org/10.2353/ajpath.2009.090202

64. Maishi, N., Annan, D., Kikuchi, H., Hida, Y., & Hida, K. (2019). Tumor Endothelial

Heterogeneity in. Cancers, 11(1511), 1–16.

65. Ohga, N., Ishikawa, S., Maishi, N., Akiyama, K., Hida, Y., Kawamoto, T., … Hida,

K. (2012). Heterogeneity of tumor endothelial cells: Comparison between tumor

endothelial cells isolated from high- and low-metastatic tumors. American Journal of

Pathology, 180(3), 1294–1307. https://doi.org/10.1016/j.ajpath.2011.11.035

Pericytes

66. Ferland-McCollough, D., Slater, S., Richard, J., Reni, C., & Mangialardi, G. (2017). Pericytes, an overlooked player in vascular pathobiology. Pharmacology and Therapeutics, 171, 30–42. https://doi.org/10.1016/j.pharmthera.2016.11.008

67. Dias Moura Prazeres, P. H., Sena, I. F. G., Borges, I. da T., de Azevedo, P. O., Andreotti, J. P. P., de Paiva, A. E., … Birbrair, A. (2017). Pericytes are heterogeneous in their origin within the same tissue. Developmental Biology, 427(1), 6–11. https://doi.org/10.1016/j.ydbio.2017.05.001

68. Yamazaki, T., & Mukouyama, Y. S. (2018). Tissue Specific Origin, Development, and Pathological Perspectives of Pericytes. Frontiers in Cardiovascular Medicine, 5(June), 1–6. https://doi.org/10.3389/fcvm.2018.00078

69. Sun, R., Kong, X., Qiu, X., Huang, C., & Wong, P. P. (2021). The Emerging Roles of Pericytes in Modulating Tumor Microenvironment. Frontiers in Cell and Developmental Biology, 9(June), 1–10. https://doi.org/10.3389/fcell.2021.676342

Mesenchymal stem cells

70. Krinner, A., Hoffmann, M., Loeffler, M., Drasdo, D., & Galle, J. (2010). Individual fates of mesenchymal stem cells in vitro. BMC Systems Biology, 4. https://doi.org/10.1186/1752-0509-4-73

71. Ridge, S. M., Sullivan, F. J., & Glynn, S. A. (2017). Mesenchymal stem cells: Key players in cancer progression. Molecular Cancer, 16(1), 1–10. https://doi.org/10.1186/s12943-017-0597-8

72. Costa, L. A., Eiro, N., Fraile, M., Gonzalez, L. O., Saá, J., Garcia-Portabella, P., …

    Vizoso, F. J. (2021). Functional heterogeneity of mesenchymal stem cells from

    natural niches to culture conditions: implications for further clinical uses. Cellular and

    Molecular Life Sciences, 78(2), 447–467. https://doi.org/10.1007/s00018-020-03600-

    0

73. Pevsner-Fischer, M., Levin, S., & Zipori, D. (2011). The Origins of Mesenchymal

    Stromal Cell Heterogeneity. Stem Cell Reviews and Reports, 7(3), 560–568.

    https://doi.org/10.1007/s12015-011-9229-7

74. Lee, H. Y., & Hong, I. S. (2017). Double-edged sword of mesenchymal stem cells:

    Cancer-promoting versus therapeutic potential. Cancer Science, 108(10), 1939–1946.

    https://doi.org/10.1111/cas.13334

Neutrophils

75. Shaul, M. E., & Fridlender, Z. G. (2018). Cancer-related circulating and tumor-

    associated neutrophils – subtypes, sources and function. FEBS Journal, 285(23),

    4316–4342. https://doi.org/10.1111/febs.14524

76. Lecot, P., Sarabi, M., Pereira Abrantes, M., Mussard, J., Koenderman, L., Caux, C.,

    … Michallet, M. C. (2019). Neutrophil Heterogeneity in Cancer: From Biology to

    Therapies. Frontiers in Immunology, 10(September), 1–19.

    https://doi.org/10.3389/fimmu.2019.02155

77. Rosales, C. (2018). Neutrophil: A cell with many roles in inflammation or several cell

    types? Frontiers in Physiology, 9(FEB), 1–17.

    https://doi.org/10.3389/fphys.2018.00113

78. Masucci, M. T., Minopoli, M., & Carriero, M. V. (2019). Tumor Associated Neutrophils. Their Role in Tumorigenesis, Metastasis, Prognosis and Therapy. Frontiers in Oncology, 9(November), 1–16. https://doi.org/10.3389/fonc.2019.01146

79. Ng, L. G., Ostuni, R., & Hidalgo, A. (2019). Heterogeneity of neutrophils. Nature Reviews Immunology, 19(4), 255–265. https://doi.org/10.1038/s41577-019-0141-8

80. Hedrick, C. C., & Malanchi, I. (2021). Neutrophils in cancer: heterogeneous and multifaceted. Nature Reviews Immunology, 0123456789. https://doi.org/10.1038/s41577-021-00571-6

Myeloid Derived Suppressor Cells

81. Bergenfelz, C., & Leandersson, K. (2020). The Generation and Identity of Human Myeloid-Derived Suppressor Cells. Frontiers in Oncology, 10(February), 17–19. https://doi.org/10.3389/fonc.2020.00109

82. Tcyganov, E., Mastio, J., Chen, E., & Gabrilovich, D. I. (2018). Plasticity of myeloid-derived suppressor cells in cancer. Current Opinion in Immunology, 51, 76–82. https://doi.org/10.1016/j.coi.2018.03.009

83. Veglia, F., Sanseviero, E., & Gabrilovich, D. I. (2021). Myeloid-derived suppressor cells in the era of increasing myeloid cell diversity. Nature Reviews Immunology, 21(8), 485–498. https://doi.org/10.1038/s41577-020-00490-y

84. Peranzoni, E., Zilio, S., Marigo, I., Dolcetti, L., Zanovello, P., Mandruzzato, S., & Bronte, V. (2010). Myeloid-derived suppressor cell heterogeneity and subset definition. Current Opinion in Immunology, 22(2), 238–244. https://doi.org/10.1016/j.coi.2010.01.021

85. Solito, S., Marigo, I., Pinton, L., Damuzzo, V., Mandruzzato, S., & Bronte, V. (2014). Myeloid-derived suppressor cell heterogeneity in human cancers. Annals of the New York Academy of Sciences, 1319(1), 47–65. https://doi.org/10.1111/nyas.12469

Natural Killer Cells

86. Larsen, S. K., Gao, Y., & Basse, P. H. (2014). NK Cells in the Tumor Microenvironment. Critical Reviews in Oncogenesis, 19(1–2), 91–105. https://doi.org/10.1615/CritRevOncog.2014011142

87. Stabile, H., Fionda, C., Gismondi, A., & Santoni, A. (2017). Role of distinct natural killer cell subsets in anticancer response. Frontiers in Immunology, 8(MAR), 1–8. https://doi.org/10.3389/fimmu.2017.00293

88. Melaiu, O., Lucarini, V., Cifaldi, L., & Fruci, D. (2020). Influence of the Tumor Microenvironment on NK Cell Function in Solid Tumors. Frontiers in Immunology, 10(January). https://doi.org/10.3389/fimmu.2019.03038

89. Sivori, S., Vacca, P., Del Zotto, G., Munari, E., Mingari, M. C., & Moretta, L. (2019). Human NK cells: surface receptors, inhibitory checkpoints, and translational applications. Cellular and Molecular Immunology, 16(5), 430–441. https://doi.org/10.1038/s41423-019-0206-4

90. Vivier, E., Tomasello, E., Baratin, M., Walzer, T., & Ugolini, S. (2008). Functions of natural killer cells. Nature Immunology, 9(5), 503–510. https://doi.org/10.1038/ni1582

91. Wu, S. Y., Fu, T., Jiang, Y. Z., & Shao, Z. M. (2020). Natural killer cells in cancer biology and therapy. Molecular Cancer, 19(1), 1–26. https://doi.org/10.1186/s12943-020-01238-x

92. Chen, B., Zhu, L., Yang, S., & Su, W. (2021). Unraveling the Heterogeneity and Ontogeny of Dendritic Cells Using Single-Cell RNA Sequencing. Frontiers in Immunology, 12(September), 1–13. https://doi.org/10.3389/fimmu.2021.711329

93. Kah-Wai, L., Jacek, T., & Jacek, R. (2006). Dendritic cells heterogeneity and its role in cancer immunity. Journal of Cancer Research and Therapeutics, 2(2), 35–40. https://doi.org/10.4103/0973-1482.25847

94. Patente, T. A., Pinho, M. P., Oliveira, A. A., Evangelista, G. C. M., Bergami-Santos, P. C., & Barbuto, J. A. M. (2019). Human dendritic cells: Their heterogeneity and clinical application potential in cancer immunotherapy. Frontiers in Immunology, 10(JAN), 1–18. https://doi.org/10.3389/fimmu.2018.03176

95. Ma, Y., Shurin, G. V., Peiyuan, Z., & Shurin, M. R. (2013). Dendritic cells in the cancer microenvironment. Journal of Cancer, 4(1), 36–44. https://doi.org/10.7150/jca.5046

96. Fricke, I., & Gabrilovich, D. I. (2006). Dendritic cells and tumor microenvironment: A dangerous liaison. Immunological Investigations, 35(3–4), 459–483. https://doi.org/10.1080/08820130600803429

97. Tran Janco, J. M., Lamichhane, P., Karyampudi, L., & Knutson, K. L. (2015). Tumor-Infiltrating Dendritic Cells in Cancer Pathogenesis. The Journal of Immunology, 194(7), 2985–2991. https://doi.org/10.4049/jimmunol.1403134

98. Gerhard, G. M., Bill, R., Messemaker, M., Klein, A. M., & Pittet, M. J. (2021). Tumor-infiltrating dendritic cell states are conserved across solid human cancers. Journal of Experimental Medicine, 218(1). https://doi.org/10.1084/JEM.20200264

99. Golubovskaya, V., & Wu, L. (2016). Different subsets of T cells, memory, effector

functions, and CAR-T immunotherapy. Cancers, 8(3).

https://doi.org/10.3390/cancers8030036

100. Kumar, B. V, Connors, T. J., & Farber, D. L. (2018). Human T Cell

Development, Localization, and Function throughout Life. Immunity.

https://doi.org/10.1016/j.immuni.2018.01.007

101. Kaplan, M. H., Hufford, M. M., & Olson, M. R. (2015). The development and in

vivo function of T helper 9 cells. Nature Reviews Immunology, 15(5), 295–307.

https://doi.org/10.1038/nri3824

102. Jiang, Q., Yang, G., Xiao, F., Xie, J., Wang, S., Lu, L., & Cui, D. (2021). Role of

Th22 Cells in the Pathogenesis of Autoimmune Diseases. Frontiers in Immunology,

12(July), 1–14. https://doi.org/10.3389/fimmu.2021.688066

103. Xia, A., Zhang, Y., Xu, J., Yin, T., & Lu, X. J. (2019). T Cell Dysfunction in

Cancer Immunity and Immunotherapy. Frontiers in Immunology, 10(July), 1719.

https://doi.org/10.3389/fimmu.2019.01719

104. Zhang, Z., Liu, S., Zhang, B., Qiao, L., Zhang, Y., & Zhang, Y. (2020). T Cell

Dysfunction and Exhaustion in Cancer. Frontiers in Cell and Developmental Biology,

8(February). https://doi.org/10.3389/fcell.2020.00017

105. Ward-Hartstonge, K. A., & Kemp, R. A. (2017). Regulatory T-cell heterogeneity

and the cancer immune response. Clinical & Translational Immunology, 6(9), e154.

https://doi.org/10.1038/cti.2017.43

106.   van der Leun, A. M., Thommen, D. S., & Schumacher, T. N. (2020). CD8+ T cell

states in human cancer: insights from single-cell analysis. Nature Reviews Cancer,

20(4), 218–232. https://doi.org/10.1038/s41568-019-0235-4

107.   Marshall, J. S., Warrington, R., Watson, W., & Kim, H. L. (2018). An

introduction to immunology and immunopathology. Allergy, Asthma and Clinical

Immunology, 14(s2), 1–10. https://doi.org/10.1186/s13223-018-0278-1

108.   Laydon, D. J., Bangham, C. R. M., & Asquith, B. (2015). Estimating T-cell

repertoire diversity: Limitations of classical estimators and a new approach.

Philosophical Transactions of the Royal Society B: Biological Sciences, 370(1675).

https://doi.org/10.1098/rstb.2014.0291

B Cells

109.   Shang, J., Zha, H., & Sun, Y. (2020). Phenotypes, Functions, and Clinical

Relevance of Regulatory B Cells in Cancer. Frontiers in Immunology, 11(October),

1–10. https://doi.org/10.3389/fimmu.2020.582657

110.   B Cells Overview (from Discovery to Therapy) - Mini-review _ Bio-Rad. (n.d.).

Retrieved from https://www.bio-rad-antibodies.com/b-cell-function-activation-

lineage-marker-antibody-

minireview.html?JSESSIONID_STERLING=84EF022F7D3C2CADB6D0F416ED78

2140.ecommerce1&evCntryLang=US-en&cntry=US&thirdPartyCookieEnabled=true

111.   Wei, Y., Huang, C. X., Xiao, X., Chen, D. P., Shan, H., He, H., & Kuang, D. M.

(2021). B cell heterogeneity, plasticity, and functional diversity in cancer

microenvironments. Oncogene, 40(29), 4737–4745. https://doi.org/10.1038/s41388-

021-01918-y

112. Tsou, P., Katayama, H., Ostrin, E. J., & Hanash, S. M. (2016). The emerging role of b cells in tumor immunity. Cancer Research, 76(19), 5591–5601. https://doi.org/10.1158/0008-5472.CAN-16-0431

113. Lebien, T. W., & Tedder, T. F. (2008). B lymphocytes: How they develop and function. Blood, 112(5), 1570–1580. https://doi.org/10.1182/blood-2008-02-078071

114. Somasundaram, R., Zhang, G., Fukunaga-Kalabis, M., Perego, M., Krepler, C., Xu, X., … Wagner, S. N. (2017). Tumor-associated B-cells induce tumor heterogeneity and therapy resistance. Nature Communications, 8(1), 1–16. https://doi.org/10.1038/s41467-017-00452-4

Platelets

115. Huong, P. T., Nguyen, L. T., Nguyen, X., & Lee, S. K. (2019). The Role of Platelets in the Tumor-Microenvironment and the Drug Resistance of Cancer Cells, 1–19. https://doi.org/10.3390/cancers11020240

116. Arbor, A., & Arbor, A. (2017). Normal platelet function, 36(2), 195–198. https://doi.org/10.1007/s10555-017-9677-x.Normal

117. Palacios-acedo, A. L., Mège, D., Crescence, L., Dignat-george, F., Dubois, C., & Panicot-dubois, L. (2019). and Cancer : Collaborating With the Enemy, 10(July), 1–7. https://doi.org/10.3389/fimmu.2019.01805

Adipocytes

118. Pallegar NK, Christian SL. Adipocytes in the Tumour Microenvironment. Adv Exp Med Biol. 2020;1234:1-13. doi: 10.1007/978-3-030-37184-5_1. PMID: 32040851.

119.   Choe, S. S., Huh, J. Y., Hwang, I. J., Kim, J. I., & Kim, J. B. (2016). Adipose

tissue remodeling: Its role in energy metabolism and metabolic disorders. Frontiers in

Endocrinology, 7(APR), 1–16. https://doi.org/10.3389/fendo.2016.00030

120.   Nieman, K. M., Romero, I. L., Van Houten, B., & Lengyel, E. (2013). Adipose

tissue and adipocytes support tumorigenesis and metastasis. Biochimica et Biophysica

Acta - Molecular and Cell Biology of Lipids, 1831(10), 1533–1541.

https://doi.org/10.1016/j.bbalip.2013.02.010

Tumor Cell Variability

121.   Lee, C. H., Yelensky, R., Jooss, K., & Chan, T. A. (2018). Update on Tumor

Neoantigens and Their Utility: Why It Is Good to Be Different. Trends in

Immunology, 39(7), 536–548. https://doi.org/10.1016/j.it.2018.04.005

122.   Shen, S., & Clairambault, J. (2020). Open Peer Review Cell plasticity in cancer

cell populations [version 1; peer review: 2 approved], 9, 1–16. Retrieved from

https://doi.org/10.12688/f1000research.24803.1

123.   Hanahan, D. (2022). Hallmarks of Cancer: New Dimensions. Cancer Discovery,

12(1), 31–46. https://doi.org/10.1158/2159-8290.CD-21-1059

124.   Werner, B., Case, J., Williams, M. J., Chkhaidze, K., Temko, D., Fernández-

Mateos, J., … Sottoriva, A. (2020). Measuring single cell divisions in human tissues

from multi-region sequencing data. Nature Communications, 11(1).

https://doi.org/10.1038/s41467-020-14844-6

125.   Grzywa, T. M., Paskal, W., & Włodarski, P. K. (2017). Intratumor and Intertumor

Heterogeneity in Melanoma. Translational Oncology, 10(6), 956–975.

https://doi.org/10.1016/j.tranon.2017.09.007

126. Seo, B. B., Jahed, Z., Coggan, J. A., Chau, Y. Y., Rogowski, J. L., Gu, F. X., … Tsui, T. Y. (2017). Mechanical contact characteristics of pc3 human prostate cancer cells on complex-shaped silicon micropillars. Materials, 10(8). https://doi.org/10.3390/ma10080892

127. Meacham, C. E., & Morrison, S. J. (2013). Tumour heterogeneity and cancer cell plasticity. Nature, 501(7467), 328–337. https://doi.org/10.1038/nature12624

Cell Turnover

128. Avanzini, S., Kurtz, D. M., Chabon, J. J., Moding, E. J., Hori, S. S., Gambhir, S. S., … Reiter, J. G. (2020). A mathematical model of ctDNA shedding predicts tumor detection size. Science Advances, 6(50), 1–10. https://doi.org/10.1126/sciadv.abc4308

129. Gallaher, J. A., Brown, J., & Anderson, A. R. A. (2018). The dynamic tumor ecosystem: How cell turnover and trade-offs affect cancer evolution. BioRxiv. https://doi.org/10.1101/270900

130. Hager T. Oncogene's point mutation produces cancer. JAMA. 1982;248(19):2418–2424. doi:10.1001/jama.1982.03330190006002

131. Hart, J. R., Zhang, Y., Liao, L., Ueno, L., Du, L., Jonkers, M., … Vogt, P. K. (2015). The butterfly effect in cancer: A single base mutation can remodel the cell. Proceedings of the National Academy of Sciences of the United States of America, 112(4), 1131–1136. https://doi.org/10.1073/pnas.1424012112

Appendix

Code for Cell Mutation Turnover Study

```python
# -*- coding: utf-8 -*-
"""
Created on Sat Mar 12 11:57:16 2022

@author: Josh
"""

import random
import csv
#import pandas as pd

export_file = open('Cell mutation turnover trials.csv', 'w')
writer = csv.writer(export_file, dialect = 'excel', lineterminator = '\n')

sim_run_info_header = ['wild population', 'wild replication rate', 'wild replication rate
    adjusment',
                'mutation population', 'mutation replication rate', 'mutation replication
    rate adjustment',
                'death rate', 'wild death rate adjustment', 'mutation death rate
    adjustment']
writer.writerow(sim_run_info_header)

death_rate = 0.153846
wild_pop = 99999
wild_rr =        1
wild_rr_adj = 1
wild_dr_adj = 2
mutant_pop = 1
mutant_rr = 1
mutant_rr_adj = 1.1
mutant_dr_adj = 2
days = range(0,1000)
actual_day = 0
total_pop = wild_pop + mutant_pop
print(f"total_pop is {total_pop}")

sim_run_info = [wild_pop, wild_rr, wild_rr_adj, mutant_pop, mutant_rr, mutant_rr_adj,
        death_rate, wild_dr_adj, mutant_dr_adj]
writer.writerow(sim_run_info)
new_data_headers = ['day', 'wild population', 'mutant population', 'total population']
```

```
            writer.writerow(new_data_headers)

            for day in days:
                if wild_pop <= 0:
                    break
                if mutant_pop <= 0:
                    break
                actual_day = actual_day + 1
                wild_death = (wild_pop * death_rate * wild_dr_adj)
                mutant_death = (mutant_pop * death_rate * mutant_dr_adj)
                total_death = round(wild_death + mutant_death)
                cell_turnover = range(0, total_death)
                wild_death_prob = wild_death / total_death
                mutant_death_prob = mutant_death / total_death
                cell_type = ['Wild','Mutant']
                new_wild = 0
                new_mutant = 0
                dead_wild = 0
                dead_mutant = 0
                for turnover in cell_turnover:
                    dead_cell = random.choices(cell_type, [wild_death_prob, mutant_death_prob])
                    if dead_cell[0] == 'Wild':
                        wild_pop = wild_pop - 1
                    else:
                        mutant_pop = mutant_pop - 1
                    total_pop = wild_pop + mutant_pop
                    prob_wild = (wild_pop * wild_rr * wild_rr_adj) / total_pop
                    prob_mutant = (mutant_pop * mutant_rr * mutant_rr_adj) / total_pop
                    new_cell = random.choices(cell_type, [prob_wild, prob_mutant])
                    if new_cell[0] == 'Wild':
                        wild_pop = wild_pop + 1
                    else:
                        mutant_pop = mutant_pop + 1
                total_pop = wild_pop + mutant_pop
                print(actual_day, wild_pop, mutant_pop, total_pop)
                new_data = [actual_day, wild_pop, mutant_pop, total_pop]
                writer.writerow(new_data)
        export_file.close()

        #pd_file = pd.read_csv('Cell mutation turnover trials.csv', skiprows = 2)
        #pd_file.plot(x = 'day',xticks = range(0,actual_day,100), y = ['wild population', 'mutant
            population'], kind = 'bar', stacked=True)
        #from IPython.display import display
        #display(pd_file)
```

Average Mutation Turnover

```python
# -*- coding: utf-8 -*-
"""
Created on Sun Mar 13 12:06:55 2022

@author: Josh
"""

import random
import csv
import numpy as np
import time
#import pandas as pd

start_time = time.time()

export_file = open('Average Cell mutation turnover trials.csv', 'w')
writer = csv.writer(export_file, dialect = 'excel', lineterminator = '\n')

sim_run_info_header = ['wild population', 'wild replication rate', 'wild replication rate
    adjusment',
            'mutation population', 'mutation replication rate', 'mutation replication
    rate adjustment',
            'death rate', 'wild death rate adjustment', 'mutation death rate
    adjustment', 'simulations']
writer.writerow(sim_run_info_header)

simulations = range(0,100)
death_rate = 0.153846
wild_pop = 99999
wild_rr =        1
wild_rr_adj = 1
wild_dr_adj = 2
mutant_pop = 1
mutant_rr = 1
mutant_rr_adj = 1.1
mutant_dr_adj = 2
days = range(0,1000)
failures = 0
total_pop = wild_pop + mutant_pop
average_data = []
complete_data_list = []
```

```
print(f"total_pop is {total_pop}")

sim_run_info = [wild_pop, wild_rr, wild_rr_adj, mutant_pop, mutant_rr, mutant_rr_adj,
        death_rate, wild_dr_adj, mutant_dr_adj, len(simulations)]
writer.writerow(sim_run_info)
new_data_headers = ['day', 'wild population', 'mutant population', 'total population']
writer.writerow(new_data_headers)

for simulation in simulations:
    wild_pop = 99999
    mutant_pop = 1
    total_pop = wild_pop + mutant_pop
    average_data_list = []
    actual_day = 0
    for day in days:
        actual_day = actual_day + 1
        wild_death = (wild_pop * death_rate * wild_dr_adj)
        mutant_death = (mutant_pop * death_rate * mutant_dr_adj)
        total_death = round(wild_death + mutant_death)
        cell_turnover = range(0, total_death)
        wild_death_prob = wild_death / total_death
        mutant_death_prob = mutant_death / total_death
        cell_type = ['Wild','Mutant']
        new_wild = 0
        new_mutant = 0
        dead_wild = 0
        dead_mutant = 0
        for turnover in cell_turnover:
            dead_cell = random.choices(cell_type, [wild_death_prob, mutant_death_prob])
            if dead_cell[0] == 'Wild':
                wild_pop = wild_pop - 1
            else:
                mutant_pop = mutant_pop - 1
            total_pop = wild_pop + mutant_pop
            prob_wild = (wild_pop * wild_rr * wild_rr_adj) / total_pop
            prob_mutant = (mutant_pop * mutant_rr * mutant_rr_adj) / total_pop
            new_cell = random.choices(cell_type, [prob_wild, prob_mutant])
            if new_cell[0] == 'Wild':
                wild_pop = wild_pop + 1
            else:
                mutant_pop = mutant_pop + 1
        total_pop = wild_pop + mutant_pop
        new_data = [actual_day, wild_pop, mutant_pop, total_pop]
        average_data_list.append(new_data)
```

```python
        complete_data_list.append(average_data_list)
    if mutant_pop <= 0:
        failures = failures + 1
    successes = len(simulations) - failures
complete_array = np.array(complete_data_list)
avg_complete = (np.sum(complete_array, 0)/len(simulations))
std_complete = np.std(complete_array, 0)
print(avg_complete)
print(successes)
for i in avg_complete:
    writer.writerow(i)
for j in std_complete:
    writer.writerow(j)
writer.writerow([f'successes are {successes}'])
export_file.close()
print('my program took', (time.time() - start_time)/60, 'minutes')
#pd_file = pd.read_csv('Cell mutation turnover trials.csv', skiprows = 2)
#pd_file.plot(x = 'day',xticks = range(0,actual_day,100), y = ['wild population', 'mutant
        population'], kind = 'bar', stacked=True)
#from IPython.display import display
#display(pd_file)
```

Identifying a Potential Novel Mechanism of Action for Metronomically Dosed Chemotherapeutics

1. **Introduction**

Metronomically dosed chemotherapy is a relatively new concept that originated from two seminal papers from Dr. Folkman's and Dr. Kerbel's labs in 2000.[1,2,13] In contrast to the maximum tolerated dose (**MTD**) chemotherapy, which generally relies on large bolus doses and long drug-free intervals to recover from significant toxicities, metronomic dosing utilizes more rapid administrations, often daily, of much smaller doses without a drug-free interval. Initially, metronomic chemotherapy was investigated as an antiangiogenic approach, which was thought to have more favorable drug resistance characteristics as endothelial cells were thought to be more genetically stable. Chemotherapeutics in general can be antiangiogenic because endothelial cells of newly forming blood vessels are dividing faster than those in older, more established blood vessels. However, during the drug-free intervals that are necessary in MTD chemotherapy, a host mediated repair process nullifies the antiangiogenic effects of MTD chemotherapy. To prevent this issue, investigators surmised that avoiding the drug-free periods would improve the angiogenic effects of chemotherapeutics. Of course, narrowing the drug-free interval required a concomitant reduction in dose to prevent excessive toxicity.[13] Although the initial investigation of metronomic chemotherapy was based on sound fundamentals, it has since produced mixed results clinically, which can be viewed in table 1.[14] Table 1 summarizes the partial response (**PR**) of a variety of different metronomic studies, which is defined as an at least 30%

reduction of the target lesion(s). For Prostate cancer, the proportion of patients that achieved a prostate specific antigen (**PSA**) response (>50% reduction in circulating PSA) was used as a marker of efficacy as this was reported more frequently. Also, for glioblastoma multiforme, the six-month progression free survival percentage was reported as this was the most reported outcome. As depicted in the clinical data, the overall response to metronomic therapy is rather mixed and variable, indicating a need to improve our understanding of the underlying mechanisms of metronomic therapy to better identify likely responders.

Table 1

Breast (PR) (N=24)	Prostate (PSA) (N=22)	Ovarian (PR) (N=13)	Hepatocellular (PR) (N=3)	Glioblastoma Multiforme (PFS) (N=8)
Mean: 26%	Mean: 41.62%	Mean: 24%	Mean: 14%	Mean: 28.62%
SD: 19.59%	SD: 16.74%	SD: 10.39%	SD: 6%	SD: 13%

2. Overview of Metronomic Mechanisms Currently Under Investigation

Currently, it is thought that multiple mechanisms of action are needed to adequately describe metronomic chemotherapy, including antiangiogenic, immunologic, and direct cytotoxic mechanisms.[5,7,8,9,10,13] As described in the introduction, metronomic chemotherapy was initially developed as an antiangiogenic strategy based on the idea that drug free intervals reverse the antiangiogenic effects of cytotoxic chemotherapy.[6,13] This initial hypothesis was investigated and confirmed. Although MTD chemotherapy causes direct endothelial apoptosis in newly forming blood vessels, it also stimulates a host response that rapidly mobilizes bone marrow-derived cells (**BMDCs**) including endothelial progenitor cells (**EPCs**). These cells are recruited to sites of vessel damage where they take up residence and stimulate growth and repair of the damaged vasculature.[13] Without drug exposure during the drug free intervals, the proangiogenic effects of MTD chemotherapy overcame the antiangiogenic effects and reversed any previously inflicted damage to the tumor vasculature.[13] On the other hand, the continuous exposure of metronomic chemotherapy (cyclophosphamide) was found to target the EPCs and prevent the reflexive proangiogenic response of MTD chemotherapy.[13,17] Additionally, it was found that metronomic chemotherapy (cyclophosphamide) could induce thrombospondin-1, which is a potent inhibitor of angiogenesis, further supporting this potential mechanism. Metronomic topotecan (**TOPO**) was found to inhibit Hypoxia inducible factor 1 α (**HIF-1α**), a well-known stimulator of angiogenesis, indicating that the specific antiangiogenic mechanism of metronomic chemotherapy may be drug specific.[13,19] Other important modulators of

angiogenesis that have been altered by metronomic therapy include reduction of VEGF by low dose paclitaxel/docetaxel (**DTX**), inhibition of IL8 by vinorelbine, and reduction of HIF-1α activity by doxorubicin.[4]

The second major mechanism of metronomic chemotherapy is immunomodulation. Traditionally, the interactions between the immune system and a tumor are defined by 3 main stages: elimination, equilibrium, and escape. The elimination phase typically occurs earlier in malignancy and is highlighted by widespread elimination of cancer cells by the immune system. The tumor is likely to shrink during this stage as the cytotoxicity of the immune system overwhelms the growth kinetics of the tumor. During the equilibrium stage, the tumor is more stable. The initial aggressive cytotoxic effects of the immune system begin to wane as the tumor begins to identify and produce less immunostimulatory cancer cells through natural selection. The tumor is held in check until, eventually, a cancer cell is produced that is not recognized as foreign and that may secrete immunosuppressive molecules to further prevent immune activation. If this occurs, cancer cells will escape tumor surveillance. During the escape phase, recruitment of immunosuppressive immune cells such as myeloid derived suppressor cells and regulatory T cells to the tumor can further inhibit antitumor immunity and eventually lead to immune tolerance. These immunosuppressive cells can inhibit immunity through direct and cytokine-based mechanisms and can prevent the adaptive and innate immune systems from activating.[6] Many metronomically dosed chemotherapeutics are able to reduce the population of regulatory T cells, however, cyclophosphamide is the most well studied. On the other hand, metronomically dosed

capecitabine is the most effective at inhibiting myeloid derived suppressor cells.

Interestingly, metronomic chemotherapy appears to eliminate immunosuppressive immune cells more aggressively than effector immune cells and overall leads to immune activation. In a mouse study, the combination of cyclophosphamide and capecitabine led to inhibition of regulatory T cells and myeloid derived suppressor cells and improved immunologic activity.[4,6,10] Depletion of immunosuppressive cells within the tumor has been used as a surrogate marker clinically and positively correlates with clinical outcomes in some cancer types such as breast or prostate cancers.[10] Additionally, metronomic chemotherapy has been found to increase the expression of tumor associated antigens and antigen-presenting molecules by tumor cells and upregulate the antigen presenting machinery of dendritic cells.[10] Metronomic chemotherapy also promotes dendritic cell maturation, further enhancing their ability to respond to antigens.[10,12] Because of these effects, metronomic chemotherapy can lead to a more robust anti-tumor immune response, which can lead to enhanced tumor reduction and improved clinical outcomes.

Metronomic chemotherapy also inhibits the tumor cells directly, but in a different way than MTD chemotherapy. Experimentally, many metronomic based regimens are at least as potent as the MTD based regimens for the same drug. This is true even when controlling for the total cumulative dose. From a cell exposure perspective, MTD chemotherapy results in higher peaks and lower troughs and metronomic chemotherapy results in a steadier drug exposure. This altered exposure is more likely to cause senescence is less likely to induce apoptosis as the maximum

exposure concentration is lower and generally not sufficient to induce apoptosis.[4,6]

Clinically, this may be more similar to a cytostatic effect that allows angiogenic,

immunomodulatory, or other mechanisms to induce apoptosis and shrink the tumor.

Another hypothetical, but unproven direct mechanism that is currently being

investigated is the "four-dimensional effect" in which cancer cells become dependent

on the therapeutic during extended intervals and sudden withdrawal leads to cell

death.[6]
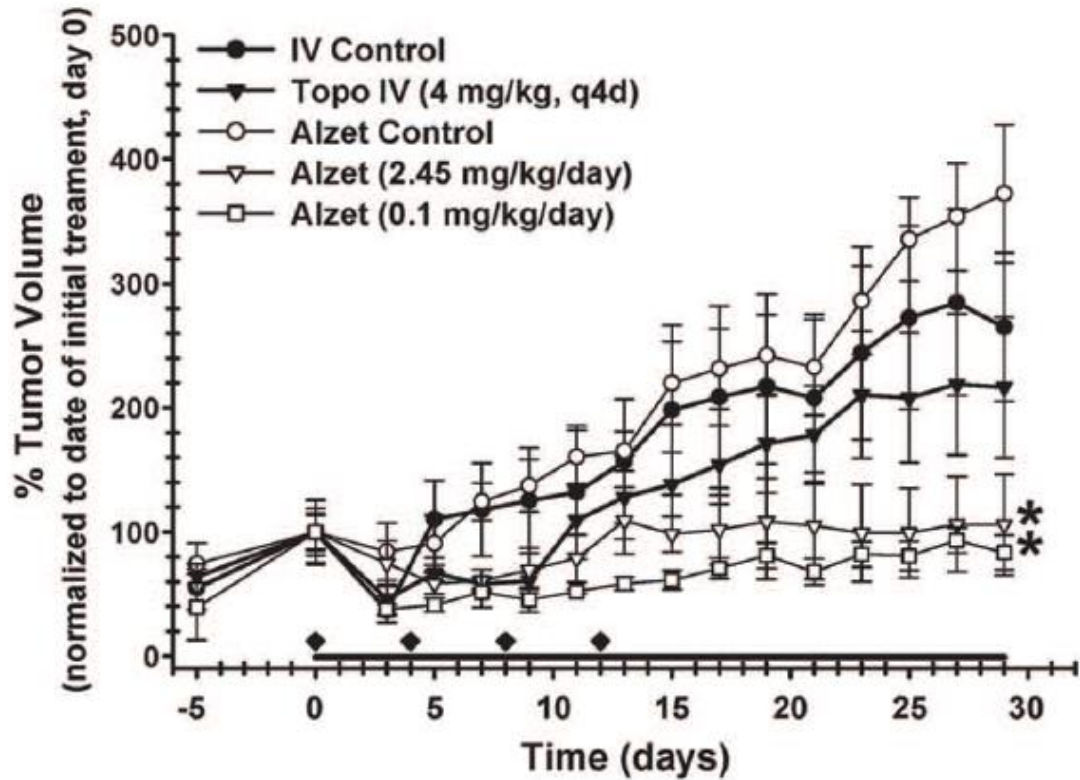
Figure 1. The effect of different dosing schedules of topotecan on tumor volumes in a PC3 xenograft mouse model. Tumor volumes were determined following topotecan administration using either IV administration via tail vein at 4mg/kg or vehicle control q4d x 4 total doses (represented by diamonds) or by a subcutaneously implanted ALZET micro-osmotic pumps at doses of 2.45mg/kg/day, 0.1mg/kg/day, or vehicle control (represented by a solid line). Data are presented as the mean +/- SEM (n=4-5). Means noted with (*) are significantly different to control (p </= 0.05).[3]

3. Review of Historical In-House Laboratory Data on Metronomic Topotecan in Prostate Cancer

Previously, our lab investigated the efficacy of metronomic topotecan in prostate cancer with LNCaP and PC3 cell-lines.[3] After successful *in vitro* experiments, an *in vivo* xenograft model of PC3 cells was used to further validate the treatment's efficacy and to determine the toxicity of the treatment. The results of this study can be viewed in **figure 1**. In this experiment, NCr nude (athymic/immune compromised) mice were implanted with PC3 cells at $1x10^7$cells/mL and diluted 1:1 in Matrigel. A 200µL subcutaneous injection occurred in the flank of each mouse. Tumors were allowed to grow until they reached an approximate size of 200-300 mm^3. Then, mice were exposed to 5 different treatments. IV treatments were given as tail vein injections every 4 days for 4 total doses. IV control was given as a vehicle control and IV topotecan was given at 4mg/kg, which was determined based on previous studies evaluating MTD topotecan. For continuous/metronomic exposure, an implantable micro-osmotic pump (Alzet) pump was implanted according to the manufacturer's instructions. The Alzet pump was designed to deliver a specific volume over a period of 28 days. The Alzet control contained only a vehicle control. The Alzet topotecan dose of 2.45mg/kg/day was evaluated using pilot mice blood samples that determined this achieved blood concentrations approximately similar to the 72H IC50 determined in the *in vitro* studies conducted previously. The Alzet topotecan dose of 0.1mg/kg/day achieved a concentration approximately 4% of the calculated IC50 concentration. No significant differences in tumor volumes were found between the IV conventional mice and the IV

control and Alzet control, however, each Alzet topotecan dose achieved a significant difference (p<0.05) when compared to the Alzet control. Additionally, there was no significant differences in animal weights for any treatment group, indicating similar toxic effects. These results indicate that continuous or metronomic dosing of topotecan results in significantly less tumor growth relative to conventional dosing of topotecan and without significantly increased toxicity.[3]

The drastic *in vivo* efficacy improvement by metronomic topotecan supported a need to better understand the underlying molecular mechanisms that drove this efficacy improvement. This would not only drive novel drug development but would also further support the use of metronomic dosing clinically. Initially, we assessed whether previously identified alternative mechanisms of metronomic dosing would help explain our findings. In general, an *in vivo* model system allows for assessment of more complex interactions including the immunologic or angiogenic mechanisms that are important to some metronomic based regimens. However, the NCr nude mouse model used in this study is athymic and lacks functional T-cells, which drastically reduces the probability that the immune system plays a significant role in our treatment response. Specifically, although a small number of T-cells are present in these mice due to alternative activation mechanisms, the overall immune system is significantly inhibited.[20] Regulatory T-cells most likely do not play a significant role in tumor response in this model system and the adaptive arm of the immune system is significantly hampered without adequate activation through helper T cells.[21] Therefore, although some aspects

of the mouse immune system remain intact in an athymic mouse model, the parts most

affected are also those that are most important in explaining the metronomic effect.

Figure 2

Factor VIII (vascular staining)
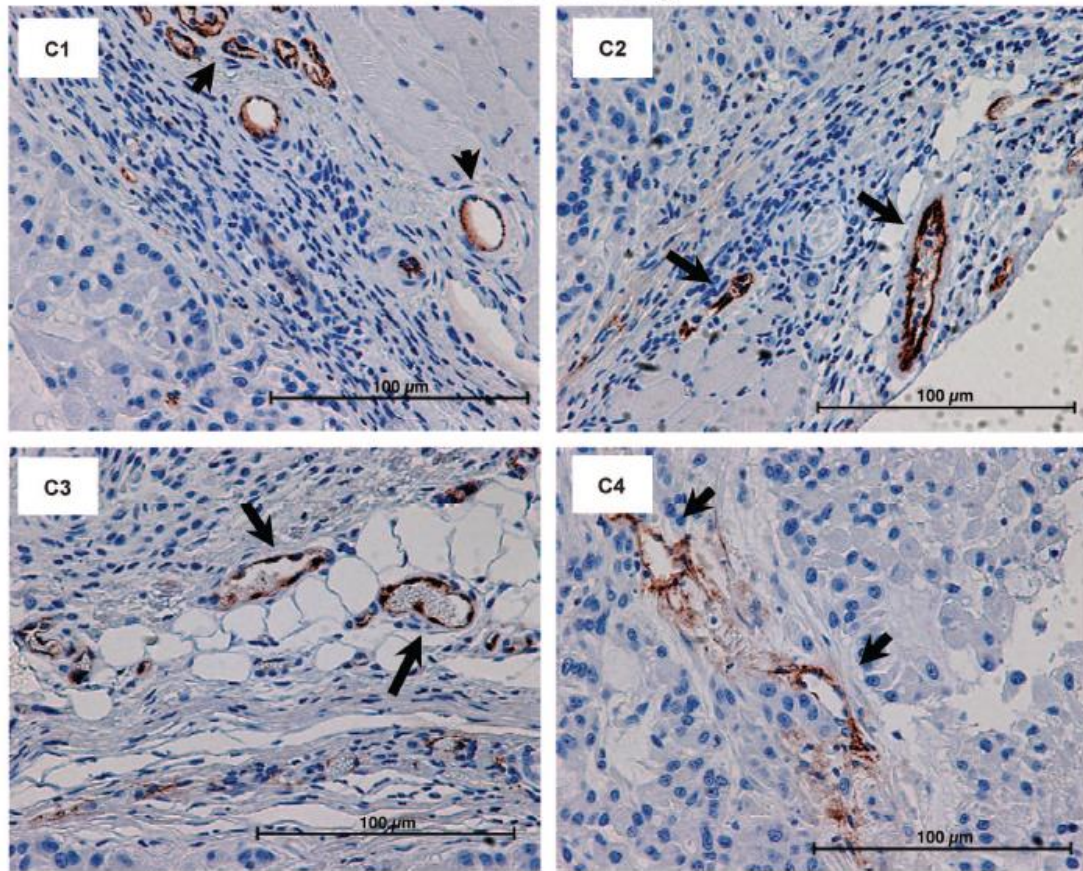
Figure 2. **The effect of different dosing schedules of topotecan on tumor vascular density in a PC3 xenograft mouse model.** Tumors were harvested after 28 days of treatment, sectioned, and stained with factor VIII. Vasculature is denoted with black arrowheads. Included are samples from the 4mg/kg conventional IV treatment (C1), the 2.45mg/kg/day ALZET treatment (C2), the 0.1mg/kg/day ALZET treatment (C3), and the ALZET vehicle control (C4). No significant differences in vascular density were found in any treatment group.[3]

Because of these issues, immunologic effects do not adequately explain the efficacy difference between metronomic and conventional topotecan in our model system.

Next, angiogenesis was assessed to determine whether it could adequately explain the metronomic effect of topotecan. **Figure 2** was generated using tumor samples from mice treated in **figure 1**. The tumors were sectioned and stained with factor VIII to visualize endothelial cells. The conventional 4mg/kg IV sample is visualized in C1, the 2.45mg/kg/day ALZET sample (metronomic) is presented in C2, the 0.1mg/kg/day ALZET sample (metronomic) is shown in C3, and the ALZET vehicle control is in C4. These samples were sent to a blinded pathologist for evaluation. No significant difference in the vascular density of any sample was found by the pathologist. This suggests that the mechanism of action of metronomic topotecan is less likely to rely heavily on angiogenesis, at least in our model system.[10]

Although traditional direct cytotoxic mechanisms may explain part of the observed response, it would be difficult to explain how a lower concentration can achieve a greater effect as this would contradict the basic dose-response-effect concept. In **figure 3**, we used a 2D *in vitro* model of PC3 cells to compare the efficacy of metronomic topotecan to conventional topotecan after 72 hours of treatment. PC3 cells (ATCC) were initially grown in F12K (Corning) /10% FBS (Hyclone) in cell culture flasks (Corning) until sufficient quantity was available to seed 96 well flat bottom flasks (Falcon). Seeded cells were allowed to grow for 24 hours prior to initiation of treatments. Conventionally dosed topotecan occurred as a single dose on day 0 at concentrations (0.001nM-10,000nM) and metronomically dosed topotecan occurred as

a fractionated dose on days 0, 1, 2 at 1/3rd the conventional concentrations to achieve 1/1 cumulative exposure. After 24 hours following the final metronomic dose, cells were analyzed using standard Thiazolyl blue tetrazolium bromide (**MTT**) (Sigma life sciences) and sulforhodamine B (**SRB**) (Biotinum) techniques. After treatment, conventionally dosed topotecan achieved an MTT IC50 of 189.6nM and an SRB IC50 of 115.3nM and metronomically dosed topotecan achieved an MTT IC50 of 177nM and an SRB IC50 of 159.5nM. None of the IC50s were statistically different. These results demonstrate similar efficacy regardless of the dosing schedule. Therefore, although the *in vitro* data shows that metronomic therapy has some direct effects, they are not sufficient to explain the efficacy differences found *in vivo*.

Metronomic chemotherapy is thought to cause antiangiogenic, immunologic, or direct cytotoxic effects, however, based on our previous *in vivo* data, angiogenic and immunologic mechanisms are not the likely causes of metronomic topotecan's increased potency. Our *in vitro* data suggests that metronomic topotecan does have some direct effects, but alone, these would not cause improved potency relative to conventional topotecan. In light of this information, a new mechanism is needed to help explain the potency differences of metronomic topotecan *in vivo*.

Figure 3

A

Conventional vs Metronomic Dosing: MTT after 72Hours of Topotecan Exposure

B

Conventional vs Metronomic Dosing: SRB after 72Hours of Topotecan Exposure
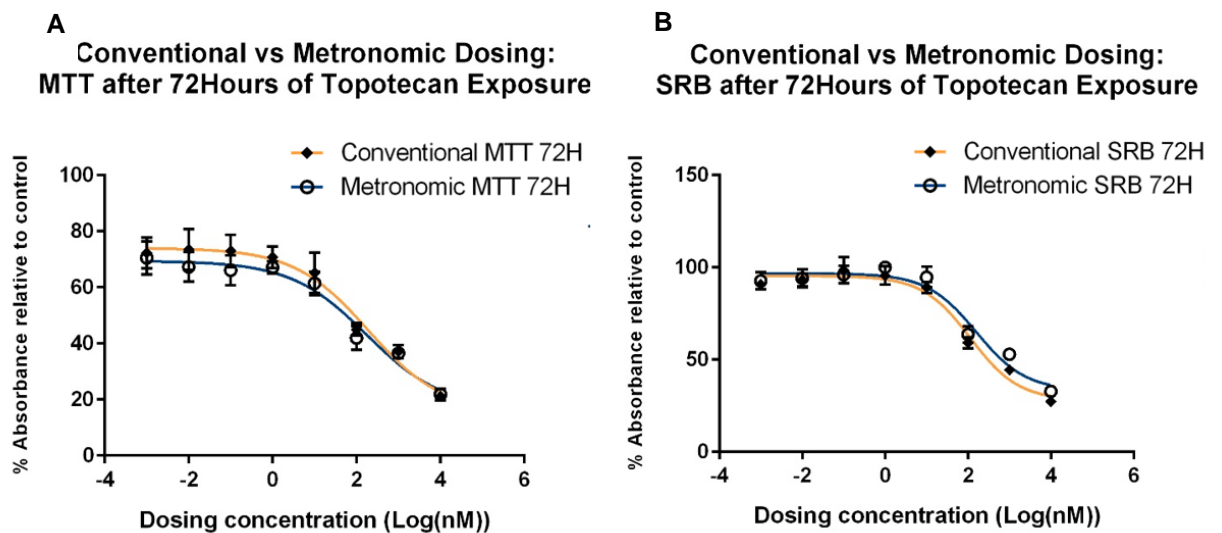
Figure 3. The effect of different dosing schedules of topotecan on PC3 cells grown *in vitro*. Cells were seeded at 5000 cells/mL in 96 well plates and grown for 24 hours prior to the first dose. The conventional dose was given at day 0 as a single bolus dose using concentrations (0.001nM-10000nM) and the metronomic dose was given at days 0, 1, 2 as a fractionated dose at 1/3 the conventional dose. At the end of the experiment, each treatment group was exposed to the same cumulative dose. (A) represents the MTT mitochondrial assay and (B) represents the SRB protein assay. Each assay was taken 24 hours following the last metronomic dose.

4. Identifying a Novel Potential Mechanism of Metronomic Topotecan

Overview of the Molecular Mechanisms of DNA Repair

Although it is common to view DNA as an inherently stable molecule that only becomes unstable from outside influences such as drugs or radiation, in reality, DNA is constantly enduring genetic insults from both endogenous and exogenous mechanisms such as metabolic accidents, heat, radiation, oxidation, hydrolysis, or environmental toxins. It is estimated that out of the tens of thousands of mutation events that occur each day, only approximately 0.02% become permanent. The remaining events are repaired with remarkable accuracy and tenacity by the cell using a variety of different repair mechanisms.[26] A brief overview of the most common types of DNA damage will be discussed below to provide context for the corresponding repair mechanism.

Endogenous DNA damage

Hydrolysis is an extremely common endogenous mutational event that occurs spontaneously and primarily affects the nucleotide base. Although hydrolysis of the phosphate backbone can occur, it doesn't occur frequently in normal metabolic conditions. Hydrolysis of the base on the other hand can occur thousands of times per day. More specifically, hydrolysis of the N-glycosyl linkage between the nucleotide base and the deoxyribose of the phosphate backbone will dislodge the base and lead to a depurination/depyrimidination event. The remaining DNA strand will lack a nucleotide base, which can lead to improper deletion of the nucleotide on both strands during replication if unrepaired. Hydrolysis can also cause deamination (**figure 4**) of cytosine to

uracil, of adenine to hypoxanthine, of guanine to xanthine, or of 5-methylcytosine, a

common epigenetic modification, to thymine. Because thymine lacks an amine group, it

does not undergo deamination. These events are problematic as they can lead to

altered complementary base binding such as cytosine to uracil binding to adenine,

which can lead to mutational events if unrepaired. Reactive oxygen species (**ROS**)

produced by the cell can also cause oxidation of nucleotide bases (**figure 5**) such as

guanine to 8-oxo guanine or thymine to thymine glycol. In total, over 100 different

oxidative base lesions and 2-deoxyribose modifications can be caused by ROS. ROS also

cause an estimated 2300 single strand breaks per hour in mammalian cells.[23]

Additionally, highly reactive methyl donors such as S-adenosylmethionine (SAM) can

spontaneously generate methylated bases such as 7-methylguanine or 3-methyladenine

and N-nitroso compounds (**NOC**) can convert guanine to O^6-methylguanine, a highly

mutagenic alkylated base.[23,26] 7 and 3 methylguanine on the other hand are not

particularly problematic as they can only impede replication and do not generally lead

to mutagenic events.[23] Endogenous topoisomerases, which cause single or double

strand nicks in the phosphate backbone to alleviate torsional strain in the DNA double

helix during replication, can cause DNA damage if the resealing subunit becomes

stabilized and leaves the nicks unrepaired. These lesions can be repaired by reversal of

the stalled topoisomerase complexes or through excision from tyrosyl DNA

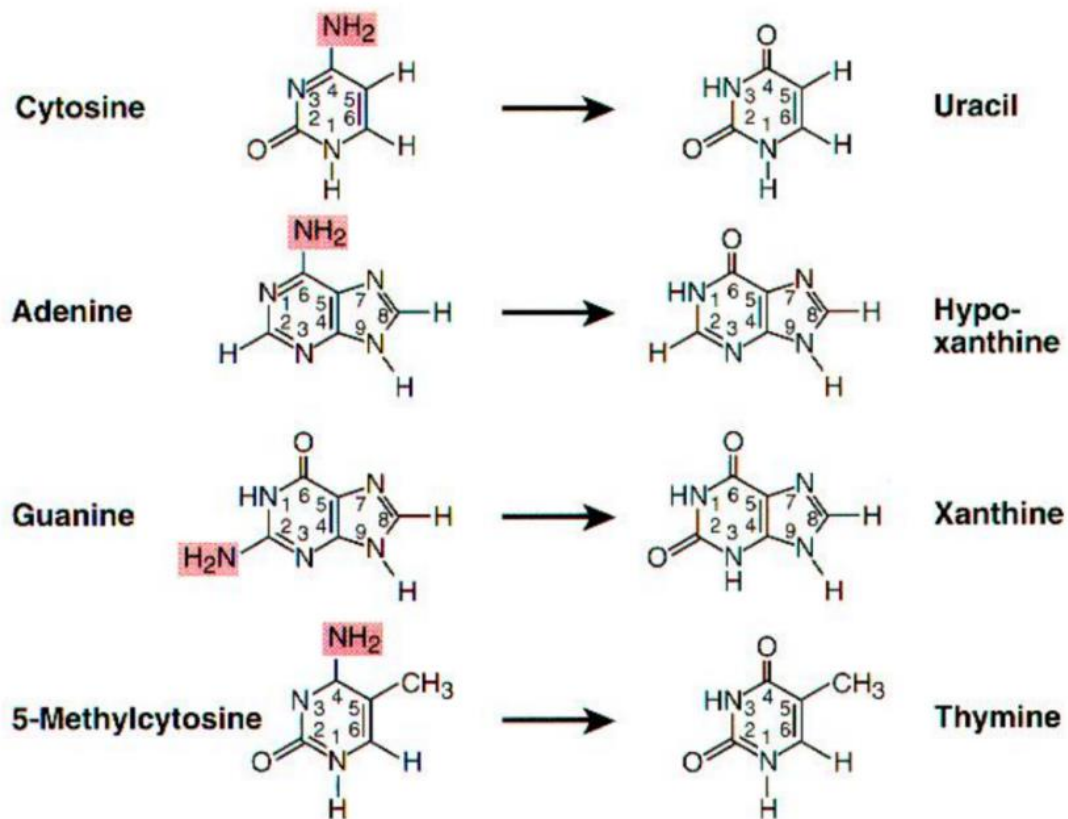phosphodiesterase 1 (**TDP1**) and endonucleases.[23]

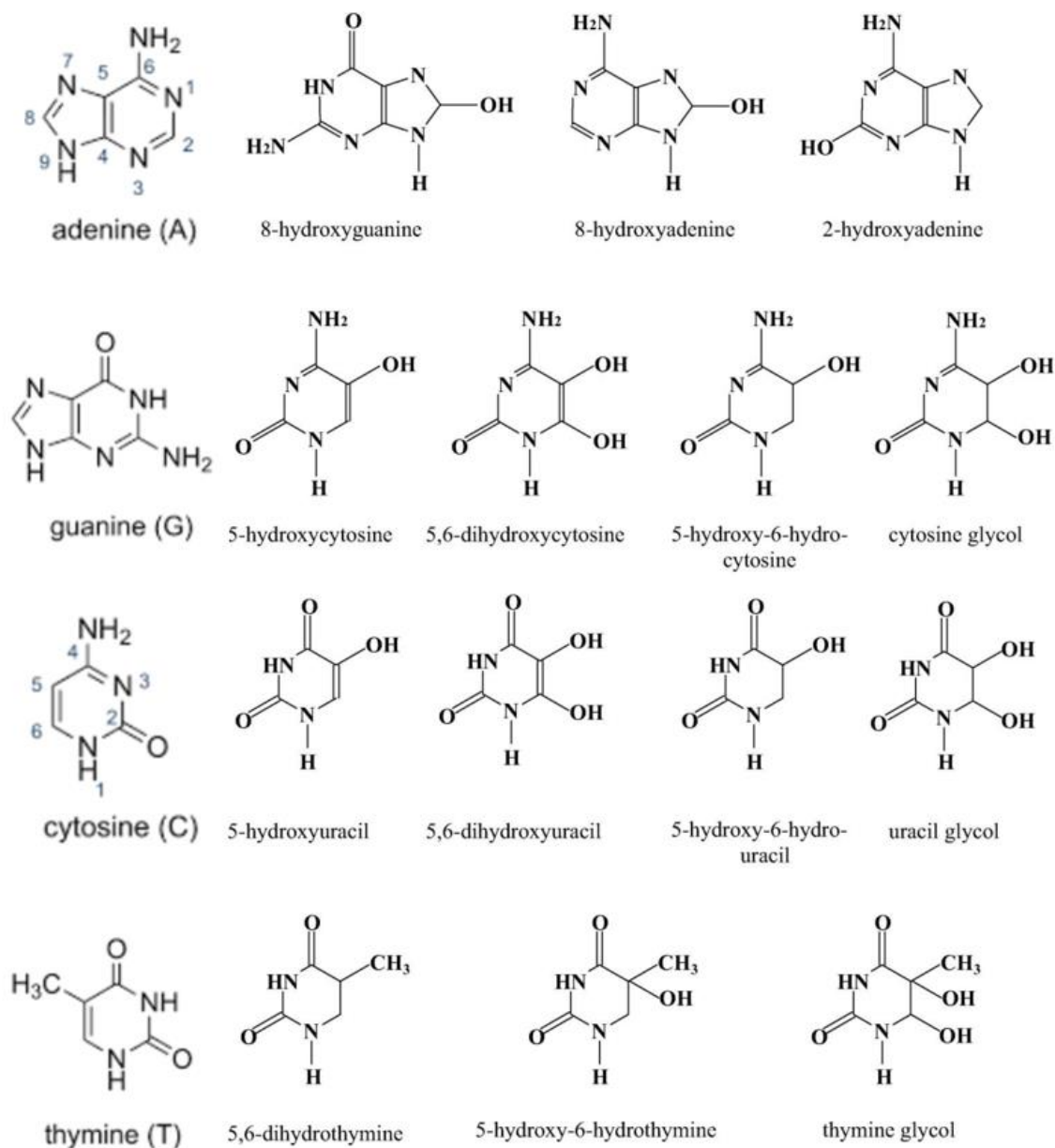**Figure 4:** Molecular structures of the common deamidation reactions and the resulting damaged byproduct.[50]

Figure 5: Molecular structures of the common oxidation reactions and the resulting damaged byproduct with normal bases added for reference.[51]

Exogenous DNA damage

The main causes of exogenous DNA damage are ionizing radiation, ultraviolet radiation, alkylating agents, and other specific drugs such as topoisomerase inhibitors, intercalators, or antimetabolites. Ionizing radiation occurs from neutron beams, alpha particles, beta particles, gamma rays, and X-rays. Neutron beams are formed only from neutrons, alpha particles contain 2 neutrons and 2 protons, beta particles are formed from electrons or positrons, and gamma and x rays are formed from photons. Ionizing radiation can be classified according to the ionization density of the underlying particle, which is the number of ions per path length. Said in another way, high ionization density leads to a greater number of ions created by the particle as it moves along its path. Alpha particles and neutron beams have high ionization density and beta particles, gamma rays, and x-rays have low ionization density. Ionizing radiation can damage DNA using two different mechanisms: direct and indirect. Direct acting ionizing radiation can cause single strand or double strand breaks in the DNA backbone, which can lead to significant mutagenesis if unrepaired. Alternatively, ionizing radiation can indirectly damage DNA by generating free radicals and ROS such as $OH^\bullet$, $O_2^\bullet$, or H_2O_2. These free radicals can produce a spectrum of base lesions similar to the hydrolysis or oxidative damage discussed in previous sections. Some of the most common lesions are 8-oxo-guanine and thymine glycol.[23]

Ultraviolet radiation, primarily from the sun, is another common exogenous cause of DNA damage. Because the depth of penetration is relatively shallow (20 to 150 μm), skin cells are the most at risk of exposure. However, the epidermal layer can be as

thick as 1500μm in areas such as the soles of the hands and feet or as thin as 50μm in

the eyelids causing some deeper dermal layers to receive some ultraviolet exposure.[28]

Ultraviolet radiation is classified according to the wavelength into UV-C (190-290nm),

UV-B (290-320nM), and UV-A (320-400nM). Because the maximal UV absorption of DNA

is at 260nM, UV-C is the most dangerous. Similar to ionizing radiation, ultraviolet

radiation can cause both direct and indirect effects by transferring excess energy to the

DNA molecule or surrounding molecules. The primary mechanism of ultraviolet

radiation depends on the type of UV radiation affecting the cell. UV-C primarily acts

through covalent linkages between pyrimidines. The most common byproduct of this

radiation is cyclobutene pyrimidine dimers (**CPDs**) (Thymine/cytosine dimers) or

pyrimidone phosphoproducts (**PPs**). However, some other byproducts such as thymine

glycol or pyrimidine hydrate are possible. The overall effect of CPDs and PPs is the

creation of bulky dimers that distort the natural helical structure of DNA and prevents

replication forks from progressing during replication. UV-B also primarily causes

pyrimidine dimers, but is less efficient than UV-C and UV-A can cause CPDs, 8-oxoG,

oxidized pyrimidines, and SSB, but is much less efficient at inducing DNA damage

relative to UV-C.[23,29,30]

Another major cause of exogenous DNA damage are alkylating agents. Alkylating

agents can be formed from aromatic amines and polycyclic aromatic hydrocarbons from

natural products such as tobacco smoke, high temperature cooking, or from some

dietary components or from natural and synthetic chemotherapeutic agents such as

cisplatin or cyclophosphamide. Alkylating agents most commonly interact with the

nucleophilic ring nitrogens and to a lesser extent, the ring oxygens. Examples of specific

vulnerable regions include the N1, N3, N6, and N7 of adenine, the N1, N2, N3, N7, and

O6 of guanine, the N3, N4, and O2 of cytosine, and the N3, O2, and O4 of thymine.[23]

Alkylating agents form adducts between the alkylating agent and the DNA base through

nucleophilic attack of the DNA base causing ejection of a leaving group on the alkylating

agent. The resulting covalent bond between the DNA base and the alkylating agent

either results in a bulky addition to the DNA molecule, preventing adequate binding of

the molecular machinery to the DNA or in cross-linked DNA strands that prevent

unwinding of the DNA by helicases. The exact mechanism depends on the number of

leaving groups present on the alkylating agent. Either way, alkylating agents will halt

replication and can lead to apoptosis if unrepaired.[23, 28]

DNA damage repair

The 5 major DNA repair mechanisms are base excision repair (**BER**), nucleotide

excision repair (**NER**), mismatch repair (**MMR**), homologous recombination (**HR**), and

non-homologous end joining (**NHEJ**).[23,26] Other pathways include direct chemical

reversal and the Fanconi anemia DNA repair pathway, which are used for a few specific

types of DNA damage. Cells can also upregulate translesion synthesis (**TLS**) polymerases,

which specialize in bypassing stalled replication forks, but at the expense of accuracy.[23]

BER is used to overcome single nucleotide damage such as the oxidation,

alkylation, or hydrolysis reactions described above. These damaged bases are identified

and targeted using a variety of DNA glycosylases, which catalyze a hydrolysis reaction to

excise the damaged base. Each DNA glycosylases can recognize a specific type of damaged base such as uracil glycosylase, which functions to correct the deamination of cytosine. There are currently at least 11 known human glycosylases.[23] The excision of the damaged base leaves an abasic gap in the nucleotide chain but preserves the phosphate backbone. DNA glycosylases can either be monofunctional or bifunctional. Monofunctional DNA glycosylases initiate short patch repair and bifunctional glycosylases initiate long patch repair. In short patch repair, an endonuclease (apurinic/apyrimidinic endonucleases 1 (**APE1**)) recognizes the abasic site and cleaves the phosphate backbone leaving an open 3' hydroxyl group and a 5' deoxyribose phosphate flap. Polymerase β (**Pol β**) is then used to remove the flap and repair the single nucleotide gap and ligase (DNA ligase 1 (**LIG1**) or LIG3/X-ray repair cross contaminating protein (**XRCC**)) is used to seal the phosphate backbone. In long patch repair, Pol δ/ε is used to elongate the repair for a short stretch (2-12 nucleotides). The repair starts at the abasic site with the elongated repair strand displacing the damaged strand as the repair progresses. Flap endonuclease (**FEN1**) removes the displaced damaged DNA strand, leaving behind a nick in the phosphate backbone, which is repaired with LIG1.[23,26]

More extensive DNA damage that distorts the normal helical structure of DNA such as bulky lesions from large adducts or from UV dimers cannot be repaired using BER and instead recruits proteins associated with NER. NER is a more broad-based repair mechanism that can overcome a variety of different types of damage. NER is further subdivided into the global genomic repair (**GGR**) pathway and the transcription

coupled repair (**TCR**) pathway depending on the initiating protein. The GGR pathway is initiated when a damage probe complex made up of DNA damage sensor protein xeroderma pigmentosum complementation group C (**XPC**), RAD23B, and centrin 2 (**CETN2**) recognizes DNA damage with the help of ultraviolet DNA damage binding (**UV DDB**) proteins. The TCR pathway is initiated by an RNA polymerase II that has stalled at a damaged lesion. A complex of Cockayne syndrome group A and B (**CSA and CSB**) is formed, which results in reverse translocation of the RNA Pol II and allows access to the lesion. After initiation, each pathway converges with the recruitment of the transcription initiation factor II H (**TFIIH**) complex. This complex contains a helicase that is used to unwind the damaged region and allow greater access. Next, the XPD subunit verifies the lesion and the XPA and XPB subunits bind to the damaged strand. Replication protein A (**RPA**) is also recruited and coats the undamaged strand to protect it from further damage. Then, XPA recruits XPF/DNA excision repair protein 1 (**ERCC1**), which makes a cut at the 5' end a few nucleotides away from the lesion. XPG then cuts the 3' end a few nucleotides away, which releases a 22-30 nucleotide long strand. Finally, proliferating cell nuclear antigen (**PCNA**) recruits DNA pol δ, DNA Pol κ, or DNA Pol ε to fill the resulting DNA gap and LIG1 or LIG3 seals the phosphate backbone.[23,26,38]

The MMR pathway is integral in postreplication processing to correct spontaneous base-base mispairs and small insertion-deletion loops that occur during replication. Combining MMR with the replication machinery drastically increases the overall fidelity (even up to 100 fold) of the repair process and improves the overall genetic stability of the cell. MMR is initiated from the MutS protein, which is responsible

for mismatch detection in double stranded DNA. The newly replicated strand is preferentially chosen to undergo repair because this strand contains nicks and is unmethylated relative to the parent strand. This is important for mismatched nucleotides, which would otherwise have a 50-50 chance of being repaired to the incorrect nucleotides. After recognition, MutS undergoes a conformational change, which allows the protein to bind to the mismatched lesion. MutL, MutH, and UvrD is recruited to the complex. Exo1 is used to nick the strand upstream from the lesion and remove a strand of DNA containing the mismatched bases. Pol δ is then used to fill the gap and LIG1 seals the phosphate backbone. [23,26,39]

For a small subset of DNA lesions including some UV lesions and alkylated bases, the cell can directly reverse the damage. It does this using specific enzymes such as O^6 alkylguanine-DNA alkyltransferase (**AGT/MGMT**) and AlkB related α-ketoglutarate-dependent dioxygenase (human homologs are **AlkBH1-8** and **FTO**). MGMT primarily reverses O^6 alkylguanine damage and can even repair O^6 intrastrand crosslinks.[23,31] It functions as a suicide repair enzyme, meaning the act of transferring the alkyl group to the enzyme leads to inactivity and degradation of the enzyme. Separately, the AlkB enzymes reverse N-alkylated base adducts. In contrast to MGMT, which is specific to the O^6 alkylguanine adducts, the AlkB enzymes are more promiscuous and function to repair many types of N-alkylated bases including the N1/N6 of adenine, the N3/N4 of cytosine, the N1/N2 of guanosine, and the N3 of thymidine.[32,33] Oxidative dealkylation reactions are used to remove the alkyl group from the damaged base in the form of an aldehyde

byproduct. In this instance, the enzyme(s) can be recycled and do not require degradation.

The Fanconi anemia proteins currently consists of 22 different functional groups (A, B, C, D1, D2, E, F, G, I, J, L, M, N, O, P, Q, R, S, T, U, V, W).[23, 34] These proteins were first identified for their role in Fanconi anemia, which is a hereditary disease characterized by bone marrow failure and hypersensitivity to interstrand crosslinks.[34] Further investigation into the function of Fanconi anemia proteins revealed a significant role in repairing interstrand crosslinks and further supported their causative role in Fanconi anemia. Through a series of complex interactions, interstrand crosslink damage is identified and Fanconi anemia proteins are recruited to the damaged stie. A core complex is assembled and the Fanconi anemia pathway is activated, which results in excision of the lesion by endonucleases and unhooking of the interstrand crosslink from the daughter strand. The crosslink remains on one parenteral strand and impedes normal replication by traditional polymerases. To overcome this, translesion synthesis polymerases are recruited to bypass the interstrand crosslink remnant. Afterward, NER is utilized to remove the interstrand crosslink remnant from the parental strand. After these steps, one parental strand and one daughter strand is fully repaired but may have sustained mutations from the TLS polymerases. At this point, the remaining parental and daughter strands have sustained a double strand break due to the endonuclease activity and must be repaired with double strand break (**DSB**) repair mechanisms. If an appropriate sister chromatid is present, then HR can be used. Otherwise NHEJ is used.[23,34,35,36,37]

As discussed in the previous section, translesion synthesis polymerases are used to help bypass damaged sections of DNA that cannot adequately be replicated using the traditional replicative polymerases α, ε, δ. Replicative polymerases stall when they encounter damaged DNA. A few of the known human translesion synthesis polymerases include REV1, Polη, Polι, Polκ, Polζ, Polμ, Polλ, Polβ, Polv, Polθ. Some TLS polymerases can recognize specific types of DNA damage and can accurately repair the DNA with the appropriate base, but overall, TLS polymerases are much lower fidelity and are much less discerning in choosing which nucleotide to incorporate relative to the traditional replicative polymerases. Although TLS polymerases may lead to increased mutational activity relative to replicative polymerases, they allow the cell to survive heavy DNA damage that would ordinarily stimulate apoptosis. The TLS polymerases differ from the replicative polymerases by lacking the 3'-5' exonuclease proofreading domain and through structural changes in the protein that allow for more flexibility in the in the catalytic site to accept more variable DNA bases.[21,23]

DSBs are extremely concerning lesions for the cell because they can fragment the DNA and can potentially lead to significant loss of genetic material. Also, the traditional approach of using the reciprocal DNA strand as a template is not appropriate for this type of damage. Therefore, a different approach is needed to repair these lesions. The two major approaches are HR and NHEJ.

Of the two, NHEJ is the simplest and easiest to understand. In response to broken double stranded DNA, NHEJ simply rejoins the strands with little concern about the accuracy of the repair. Commonly, this method of repair leads to insertions and

deletions of genetic material and is a notoriously low fidelity repair mechanism. An

additional issue of NHEJ is the lack of regulatory proteins preventing interactions

between different DNA strands, which can make rearrangements relatively likely.

However, because the potential risk from an unrepaired DSB is so high, it is an

apparently acceptable tradeoff for the cell. NHEJ begins with the attachment of Ku

heterodimers (Ku70/Ku80) to the ends of the DSB to prevent end resection and to serve

as a scaffold for the remaining NHEJ components. DNA-dependent protein kinases

(**DNA-PKcs**) is then recruited to the area which functions to phosphorylate itself and

other NHEJ components. XRCC4 is then recruited to help tether the Ku heterodimers

together and act as a scaffold for other components. These include the nuclease,

polymerase, and ligase components. The nuclease component consists of an Artemis—

DNA PKcs complex, which can act as an endonuclease or an exonuclease and mainly

functions to remove any undesirable overhangs to allow strand joining. The polymerase

component uses either Pol μ or Pol λ. Pol μ is particularly beneficial as it can undergo

template independent and template dependent synthesis. Finally, the ligase complex

consists of a XLF—XRCC4 complex and LIG4, which is the most flexible ligase known and

has the capability to ligate across gaps and to ligate incompatible DNA ends. It can also

ligate individual strands when the reciprocal strand cannot yet be ligated due to flaps or

other DNA complexes. Other important components include polynucleotide kinase

(**PNKP**), which functions as a phosphatase and kinase to help process the damaged ends,

aprataxin and PNKP like factor (**APLF**), which functions as an endonuclease and 3'

exonuclease, and aprataxin, which functions to remove adenosine monophosphate

(**AMP**) from DNA ends after aborted ligation attempts. Simplified, NHEJ recognizes the DSB, processes the DNA termini, and then joins the processed termini.[23,26,40]

In contrast to NHEJ, HR is a much higher fidelity repair mechanism and is generally error free. HR is a templated repair process that uses the sister chromatid as a frame of reference. Because of this, HR is usually only used when duplicate chromatids are available, which is predominately in the S and G2 phase of the cell cycle. Overall, NHEJ is used most frequently in the G1 phase, HR is used most frequently in the S phase, NHEJ and HR compete during the G2 phase and both are down regulated during the M phase.[41] HR is initiated when the MRN complex (meiotic recombination 11 (**MRE11**), RAD50, Nijmegen breakage syndrome 1 (**NBS1**)) recognizes and binds to the DSB and recruits ataxia-telangiectasia mutated (**ATM**) and lysin acetyltransferase (**TIP60**). ATM is an extremely important protein that phosphorylates hundreds of downstream proteins to bring about HR and to cause cell cycle arrest. ATM also phosphorylates H2AX variant histone (**H2AX**), which is a type of histone protein that functions as a DNA damage sensor and helps to recruit other proteins to the area, including additional ATM molecules, which phosphorylate additional H2AX proteins in a positive feedback loop. Mediator of DNA damage checkpoint 1 (**MDC1**) is also phosphorylated by ATM and functions as a scaffold for ring finger protein (**RNF**)8 and RNF168, which functions to ubiquitinate H2AX, allowing binding of tumor protein P53 binding protein 1 (**TP53BP1**) and breast cancer gene 1 (**BRCA1**). Interaction between 53BP1 and BRCA1 acts to regulate HR and prevent activation during phases of the cell cycle when sister chromatids are not present.[42] If HR occurs when the sister chromatids are not present,

an exchange between the maternal and paternal chromatics could occur leading to a loss of heterozygosity. This is most important when the cell possesses one functional and one non-functional gene. Although repairing the functional gene using the non-functional gene as a template would result in an accurate repair, the loss of heterozygosity would impede cellular function and could potentially lead to oncologic events. To prevent these issues, TP53BP1 negatively regulates the HR pathway during the G1 phase and must be removed by BRCA1 to allow progression of the HR pathway. BRCA1 is upregulated during S phase and promotes HR. In cells lacking BRCA1, NHEJ is used and leads to gross chromosomal rearrangements during the S phase. One HR is chosen, additional HR components are recruited and short end resection occurs using MRN and CtIP generating a 3' overhang and committing the cell to the HR pathway. Next, long resection occurs using exonuclease 1 (**EXO1**), DNA replication helicase/nuclease 2 (**DNA2**), and BLM RecQ like helicase (**BLM**). The resection is coated with RPA, which recruits ATR serine/threonine kinase (**ATR**) and ATR interacting protein (**ATRIP**), which function with ATM to unleash a second wave of phosphorylation events. Next, a complex of BRCA2, partner and localizer of BRCA2 (**PALB2**), BRCA1 associated RING domain 1 (**BARD1**), and BRCA1 lead to displacement of RPA with RAD51, which generates a RAD51 nucleoprotein filament with the damaged DNA strand. The RAD51-DNA filament is an important structure for homology search and strand invasion of the sister chromatid. This filament invades a nearby DNA duplex and forms a D-loop. RAD54 and RAD54B then remove RAD51 to expose the DNA strand and initiate priming by RNA polymerase. From here, a number of different pathways of HR can occur including

synthesis dependent strand annealing, break induced replication, and holiday junction

resolution. The regulation of these pathways and the repair is extremely complex and

utilizes a large number of different complexes such as BLM-TOPOIII-RMI1-RMI2 (RecQ

mediated genome instability 1/2 (**RMI1/2**)) complex, GEN1 holliday junction 5' flip

endonuclease (**GEN1**), MUS81 structure specific endonuclease subunit-Essential meotic

structure specific endonuclease (**MUS81-EME1**) complex, and the SLX1-4 homolog A

structure specific endonuclease subunit (**SLX1-SLX4**) complex for resolution of the

holiday junction. Overall, the main difference between each of these subpathways is the

probability of cross overs occurring. A cross over is the connection of two distinct DNA

molecules that results in two unique sister chromatids with genetic material from each

sister chromatid. SDSA is the predominate HR pathway and results in no cross over DNA

while HJ resolution has a 50% probability of a cross over.[23,26,42,43,44,45,46]

A schematic of the DSB repair pathways is included (**figure 6**) to help visualize

these processes. An important characteristic of each repair process, which will become

important later when describing the overall hypothesis, is the complexity of each

pathway. Not only does NHEJ rely on fewer proteins to function, it is also a simpler,

quicker, and more straightforward process. HR on the other hand is much more complex

and requires a significantly greater number of proteins. Currently, there are 7 specific

genes used in NHEJ and over 35 unique genes in HR.[53] HR also includes multiple

subpathways, which further adds complexity. The act of pulling sister chromatids

together, searching for sequence homology, and using the sister chromatid as a

template is an extremely complex process. Additionally, the repair fidelity of each

pathway is extremely important. NHEJ is typically a lower fidelity repair mechanism that results in a high frequency of insertions and deletions and can drastically increase the mutation rate of the cell if used extensively. HR typically is a high-fidelity repair mechanism that can frequently repair the DNA error free. Importantly, though the fidelity of each pathway is generally low or high, there are exceptions depending on the specific repair that can sometimes result in a higher fidelity repair from NHEJ relative to HR. However, generally, HR is the less error prone pathway.
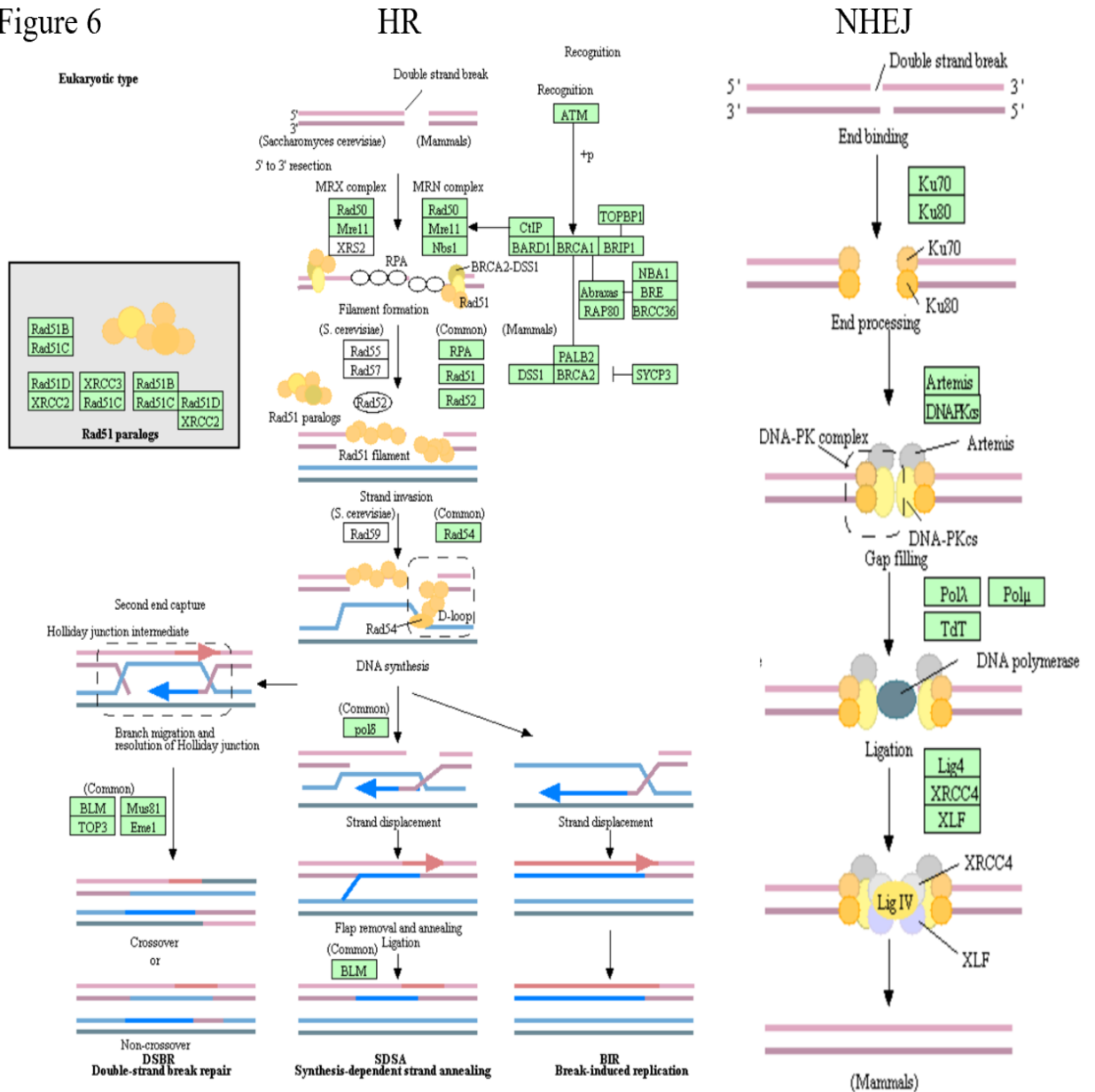
Figure 6: Schematic depicting the multi-step processes of homologous recombination (HR) and non-homologous end joining (NHEJ).[47,48,49]

5. The mechanism of action of topotecan

For replication to occur, DNA must be unwound and separated to provide access to the replication machinery. However, unwinding creates a supercoiling problem that increases tension across the DNA strand as the replication fork moves along the DNA. Eventually, if left alone, this tension would lead to breaks in the phosphate backbone. To prevent this issue, the cell has developed mechanisms such as topoisomerases to help relieve this strain. Topoisomerases create nicks in the phosphate backbone, which allows the two sections on either side of the replication fork to move freely, which relieves the torsional strain. Topoisomerase I causes a single nick and topoisomerase II causes two nicks and forms a DSB. The nicks are temporary and can be repaired by the topoisomerases when they are no longer needed.[23,36]

Topotecan is a topoisomerase I inhibitor that can bind to the topoisomerase-DNA complex, can prevent religation of the nicks, and can prevent detachment of the enzyme. When the replication fork collides with the inhibited topoisomerase I enzyme, a double strand break occurs. As described above, these DSBs can be particularly dangerous for the cell and must be repaired to prevent massive loss of genetic material. However, if the cell is unable to appropriately repair the damage, it will undergo apoptosis.[26,53]

6. Metronomic topotecan may alter the repair mechanism of DSBs

Based on topotecan's mechanism of action, the quantity of DSBs created by the drug is directly proportional to the number of topoisomerase I molecules that are

inhibited, up to a point of potential saturation. As the concentration of topotecan increases, the number of inhibited topoisomerase I molecules also increases, leading to a greater number of DSBs. Conventional topotecan is given as a large dose over a short period of time, which leads to a very large number of DSBs. Thus, for a cell to resume replication, a significant repair process must occur. Since HR is a slower, more complex, and more energetically demanding repair process, it is possible that NHEJ would be utilized relatively more frequently during times of crisis to ensure cell survival at the expense of accuracy. Based on the overall fidelity of each repair process, cells that utilize NHEJ more frequently would have an increased mutation rate relative to cells that more frequently rely on HR. Therefore, cells that survive conventional topotecan may have done so by relying more heavily on NHEJ, which may have increased the mutation rate of the cells. On the other hand, metronomic topotecan utilizes a lower dose and a longer exposure time, which decreases the intensity of DNA damage. Cells that encounter this type of damage may rely less on NHEJ, and therefore have a more genetically stable genome relative to conventionally dosed cells.

The probability of tumor resistance is directly related to the quantity of cancer cells, the environmental variability, the frequency of mutation, and the durability of the drug. Essentially, if resistance is based on achieving a specific mutation that reduces the activity of the drug, then the probability of achieving drug resistance is calculated based on the mutation frequency and the number of mutations that are needed to achieve resistance. If an enzyme requires 4 simultaneous mutations to reduce the drug's binding affinity, then the probability of achieving resistance is much lower than an enzyme that

only requires 1 mutation. Similarly, a cell that mutates more frequently will have more chances to hit the right combination of mutations to achieve drug resistance.

Clinical drug exposure to chemotherapy is limited by how much toxicity the patient can endure and makes killing every cancer cell nearly impossible. Therefore, it is imperative to focus not only on reducing tumor growth, but also on what happens to the cells that survive each round of chemotherapy. Long-term treatment efficacy is not based on a single potency measurement, but rather on the average potency over time. If a drug is extremely potent on the first dose but causes the surviving cells to become more adaptable (genetically unstable), then the average potency over time will be reduced and the long-term efficacy will decrease. Similarly, a therapy that is less aggressive and does not increase the adaptability of cancer cells may appear less efficacious initially but can still achieve acceptable long-term potency.

Based on the above theoretical mechanisms, while conventional topotecan may lead to higher initial potency, it also creates more genetically unstable cells. These cells are able to adapt to a greater and greater degree based on the mutation frequency of the cells. Metronomic topotecan might kill fewer cells initially but will result in a more genetically stable tumor population for subsequent doses. Conventional topotecan will generate resistance much faster than metronomic topotecan, which explains the long-term potency differences seen in the previous animal model. While both therapies were efficacious for the first few weeks, over time, conventional topotecan lost potency as the treated population became more and more resistant. Metronomic topotecan maintains its potency for a longer period of time by maintaining a more consistent

tumor cell population. Experimentally, this led to a stable and consistent drug response for the entirety of the experiment.

7. Conclusion

The effects of metronomic dosing have been explained using antiangiogenic, direct cytotoxic, and immunologic mechanisms. However, based on our previous *in vivo* model system, these mechanisms do not adequately explain the significant efficacy difference between metronomic and conventional topotecan. In order to more accurately explain these results, a more appropriate mechanism needed to be identified. Because we were seeing improved long-term potency without improved short-term potency, it was hypothesized that metronomic topotecan improved potency by maintaining sensitivity over a longer period of time relative to conventional topotecan. Based on the underlying mechanism of action of topotecan, the DSB repair pathway had the highest potential to explain our results. The high intensity of the conventional regimen may force cells to make a decision between survival and genomic stability. Cells that survive conventional therapy may have significantly increased mutation rates, which directly increases the potential for drug resistance. Metronomic uses a more constant exposure with a lower dose that allows more accurate repair. The cells that survive metronomic therapy may be more genetically stable and less likely to develop drug resistance. While each regimen can inhibit tumor cells, metronomic dosing may lead to a more durable response.

References

1. Hanahan D, Bergers G, Bergsland E (2000) Less is more, regularly: metronomic dosing of cytotoxic drugs can target tumor antiangiogenesis in mice. J Clin Invest 105:1045–1047

2. Man S, Bocci G, Francia G, Green SK, Jothy S, Hanahan D, Bohlen P, Hicklin DJ, Bergers G, Kerbel RS (2002) Antitumor effects in mice of low-dose (metronomic) cyclophosphamide administered continuously through the draining water. Cancer Res 15:2731–2735

3. Aljuffali, I. A., Mock, J. N., Costyn, L. J., Nguyen, H., Nagy, T., Cummings, B. S., & Arnold, R. D. (2011). Enhanced antitumor activity of low-dose continuous administration schedules of topotecan in prostate cancer. *Cancer Biology and Therapy*, *12*(5), 407–420. https://doi.org/10.4161/cbt.12.5.15950

4. Biziota, E., Mavroeidis, L., Hatzimichael, E., & Pappas, P. (2017). Metronomic chemotherapy: A potent macerator of cancer by inducing angiogenesis suppression and antitumor immune activation. *Cancer Letters*, *400*, 243–251. https://doi.org/10.1016/j.canlet.2016.12.018

5. Chen, Y.-L., Chang, M.-C., & Cheng, W.-F. (2017). Metronomic chemotherapy and immunotherapy in cancer treatment. *Cancer Letters*, *400*, 282–292. https://doi.org/10.1016/j.canlet.2017.01.040

6. Maiti, R. (2014). Metronomic chemotherapy. *Journal of Pharmacology and Pharmacotherapeutics*, *5*(3), 186. https://doi.org/10.4103/0976-500X.136098

7. Romiti, A., Falcone, R., Roberto, M., & Marchetti, P. (2017). Current achievements and future perspectives of metronomic chemotherapy. *Investigational New Drugs*, *35*(3), 359–374. https://doi.org/10.1007/s10637-016-0408-x

8. Rajasekaran, T., Ng, Q. S., Tan, D. S. W., Lim, W. T., Ang, M. K., Toh, C. K., … Tan, E. H. (2017). Metronomic chemotherapy: A relook at its basis and rationale. *Cancer Letters*, *388*, 328–333. https://doi.org/10.1016/j.canlet.2016.12.013

9. Kareva, I., Waxman, D. J., & Klement, G. L. (2015). Metronomic chemotherapy: An attractive alternative to maximum tolerated dose therapy that can activate anti-tumor immunity and minimize therapeutic resistance. *Cancer Letters*, *358*(2), 100–106. https://doi.org/10.1016/j.canlet.2014.12.039

10. Hao, Y. Bin, Yi, S. Y., Ruan, J., Zhao, L., & Nan, K. J. (2014). New insights into metronomic chemotherapy-induced immunoregulation. *Cancer Letters*, *354*(2), 220–226. https://doi.org/10.1016/j.canlet.2014.08.028

11. Wichmann, V., Eigeliene, N., Saarenheimo, J., & Jekunen, A. (2020). Recent clinical evidence on metronomic dosing in controlled clinical trials: a systematic literature review. *Acta Oncologica*, *59*(7), 775–785. https://doi.org/10.1080/0284186X.2020.1744719

12. Cazzaniga, M. E., Cordani, N., Capici, S., Cogliati, V., Riva, F., & Cerrito, M. G. (2021). Metronomic chemotherapy. *Cancers*, *13*(9), 1–27. https://doi.org/10.3390/cancers13092236

13. Bocci, G., & Francia, G. (2014). *Metronomic chemotherapy: Pharmacology and clinical applications*. (G. Bocci & G. Francia, Eds.), *Metronomic Chemotherapy:*

Pharmacology and Clinical Applications (Vol. 5). Berlin, Heidelberg: Springer Berlin Heidelberg. https://doi.org/10.1007/978-3-662-43604-2

14. Simsek, C., Esin, E., & Yalcin, S. (2019). Metronomic Chemotherapy: A Systematic Review of the Literature and Clinical Experience. *Journal of Oncology*, *2019*(November 2017). https://doi.org/10.1155/2019/5483791

15. Mross, K., & Steinbild, S. (2012). Metronomic anti-cancer therapy – an ongoing treatment option for advanced cancer patients. *Journal of Cancer Therapeutics and Research*, *1*(1), 32. https://doi.org/10.7243/2049-7962-1-32

16. Torimura, T., Iwamoto, H., Nakamura, T., Koga, H., Ueno, T., Kerbel, R. S., & Sata, M. (2013). Metronomic chemotherapy: Possible clinical application in advanced hepatocellular carcinoma. *Translational Oncology*, *6*(5), 511–519. https://doi.org/10.1593/tlo.13481

17. Bertolini F, Paul S, Mancuso P, Monestiroli S, Gobbi A, Shaked Y, Kerbel RS (2003) Maximum tolerable dose and low-dose metronomic chemotherapy have opposite effects on the mobilization and viability of circulating endothelial progenitor cells. Cancer Res 63:4342–4346

18. Bocci G, Francia G, Man S, Lawler J, Kerbel RS (2003) Thrombospondin-1, a mediator of the antiangiogenic effects of low-dose metronomic chemotherapy. Proc Natl Acad Sci U S A 100:12917–12922

19. Rapisarda A, Zalek J, Hollingshead M, Braunschweig T, Uranchimeg B, Bonomi CA, Borgel SD, Carter JP, Hewitt SM, Shoemaker RH, Melillo G (2004) Schedule-dependent inhibition of hypoxia-inducible factor-1 alpha protein accumulation,

angiogenesis, and tumor growth by topotecan in U251-HRE glioblastoma xenografts. Cancer Res 64:6845–6848

20. Sim, G. K. (1995). Intraepithelial Lymphocytes and the Immune System. *Advances in Immunology*, *58*(C), 297–343. https://doi.org/10.1016/S0065-2776(08)60622-7

21. Alberts B, Johnson A, Lewis J, et al. Molecular Biology of the Cell. 6th edition. New York: Garland Science; 2002. Helper T Cells and Lymphocyte Activation. Available from: https://www.ncbi.nlm.nih.gov/books/NBK26827/

22. Turgeon, M. O., Perry, N. J. S., & Poulogiannis, G. (2018). DNA damage, repair, and cancer metabolism. *Frontiers in Oncology*, *8*(FEB). https://doi.org/10.3389/fonc.2018.00015

23. Chatterjee, N., & Walker, G. C. (2017). Mechanisms of DNA damage, repair, and mutagenesis. *Environmental and Molecular Mutagenesis*, *58*(5), 235–263. https://doi.org/10.1002/em.22087

24. Li, L. Y., Guan, Y. Di, Chen, X. S., Yang, J. M., & Cheng, Y. (2021). DNA Repair Pathways in Cancer Therapy and Resistance. *Frontiers in Pharmacology*, *11*(February), 1–13. https://doi.org/10.3389/fphar.2020.629266

25. Torgovnick, A., & Schumacher, B. (2015). DNA repair mechanisms in cancer development and therapy. *Frontiers in Genetics*, *6*(APR), 1–15. https://doi.org/10.3389/fgene.2015.00157

26. Alberts, B., Johnson, A., Lewis, J., Morgan, D., Raff, M., Roberts, K., & Walter, P. (2017). *Molecular Biology of the Cell*. (J. Wilson & T. Hunt, Eds.). W.W. Norton & Company. https://doi.org/10.1201/9781315735368

27. Weinberg, R. A. (2013). *The Biology of Cancer*. W.W. Norton & Company.

    https://doi.org/10.1201/9780429258794

28. Sandby-Møller, J., Poulsen, T., & Wulf, H. C. (2003). Epidermal Thickness at Different

    Body Sites: Relationship to Age, Gender, Pigmentation, Blood Content, Skin Type and

    Smoking Habits. *Acta Dermato-Venereologica*, *83*(6), 410–413.

    https://doi.org/10.1080/00015550310015419

29. Rochette, P. J., Therrien, J. P., Drouin, R., Perdiz, D., Bastien, N., Drobetsky, E. A., &

    Sage, E. (2003). UVA-induced cyclobutane pyrimidine dimers form predominantly at

    thymine-thymine dipyrimidines and correlate with the mutation spectrum in rodent

    cells. *Nucleic Acids Research*, *31*(11), 2786–2794.

    https://doi.org/10.1093/nar/gkg402

30. Dunkern, T. R., Fritz, G., & Kaina, B. (2001). Ultraviolet light-induced DNA damage

    triggers apoptosis in nucleotide excision repair-deficient cells via Bcl-2 decline and

    caspase-3/-8 activation. *Oncogene*, *20*(42), 6026–6038.

    https://doi.org/10.1038/sj.onc.1204754

31. Pegg, A. E. (2011). Multifaceted Roles of Alkyltransferase and Related Proteins in

    DNA Repair, DNA Damage, Resistance to Chemotherapy, and Research Tools.

    Chemical Research in Toxicology, *24*(5), 618–639.

    https://doi.org/10.1021/tx200031q

32. Xu, B., Liu, D., Wang, Z. *et al.* Multi-substrate selectivity based on key loops and non-

    homologous domains: new insight into ALKBH family. *Cell. Mol. Life Sci.* **78,** 129–141

    (2021). https://doi.org/10.1007/s00018-020-03594-9

33. Fedeles, B. I., Singh, V., Delaney, J. C., Li, D., & Essigmann, J. M. (2015). The AlkB family of Fe(II)/α-ketoglutarate-dependent dioxygenases: Repairing nucleic acid alkylation damage and beyond. *Journal of Biological Chemistry*, *290*(34), 20734–20742. https://doi.org/10.1074/jbc.R115.656462

34. Xu, X., Xu, Y., Guo, R., Xu, R., Fu, C., Xing, M., … Xu, D. (2021). Fanconi anemia proteins participate in a break-induced-replication-like pathway to counter replication stress. Nature Structural and Molecular Biology, 28(6), 487–500. https://doi.org/10.1038/s41594-021-00602-9

35. Kim, H., & D'Andrea, A. D. (2012). Regulation of DNA cross-link repair by the Fanconi anemia/BRCA pathway. *Genes and Development*, *26*(13), 1393–1408. https://doi.org/10.1101/gad.195248.112

36. Moldovan, G. L., & D'Andrea, A. D. (2009). How the fanconi anemia pathway guards the genome. *Annual Review of Genetics*, *43*(101), 223–249. https://doi.org/10.1146/annurev-genet-102108-134222

37. Liu, W., Palovcak, A., Li, F., Zafar, A., Yuan, F., & Zhang, Y. (2020). Fanconi anemia pathway as a prospective target for cancer intervention. *Cell and Bioscience*, *10*(1), 1–14. https://doi.org/10.1186/s13578-020-00401-7

38. Marteijn, J. A., Lans, H., Vermeulen, W., & Hoeijmakers, J. H. J. (2014). Understanding nucleotide excision repair and its roles in cancer and ageing. *Nature Reviews Molecular Cell Biology*, *15*(7), 465–481. https://doi.org/10.1038/nrm3822

39. Pećina-Šlaus, N., Kafka, A., Salamon, I., & Bukovac, A. (2020). Mismatch Repair Pathway, Genome Stability and Cancer. *Frontiers in Molecular Biosciences*, *7*(June), 1–12. https://doi.org/10.3389/fmolb.2020.00122

40. Lieber, M. R. (2010). The Mechanism of Double-Strand DNA Break Repair by the Nonhomologous DNA End-Joining Pathway. *Annual Review of Biochemistry*, *79*(1), 181–211. https://doi.org/10.1146/annurev.biochem.052308.093131

41. Her, J., & Bunting, S. F. (2018). How cells ensure correct repair of DNA double-strand breaks. *Journal of Biological Chemistry*, *293*(27), 10502–10511. https://doi.org/10.1074/jbc.TM118.000371

42. Daley, J. M., & Sung, P. (2014). 53BP1, BRCA1, and the Choice between Recombination and End Joining at DNA Double-Strand Breaks. *Molecular and Cellular Biology*, *34*(8), 1380–1388. https://doi.org/10.1128/MCB.01639-13

43. Mitchel, K., Zhang, H., Welz-Voegele, C., & Jinks-Robertson, S. (2010). Molecular Structures of Crossover and Noncrossover Intermediates during Gap Repair in Yeast: Implications for Recombination. *Molecular Cell*, *38*(2), 211–222. https://doi.org/10.1016/j.molcel.2010.02.028

44. Sun, Y., McCorvie, T. J., Yates, L. A., & Zhang, X. (2020). Structural basis of homologous recombination. *Cellular and Molecular Life Sciences*, *77*(1), 3–18. https://doi.org/10.1007/s00018-019-03365-1

45. Elbakry, A., & Löbrich, M. (2021). Homologous Recombination Subpathways: A Tangle to Resolve. *Frontiers in Genetics*, *12*(August). https://doi.org/10.3389/fgene.2021.723847

46. Li, X., & Heyer, W. D. (2008). Homologous recombination in DNA repair and DNA damage tolerance. *Cell Research*, *18*(1), 99–113. https://doi.org/10.1038/cr.2008.1

47. Kanehisa, M. and Goto, S.; KEGG: Kyoto Encyclopedia of Genes and Genomes. Nucleic Acids Res. 28, 27-30 (2000). [pubmed] [doi]

48. Kanehisa, M; Toward understanding the origin and evolution of cellular organisms. Protein Sci. 28, 1947-1951 (2019) [pubmed] [doi]

49. Kanehisa, M., Furumichi, M., Sato, Y., Ishiguro-Watanabe, M., and Tanabe, M.; KEGG: integrating viruses and cellular organisms. Nucleic Acids Res. 49, D545-D551 (2021). [pubmed] [doi]

50. Deamidation reaction structures. DNA Damage – Biotech Khan (wordpress.com).

51. Svobodová, A., & Vostálová, J. (2010). Solar radiation induced skin damage: Review of protective and preventive options. *International Journal of Radiation Biology*, *86*(12), 999–1030. https://doi.org/10.3109/09553002.2010.501842

52. Wood RD, Mitchell M, & Lindahl T Mutation Research, 2005, in Science, 2001, in the reference book DNA Repair and Mutagenesis, 2nd edition, 2006, and in Nature Reviews Cancer, 2011.

53. Kollmannsberger, C., Mross, K., Jakob, A., Kanz, L., & Bokemeyer, C. (1999). Topotecan – A Novel Topoisomerase I Inhibitor: Pharmacology and Clinical Experience. *Oncology*, *56*(1), 1–12. https://doi.org/10.1159/000011923

Evaluating a Novel Model System Designed to Assess the Long-Term Therapeutic Resistance of Chemotherapeutics.

1. Introduction

The earliest known description of cancer is documented in the Edwin Smith Papyrus, a piece of an ancient Egyptian surgical textbook that dates back to 3000 BC and describes the use of cauterization for the treatment of breast "ulcers".[1] However, the term cancer wasn't used until around 400 BC when Hippocrates first used the terms carcinos or carcinoma (Greek for cancer) to describe the finger-like spreading projections commonly found in many malignant tumors.[1] Also in this ancient textbook is the realization that "there is no treatment" that will completely cure a patient from these breast "ulcers".[1] Even in the earliest days of civilization, cancer was identified as an untreatable and fatal disease. Fast forward a few millennia and, unfortunately, "there is no treatment" still applies to far too many cancer diagnoses. In the US, cancer is the second leading cause of death following heart disease but is slowly becoming the leading cause of death as treatments for heart disease become more effective.[2,3] Although some significant progress has been made in the treatment of blood cancers, solid tumors, especially malignant tumors, still lack effective therapeutic options. This is despite numerous oncologic therapeutic approvals that have occurred over the past few decades.

A comprehensive review by Dr. Hess, et al. highlights the challenge of developing clinically beneficial oncologic therapeutics. They reviewed 192 unique clinical trials

between 2007 and 2017 that compared novel biologic/targeted agents to non-biologic/targeted comparators. The average post progression-free survival (overall survival – progression-free survival) for the biologic/targeted group and non-biologic/targeted comparators were 9.7 and 9.8 months, respectively. The addition of a biologic/targeted agent increased the overall survival and progression-free survival by an average of 1.2 months (+/- 3.8 (OS) and 2.5 (PFS) (SD)).[4] Another review of 62 oncologic agents approved by the FDA and EMA between 2003 and 2015 demonstrated an average overall survival benefit of 3.43 (0.63 SD) months relative to the existing standard of care.[5] These data show that there is some elimination of ineffective therapeutics in the clinical trial stage of drug development (phase I-III), which is evident by the overall survival difference between the first group of investigational drugs and the second group of approved drugs; however, decades of research culminating in a survival benefit of a few months is surely disheartening. While we have continued to develop drugs with novel mechanisms of action in the hopes of a breakthrough therapeutic, these studies suggest that our current developmental strategy does not generate therapeutic agents with significant clinical benefit.

Each drug approval requires years of target validation and billions of dollars to reach the market. It is estimated that only 1 drug out of every 5,000 in preclinical testing will be approved by the FDA.[6] A major contributing factor to these poor probabilities is the extraordinary complexity of the body that can cause unpredictable responses to novel therapeutics. Currently, a human cell contains an estimated 30,000 genes, which each make an average of 3 proteins.[7] Many of these proteins play a simultaneous role in

multiple functional pathways, creating an interconnected web that can cause unintended effects when a protein is inhibited. This internal interconnected web is then further complicated by external interactions from the surrounding microenvironment. The microenvironment contains multiple different cell types each with unique therapeutic responses that can exponentially alter the microenvironment in unpredictable ways. Variability in the drug exposure profiles for each cell further complicates the expected response, which is compounded further by interpatient variability. Unfortunately, the model systems that have become the foundation for drug discovery, namely two-dimensional high throughput microwell plates, possess limited complexity relative to the highly interconnected physiology of the human body. It is likely that many of the highly efficacious therapeutic mechanisms found in such simplistic tumor models will not translate clinically because cancer cells can become heterogeneous depending on the underlying environmental context. Additionally, the underlying cancer cell population can be altered in such model systems because the selective pressure associated with the model system may differ significantly from the selective pressure within the body, leading to clonal selection of a cell population that differs from the target cell population.

Another cause of poor clinical translation is the use of short-term treatment efficacy as a screening tool for identifying novel therapeutics. Currently, most drugs are either screened based on their ability to impact cell viability or for their ability to inhibit a target protein with the goal of inhibiting cell viability. According to the FDA's guidance for the nonclinical evaluation of anticancer pharmaceuticals, in order for a drug to

progress to clinical trials, it must have a well-characterized mechanism of action and demonstrate anti-tumor activity.[8] Although the FDA also appropriately mentions other requirements such as assessments of pharmacokinetics and safety, it makes no mention of treatment resistance. It also does not specify how long a drug must maintain anti-tumor efficacy. It's estimated that over 90% of all cancer-related deaths are caused by treatment resistance.[9] Yet, we currently do not prioritize drug resistance in the drug development process. In the same way that some drugs can be more efficacious, some drugs can have higher barriers to resistance. A simple example is to consider a drug that requires three simultaneous mutations to reduce efficacy compared to a drug that only requires one mutation. More time is needed for a cell population to acquire the mutations necessary to protect a cell from the higher-barrier drug, allowing the drug to maintain efficacy for longer.

Drug resistance is highlighted to a much greater degree in infectious disease where drugs are selected clinically based on their resistance profiles by using antibiograms or culture and sensitivity assays.[10,11] There have been no studies evaluating whether the potency of a chemotherapeutic can predict the clinical durability of a chemotherapeutic, however, some inferences can be made based on HIV regimens. Some drugs such as darunavir require 4 simultaneous mutations before the virus acquires resistance, while others such as atazanavir require only 2 mutations. Importantly, both drugs target the same mechanism of action.[12] The genetic barrier to resistance of an HIV regimen also does not directly correlate with its effectiveness.[13] Therefore, the potency of the drug with the higher barrier to resistance may be higher,

lower, or equal to the lower barrier drug. This also suggests that using anti-cancer activity as a screening mechanism does not necessarily select for drugs with high barriers to drug resistance. An extreme example of these concepts could be a drug that can only impede tumor growth by 1% but can never succumb to resistance. This drug would never be identified in our current developmental process but would have immense benefits as an additive medication. Because resistance is the most significant cause of treatment failure, it is imperative to identify and select the most durable therapeutics for further development. Unfortunately, identifying therapeutics with high barriers to resistance is currently difficult as most model systems are not equipped to assess potency changes over time. To help address this problem, we developed a high throughput three-dimensional spheroidal model system of castration resistant prostate cancer that is capable of assessing long-term potency changes over weeks to months.

Currently, there is no model system designed specifically to screen for high durability drugs, however, a significant number of new models have been developed to address other challenges. We will briefly review some of these newer models to provide context for our model system. Broadly speaking, most model systems under investigation either attempt to replicate the tumor microenvironment more accurately or mimic the drug resistance profile of the drug. An excellent recent review by Dr. Kitaeva et al. highlights many of the newer model systems designed to better replicate the tumor microenvironment.[14] Among these models are co-culture 2D models, 3D spheroidal models, Boyden chamber models, and microfluidic devices. Co-culture models increase the complexity of the model system through the addition of stromal

cells, which have increasingly been shown to significantly impact the aggressiveness, resistance, and progression of the tumor.[15,16,17,18] Co-culturing can occur in both 2D and 3D models, however, 3D models increase the structural complexity of the tumor model. This increases intercellular interactions, increases the release of extracellular matrix components, increases the drug barrier properties of the model, and increases the heterogeneity of the model.[24,25] The transcriptomic profile of 3D models is more similar to *in vivo* and clinical tumors than traditional 2D models.[19,20,21] These 3D models can be generated using a variety of different techniques with unique applications and benefits, depending on the specific model system. Some of these techniques include ultra-low attachment plates, matrix or hydrogel encapsulation[23], spinner flasks, micropattern plates, magnetic nanoparticles, or bioprinting.[14,22,26] Of these techniques, bioprinting is currently the most versatile. Most of these techniques rely on simple mixing or overlaying of cells, which create relatively simple models, however, bioprinting techniques can place cells in specific locations generating unique tumor regions that increase the spheroid's complexity.[14,22] The Boyden chamber is another unique model that is used to study cell motility and invasion and uses a two-compartment setup separated by a microporous membrane. Invasive cells can migrate across this membrane in response to environmental stimuli placed in the compartments. A representation of this model can be found in the appendix to help readers conceptualize the model. Lastly, microfluidic devices can be used to recreate the microenvironment and microcirculation of the tumor tissue. These systems can be extremely fine-tuned by

adjusting the fluid flow, temperature, and pressure, and can be used to create artificial chemical gradients.[14]

In addition to assessing drug efficacy, some model systems are being developed to specifically assess drug resistance mechanisms. One of the simpler resistance models relies on prolonged drug exposure with increasing concentrations of chemotherapeutics to generate resistant cell lines.[27,28] These model systems are usually employed to test drug resistance mechanisms such as MDR efflux pumps in the hopes of overcoming this resistance.[29,30,31,33] An alternative to this model system can be achieved using cell lines derived from drug resistant human tumors.[31,33] Three dimensional models[34] are also used to test resistance mechanisms such as extracellular matrix interactions,[25,32] heterogeneity[32], or transport barriers.[32] An excellent review by Dr. Nunes, et. al. highlights characteristics of 3D model that allow for more accurate assessment of drug resistance.[24] An alginate and gelatin microcapsule based 3D spheroid model has also been recently developed and has demonstrated enhanced resistance to cisplatin relative to traditional 2D models and may offer another option to assess drug resistance.[23] Finally, some animal models such as xenografts, syngeneic, or genetically engineered mouse models (**GEMMs**) have been used to assess drug resistance mechanisms as an alternative to *in vitro* models.[31]

Importantly, the models depicted above have been used to investigate drug resistance mechanisms and have not been used to differentiate investigational drugs based on their treatment durability. **The remaining focus of this paper will be to describe a novel approach for identifying drugs with high barriers to drug resistance.**

In this project, we have adapted a high-throughput spheroidal model system of PC3 cells that is capable of long-term oncologic drug exposure, a necessary trait for evoking drug resistance in cancer cell populations. We then assessed the predictability of model system using docetaxel, the treatment standard for prostate cancer and topotecan, a drug that clinically failed in prostate cancer.[40,41]

2. Materials and Methods

2.1. Cell line and cell culture

The human prostate cancer (PC3) cell line was purchased from ATCC and was maintained as monolayers in complete medium using F12K (Corning) and 10% (v/v) fetal bovine serum (**FBS**) (Hyclone) at 37°C in a 5% CO_2 atmosphere using a Heracell bios 160i incubator (Thermoscientific). The PC3-Luc-GFP cell line was initially purchased from ATCC but was infected using a lentiviral vector[37] that contained genes for enhanced green fluorescent protein (**eGFP**) and was maintained in similar culture conditions to the PC3 cell line. The murine macrophage (RAW 264.7) cell line was maintained in DMEM (Biowhitiker) with 10% FBS at 37°C and in a 5% CO_2 atmosphere. The endothelial (HUVEC) Cells were maintained in EGM2 (Lonza) with the EGM2 SingleQuot kit (Lonza) at 37°C in a 5% CO_2 atmosphere. All cells were kept at lower passage numbers (<10 PC3 and RAW264.7) (<5 for HUVEC) throughout the experiment to maintain genotypic and phenotypic consistency. Cells were passaged using 0.25% (w/v) trypsin (Hyclone) for 2-3 minutes every 2-4 days according to confluency, which was determined using a Primovert microscope (Zeiss). During the experiment, the PC3 cell line was forked into multiple sub cell lines according to the treatment group, which will be described in

greater detail below. Each of these sub cell lines was treated as a unique cell line (separate flasks, no mixing, ect.) throughout the experiment using the same methods described above.

2.2. Spheroid formation

Our spheroid protocol was largely adapted from a high-throughput liquid overlay technique developed by Metzger, et al.[35] This technique rapidly generates many spheroids with minimal incubation time (24 hr), which is necessary for drug screening protocols. Briefly, 96 well U bottom plates (Grenier bio-one) are coated with a 1.2% w/v poly-HEMA (Sigma Aldrich) solution in 95% v/v ethanol. This solution was produced by incubating poly-HEMA crystals overnight with a magnetic stir rod at 80°C to ensure full dissolution. The poly-HEMA solution is kept warm throughout the coating process to prevent precipitation during the evaporation step. 60 µL of the poly-HEMA solution is added to each well and the plates are heated using a 10x10 hot plate (VWR). Plates are then left on the hot plate for approximately 1 hour with the lid raised to evaporate the ethanol. Plates are then sealed using Parafilm (Bemis) for future use. After cells have been passaged and placed into a separate conical tube, they are mixed thoroughly, and a small sample is removed for counting using a TC10 automated cell counter (Biorad). A minimum of two counts are taken per cell line to ensure accurate counts for cell seeding. Cells are diluted to achieve a concentration of 50,000 cells per mL and are placed on ice. 2.5% v/v of Matrigel (Corning) is added to the cell suspension using an ice-cold syringe and needle. The cells are then plated using 100 µL of the cell suspension to achieve 5,000 cells per well. The plates are then centrifuged at 400 g for 5 to 10 minutes

at 4°C. This protocol rapidly generates fully formed spheroids within 24 hours for the PC3 cell line.

2.3. Co-culture spheroids

Co-culture spheroids were generated using a similar high-throughput liquid overlay technique as the PC3 spheroids, but with differing combinations of macrophages (RAW264.7), endothelial (HUVEC), and PC3 cells. These combinations included PC3, RAW264.7, and HUVEC cells alone, in combination with PC3 cells (10, 20, 40% stromal to 90, 80, 60% PC3), and altogether in differing concentrations (Raw264.7/HUVEC/PC3, 10/10/80, 10/20/70, 10/30/60, 10/40/50, 20/10/70, 30/10/60, 40/10/50). These combinations were generated by initially making up 50,000 cells/mL stock suspensions of each cell line and then mixing the cell lines using appropriate volumes in each well. These mixed suspensions were plated to achieve a total of 5,000 cells per well. The type of media was selected based on the most sensitive cell line. PC3 and RAW264.7 were grown in DMEM and the endothelial cells were grown in EGM2 with appropriate growth factor additives. However, for the combinations that included endothelial cells, the EGM2 media was chosen for all cells to accommodate the endothelial cells, which were not immortalized and were much more sensitive to culture conditions.

2.4. Dosing and spheroid handling

Two days after initial seeding and spheroid formation, spheroids received an additional 100 μL of media +/- drug with the total volume reaching 200 μL for the remainder of the experiment. On days 3 and 5, a media exchange was executed by

removing 100 μL of media per well and replacing it with 100 μL of fresh media +/- drug. Limiting the media exchanges and leaving some residual old media prevented lost spheroids throughout the experiment. On off media exchange days, 10 μL was removed and replaced with 10 μL of media or treatment solution, depending on the treatment group. Dosing of topotecan (Chempac) and docetaxel (Fluka) occurred using 20x concentrated solutions which could be directly spiked into the wells at 10 μL in 190 μL of media. Each treatment was dosed as a bolus dose on day 0. There were 3 treatment groups: control, topotecan, and docetaxel. Dosing occurred at 100 nM for topotecan during each treatment week and from 1 to 100,000 nM for the IC50 assay and at 2.5 nM for docetaxel and from 0.01 to 1000 nM for the IC50.

2.5. Study Protocol

Spheroids were generated according to the protocol depicted in Section 2.2 and were allowed to grow for approximately 2-3 days to allow size-dependent drug barriers to form. Spheroids were then dosed according to protocol in Section 2.3 for a total of 7 days of exposure. During the first week of exposure, samples were taken for genomic and proteomic analysis on days 0, 1, 3, and 7. The remaining spheroids were saved for future weeks by digesting using Accumax (Innovative cell technologies) for approximately 1 hour until a single cell suspension was achieved. At this point, a total of 3 treatment groups generated 3 unique cell-lines that were maintained throughout the experiment: PC3-Control, PC3-Topotecan, and PC3-Docetaxel. The digested spheroids were grown in 2D for approximately 1-2 weeks until the cell population was replenished sufficiently to plate additional spheroids. Each cell population was then used to

generate two groups of spheroids. One group (3D) was exposed to an additional week of

treatment and one group (3D) was used to assess the resulting sensitivity of the drug

(Topotecan or docetaxel) from the previous week(s) of drug exposure. After another full

week of exposure, some spheroids were harvested for genomic and proteomic analysis,

and some were digested to prepare for another week of exposure and analysis. This

cycle was repeated throughout the experiment. A schematic is depicted below (**figure 1**

and **figure 2**) to help better orient readers to the study protocol. For scRNAseq, digested

spheroids from week 5 that had been grown in 2D and were ready to be reseeded as

spheroids were instead analyzed using scRNAseq. We also analyzed the 3D-treated
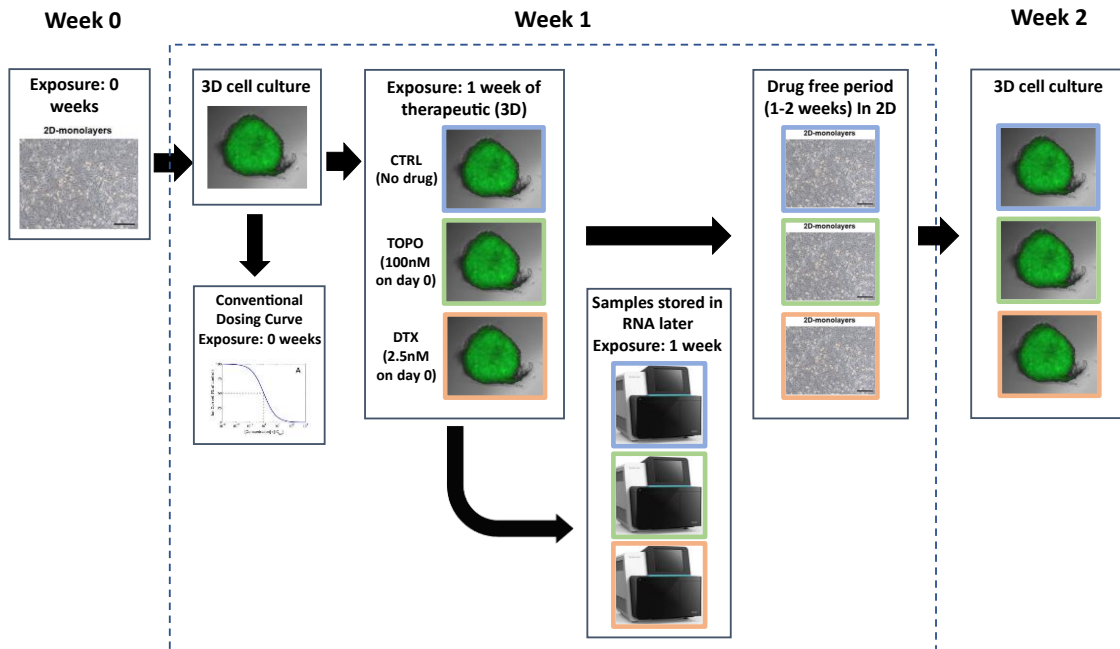
samples from week 6 using scRNAseq.

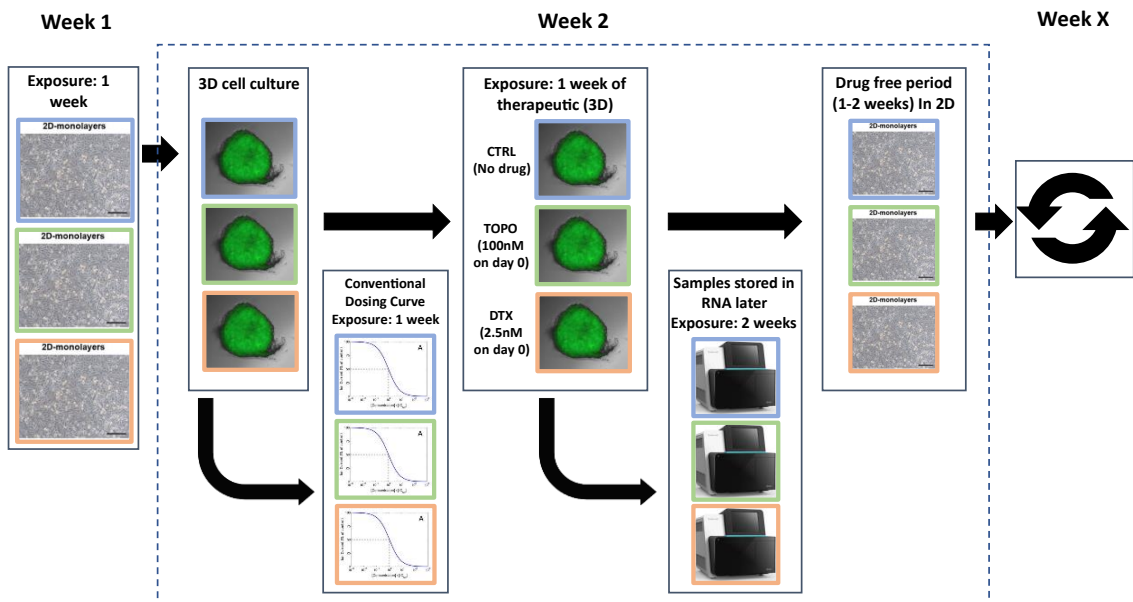**Figure 1.** Schematic depicting the first week of the study protocol, starting from the base cell line (PC3).

Figure 2. Schematic depicting the second week of the study protocol, starting from the treatment exposed cell lines.

2.6. Resazurin assay (Cytotoxicity)

Resazurin was used to measure the mitochondrial activity of the cells as a surrogate for cell viability because the reductive conversion of resazurin to resorufin creates a water-soluble end-product. This prevents the need for a solubilizing step, which would be untenable in a 3D format. Resazurin (Alfa Aesar) was made fresh for each experiment at a 0.015% w/v concentration in PBS and was sterilized using a 0.22 μm filter. Before resazurin was added to the spheroids, the spheroids were moved from U bottom 96 well plates to flat bottom black, fluorescent plates (Grenier bio-one). This was accomplished by using a 1 mL pipette tip to move the spheroid with 100 μL media. Moving the spheroids allows for more accurate imaging and plate reading. This also ensured that any alterations in well volumes from inconsistent evaporation dynamics that occur over the duration of the experiment would not alter the resorufin concentrations, preventing additional assay variability. Resazurin was added at a ratio of 10 μL per 100 μL of media and was incubated for 4 to 12 hours with readings taken over time (2, 4, 6, 8, 12). Generally, 4-6 hours was the most appropriate time point and achieved the lowest CV values with the greatest sensitivity and limited assay saturation. Fluorescent measurements for each plate were read using a Cytation 5 plate reader (BioTek) with excitation set at 560 nm and emission set at 590 nm.

2.7. PI Stain protocol

The nuclei of cells within the spheroids were stained with propidium iodide (PI) using a 1 mg/mL stock solution that was diluted 1:100 using 10 μL of PI stock solution

and 1 mL of FBS free media. This solution was incubated for 5 minutes at room temperature while being protected from light. The staining solution was then removed, and the spheroids were washed using PBS. Finally, the FBS free media was added to the spheroids and they were imaged using the Cytation 5 plate reader using the Texas red filter set. Spheroids were discarded after each day of imaging and, therefore, different spheroids are viewed each day.

2.8. RNA storage protocol

Cells and spheroids are separated into individual microfuge tubes at approximately 1,000,000 cells/mL and washed 2x using phosphate buffered saline (**PBS**) (Wards science) and the Heraeus Fresco 21 microcentrifuge (Thermoscientific) set at 400g and 4°C for 10 minutes. Samples are maintained on ice for the duration of the protocol. The PBS is then aspirated and replaced with 300µL of RNA later (Qiagen). Samples are stored overnight (24H) at 4°C before moving to -80C for long-term storage. For scRNAseq, live samples are necessary and therefore, RNA later is not appropriate. Instead, we stored samples by cryopreservation using 10% dimethyl sulfoxide (**DMSO**) in complete media and stored in liquid nitrogen.

2.9. scRNAseq

The top 500 genes were selected based on their generated p-value and based on a fold change >1.5 relative to control (Untreated spheroids at time 0 d, which is 2 d post seeding). Reactome was then used to identify the most significant pathways that were overrepresented within the submitted gene lists. The most pertinent pathways were

included in our analysis. Pathways that were significantly overrepresented are displayed as blue in the tables and graphics in **figures 7, 8, and 9**.

2.10.   Statistics

The curve fitting and statistical analysis of the IC50 data were performed using Graphpad Prism (Dotmatics, Boston MA, USA). The IC50 was determined at ½ of fitted maximal activity. Usually, an extra sum-of-squares F test was used to compare IC50 values between treated and control samples. The statistics generated during the gene enrichment analysis were produced using Reactome.

3. Results

3.1. Reproducibility and morphological characteristics of the spheroidal model

The methods used to produce our spheroids generated rapid (within 24 hours), well-developed, and reproducible spheroids in relatively high quantities. During our studies, we generated up to 10 full 96-well plates at once, which equates to around 1,000 spheroids created within a day when excluding 2D culturing time. Although unnecessary for our particular experiment, this value can easily scale further with additional plates and the use of automated culturing methods. Examples of these spheroids can be found in **figure 3**, which were imaged 24 hours after seeding. Initially, spheroids grew to a diameter below 500 μm, but eventually, their diameter exceeded 1000 μm as shown in **figure 5**. We found that spheroid growth tended to be most robust earlier in the experiment and tended to plateau as the spheroid grew larger. The spheroids were most uniform and spherical initially after seeding, but over time, some

spheroids grew in more amorphous shapes. Despite this variability, we routinely

achieved coefficient of variation values for the resazurin assay of our control and

treated spheroids in the mid to low single digits with a trend of lower coefficient of

variability (**CV**) values with higher treatment concentrations (Mean coefficient of

variation for our control spheroids for the full topotecan experiment was 8.18 and for

our highest treatment samples was 3.52).
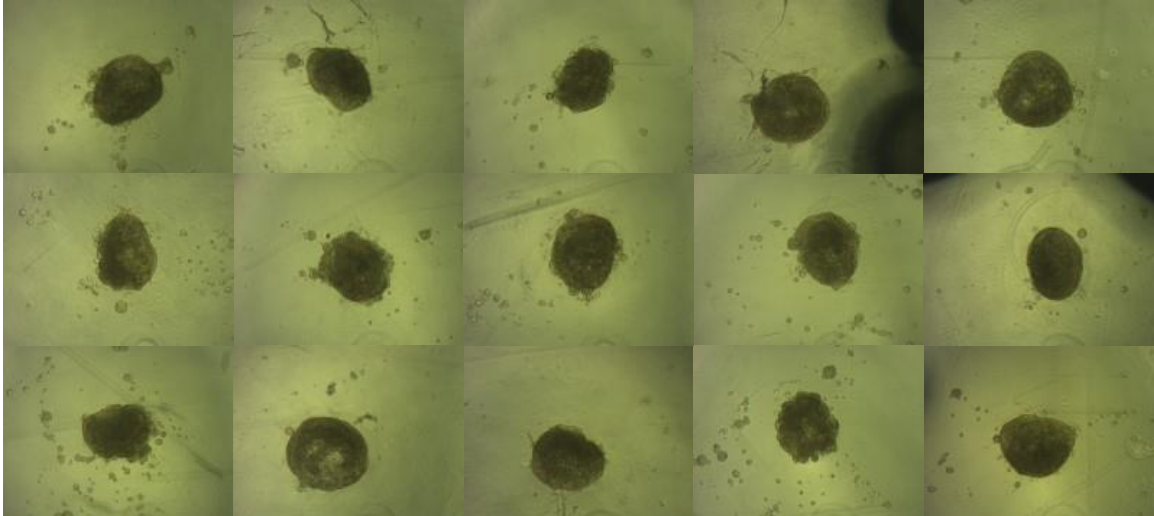
Brightfield Images of PC3 Spheroids

Figure 3. Example brightfield images of PC3 spheroids generated 24 hours after initial seeding. Images were taken manually with the Primovert microscope.

3.2. Flexibility of the model system

Although the overall parameters of our model system were designed specifically to address resistance using a more clinically tailored regimen, in **figure 4**, we highlight adjustments and additional complexities that can be introduced into the model to address other investigator questions. In panel A, PC3 only spheroids were grown over a total of 16 days with 2 days allowed for initial formation and a 14-day treatment window. As indicated by the bright green fluorescence from the eGFP producing cells, these spheroids remain viable. Although not shown, spheroids also maintained integrity for up to 21 days, however, over time, debris, and extra-spheroidal cells can begin to accumulate within the wells, which can create unintended microenvironmental conditions that can alter experimental results. In panels B, C, and D, different combinations of PC3, macrophage (RAW264.7), and endothelial (HUVEC) cells were used to generate co-culture spheroids, which were imaged after 24 hours. Panel B contained 80% PC3, 10% macrophage, and 10% endothelial cells. Panel C contained 50% PC3, 40% macrophage, and 10% endothelial cells. Panel D contained 50% PC3, 10% macrophage, and 40% endothelial cells. These spheroids were grown over a total of 4 days to achieve a 72-hour exposure. The PC3-Luc-GFP cell line was the only cell line capable of expressing GFP, which is evident in panels C and D as they show significantly darker spheroids due to the reduced PC3 cell composition. As shown in **figure 5**, the spheroidal model can generate reproducible co-culture spheroids that are well developed within 24 hours. Over time, however, the cellular composition of the spheroids can shift depending on the growth kinetics of each cell line. In our case, the

macrophage composition increased drastically over the study duration relative to the

other cell lines (Panel E), especially for the spheroids in panel C (highest initial

macrophage concentration), which indicates that further optimization may be necessary

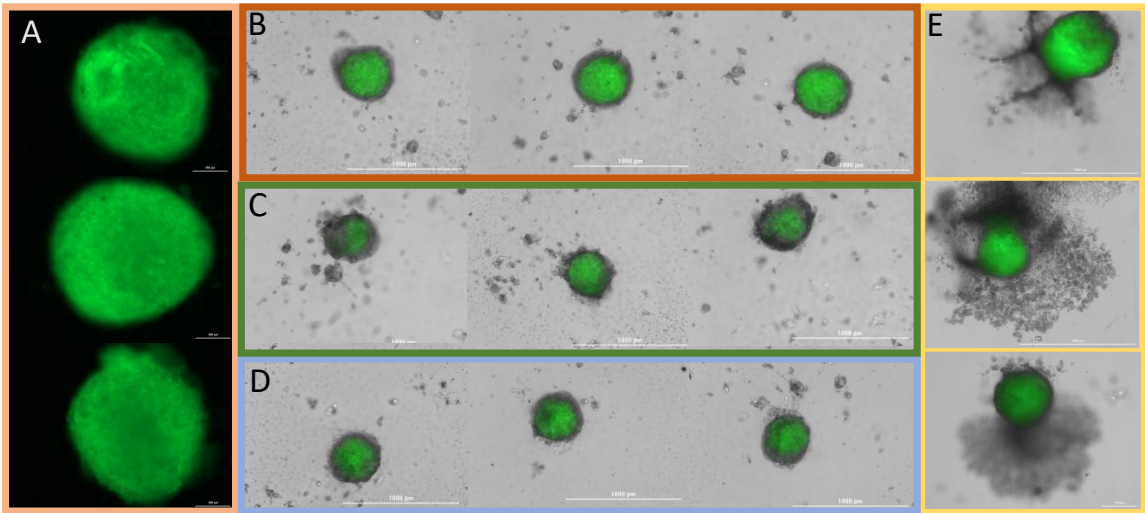to address specific investigator needs.

Figure 4. Images of spheroids depicting the versatility of the model system Green florescence is GFP. **A.** PC3 spheroids grown over a total of 16 days. **B.** Co-culture Spheroids grown over 24H using 10% endothelial cells (Huvec), 10% macrophages (Raw264.7), and 80% PC3 cells. **C.** Co-culture spheroids at 24H containing 40% macrophages, 10% endothelial cells, and 50% PC3 cells. **D.** Co-culture spheroids at 24H containing 10% Macrophages, 40% endothelial cells, and 50% PC3 cells. **E.** Co-culture spheroids at 72H for each of the cell compositions in B, C, and D. Small scale bar is 300 µm and large-scale bar is 1000 µm.

3.3. Analyzing the heterogeneity of the spheroidal model

Next, we assessed the underlying heterogeneity of the model system to further characterize the model's ability to accurately assess drug resistance. We stained spheroids nuclei using PI (Fig. 5), which revealed heterogeneous regions of necrosis (red) that formed initially on day 1 (3 total days as a spheroid) and were maintained throughout the duration of the experiment. In this experiment, spheroids grew to approximately 600-1000 nm in diameter. We also demonstrated cell viability throughout the experiment (green) using GFP as a marker of activity. We further assessed the heterogeneity of the model system using scRNAseq (Fig. 6) of samples taken during the long-term exposure experiment (Fig. 8). Specifically, the samples analyzed using scRNAseq include control cells (2D) taken during the drug-free interval, immediately before cells were reformed into spheroids for the 6th week of treatment and control cells (3D) after the completion of the 6th week of treatment. Using t-distributed stochastic neighbor embedding (t-SNE) of the scRNAseq data, we can visualize the heterogeneity of each sample. Because converting a higher dimensional graph (3D) to a lower dimensional graph (2D) can be difficult, different methods such as principal components analysis (**PCA**), multidimensional scaling (**MDS**), and t-distributed stochastic neighbor embedding (**tSNE**) have been used to try to faithfully approximate the underlying higher dimensional structure in a lower dimension. Datapoints in the t-SNE graphs are arranged according to similarity based on the gene expression of the underlying cell. During the analysis, cells that are more similar are attracted to each other, and cells that are less similar are repelled. This analysis does a great job of

faithfully maintaining the local structure from the original dataset but does not

necessarily maintain the larger structure. The main goal of the algorithm is to accurately

place the closest neighbors to each other. The distance between clusters is not linear

and this distance does not accurately depict the inter-cluster similarity. However, the

control 3D data appears to have many cells that are not neighbors and thus the

heterogeneity of the sample is increased relative to the control 2D sample.

In **figure 7**, we analyzed the effect of the 3D spheroid model system on genes

associated with the cell cycle. Overrepresentation analysis of the top 500 genes by

significance with fold changes > 1.5 for each scRNAseq sample was completed using

Reactome, an open-source, open access, manually curated, and peer-reviewed pathway

database.[38] In these figures, blue fill represents a p-value below 0.05 and is considered

significantly enriched. A significantly enriched pathway comprises a greater percentage

of genes within the submitted list than expected based on a control reference sample.

For instance, based on a list of 500 genes, the program might expect the list to contain

10/500 genes related to the cell cycle, but instead, the list contains 20/500 genes

related to the cell cycle, overcoming the threshold for significance. In this analysis, cells

from the 3D spheroids demonstrated significant enrichment of the broad cell cycle

category as well as many subpathways, however, cells from the 2D microenvironment

did not demonstrate significant enrichment in the broad cell cycle category and only

demonstrated enrichment for a few subpathways.
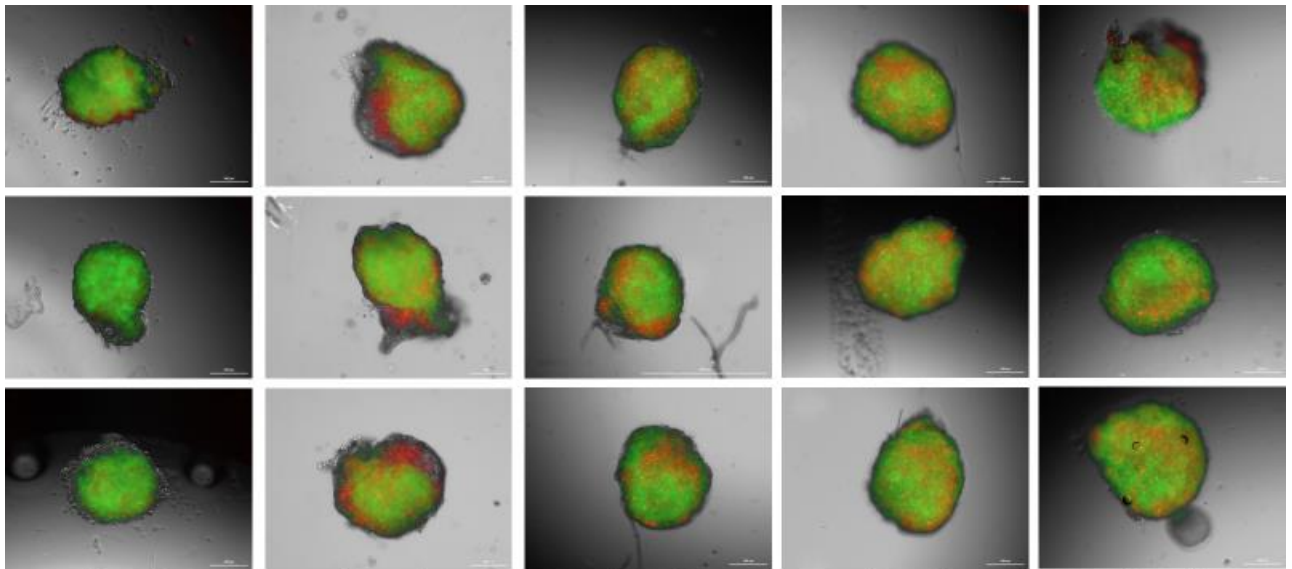
Day 0   Day 1   Day 3   Day 5   Day 7

Figure 5. Images of PI-stained spheroids over a 7-day timepoint. Green fluorescence denotes GFP expressing PC3 cells. Red fluorescence denotes the PI stain. Day 0 occurs after a total of two days of prior growth. Small scale bar is 300µm and large-scale bar is 1000µm.

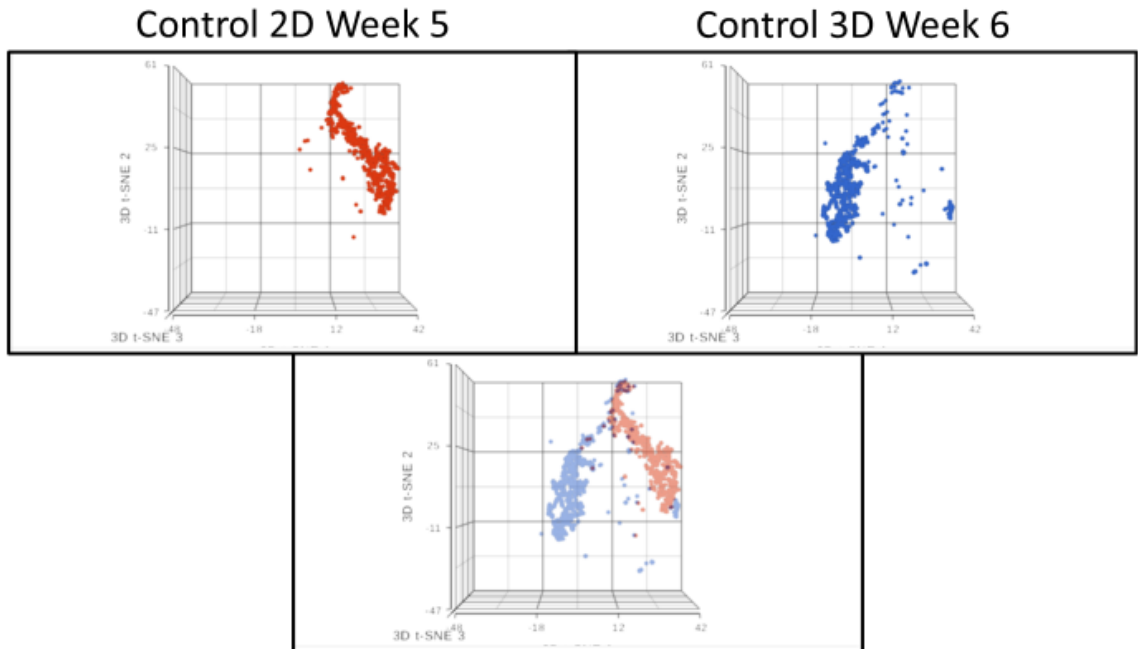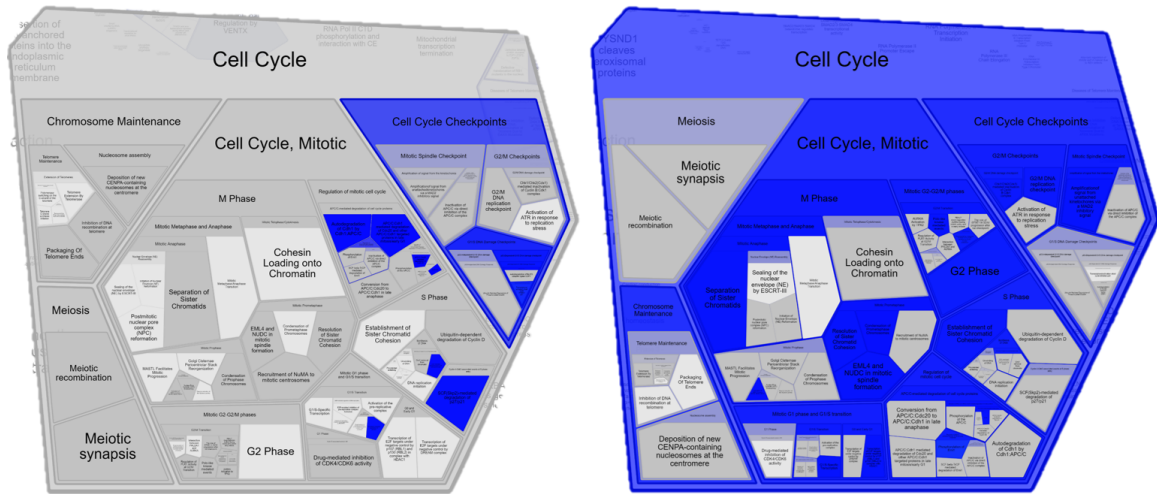**Figure 6.** t-SNE analysis of scRNAseq data obtained from control spheroids taken after 5 (red) and 6 (blue) model system cycles.

Control 2D Week 5   **Control 3D Week 6**

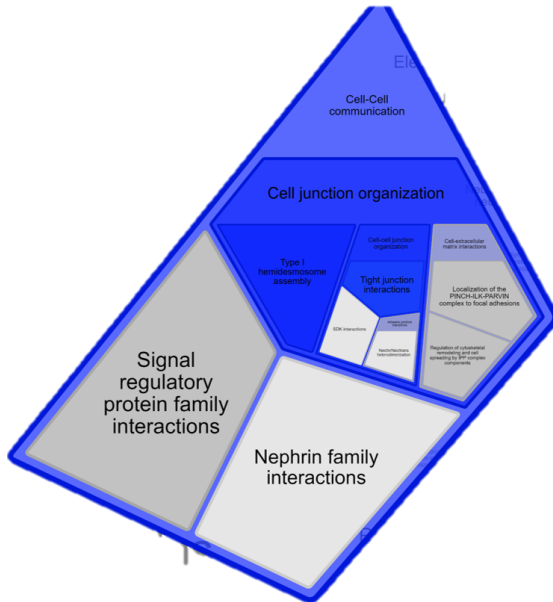| Week 5	Week 6
Cell cycle	Cell cycle
Meiosis	Meiosis
Cell cycle checkpoints	Cell cycle checkpoints
G2/M checkpoints	G2/M checkpoints
Mitotic spindle checkpoint	Mitotic spindle checkpoint
G1/S DNA Damage checkpoint	G1/S DNA Damage checkpoint
Cell cycle mitotic	Cell cycle mitotic
M Phase	M Phase
Mitotic G2-G2/M phage	Mitotic G2-G2/M phage
S Phase	S Phase
G2 Phase	G2 Phase
Mitotic G1 phase and G1/S transition	Mitotic G1 phase and G1/S transition
Regulation of mitotic cell cycle	Regulation of mitotic cell cycle
Chromosome maintenance	Chromosome maintenance

Figure 7. Overview of the cell cycle data from an overrepresentation analysis of the top 500 most significant genes with a fold change > 1.5 from the control WK5 and WK6 scRNAseq data.

3.4. Assessing the impact of the spheroidal model system on genes associated with

barriers to drug delivery.

We also investigated the impact of the 3D spheroidal model system on genes known to alter drug delivery. **Figure 8** highlights the impact of the 3D microenvironment on genes related to cell-cell communication. Some important genes found within this broad category include laminins, tight junction proteins, and adherens and junction proteins. The 3D spheroid demonstrated similar enrichment to the 2D microenvironment for many subpathways within cell-cell communication, however, genes associated with adherens and junction interactions were significantly enriched in the 3D spheroids and not by the 2D cells. Extracellular matrix genes are assessed in **figure 9** and were enriched significantly by cells from the 3D spheroids, but not by cells from the 2D microenvironment. The subpathways within the broad extracellular matrix pathway were also differentially enriched and these differences are highlighted in the **figure 9** Table.

The 3D spheroid model system also influenced the expression of efflux pumps, which can be seen in **figure 10**. Broadly, a greater proportion of cells from the 3D spheroid model expressed some form of efflux pump relative to cells from the 2D model. This can be seen in **figure 10** as a greater proportion of cells are colored in the WK6 3D plot relative to the WK5 2D plot. Most notable is an increase in the expression of ATP binding cassette (**ABC**)C3 and ABCC5, which are shown as pink and dark red in **figure 10**. ABCC3 and ABCC5 are well-known multidrug resistance pumps and may negatively impact drug delivery.
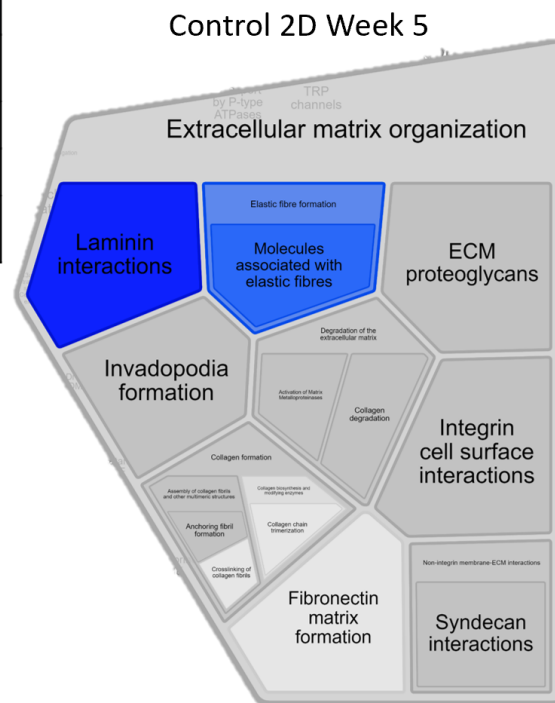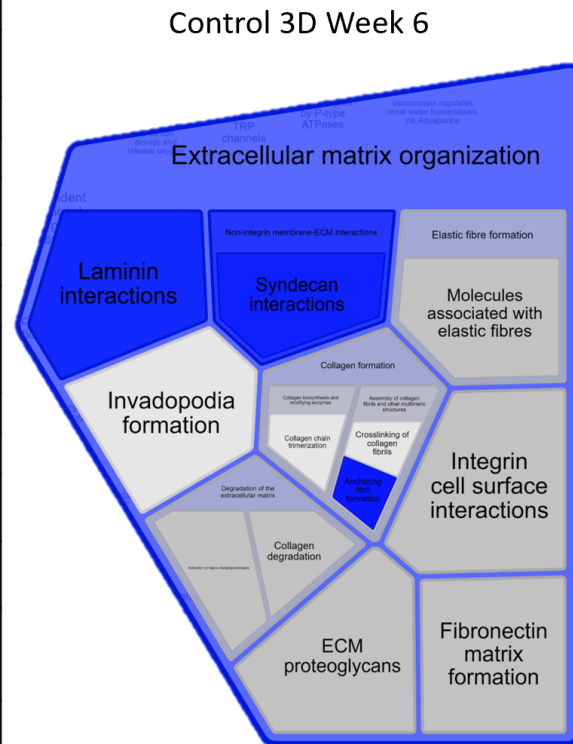
Control 2D Week 5

Control 3D Week 6
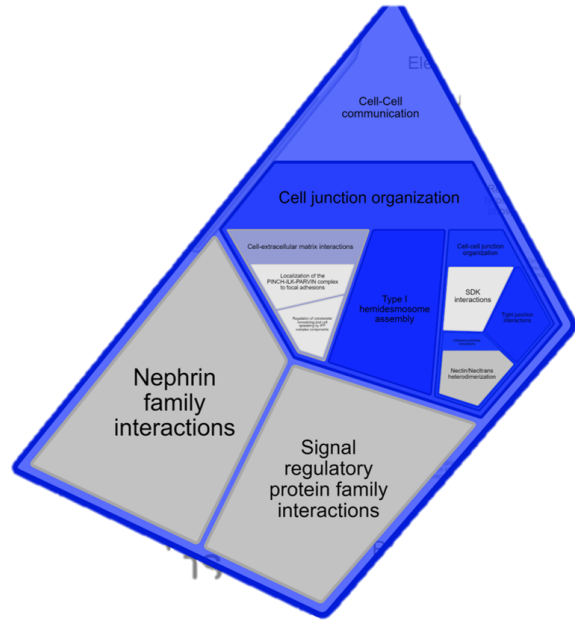
Week 5	Week 6
Cell-Cell Communication	Cell-Cell Communication
Cell junction organization	Cell junction organization
Type I hemidesmosome assembly	Type I hemidesmosome assembly
Cell-cell junction organization	Cell-cell junction organization
Tight junction interactions	Tight junction interactions
SDK interaction	SDK interaction
Adherens junction interactions	Adherens junction interactions
Nectin/necltrans heterodimerization	Nectin/necltrans heterodimerization
Cell-extracellular matrix interactions	Cell-extracellular matrix interactions
Localization of the PINCH-ILK-PARVIN complex to focal adhesions	Localization of the PINCH-ILK-PARVIN complex to focal adhesions
Regulation of cytoskeletal remodeling and cell spreading by IPP complex components	Regulation of cytoskeletal remodeling and cell spreading by IPP complex components
Nephrin family interactions	Nephrin family interactions
Signal regulatory protein family interactions	Signal regulatory protein family interactions

Figure 8. Overview of the cell-cell communication data from an overrepresentation analysis of the top 500 most significant genes with a fold change > 1.5 from the control WK5 and WK6 scRNAseq data.

Week 5	Week 6
Extracellular matrix organization	Extracellular matrix organization
Laminin interactions	Laminin interactions
Elastic fibre formation	Elastic fibre formation
Molecules associated with elastic fibres	Molecules associated with elastic fibres
ECM proteoglycans	ECM proteoglycans
Invadopodia formation	Invadopodia formation
Non-integrin membrane ECM interactions	Non-integrin membrane ECM interactions
Syndecan interactions	Syndecan interactions
Collagen formation	Collagen formation
Collagen biosynthesis and modifying enzymes	Collagen biosynthesis and modifying enzymes
Collagen chain trimerization	Collagen chain trimerization
Assembly of collagen fibrils and other multimeric structures	Assembly of collagen fibrils and other multimeric structures
Crosslinking of collagen fibrils	Crosslinking of collagen fibrils
Anchoring fibril formation	Anchoring fibril formation
Integrin cell surface interactions	Integrin cell surface interactions
Degradation of the ECM	Degradation of the ECM
Collagen degradation	Collagen degradation
Activation of matrix metalloproteinases	Activation of matrix metalloproteinases

Figure 9. Overview of the extracellular matrix organization data generated from an overrepresentation analysis of the top 500 most significant genes with a fold change > 1.5 from the control WK5 and WK6 scRNAseq data.

Control 3D Week 6

Control 2D Week 5

Control 2D Week 5   **Control 3D Week 6**

Efflux Pumps
- ABCA1
- ABCA7
- ABCB1
- ABCB4
- ABCC1
- ABCC2
- ABCC3
- ABCC4
- ABCC5
- ABCG1
- ABCG2
- ABCG4
- N/A
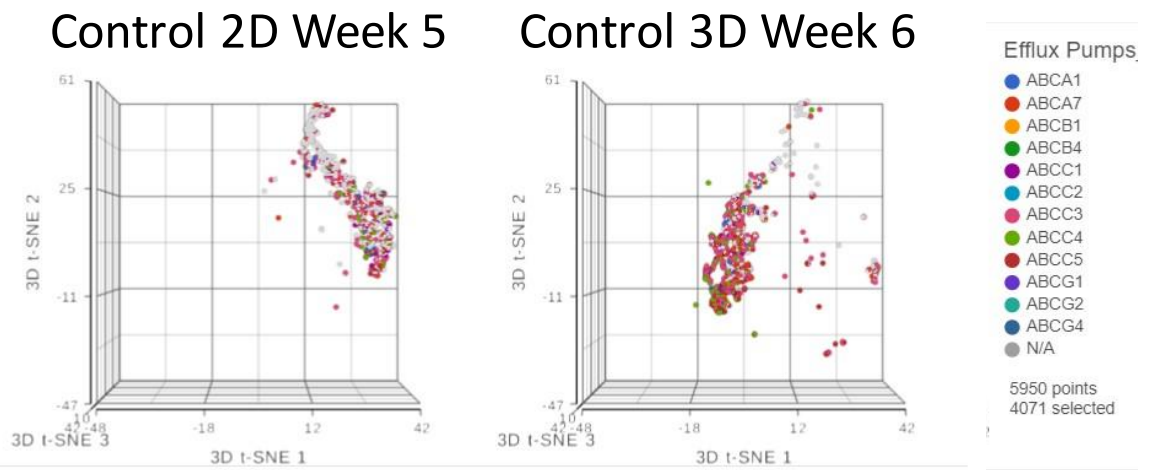
5950 points
4071 selected

Figure 10. scRNAseq analysis comparing the expression of efflux pumps between control cells grown in 2D to those grown in 3D.

3.5. Applying the model system to therapeutics with known clinical efficacy to assess

     model accuracy

     Finally, we used two chemotherapeutics with known clinical efficacy in prostate

cancer to assess whether the model system can differentiate between effective clinical

therapies and clinical failures based on the long-term potency data generated from the

in vitro spheroid model. **figure 11** demonstrates the long-term potency of topotecan

after a total of 6 treatments at the previously determined IC50 (100 nM). Cells were

grown initially in 2D before forming spheroids. The spheroids were treated for a total of

1 week using a bolus dose of topotecan on day 0. After treatment, spheroids were

digested and grown in 2D to recover before spheroids were reformed and a new week

of treatment was initiated. Typically, recovery took approximately 2 weeks. Thus, a full

treatment cycle was approximately 1 week of therapy and 2 weeks of recovery, which

closely mimics a true treatment cycle.

     After the first week of exposures, each treatment group was treated as a unique

cell line that was carried forward for the remainder of the experiment. Cells were

formed as spheroids when assessing the IC50 to ensure that the same

microenvironment that generated the underlying resistance mechanism would also be

present when assessing the impact of the resistance mechanism on drug potency.

Weeks with significantly decreased potency relative to control are identified with three

asterisks. Plots A and B show the same data using two different types of graphs to help

better visualize the data and plot C was generated by calculating the fold change in the

IC50 between control cells and topotecan exposed cells. Our data demonstrated that

topotecan exposed cells quickly developed an initial underlying level of resistance that significantly increased the IC50 relative to the control sample as soon as the first week of exposure. This lower level of resistance was maintained for 4 weeks before a more significant level of drug resistance developed after 5 weeks of topotecan exposure. This significant jump in IC50 from ~300 nM to ~2,200 nM was further confirmed after another week of topotecan exposure. After 6 full weeks of topotecan exposure, the underlying cell population required a 26-fold increase in dose relative to the 6-week control cells and a 58-fold increase in dose relative to the initial PC3 population to achieve a similar effect.

The effect of long-term exposure of docetaxel on treatment potency is shown in **figure 12**. The model and treatment protocol were similar to **figure 11**, but with docetaxel as the investigational treatment. Docetaxel was also given as a single bolus dose on day 0. The graphs displayed in **figure 12 and 13** are also similar to **figure 11** and represent the same type of data. In this study, the docetaxel-treated cells did demonstrate some weeks with significantly reduced potency relative to the control population, however, it was much more variable relative to the topotecan study. Docetaxel exposed cells during the final week of the study did not show significantly reduced potency relative to the week 5 control cells and over the entire experiment, docetaxel exposed cells did not achieve a fold change greater than 2 relative to the corresponding control population. The docetaxel exposed cells did achieve a ~2.4-fold change relative to the initial study IC50.
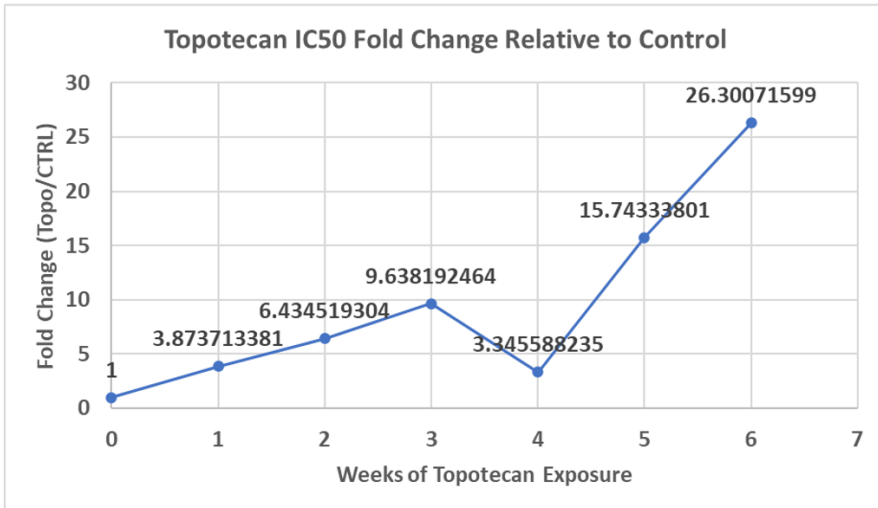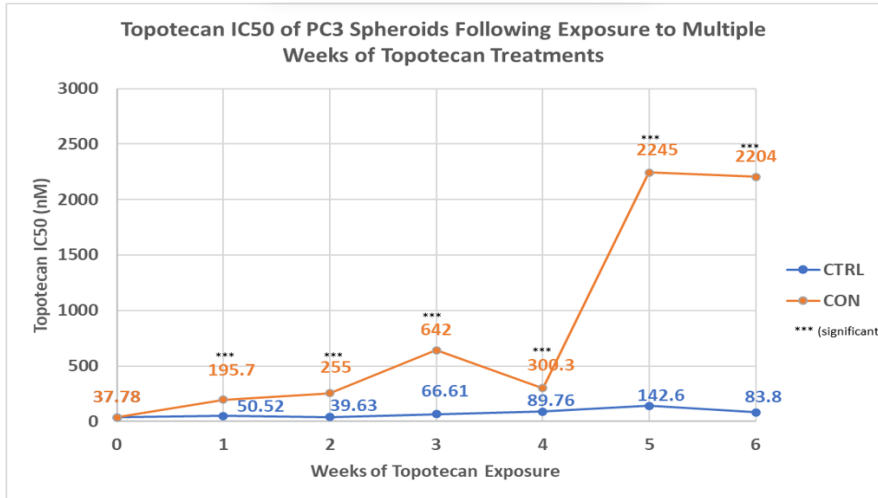
Figure 11. Summary of the IC50 data from either control spheroids or spheroids exposed to 6 weeks of topotecan therapy. Plots **A** and **B** present similar data using different graph styles and plot **C** illustrates the fold change between the topotecan treated cell line and the control cell line.
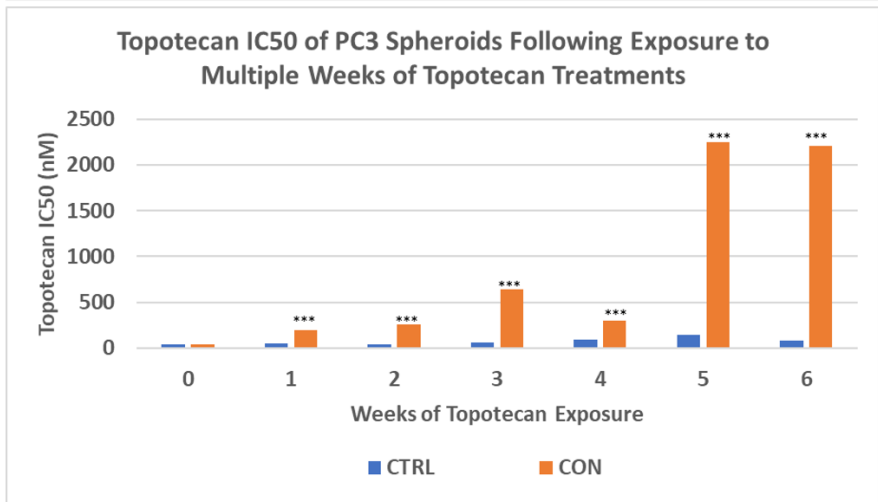
Figure 12. Summary of the IC50 data from either control spheroids or spheroids exposed to 5 weeks of docetaxel therapy. Plots **A** and **B** present similar data using different graph styles and plot **C** illustrates the fold change between the docetaxel treated cell line and the control cell line.
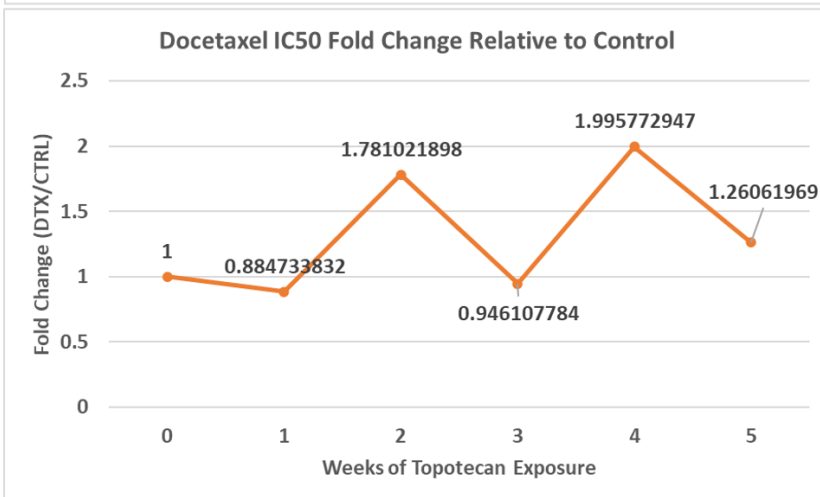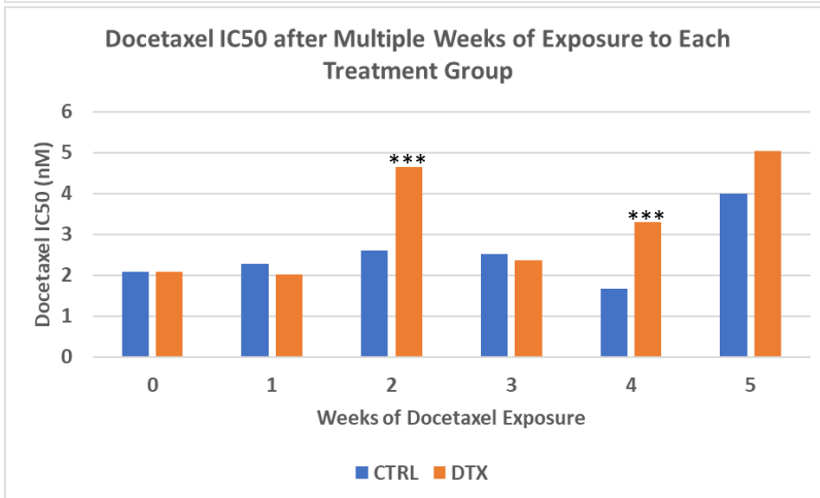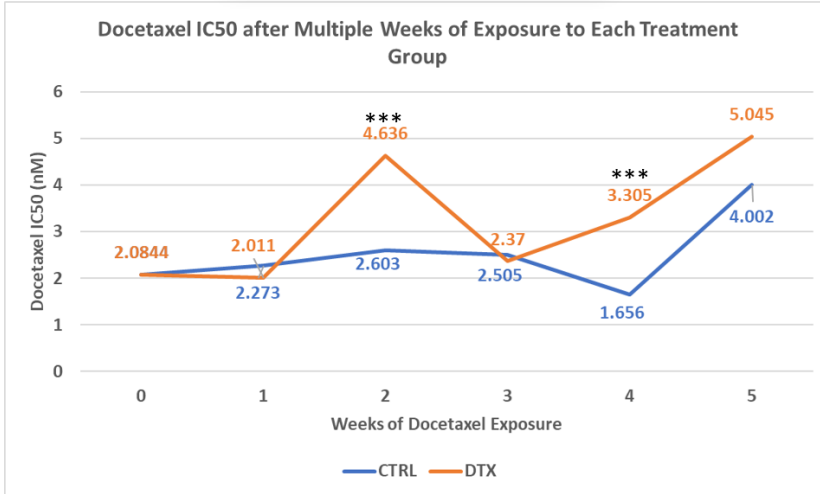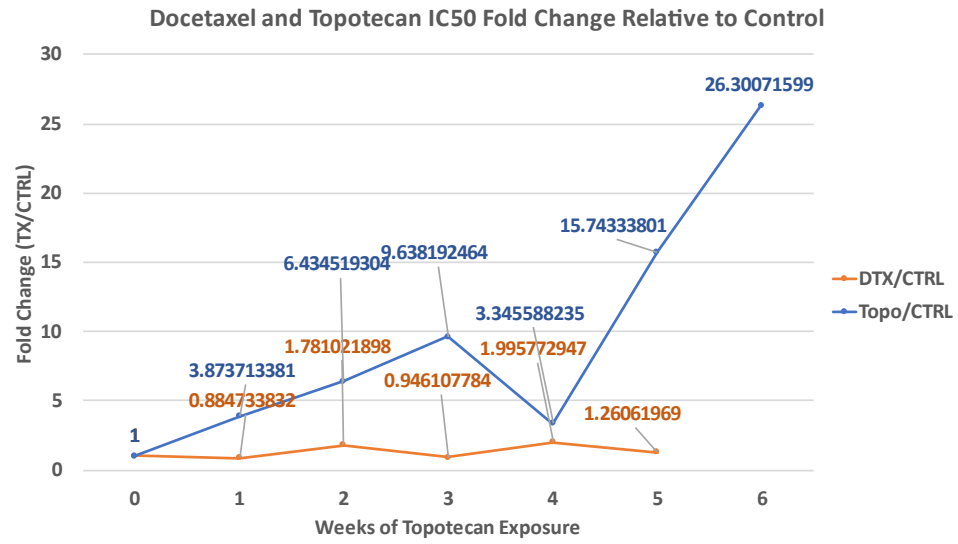
Figure 13. Comparison of the fold change relative to control of the docetaxel treatment group to the topotecan treatment group.

Discussion

Many different tumor models are being used or are being developed to provide researchers with a more accurate clinical representation of a target disease or a more appropriate microenvironment to answer different questions. The number of available models is evidence of the difficulty in designing a one-size-fits-all model to address all possible challenges. A more generalized model such as the standard 2D single cell model does have some advantages as a drug screening tool despite its limited ability to approximate the tumor microenvironment. Namely, the model's low-cost scalability, uniformity and reproducibility, limited instrumentation requirements, and easy manipulation techniques greatly enhance its usefulness as a drug screening tool. Unfortunately, the model has limited tumor barrier properties, limited co-culture interactions, limited heterogeneity, limited gradient properties, and can only support a limited duration of exposure. These issues can significantly reduce the types of resistance mechanisms that can be evaluated by the 2D single cell model. For instance, adaptable resistance, or the ability to generate resistance inducing mutations, is highly unlikely in a model system with uniform drug exposure and limited heterogeneity. A sensitive cell must have sufficient protection for enough time to develop novel resistance, otherwise, the model is simply screening out sensitive cells. Heterogeneity is also necessary to increase the number of potential resistance mechanisms and to increase the likelihood of resistance developing.

We sought to develop a model system better equipped to assess drug resistance without losing many of the characteristics that make the 2D model ideal for drug

screening. To that end, the model may not be ideal for all studies, but should be sufficient in many situations. The model is highly scalable with the potential to generate thousands of spheroids within 24 hours. It does not require specialized equipment, should be easily accessible, and is relatively cheap compared to other spheroidal models. However, based on our experience, spheroid handling is more tedious relative to the traditional 2D model and is more time intensive. Exceptional sterile technique is necessary to prevent spheroid contamination during the months-long study, which can be difficult due to the many touchpoints that occur throughout the study. Although less accessible, automated media exchange and dosing systems such as the Multiflo FX by Biotek could dramatically increase the scalability of the model and decrease the possibility of contamination.

As shown in **figure 3**, the model is highly reproducible and produces relatively large spheroids (600-1000 µm) that should contain diffusion gradients based on the diffusion distance of oxygen, which is approximately 100-200 µm.[43] The spheroids contained heterogeneous regions of necrosis as shown in **figure 5**, which further suggests that the model displays variability in nutrient and oxygen exposure and presumably drug exposure. To further confirm this finding, we utilized single cell RNAseq analysis and determined that cells from the 3D microenvironment were more heterogenous than cells from the 2D microenvironment (**figure 6**). We also observed differential expression of cell-cycle genes between the 3D and 2D models (**figure 7**), which might suggest increased cell turnover or increased cell cycle diversity in the 3D model, although additional studies are necessary to confirm this.

The environmental heterogeneity of the model system can be increased, if necessary, through the addition of stromal cells, which appear to grow well in the spheroid model (**figure 4**). We initially created the co-culture spheroids as a proof of concept to assess the flexibility of the model system in the context of drug resistance screening and to determine whether co-culture spheroids could easily be integrated into the model system. Based on our experience, to address a specific need, the establishment of spheroids co-cultured with other cell types could reasonably be incorporated into the drug resistance model, however, a few significant issues would need to be addressed. As shown in **figure 4**, although co-culture spheroids may initially appear to form reproducible, round spheroids, over time, the stromal cells may begin to disaggregate depending on their natural tendency to form spheroids. Although not shown, endothelial cells (HUVEC) tended to form tighter spheroids and macrophages (RAW 264.7) tended to form looser spheroids, when compared to spheroids composed of PC3 cells . Over time, PC3 spheroids maintained their integrity the best followed by endothelial cells and then macrophages. The macrophage spheroids were only loosely aggregated by 72 hours. The hazy outgrowth in **figure 4** highlights the macrophage's aggregation issues. While incorporation of stromal cells within the spheroid is possible, additional optimization is necessary to ensure adequate spheroid production and to ensure the desired stromal influence is maintained throughout the experiment. Additionally, flow-based cell-sorting would be necessary to grow the cancer cells in future weeks. Because these issues will vary depending on which stromal cells are

introduced, a few weeks of optimization is necessary for any lab attempting co-culture spheroids.

We also evaluated the drug barrier properties of the spheroid model system using Reactome to complete an overrepresentation analysis of the top 500 differentially expressed genes by p-value and fold change > 1.5 from the scRNAseq expression data. In **figures 8 and 9**, we evaluate the impact of the spheroid model system on genes related to cell-cell communication and the extracellular matrix. Within the cell-cell communication pathway, genes related to cell junctions and adherens will have the most important impact on drug delivery. These proteins can limit the number of intercellular gaps available for drug transport and have been found to significantly impact drug delivery.[39] Surprisingly, the 2D model and the 3D model demonstrated similar overrepresentation of these pathways, though the 3D model did show an overrepresentation of the adherens and junction genes while the 2D model did not. Cells within the 2D model do interact across the 2D plane, however, we expected the physical requirements necessary to maintain the spheroidal structure would have led to increased utilization of cell-cell junction interactions. It's possible that the use of Matrigel initially to supplement the spheroid may have lessened the structural burden of the cells or it's possible that the extracellular matrix plays a larger tissue structure role relative to cell-cell interactions. Genes related to the extracellular matrix were overrepresented in the 3D model and were not overrepresented in the 2D model. However, some subpathways were overrepresented in the 2D model. When comparing these subpathways, the 3D model appeared to express more genes related to the

structural integrity of the spheroid, which can be seen in the overrepresentation of the laminin interaction, the non-integrin ECM interaction, and the anchoring fibril formation genes. Importantly, although the 2D cells may express genes associated with drug barriers, it's nearly impossible for these genes/proteins to have a substantial impact on drug exposure as the drug is typically dosed in solution and therefore planer junctions would not alter uptake and a thin ECM layer would not prevent drug uptake. Finally, we analyzed the impact of the 3D model on the expression of efflux pump genes, which is shown in **figure 10**. The 3D model significantly increased the number of cells expressing efflux pumps, especially ABCC3 and ABCC5, which are well known multidrug resistance (**MDR**) pumps. This data suggests that the microenvironment generated by the spheroid model may lead to more resilient cells and more variable drug exposure.

The model system was then tested to determine whether it was sensitive enough to detect changes in drug potency, how many weeks would be necessary before drug resistance could be detected, and whether the model system would accurately predict the most effective drug clinically. We demonstrated a drastic decrease in potency over the study duration for the topotecan treated spheroids (**figure 11**). After 6 weeks of therapy, topotecan treated spheroids required a 26-fold higher dose to achieve the same treatment efficacy as the control spheroids. Even more shocking, the topotecan spheroids required a 4-fold higher dose after a single treatment. This suggests that the therapeutic index of an oncologic agent may decrease significantly after initial exposure. Said in another way, for some therapeutics, in some cancers, we may cause patient harm as quickly as the second dose. Typically, patients receive 2-3

treatment cycles before efficacy is determined, which could mean 2 to 3 months of

ineffective and harmful therapy before the treatment is altered. In stark contrast, after

5 weeks of therapy, the docetaxel treated spheroids only required a 1.2-fold higher dose

to achieve the same efficacy as the control spheroids (**figure 12**). Throughout the entire

experiment, the docetaxel treated spheroids displayed a statistically higher IC50 twice

and displayed a peak IC50 fold change of 2 after 4 weeks of treatment. However, these

changes were not consistent as the weeks 1, 3, and 5 IC50s were near control.

Additionally, we did not observe a significant breakout of the IC50 in the docetaxel

treated spheroids. This data suggests that the long-term therapeutic efficacy of

docetaxel is more stable than topotecan in PC3 cells (**figure 13**) and also suggests that

docetaxel's barrier to drug resistance is higher than topotecan in PC3 cells. While PC3

cells may not represent all forms of prostate cancer, it does act as a surrogate for

castration-resistant prostate cancer, which is the typical target for oncologic

medications. The model also correctly predicted that docetaxel is clinically effective in

metastatic prostate cancer and correctly predicted that topotecan would fail clinically.

While these results are extremely hopeful, many more confirmatory studies are needed

before this method of initial drug screening can become the gold standard. In future

studies, we would like to further investigate our drug screening method using different

cancer types with many more oncologic agents.

References

1. Understanding What Cancer Is: Ancient Times to Present. (2018, January 4). American Cancer Society. https://www.cancer.org/treatment/understanding-your-diagnosis/history-of-cancer/what-is-cancer.html#:~:text=Our%20oldest%20description%20of%20cancer,back%20to%20about%203000%20BC.

2. FastStats – Leading Causes of Death (cdc.gov) (Last updated 2022, September 6). (Viewed 2022 October 1). https://www.cdc.gov/nchs/fastats/leading-causes-of-death.htm.

3. Cancer overtakes CVD to become leading cause of death in high-income countries | The BMJ

4. Hess, L. M., Brnabic, A., Mason, O., Lee, P., & Barker, S. (2019). Relationship between progression-free survival and overall survival in randomized clinical trials of targeted and biologic agents in oncology. Journal of Cancer, 10(16), 3717–3727. https://doi.org/10.7150/jca.32205

5. Salas-Vega, S., Iliopoulos, O., & Mossialos, E. (2017). Assessment of Overall survival, quality of life, and safety benefits associated with new cancer medicines. JAMA Oncology, 3(3), 382–390. https://doi.org/10.1001/jamaoncol.2016.4166

6. Drug Approvals - From Invention to Market...12 Years! (medicinenet.com)

7. Human Genome Project FAQ

8. FDA. (2010). Nonclinical Evaluation for Anticancer Pharmaceuticals, (March).

9. Goldie, J. H., & Coldman, A. J. (2009). Drug Resistance in Cancer: Mechanisms and Models, 256. Retrieved from

   http://books.google.com/books?id=nAR0deuqpyAC&pgis=1

10. Soiza, R. L., Donaldson, A. I. C., & Myint, P. K. (2018). Vaccine against arteriosclerosis: an update. Therapeutic Advances in Vaccines, 9(6), 259–261.

    https://doi.org/10.1177/https

11. Jorgensen, J. H., & Ferraro, M. J. (2009). Antimicrobial susceptibility testing: A review of general principles and contemporary practices. Clinical Infectious Diseases, 49(11), 1749–1755. https://doi.org/10.1086/647952

12. Tang, M. W., & Shafer, R. W. (2012). HIV-1 antiretroviral resistance: Scientific principles and clinical applications. Drugs, 72(9), 1–25.

    https://doi.org/10.2165/11633630-000000000-00000

13. Luber, A. D. (2005). Genetic barriers of resistance and impact on clinical response. MedGenMed Medscape General Medicine, 7(3). https://doi.org/10.1186/1758-2652-7-3-69

14. Kitaeva, K. V., Rutland, C. S., Rizvanov, A. A., & Solovyeva, V. V. (2020). Cell Culture Based in vitro Test Systems for Anticancer Drug Screening. Frontiers in Bioengineering and Biotechnology, 8. https://doi.org/10.3389/fbioe.2020.00322

15. Quail, D. F., & Joyce, J. A. (2013). Microenvironmental regulation of tumor progression and metastasis. Nature Medicine, 19(11), 1423–1437.

    https://doi.org/10.1038/nm.3394

16. Giraldo, N. A., Sanchez-Salas, R., Peske, J. D., Vano, Y., Becht, E., Petitprez, F., … Sautès-Fridman, C. (2019). The clinical role of the TME in solid cancer. British Journal of Cancer, 120(1), 45–53. https://doi.org/10.1038/s41416-018-0327-z

17. Brassart-Pasco, S., Brézillon, S., Brassart, B., Ramont, L., Oudart, J. B., & Monboisse, J. C. (2020). Tumor Microenvironment: Extracellular Matrix Alterations Influence Tumor Progression. Frontiers in Oncology, 10(April), 1–13. https://doi.org/10.3389/fonc.2020.00397

18. Klemm, F., & Joyce, J. A. (2015). Microenvironmental regulation of therapeutic response in cancer. Trends in Cell Biology, 25(4), 198–213. https://doi.org/10.1016/j.tcb.2014.11.006

19. Takagi, A., Watanabe, M., Ishii, Y., Morita, J., Hirokawa, Y., Matsuzaki, T., & Shiraishi, T. (2007). Three-dimensional cellular spheroid formation provides human prostate tumor cells with tissue-like features. Anticancer Research, 27(1 A), 45–54.

20. Árnadóttir, S. S., Jeppesen, M., Lamy, P., Bramsen, J. B., Nordentoft, I., Knudsen, M., … L. Andersen, C. (2018). Characterization of genetic intratumor heterogeneity in colorectal cancer and matching patient-derived spheroid cultures. Molecular Oncology, 12(1), 132–147. https://doi.org/10.1002/1878-0261.12156

21. Gheytanchi, E., Naseri, M., Karimi-Busheri, F., Atyabi, F., Mirsharif, E. S., Bozorgmehr, M., … Madjd, Z. (2021). Morphological and molecular characteristics of spheroid formation in HT-29 and Caco-2 colorectal cancer cell lines. Cancer Cell International, 21(1), 1–16. https://doi.org/10.1186/s12935-021-01898-9
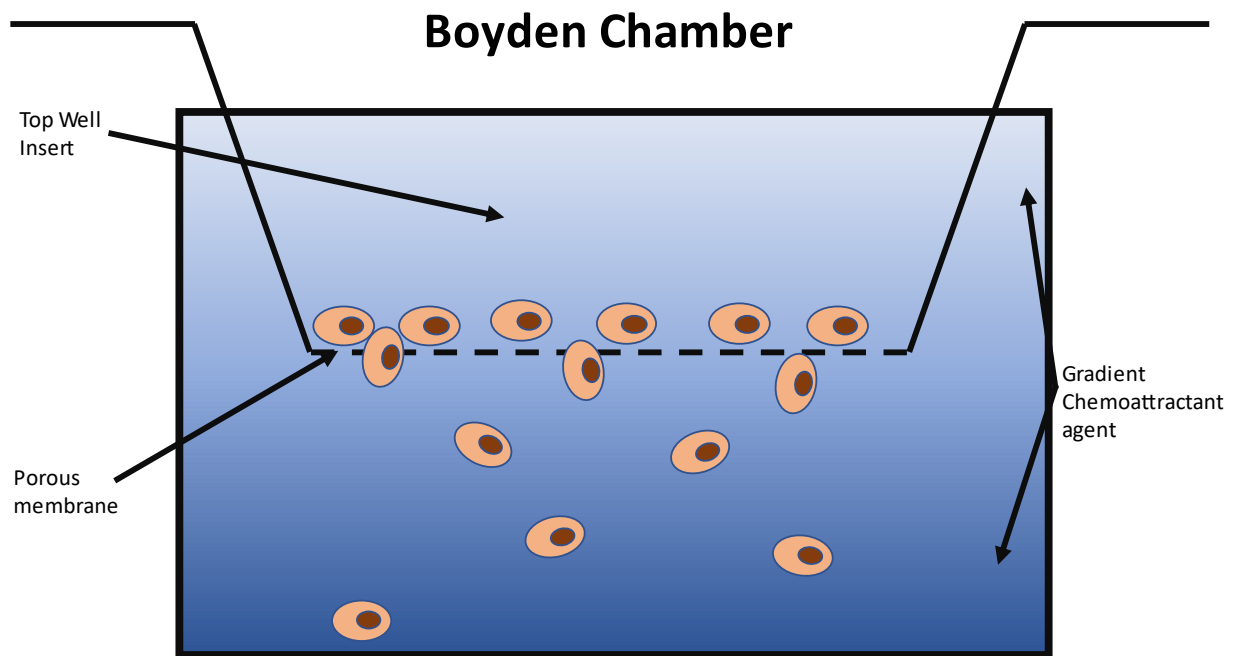
22. Nath, S., & Devi, G. R. (2016). Three-dimensional culture systems in cancer research: Focus on tumor spheroid model. Pharmacology and Therapeutics, 163, 94–108. https://doi.org/10.1016/j.pharmthera.2016.03.013

23. Ertekin, Ö., Monavari, M., Krüger, R., Fuentes-Chandía, M., Parma, B., Letort, G., … Leal-Egaña, A. (2022). 3D hydrogel-based microcapsules as an in vitro model to study tumorigenicity, cell migration and drug resistance. Acta Biomaterialia, 142, 208–220. https://doi.org/10.1016/j.actbio.2022.02.010

24. Nunes, A. S., Barros, A. S., Costa, E. C., Moreira, A. F., & Correia, I. J. (2019). 3D tumor spheroids as in vitro models to mimic in vivo human solid tumors resistance to therapeutic drugs. Biotechnology and Bioengineering, 116(1), 206–226. https://doi.org/10.1002/bit.26845

25. Loessner, D., Stok, K. S., Lutolf, M. P., Hutmacher, D. W., Clements, J. A., & Rizzi, S. C. (2010). Bioengineered 3D platform to explore cell-ECM interactions and drug resistance of epithelial ovarian cancer cells. Biomaterials, 31(32), 8494–8506. https://doi.org/10.1016/j.biomaterials.2010.07.064

26. Katt, M. E., Placone, A. L., Wong, A. D., Xu, Z. S., & Searson, P. C. (2016). In Vitro Tumor Models: Advantages, Disadvantages, Variables, and Selecting the Right Platform. Frontiers in Bioengineering and Biotechnology, 4(February). https://doi.org/10.3389/fbioe.2016.00012

27. McDermott, M., Eustace, A. J., Busschots, S., Breen, L., Crown, J., Clynes, M., … Stordal, B. (2014). In vitro development of chemotherapy and targeted therapy

drug-resistant cancer cell lines: A practical guide with case studies. Frontiers in Oncology, 4 MAR(March). https://doi.org/10.3389/fonc.2014.00040

28. Michaelis, M., Wass, M. N., & Cinatl, J. (2019). Drug-adapted cancer cell lines as preclinical models of acquired resistance. Cancer Drug Resistance, 2(3), 447–456. https://doi.org/10.20517/cdr.2019.005

29. Kars, M. D., Işeri, Ö. D., Gündüz, U., Ural, A. U., Arpaci, F., & Molnár, J. (2006). Development of rational in vitro models for drug resistance in breast cancer and modulation of MDR by selected compounds. Anticancer Research, 26(6 B), 4559–4568.

30. Romney, E., & Nagaraj, V. J. (2015). <i>In Vitro</i> Model Systems to Investigate Drug Resistance Mechanisms in Pancreatic Cancer Cells. Advances in Biological Chemistry, 05(07), 286–292. https://doi.org/10.4236/abc.2015.57026

31. Rosa, R., Monteleone, F., Zambrano, N., & Bianco, R. (2014). In Vitro and In Vivo Models for Analysis of Resistance to Anticancer Molecular Therapies, 1595–1606.

32. Rahmanian, M., Seyfoori, A., Ghasemi, M., Shamsi, M., & Majidzadeh-a, K. (2021). In-vitro tumor microenvironment models containing physical and biological barriers for modelling multidrug resistance mechanisms and multidrug delivery strategies. Journal of Controlled Release, 334(April), 164–177. https://doi.org/10.1016/j.jconrel.2021.04.024

33. Mohammad Azharuddin1,#, Karin Roberg1, 2, Ashis Kumar Dhara3, Mayur Vilas Jain4, P., & D´arcy 5, Jorma Hinkula1, Nigel K H Slater6, Hirak K Patra1, 6, #. (2019).

Multicellular tumor spheroids- an effective in vitro model for understanding drug resistance in head and neck cancer, 1–26.

34. Nowacka, M., Sterzynska, K., Andrzejewska, M., & Nowicki, M. (2021). Biomedicine & Pharmacotherapy Drug resistance evaluation in novel 3D in vitro model. Biomedicine & Pharmacotherapy, 138, 111536.

https://doi.org/10.1016/j.biopha.2021.111536

35. Metzger, W., Sossong, D., & Chle, A. B. Ä. (2011). The liquid overlay technique is the key to formation of co-culture spheroids consisting of primary osteoblasts , fi broblasts and endothelial cells, (August 2010), 1000–1012.

https://doi.org/10.3109/14653249.2011.583233

36. Wang, Peggy. Visualizing Single-Cell RNA-Seq Data with t-SNE: Researcher Interview with Dmitry Kobak and Philipp Berens. 2020. Single-Cell RNA-Seq Visualization with t-SNE - NCI (cancer.gov)

37. Roy Chaudhuri T, Arnold RD, Yang J, Turowski SG, Qu Y, Spernyak JA, Mazurchuk R, Mager DE, Straubinger RM. Mechanisms of tumor vascular priming by a nanoparticulate doxorubicin formulation. Pharm Res. 2012 Dec;29(12):3312-24. doi: 10.1007/s11095-012-0823-4. Epub 2012 Jul 14. PMID: 22798260; PMCID: PMC3631713.

38. Roy Chaudhuri T, Arnold RD, Yang J, Turowski SG, Qu Y, Spernyak JA, Mazurchuk R, Mager DE, Straubinger RM. Mechanisms of tumor vascular priming by a nanoparticulate doxorubicin formulation. Pharm Res. 2012 Dec;29(12):3312-24. doi:

10.1007/s11095-012-0823-4. Epub 2012 Jul 14. PMID: 22798260; PMCID: PMC3631713.

39. Tscheik, C., Blasig, I. E., & Winkler, L. (2013). Trends in drug delivery through tissue barriers containing tight junctions. Tissue Barriers, 1(2), e24565. https://doi.org/10.4161/tisb.24565

40. Mohler, J. L., Antonarakis, E. S., Armstrong, A. J., D'Amico, A. V., Davis, B. J., Dorff, T., … Freedman-Cass, D. A. (2019). Prostate cancer, version 2.2019. JNCCN Journal of the National Comprehensive Cancer Network, 17(5), 479–505. https://doi.org/10.6004/jnccn.2019.0023

41. Hudes GR, Kosierowski R, Greenberg R, Ramsey HE, Fox SC, Ozols RF, McAleer CA, Giantonio BJ. Phase II study of topotecan in metastatic hormone-refractory prostate cancer. Invest New Drugs. 1995;13(3):235-40. doi: 10.1007/BF00873806. PMID: 8729952.

42. Marín-Aguilera, M., Codony-Servat, J., Kalko, S. G., Fernández, P. L., Bermudo, R., Buxo, E., … Mellado, B. (2012). Identification of docetaxel resistance genes in castration-resistant prostate cancer. Molecular Cancer Therapeutics, 11(2), 329–339. https://doi.org/10.1158/1535-7163.MCT-11-0289

43. Place, T. L., Domann, F. E., Case, A. J., City, I., City, I., Physiology, I., & City, I. (2017). Limitations of oxygen delivery to cells in culture: An…. Free Radic Biol Med, 113, 311–322. https://doi.org/10.1016/j.freeradbiomed.2017.10.003.Limitations

Boyden Chamber

Top Well
Insert

Porous
membrane

Gradient
Chemoattractant
agent

Extended Exposure Topotecan Significantly Improves Long-Term Drug Sensitivity by Decreasing Malignant Cell Heterogeneity and Preventing Epithelial-Mesenchymal Transition in a 3D Spheroid Model of Castration-Resistant Prostate Cancer

1. Introduction

Metronomic or extended exposure (**EE**) dosing of chemotherapeutics was first introduced in 2000 as an antiangiogenic therapy.[1,2,3] In contrast to maximum tolerable dosing (**MTD**), which usually involves administering a large single-dose or a short course of therapy at a level just below life-threatening toxicity, EE dosing is usually administered much more frequently at much lower doses and at a cumulative dose that may be at or significantly below MTD. It was hypothesized that EE dosing would more effectively target endothelial cells and would prevent the reflexive regeneration of endothelial cells that can occur during the drug-free periods of conventional therapy. It was also thought that endothelial cells would not develop resistance because they were genetically stable. The antiangiogenic mechanism of EE chemotherapy would later be confirmed with multiple agents and in multiple cancer types, however, malignant cells proved more versatile than anticipated and, in many instances, developed drug resistance.[3,4,5,6,7,8] It was later revealed that the mechanism of action of EE therapy was likely multimodal. Some major mechanisms identified include inhibiting angiogenesis, activating the immune system, and inducing tumor dormancy and senescence.[3,5,9,10]

Our lab first investigated EE dosing of topotecan using an *in vivo* xenograft model of subcutaneously implanted PC3 cells. EE topotecan, which was administered using a

subcutaneously implanted osmotic pump, was compared to MTD topotecan, which was administered as a bolus dose using tail vein injections. EE topotecan significantly reduced tumor growth relative to MTD topotecan. Importantly, we used an athymic mouse model, which found no significant differences in the tumor vasculature of any treatment group.[11] Also, in our *in vitro* experiments, when controlling for cumulative exposure, clinically meaningful changes to the IC50 could not be produced over a 72-hour timepoint (MTD IC50-189.6nM, EE IC50- 177.0nM). Therefore, seemingly, the three major mechanisms of EE dosing (angiogenesis, immunity, and direct effects) could not adequately explain our results. Thus, EE topotecan, somewhat paradoxically, produced similar short-term efficacy and greater long-term efficacy relative to MTD topotecan. We determined the most plausible explanation for these seemingly incongruous results was a change in drug sensitivity over time by the underlying malignant cell population. Or, said in another way, that MTD topotecan led to rapid regimen crippling resistance, which was attenuated by EE topotecan. The remainder of this article will describe the methods used and the evidence obtained to evaluate this underlying hypothesis.

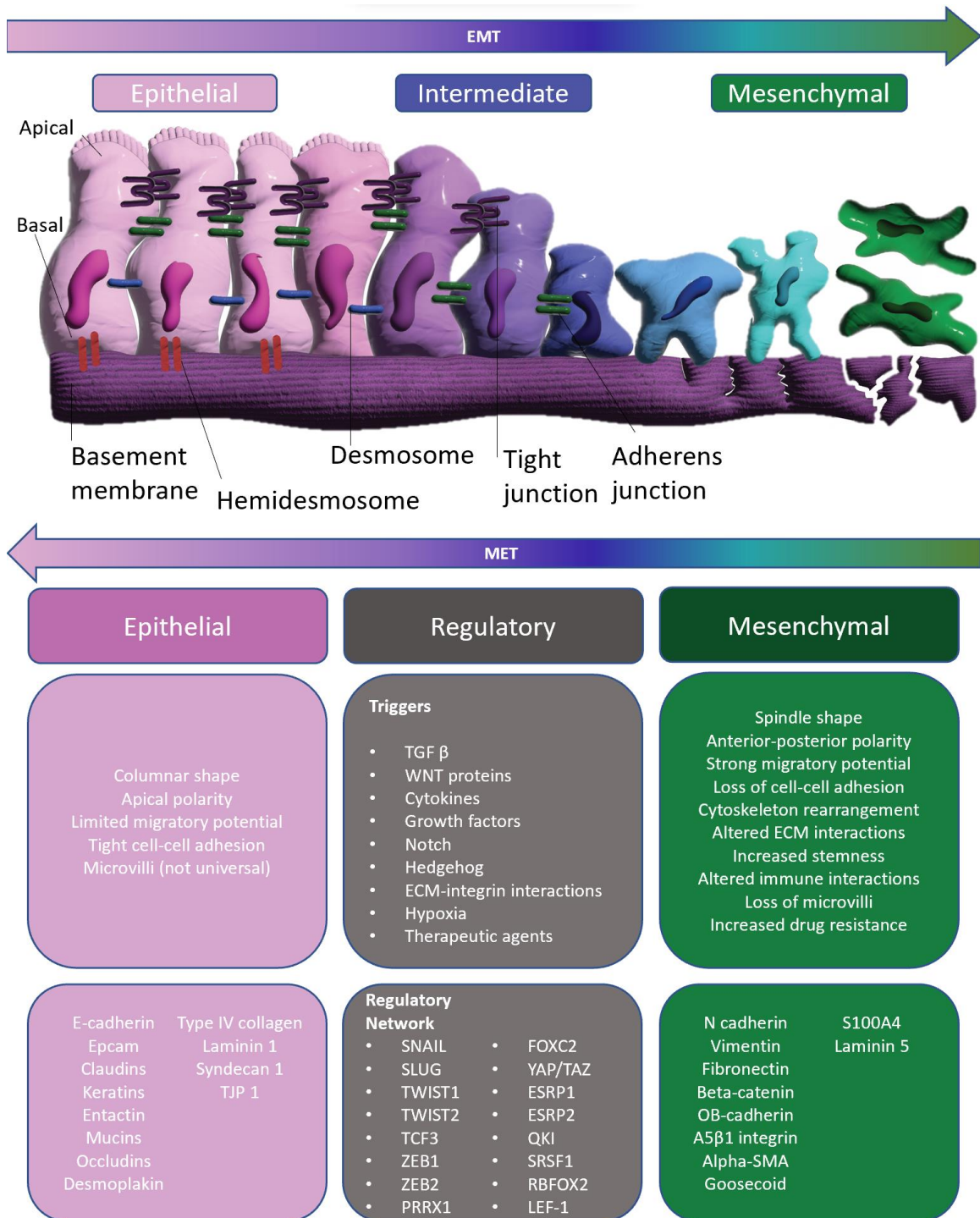## 2. Overview of epithelial mesenchymal transition (EMT)

Figure 1. Overview of epithelial mesenchymal transition (EMT)[14,15,16,17,18,19]

Epithelial mesenchymal transition (**EMT**) is the phenotypic transition of a cell from an epithelial-like state to a mesenchymal-like state. Typical characteristics of epithelial cells include apical-basal polarity, structural cell-cell connections with adherens junctions, tight junctions, and desmosomes, and connection to the basement membrane through hemidesmosomes. Mesenchymal cells on the other hand typically lose cell-cell connections, possess anterior-posterior polarity, and have strong migratory properties. EMT is induced during three main physiological events: embryonic development, tissue regeneration, and cancer progression.[17,20] Cells undergoing EMT being to lose classic epithelial markers such as E-cadherin or epithelial cell adhesion molecule (**EPCAM**), begin to decrease production of mucins and other epithelial matrix molecules, and begin to shed adhesion molecules. These cells also begin to increase production of mesenchymal markers such as N-cadherin, vimentin, and fibronectin. Importantly, this transition is usually more gradual, and cells usually will fall within a range between highly epithelial to highly mesenchymal. This process is also reversible and more mesenchymal-like cells can become more epithelial-like through mesenchymal-epithelial transition (**MET**). EMT can be triggered by many different environmental factors such as hypoxia, cytokines, growth factors, and therapeutic agents. The most common regulatory factors for EMT include Snail (**SNAI1**), Slug (**SNAI2**), twist related protein 1/2 (**TWIST 1/2**), Zinc finger E-box binding homobox 1/2 (**Zeb1/2**). Cancer cells that have undergone EMT can also display other characteristics such as increased stemness, increased migratory potential, increased chemoresistance,

and decreased immune sensitivity.[17,20,21] **Figure 1** summarizes the bulk of the information presented in this overview paragraph.

3. Materials and Methods

3.1. Cell line and cell culture

The human prostate cancer (**PC3**) cell line was obtained from ATCC and was maintained as monolayers in complete medium using F12K (Corning) and 10% (v/v) FBS (Hyclone) at 37°C in a 5% CO_2 atmosphere using a Heracell bios 160i incubator (Thermoscientific). Cells were kept at lower passage numbers (<10 PC3) throughout the experiment to maintain genotypic and phenotypic consistency. Cells were passaged using 0.25% (w/v) trypsin (Hyclone) for 2-3 minutes every 2-4 days according to confluency, which was determined using a Primovert microscope (Zeiss). During the experiment, the PC3 cell line was forked into multiple sub cell lines according to the treatment group, described in greater detail below. Each of these sub cell lines was treated as a unique cell line (separate flasks, no mixing, etc.) throughout the experiment using the same methods described above.

3.2. Spheroid formation

Our spheroid protocol was largely adapted from a high-throughput liquid overlay technique developed by Metzger, et al.[12] This technique rapidly generates many spheroids with minimal incubation time (24 hr), which is necessary for drug screening protocols. Briefly, 96 well U bottom plates (Grenier bio-one) are coated with a 1.2% w/v poly-HEMA (Sigma Aldrich) solution in 95% v/v ethanol. This solution was produced by

incubating poly-HEMA crystals overnight with a magnetic stir rod at 80°C to ensure full

dissolution. The poly-HEMA solution is kept warm throughout the coating process to

prevent precipitation during the evaporation step. 60 µL of the poly-HEMA solution is

added to each well and the plates are heated using a 10x10 hot plate (VWR). Plates are

then left on the hot plate for approximately 1 hour with the lid raised to evaporate the

ethanol. Plates are then sealed using Parafilm (Bemis) for future use. After cells have

been passaged and placed into a separate conical tube, they are mixed thoroughly, and

a small sample is removed for counting using a TC10 automated cell counter (Biorad). A

minimum of two counts are taken per cell line to ensure accurate counts for cell

seeding. Cells are diluted to achieve a concentration of 50,000 cells per mL and placed

on ice. 2.5% v/v of Matrigel (Corning) is added to the cell suspension using an ice-cold

syringe and needle. The cells are then plated using 100 µL of the cell suspension to

attain 5,000 cells per well. The plates are then centrifuged at 400 g for 5 to 10 minutes

at 4°C. This protocol rapidly generates fully formed spheroids within 24 hours for the

PC3 cell line.

3.3. Dosing and spheroid handling

   Two days after initial seeding and spheroid formation, spheroids received an

additional 100 µL of media +/- drug, reaching a total volume 200 µL for the remainder of

the experiment. On days 3 and 5, a media exchange was executed by removing 100 µL

of media per well and replacing it with 100 µL of fresh media +/- drug. Limiting the

media exchanges and leaving some residual, old media prevented spheroid loss

throughout the experiment. On off media exchange days, 10 µL of media was removed

and replaced with 10 µL of media or treatment solution according to the treatment group. Dosing of topotecan (Chempac) occurred using 20x concentrated solutions which could be directly spiked into the wells at 10 µL in 190 µL of media. The conventional or MTD treatment was given as a bolus dose on day 0. Metronomic or EE treatment was given daily as a fractionated dose at 1/7th the MTD. The cumulative dose for the MTD and EE treatments were equal throughout the experiment. In total, there were 3 treatment groups: control, MTD topotecan, and EE topotecan. Topotecan dosing occurred at 100 nM during each week of therapy and occurred between 1 to 100,000 nM for the IC50 assays.

3.4. Study Protocol

Spheroids were generated according to the protocol described in Section 2.2 and were grown for approximately 2-3 days to allow size-dependent drug barriers to form. Spheroids were then dosed according to the protocol in Section 2.3 for a total of 7 days. During the first week of exposure, samples were taken for genomic and proteomic analysis on days 0, 1, 3, and 7. The remaining spheroids were saved for future weeks by digestion using Accumax (Innovative cell technologies) for approximately 1 hour until a single cell suspension was achieved. At this point, a total of 3 treatment groups generated 3 unique cell-lines that were maintained throughout the experiment: PC3-Control, PC3-EE-Topotecan, and PC3-MTD-Topotecan. The digested spheroids were grown in 2D for approximately 1-2 weeks until the cell population was replenished sufficiently to plate additional spheroids. Each cell population was then used to generate two groups of spheroids. One group (3D) was exposed to an additional week of

treatment and one group (3D) was used to assess the resulting sensitivity of the drug

(Topotecan) from the previous week(s) of drug exposure. After another full week of

exposure, some spheroids were harvested for genomic and proteomic analysis, and

some were digested to prepare for another week of exposure and analysis. This cycle

was repeated throughout the experiment. A schematic is depicted below (**figure 1 and**

figure 2) to help better orient readers to the study protocol. Specifically, for scRNAseq,

we analyzed digested spheroids from week 5 (2D) and treated 3D samples from week 6.

Week 5 samples had been grown in 2D for approximately 1 to 2 weeks in drug-free
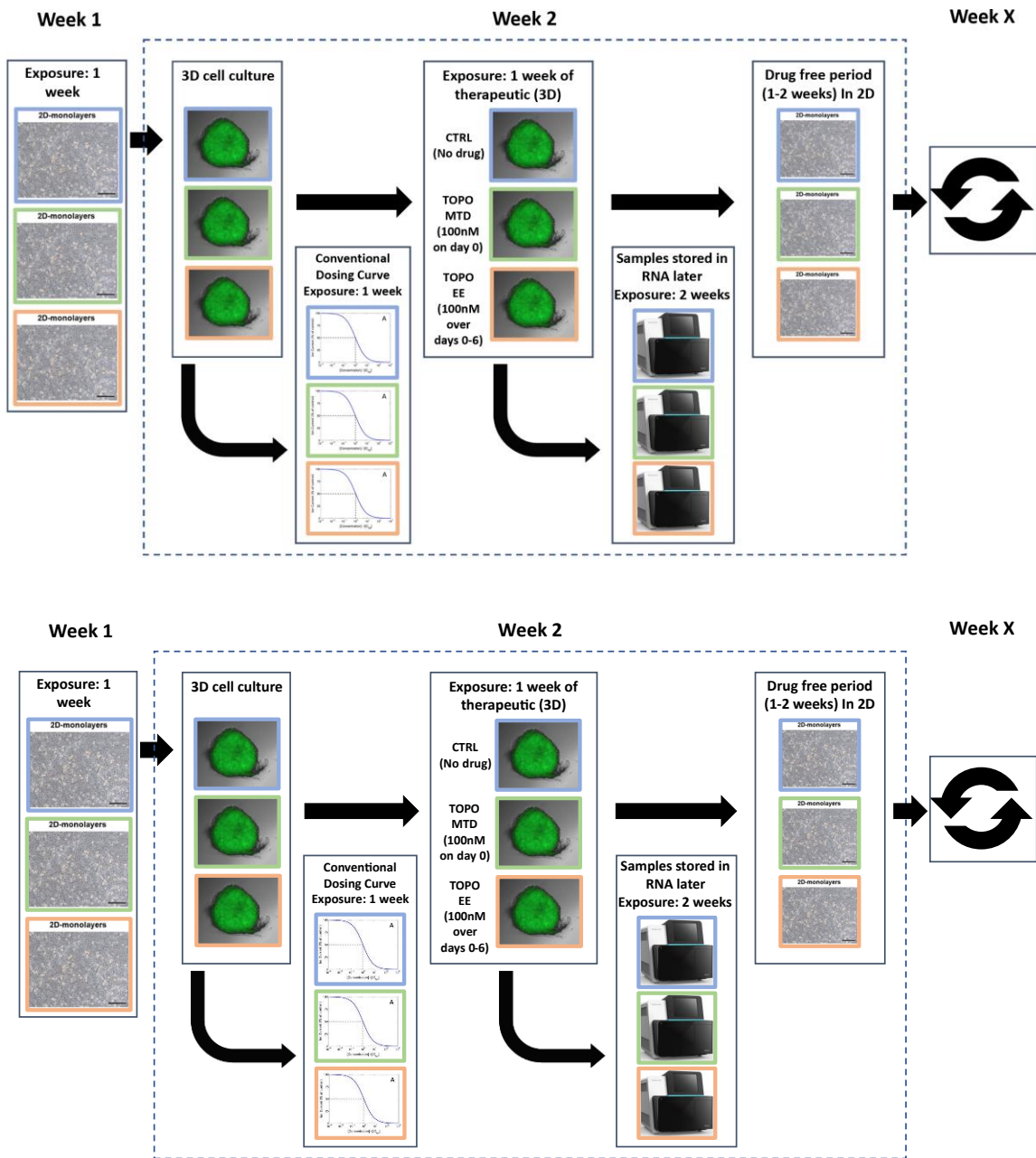
media before analysis.

Figure 3. Schematic depicting the second week of the study protocol, starting from the treatment exposed cell lines.

3.5. Resazurin assay (Cytotoxicity)

Resazurin was used to measure the mitochondrial activity of the cells as a surrogate for cell viability because the reductive conversion of resazurin to resorufin creates a water-soluble end-product. This prevents the need for a solubilizing step, which would be untenable in a 3D format. Resazurin (Alfa Aesar) was made fresh for each assay at a 0.015% w/v concentration in PBS and was sterilized using a 0.22 μm filter. Before resazurin was added to the spheroids, the spheroids were moved from U bottom 96 well plates to flat bottom black, fluorescent plates (Grenier bio-one). This was accomplished using a 1 mL pipette tip to move the spheroid and 100 μL media. Moving the spheroids increased the accuracy of the imaging and spectrophotometry. This also ensured that well volume variability from inconsistent evaporation dynamics that occur over the duration of the experiment would not alter the resorufin concentrations. Resazurin was added at a ratio of 10 μL per 100 μL of media and was incubated for 4 to 12 hours with readings taken over time (2, 4, 6, 8, 12). Generally, 4-6 hours was the most appropriate time point and achieved the lowest CV values with the greatest sensitivity and limited assay saturation. Fluorescent measurements for each plate were read using a Cytation 5 plate reader (BioTek) with excitation set at 560 nm and emission set at 590 nm.

3.6. RNA storage protocol

Cells and spheroids are separated into individual microfuge tubes at approximately 1,000,000 cells/mL and washed 2x using PBS (Wards science) and the Heraeus Fresco 21 microcentrifuge (Thermoscientific) set at 400g and 4C for 10 minutes. Samples are

maintained on ice for the duration of the protocol. PBS is aspirated and replaced with

300μL of RNA later (Qiagen). Samples are stored overnight (24H) at 4C before moving to

-80C for long-term storage. For scRNAseq, live samples are necessary and therefore,

RNA later is not appropriate. Instead, we stored samples by cryopreservation using 10%

DMSO in complete media and stored in liquid nitrogen.

RNA Isolation

Total RNA was isolated from cultured cells and 3D spheroid model using standard

RNA extraction kits (RNeasy Kits–QIAGEN). RNA concentration and integrity were

estimated by a NanoDrop 2000 UV-Vis spectrophotometer (Thermo Scientific, United

States), Qubit® 2.0 Fluorometer (Invitrogen, Carlsbad, CA, United States), and Agilent

2,100 Bioanalyzer (Applied Biosystems, Carlsbad, CA, United States). RNA integrity

number threshold of eight was used for RNAseq analysis.

3.7. RNAseq

RNAseq libraries were constructed using Illumina TruSeq RNA Sample Preparation

Kit v2. Libraries were then size selected to generate inserts of approximately 200 bp.

RNA sequencing was performed on llumina's NovaSeq next-generation highthroughput

sequencing system using 150 bp paired-end protocol with a depth of more than 20

million reads per sample. The average quality scores were above Q30 for all libraries in

both R1 and R2.

RNAseq Data Processing

RNAseq data were normalized, and fragments per kilobase million values were used in further analysis using Partek Genomics Suite and Galaxy data analysis software, an open source, web-based platform that provides tools necessary to create and execute RNA-seq analysis. In brief, RNA-seq data analysis pipeline was developed using Galaxy software workflow. Quality control (**QC**) check on the RNAseq raw reads was performed using the FastQC tool, followed by read trimming to remove base positions with a low median (or bottom quartile) score. Tophat2 Aligner tool mapped processed RNAseq reads to the hg19 human genome build. Picard's CollectInsertSizeMetrics tool was applied on the initial tophat2 run to obtain estimated insert sizes, which was then used to calculate mean inner distance between mate pairs (mean = estimated_insert-size−2×read_length). Tophat2 was re-run using corrected mean value and Cufflinks tool was to assemble the reads into transcripts.

Bioinformatics Analysis.

Gene expression data were filtered using the following criteria: genes with mean FPKM < 1 were removed. Global gene expression profile (**GEP**) data were analyzed further using a combination of R and Partek Flow to perform differential expression testing to identify GEP signatures of drug response. Mean fold-change > j1j and P < 0.05 were considered thresholds for reporting significant differential gene expression. Differentially expressed gene analysis was performed between two groups of gene expression datasets (e.g., treated vs. untreated). Heatmaps were generated using unsupervised hierarchical clustering analysis based on the differentially expressed genes (**DEGs**). Owing to the small sample size, Limma, an empirical Bayesian method, was used

to detect DEGs, obtain P values, and further provided a false discovery rate based on the

P value using the Benjamini-Hochberg procedure to detect the DEGs.[51] The advantage of

Limma compared with a traditional t test is that it provides a moderated t test statistic

by shrinking the variance statistics and therefore improves the statistical power.

All samples were initially normalized to control day 0. Then, each MTD and EE

timepoint was normalized to the corresponding control timepoint, e.g. day 7 MTD and

EE samples were normalized to day 7 control. After normalization, the top 1000 genes

with the lowest p-value were selected. Then, MTD and EE samples with a relative fold

change difference less than 2 were removed. Finally, each gene required at least 2

timepoints with a fold change difference greater than 1.5 to remove one-off gene

changes. Each gene was then manually investigated to determine its role and function

using databases such as GeneCards as well as literature searches using Pubmed.[25] Genes

without a well-defined function or genes without a clear role were labeled as unknown.

Heatmaps were generated using heatmapper, a web-based tool.[13]

Statistical Analysis

All statistical analyses were performed using R for statistical computing and

graphics, v3.4.2, and GraphPad Prism v7.0. We used parametric methods to analyze

differences between two groups of cells. If the assumption appeared violated,

appropriate nonparametric procedures were used. All tests were two-sided, and

differences with a $P < 0.05$ were considered statistically significant.

Ingenuity Pathway Analysis.

Ingenuity pathway analysis (**IPA**) software (QIAGEN) was used to identify the most significantly affected 1) molecular pathways predicted to be activated or inhibited, 2) upstream regulator molecule like miRNA, transcription factors, 3) downstream effects and biologic processes that are increased or decreased, and 4) predicted causal networks, relationships, mechanisms and functions relevant to changes observed in our dataset and 5) perform predictive toxicology analysis using toxicogenomics approaches (IPA-Tox).[52]

3.8. scRNAseq

The presence of drug-resistant single-cell subpopulations (subclones) may influence differential response to METRO therapy in PCa tumors. Therefore, we performed single-cell transcriptomics to identify resistant and sensitive subclones based on single-cell GEP signatures. Briefly, automated single-cell capture, and cDNA synthesis was performed at ~5000 tumor cells/sample using 10X Genomics Chromium platform. Single-cell RNAseq-based gene expression analysis was performed on Illumina HiSeq 2500 NGS platform (Paired end. 2*125bp, 100 cycles. v3 chemistry) at ~5 million reads per sample. scRNAseq data was analyzed using R, Seurat and Partek Flow software packages. All *statistical analyses* were performed using the R statistical package, and GraphPad Prism with a two-sided p-value <0.05 considered as statistically significant. Total sample numbers and replicates were determined by performing a *power analysis* with an effect size of 0.25 and a significance level of 0.05 with a power of 80%. **IPA analysis:** was performed to identify regulators, relationships, mechanisms, functions and pathways relevant to changes observed in our dataset.

3.9. Immunoblotting

Treatment-mediated effects on most differentially expressed genes will be assessed at the calculated IC50 of specific drug for each treatment protocol in PCa cell lines and 3D tumor spheroids after drug exposure (*MTD* and *EE*). Cells or 3D spheroid were harvested, washed, and lysed using radioimmunoprecipitation assay lysis buffer containing 50 mM Tris-HCl, pH 7.5, 150 mM NaCl, 1% Nonionic polyoxyethylene (**NP40**), 5 mM Ethylenediaminetetraacetic acid (**EDTA**), 1 mM dithiothreitol (**DTT**), phosphatase, and protease inhibitors cocktail (Sigma) and incubated on ice for 15 min. Samples were then centrifuged at 18,500 g at 4°C for 30 mins. The supernatant was then aspirated and quantified using Pierce BCA Protein Assay Kit (Thermo Scientific). At each time point, samples were solubilized in sodium dodecyl sulfate polyacrylamide gel electrophoresis sample buffer, and equal amounts of protein were loaded per lane of 4-15% tris-glycine-extended (**TGX**) stain-free precast gels for separation under reducing conditions, transferred to a Polyvinylidene difluoride (**PVDF**) membrane (Millipore; Billerica, MA). Membranes were blocked in tris-buffered saline (**TBS**) with SuperBlock blocking buffer (Thermo Fisher) and incubated with primary antibodies for target gene/proteins, Actin-β (housekeeping/ control) and then with the appropriate secondary antibody in TBS with 0.2% Tween 20 and 2.5% bovine serum albumin. Immunoreactivity (bands) detected and quantified using Chemiluminescent horseradish peroxidase (**HRP**) substrate (Bio-Rad), Pierce ECL Western Blotting substrate (Bio-Rad, CA). Images were captured and quantify by Gel Doc™ EZ Gel Documentation System and ImageLab™

Software (Bio-RAD, CA). Densitometry analysis was performed (in triplicates) using standard image analysis software ImageJ.

3.10. Statistics

The curve fitting and statistical analysis of the IC50 data were performed using Graphpad Prism (Dotmatics, Boston MA, USA). The IC50 was determined at ½ of fitted maximal activity. Usually, an extra sum-of-squares F test was used to compare IC50 values between treated and control samples.

4. Results

4.1. Comparing the long-term potency of EE and MTD topotecan.

We first wanted to determine whether different dosing schedules of topotecan could alter long-term topotecan potency. To do this, we used a 3D spheroid model of PC3 cells that could be maintained and dosed for weeks to months. We used an initial weekslong exposure with intervening drug-free intervals (in 2D) to better simulate MTD dosing. The intervening drug-free intervals also allowed us to accurately replate cells for each IC50 assay. This prevented an ever-increasing week-to-week sample variability that could occur in a strict longitudinal assay. The EE dose (14.28nM) was given daily at $1/7^{th}$ the MTD dose (100nM), which was given as a bolus on day 0. The total cumulative exposure for each treatment was equal throughout the experiment. We also included untreated spheroids, which served as a model control for the experiment. Each treatment was administered for 6 total weeks of exposure, which amounted to roughly 3-4 months of total study duration when accounting for the drug-free intervals. After

the first treatment, each treatment group was maintained as a separate cell-line for the

remainder of the experiment. After each week of exposure, an IC50 assay was

performed, and samples were stored for future genomic, transcriptomic, and proteomic

analysis. A plot of the long-term potency changes can be found in **figure 4**. **Overall, over**

the entire study period, we found that the topotecan IC50 increased 2.21-fold for

control spheroids, increased 1.44-fold for EE spheroids, and increased 58.34-fold for

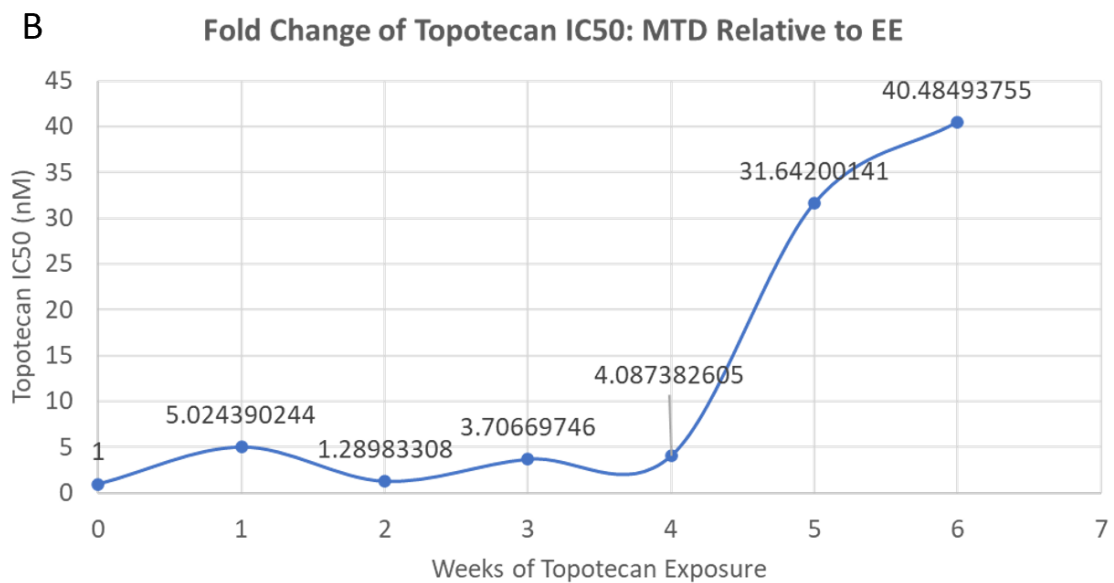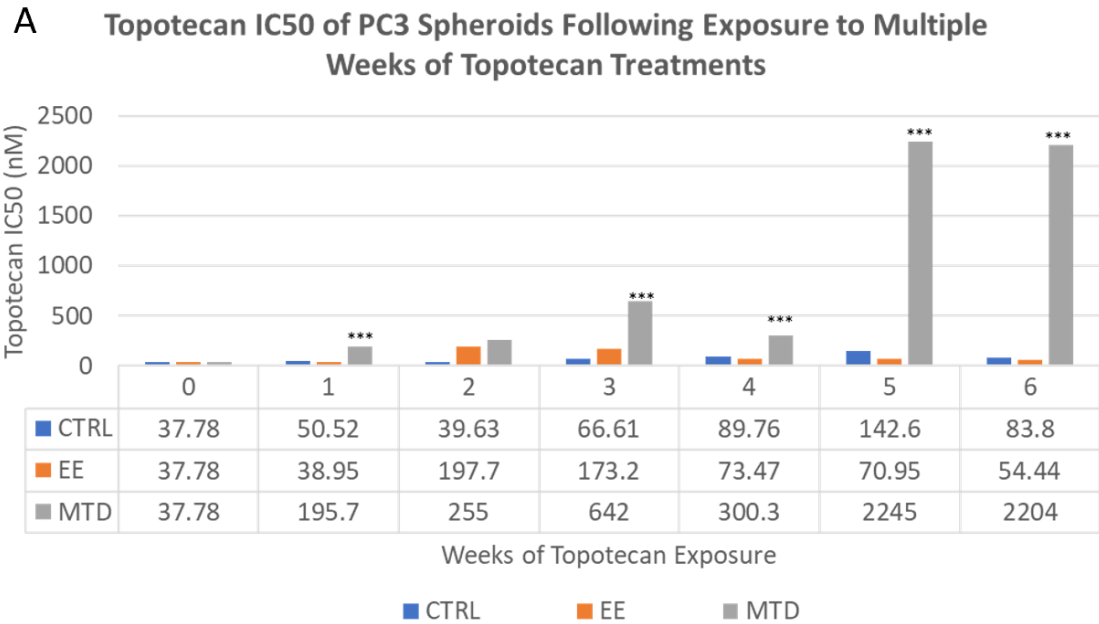**MTD spheroids relative to the initial untreated control sample, which was statistically**

significant.

A Topotecan IC50 of PC3 Spheroids Following Exposure to Multiple Weeks of Topotecan Treatments

	0	1	2	3	4	5	6
CTRL	37.78	50.52	39.63	66.61	89.76	142.6	83.8
EE	37.78	38.95	197.7	173.2	73.47	70.95	54.44
MTD	37.78	195.7	255	642	300.3	2245	2204

Weeks of Topotecan Exposure

CTRL   EE   MTD

B Fold Change of Topotecan IC50: MTD Relative to EE

Weeks of Topotecan Exposure

Figure 4
A) Comparison of the long-term IC50 data of three treatment groups:
* **Control** (CTRL)(no treatment)
* **Extended exposure topotecan** (EE)(daily fractionated dose (14.28nM) given as 1/7th the MTD dose)
* **Maximum tolerable topotecan** (MTD)(bolus dose (100nM) given at the start of each week)

Spheroids were dosed weekly with intervening drug-free intervals for a total of 6 weeks. The IC50 was assessed weekly. The cumulative total exposure of topotecan was equal for the EE and MTD treatment groups.
*** demonstrate statistical differences between MTD and EE treatments
B) Relative fold change (MTD/EE) for the weekly IC50 data.

4.2. Determining the impact of different dosing strategies on population heterogeneity

Intratumor heterogeneity is a major cause of drug resistance and can result in worse clinical outcomes for patients. Heterogenous populations are more genetically and phenotypically diverse, which increases the probability that a resistance inducing phenotype or mutation is present in the underlying cell population. Heterogenous populations also possess a more variable exposure response profile at an individual level, which may protect some cells from death and allow further resistance to develop over time.[22,23,24] Because of these factors, it was important to determine the impact of MTD and EE treatments on the underlying heterogeneity of the population as this could affect drug potency over time. We analyzed our scRNAseq data using t-SNE, which is a nonlinear dimensionality reduction technique that arranges similar objects as nearby points and dissimilar objects as distant points.[27] In this analysis, we used samples that were obtained from the IC50 study at different timepoints. In particular, we compared 2D samples taken on the last day of their drug-free interval, just prior to reseeding for the 6th week of treatment to 3D samples taken after the final day of the 6th week of treatment. This helped us understand the impact of the 3D model on heterogeneity (red/blue), to understand the immediate impact of drug treatment on heterogeneity (yellow/cyan and green/purple vs red/blue), and to understand the long-term impact of drug treatment on heterogeneity (yellow/green vs red). This data is presented in **figure 5**. The control 2D (red) and 3D (blue) graphs show a modest increase in heterogeneity in the 3D sample. The MTD treated 3D sample (cyan) is more heterogeneous than the 3D control sample (blue), is more heterogeneous than the 2D drug-free interval MTD

sample (yellow) and is more heterogeneous than the EE treated 3D sample (purple). The

EE treated 3D sample (purple) is more uniform than the 2D drug-free interval EE sample

(green) and is relatively similar to the 3D control sample (blue). The MTD (yellow) and

EE (green) drug-free interval 2D samples are more heterogeneous than the 2D drug-free

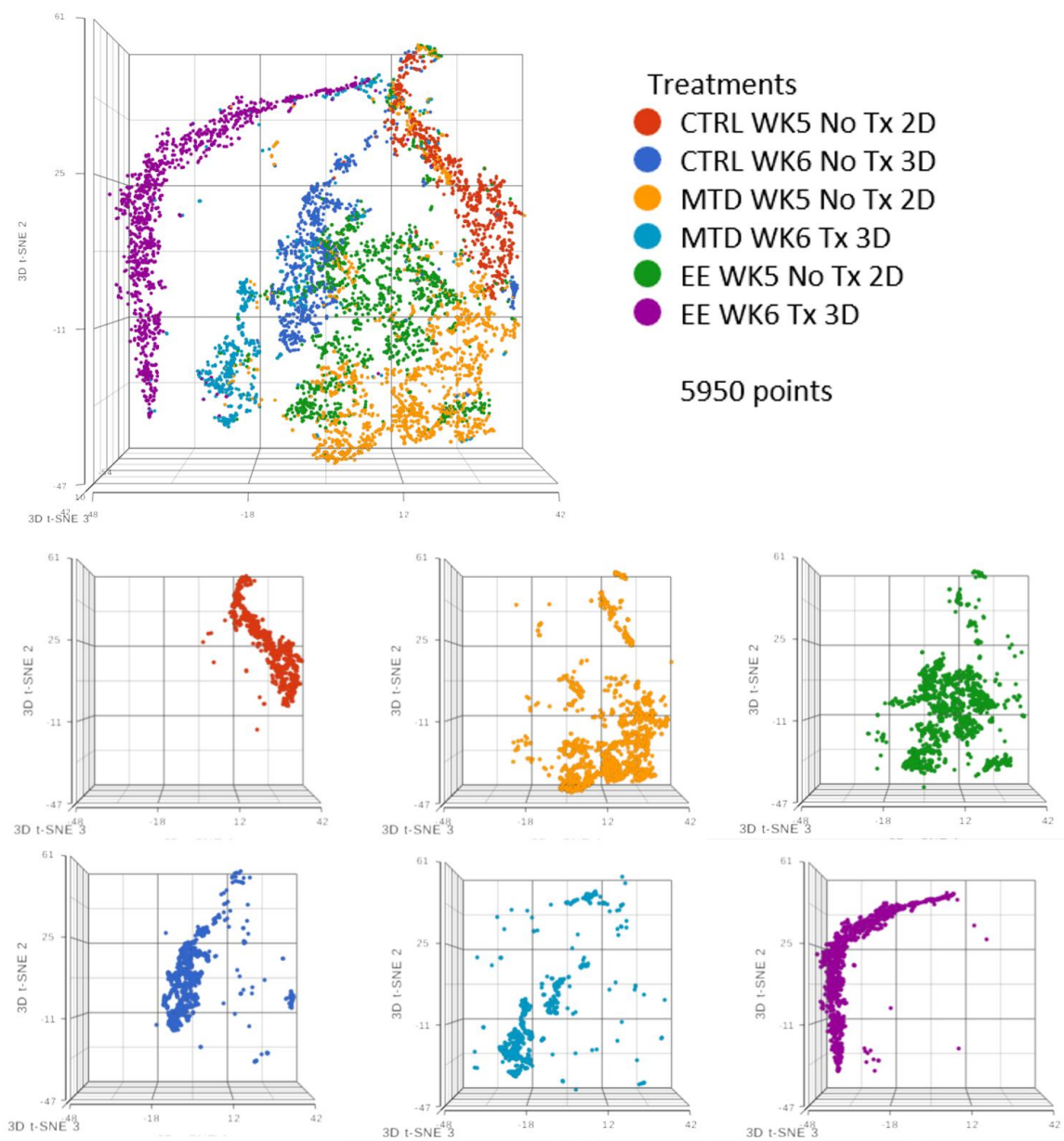interval control sample (red).

Figure 5 t-SNE analysis of scRNAseq data from pre-treated 2D cells after 5 full weeks of treatment and following a 2-week drug-free interval and from post-treated 3D cells after the final day of the week 6 treatment.

4.3. Evaluating the underlying molecular causes of MTD induced drug resistance

We used RNAseq to identify underlying transcriptomic differences between the MTD and EE treated cells. Out of an initial list of 1000 genes selected based on lowest p-value, 189 genes were selected for further analysis. A total of 51 out of the 189 genes did not have a well-defined function or had limited information available in the literature (see appendix). After additional screening criteria, 94 total genes were selected for analysis. The overall expression pattern for the complete list of 94 genes is shown in the heatmap (**Figure 6**). These genes had well-known functions in cell adhesion, tumor suppression, malignancy progression, or are well known epithelial markers. The heatmap (**Figure 6**) revealed a significant deviation from the control for the MTD-treated cells over time. During the first week (Days 1, 3, 7), most genes were not differentially expressed relative to control (grey boxes), indicating transcriptomic similarity to the control cells. However, CXCL8 is a notable exception for MTD cells, which generated a 14.45-fold change relative to control on day 1. EE treated cells generated a 1.5-fold change for CXCL8 on day 1. After 2 weeks of treatment, most genes from the MTD and EE-treated cells were significantly different to control but were not drastically different. At this point, the MTD and EE-treated cells look relatively similar. Over the next few weeks, however, the MTD-treated cells began to significantly diverge from both the control group and the EE-treated cells. In many instances, genes that were perturbed in week 3 became directionally more perturbed throughout the experiment with some genes registering a change of over 300-fold.
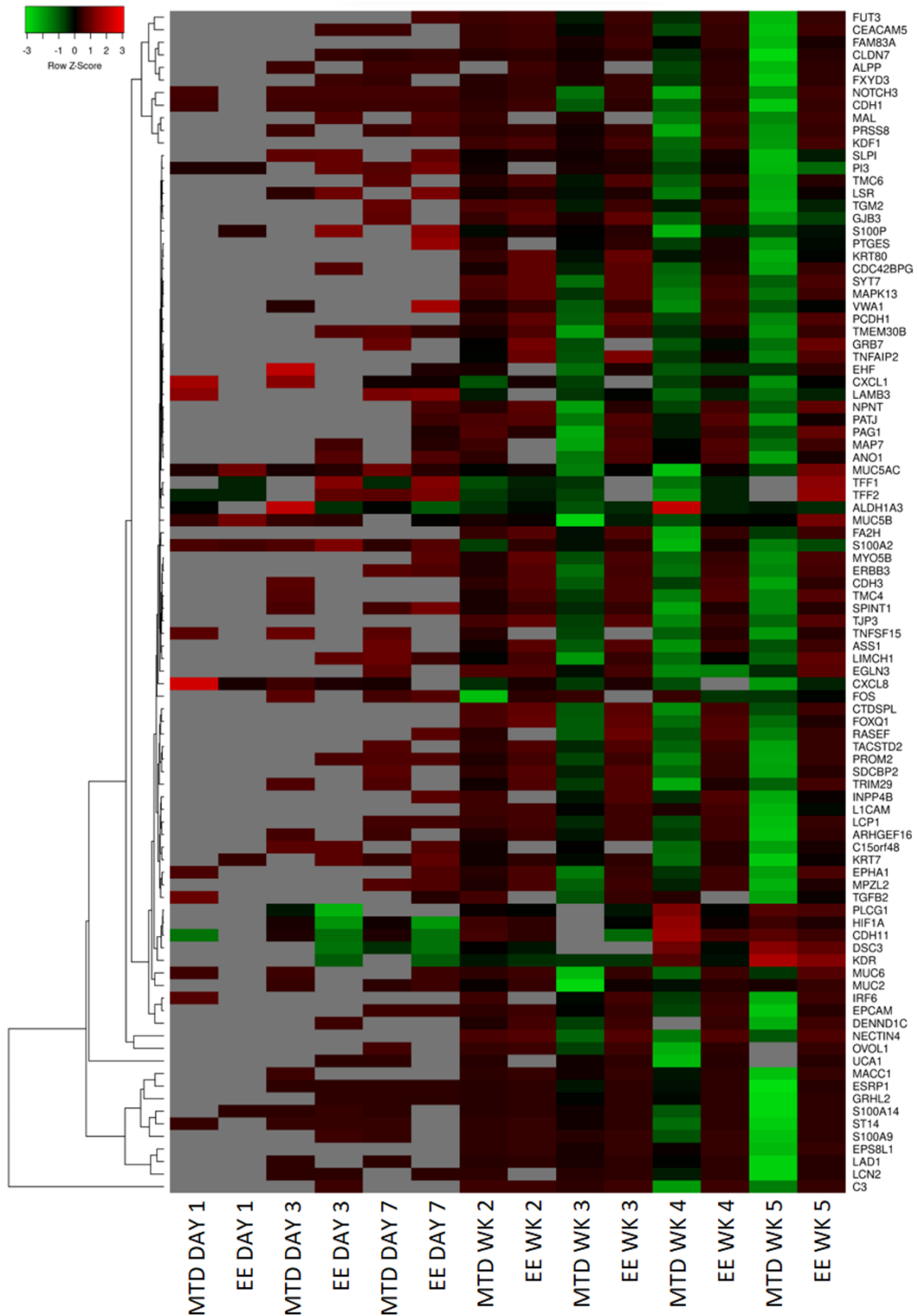
Figure 6. Heatmap of the top differentially expressed genes (RNAseq) over a five-week period from MTD and EE dosed spheroids. Grey boxes did not meet statistical significance. Green boxes are downregulated, and red boxes are upregulated.

In **figures 7, 8, and 9**, we highlight a few specific genes associated with EMT and provide a graph of the fold change over time for the MTD and EE treated cells. Only points that were statistically significant were included in each graph. In **Figure 7**, we identify a few important epithelial markers that are significantly downregulated during EMT. A few important gene types in this list are claudins (**CLDN7**), adhesion molecules (**CDH1**/E-Cadherin, EpCAM, or laminin beta 3 (**LAMB3**)), mucins (**MUC2**, **MUC5AC**, or **MUC6**), keratins (**KRT7**, **KRT80**), and PATJ crmbs cell polarity complex component (**PATJ**), which regulates both tight junctions and cell polarity.[26] The orange line for all graphs represents fold change over time relative to control for the MTD treated cells. Almost every gene identified in this graph is significantly downregulated by the MTD treated cells. In contrast, the expression profile of the EE treated cells (blue line) is relatively stable throughout the experiment. In **Figure 8**, we highlight a few genes that are known to regulate EMT. In this graph, we also included genes that were not included in the heatmap in **figure 6** to help provide a comprehensive view of the EMT transition for these cells. These genes are marked with a red dot. Epithelial splicing regulatory protein 1/2 (**ESRP1**, **ESRP2**), grainyhead like transcription factor 2 (**GRHL2**), Notch3, Ovo like transcriptional repressor 1 (**OVOL1**), and ZEB1 are the most significantly altered by the MTD treatment. Similar to the epithelial markers listed in **figure 7**, gene expression from the EE treated cells were mostly stable throughout the experiment. The remaining genes, Quaking homolog KD domain RNA binding (**QKI**), RNA binding motif protein 9 (**RBFOX2**), Serinine/arginine rich splicing factor 1 (**SRSF1**),

transcription factor 3 (**TCF3**), and Yes1 associated transcription regulatory (**YAP1**) did

not have many significant datapoints for either treatment and the few datapoints there

were significant were not significantly different between each treatment group. In

Figure 9, we reveal the long-term gene expression profile of MTD and EE treated cells

for many well-known mesenchymal markers. It should be noted that no gene in this list

met the inclusion criteria for our gene list in **figure 6**. N-cadherin (**CDH2**), beta-catenin

(**CTNNB1**), and S100 calcium binding protein A 4 (**S100A4**) had many missing

(insignificant) datapoints, but the datapoints available were not significantly different

from each other or from control. OB-cadherin (**CDH11**), fibronectin (**FN1**), integrin-α5

(**ITGA5**), laminin 5 (**LAMA5**), and vimentin (**VIM**) were not significantly altered by either

treatment group relatively, and were not significantly different from control.
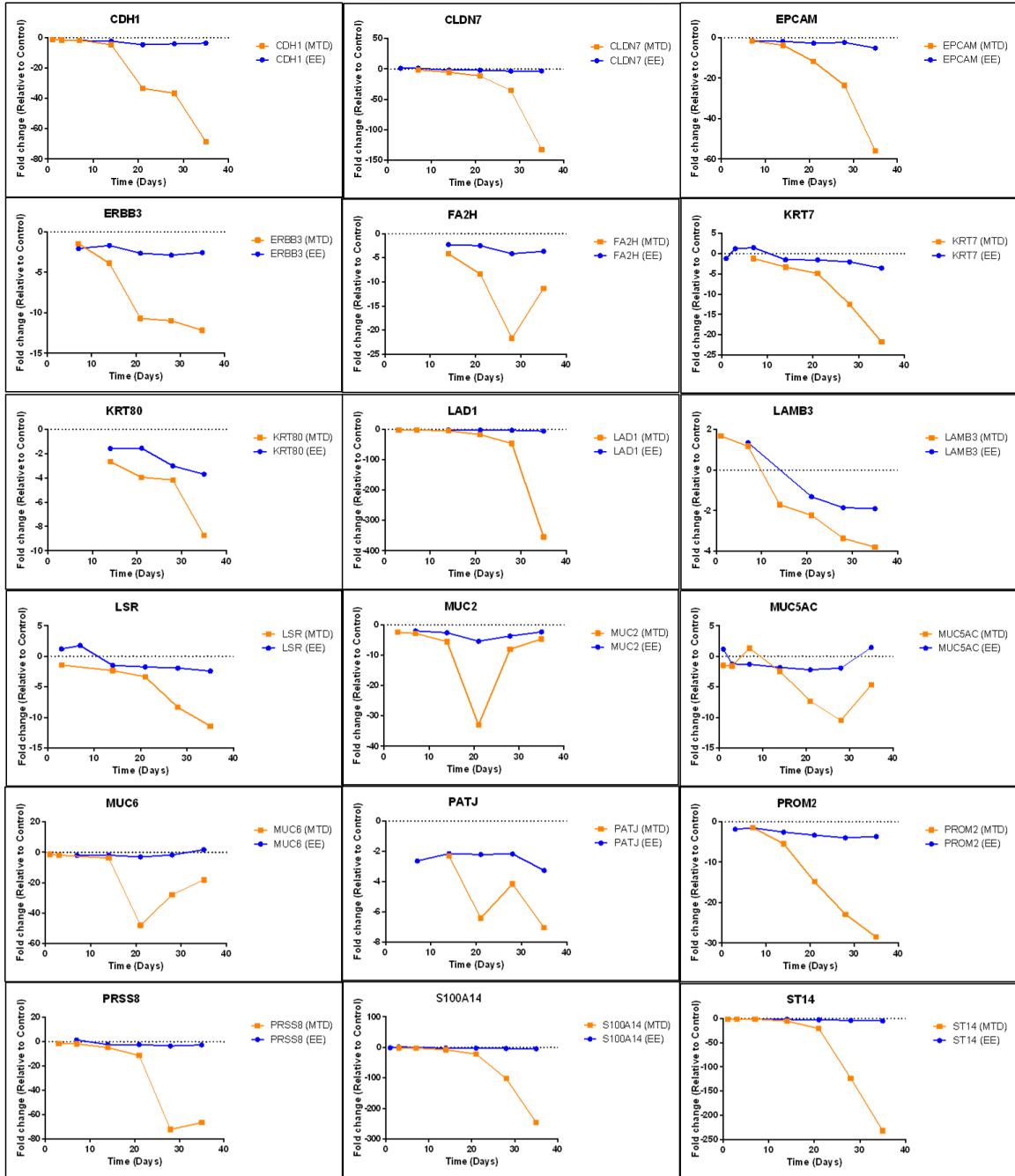
Figure 7. Gene expression over time for select epithelial markers
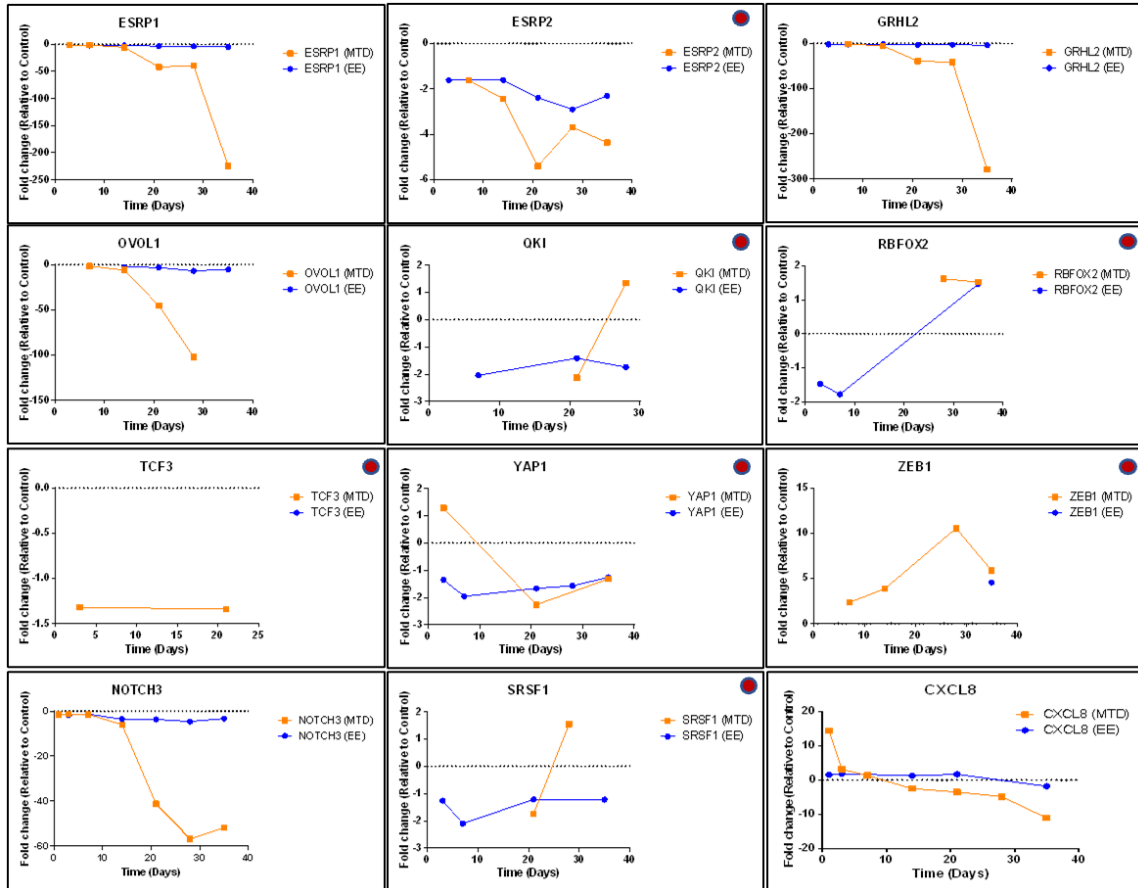
Figure 8. Gene expression over time for key EMT regulatory genes
** SNAI1, SNAI2, TWIST1, TWIST2, ZEB2, PRRX1, FOXC2, and LEF1 were not found to significantly differ from control in any timepoint

🔴 Did not meet initial screening criteria, but are included to provide a more comprehensive view of the EMT transition

Figure 9. Gene expression over time for key mesenchymal markers
** ACTA2 and GSC were not found to significantly differ from control in any timepoint

● Did not meet initial screening criteria, but are included to provide a more comprehensive view of the EMT transition

4.4. Assessing whether different administration schedules can affect efflux pump and

topoisomerase expression.

We wanted to explore whether efflux pump and topoisomerase expression

patterns could be altered by alternative dosing strategies because of their potential role

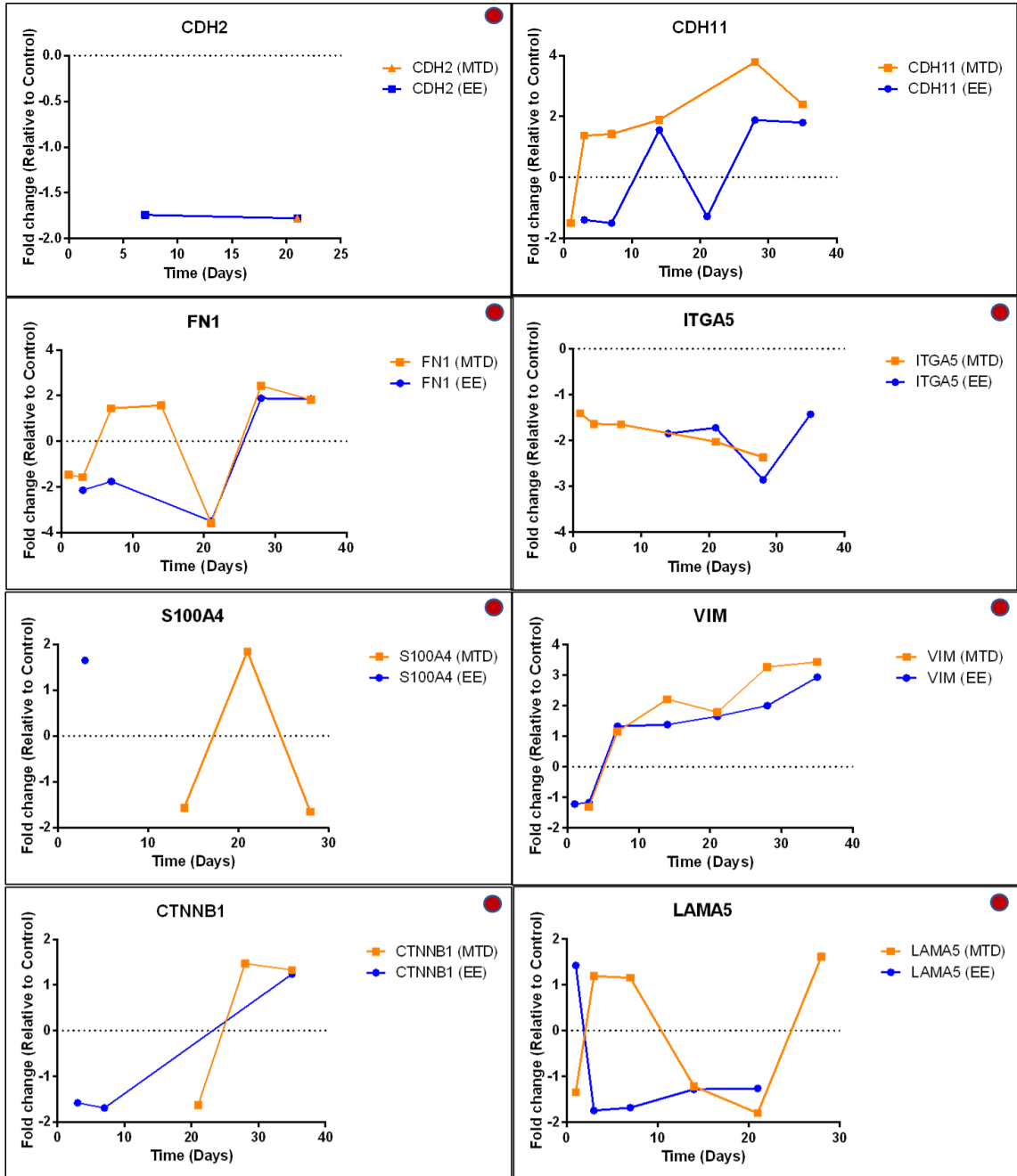in causing topotecan drug resistance. To do this, we utilized scRNAseq, which provides a

more in depth understanding of the individual expression patterns within a cancer

population. We used the same sample set that was used in **figure 5**. These samples are

identified using a colored square in **figures 10 and 11**. The efflux pump expression

pattern can be found in **figure 10**. When comparing the 2D control (red) to the 3D

control (blue), an increase in the density of efflux pump expression can be seen with

many more cells expressing efflux pumps. The 3D control group increased expression of

the ABCA7, ABCC3, and ABCC4 efflux pumps. Interestingly, the 2D MTD (yellow) and EE

(green) drug free interval populations also showed increased efflux expression

frequency with both groups highly expressing ABCC3, ABCC4, ABCC5, and ABCG1. The

treated 3D MTD (cyan) sample also increased the density of cells expressing efflux

pumps with ABCC3 and ABCC5 being the most prominent. On the other hand, the 3D EE

treated sample (purple) did not display increased efflux pump expression relative to the

2D control sample. In fact, it could be argued that the EE treated sample reduced efflux

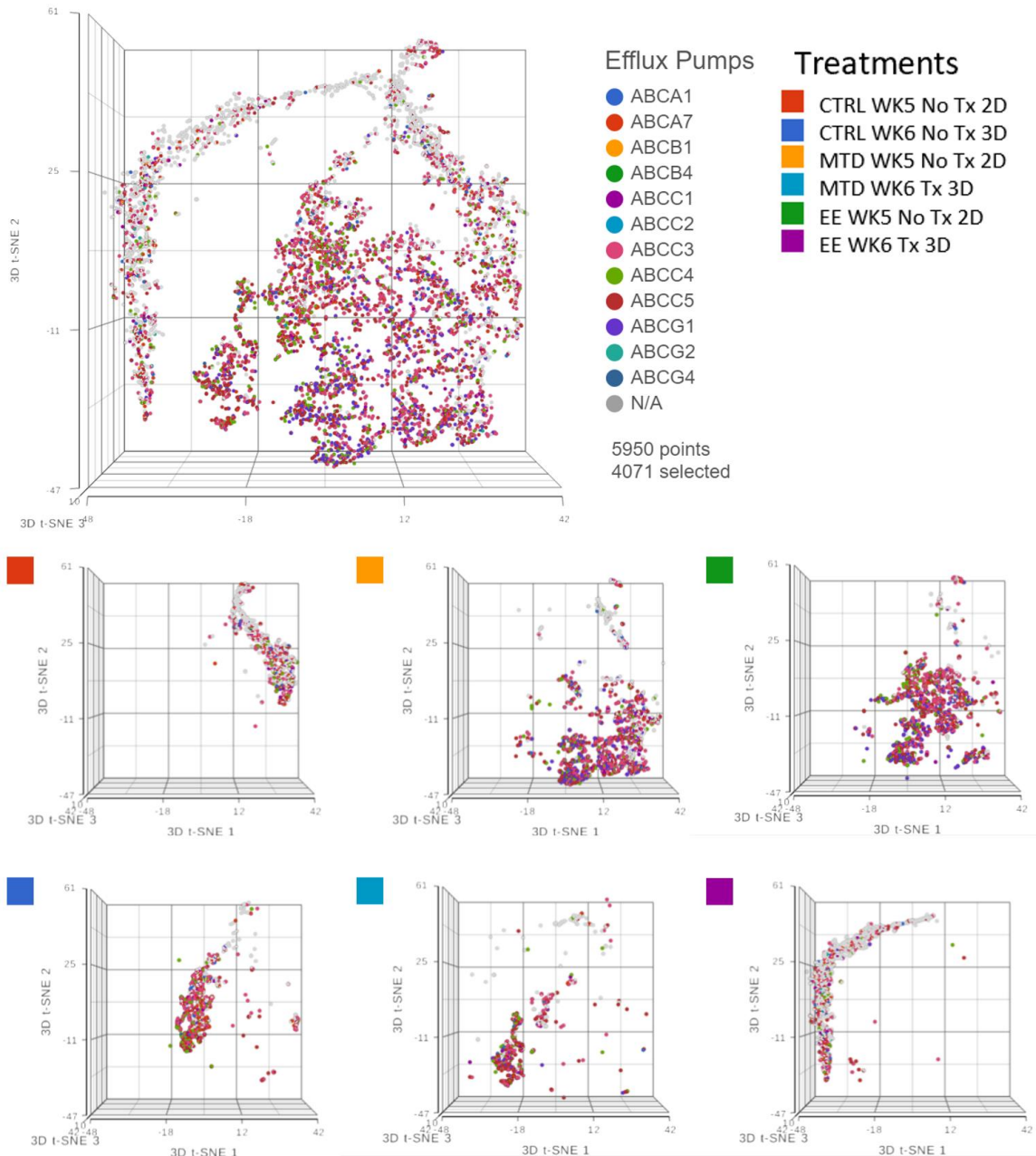pump expression relative to the control 2D sample.

Figure 10. Analysis of the impact of different dosing strategies of topotecan on efflux pump expression using scRNAseq.

Next, because topoisomerases are the main target of topotecan (specifically topoisomerase I), we wanted to assess whether alternative dosing strategies could alter the topoisomerase expression patterns, which could play a role in drug resistance. This data is shown in **figure 11**. Although there are several insights that can be identified in this data, one of the most striking sample characteristics is the relative expression of topoisomerase I (**TOP1**) to topoisomerase II (**TOP2**) and topoisomerase III (**TOP3**). The control 2D (red) sample produced more TOP1 and less TOP2 with limited TOP3 expression. The control 3D (blue) sample showed increased TOP2 relative to TOP1, but with still limited TOP3. The drug-free interval 2D MTD sample (yellow) drastically increased its TOP2 expression relative to TOP1, but also increased its TOP3 expression. The 2D EE sample (green) also showed a similar increase in TOP2 and TOP3 expression relative to TOP1. The 3D MTD treated sample (cyan) also increased its TOP2 and TOP3 expression relative to TOP1 but had the lowest amount of TOP1 of all samples. The 3D EE treated sample (purple) displayed much higher TOP1 expression relative to the MTD treated samples and rivaled even the control 2D group. This sample also produced some TOP2, but limited TOP3.
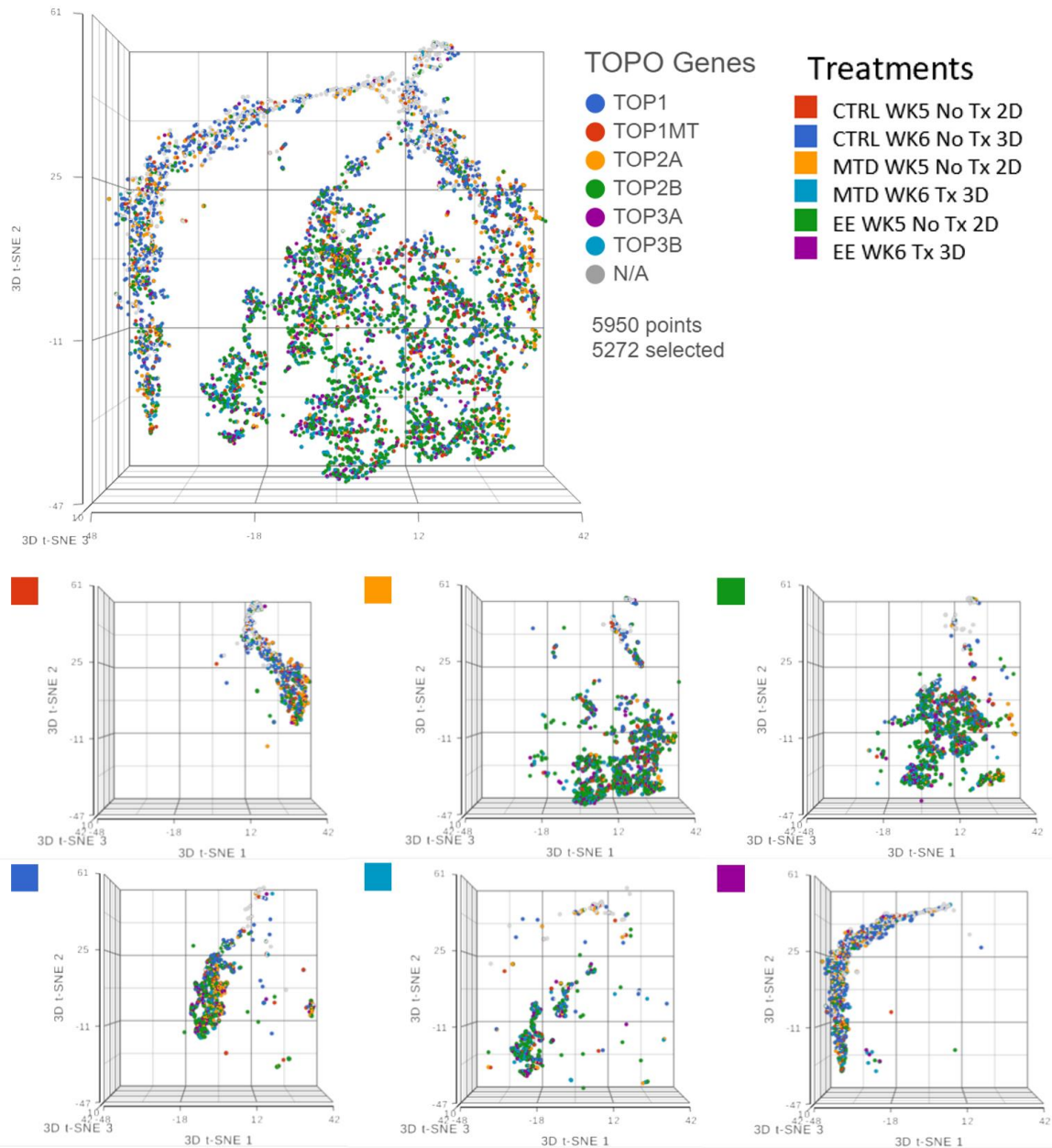
Figure 11. Analysis of the impact of different dosing strategies of topotecan on topoisomerase gene expression using scRNAseq.

5. Discussion

Metronomic or extended exposure dosing of oncologic agents is a relatively new paradigm with the potential to improve efficacy and reduce toxicity in some patients. To date, this treatment modality has demonstrated the ability to impact angiogenic and immunologic targets, however, in this article, we investigate a potential novel mechanism impacting drug resistance. In **figure 4**, we used a long-term spheroidal model of PC3 cells to investigate the potency of topotecan over time after multiple weeks of treatment with either MTD or EE dosed topotecan. After 6 full weeks of drug exposure or approximately 3-4 months total, we demonstrated decreased potency by the MTD treated cells. On the other hand, the EE treated cells maintained potency in line with the control cells. These data suggest that drug dosing can have a substantial impact on the underlying cell population, which can drastically affect efficacy. This also calls into question how our therapeutics impact patients' tumor cells and whether, long-term, we are creating more aggressive and resistant tumor cells to acutely reduce tumor volume. It also suggests that drug screening and evaluation should occur in longer-term model systems to appropriately identify treatments that can achieve sustained success. If we were to convert the potency data for MTD topotecan into a clinical scenario, it would suggest that after a single treatment, a patient would require approximately 4-5x the initial dose to have a similar impact on tumor cells. After 5 weeks of treatment, a patient would require 40x. If a treatment cannot eliminate tumor cells completely, which is currently true for almost all oncologic therapeutics, then maintaining a sensitive cancer cell population is vitally important.

To appropriately evaluate the impact of drug dosing on treatment resistance, we wanted a model system with adequate exposure duration, variable individual cell exposure through physical barriers and treatment gradients, and increased intratumor-like heterogeneity through added model complexity. Using scRNAseq (**figure 5**), we evaluated the impact of each treatment as well as the model system on population heterogeneity. Although the 3D spheroid did show increased heterogeneity relative to the 2D cells, it was less than initially expected. This was most likely caused by carryover effects from prior exposure to the spheroid model, similar to what was shown in the EE and MTD drug-free interval samples. Regardless, the most striking results from this experiment were found in the EE and MTD treated 3D samples. The MTD treated 3D samples drastically increased heterogeneity, even relative to an elevated level of heterogeneity found in the underlying 2D drug-free interval MTD cells. Although the 2D drug-free interval EE cells were found to possess similar heterogeneity to the 2D drug-free interval MTD cells, the EE treated 3D cells displayed significantly reduced heterogeneity. These cells seemed to phenotypically align in response to a more drawn-out topotecan exposure. This result could highlight a potential role of EE topotecan as a modulator of cancer cell heterogeneity. Because increased heterogeneity has been shown to increase drug resistance and lead to poor clinical outcomes, reducing the genetic diversity of cancer cells prior to therapy might increase the efficacy of combination therapeutics.[22,23,24] These results also highlight the need to further understand the impact of other therapeutics on cancer cell heterogeneity. Doing so may permit the ranking of therapeutics based on their heterogeneity impact, which may

allow clinicians to identify regimens that negatively impact cancer cell populations to a lesser degree.

To further understand why MTD dosed topotecan led to such a divergent potency response, we used RNAseq to help identify the top differentially expressed genes from the EE and MTD treated cells. A summary of these results is presented as a heatmap in **figure 6**. For this set of genes, both treatment groups remained relatively stable after the first and second weeks of exposure, but significant changes to the MTD treated cells started occurring after 3 weeks of exposure and further progressed over weeks 4 and 5. These changes also correlated well with our IC50 data, which supported further probing to determine each gene function and to determine if a mechanism of resistance could be identified.

Fortunately, a pattern quickly began to emerge and EMT became the most likely cause of the potency differences found between EE and MTD topotecan treated cells. Many of the genes that support this hypothesis can be found in **figures 7, 8, and 9**, but will be discussed further below. As a reminder, EMT usually involves the loss of epithelial markers and the gain of mesenchymal markers. In particular, the MTD treated cells significantly downregulated keratins, which are found in cornified and stratified epithelial and are known to be inhibited in EMT.[15,16,28] They also downregulated each of the secreted mucins (MUC2, MUC5AC, MUC5B, and MUC6). Of these, MUC2 has been found to be the most impactful in oncologic disease. Loss of MUC2 expression in mice is associated with increased proliferation and survival of intestinal epithelial cells and is associated with invasive adenocarcinomas.[29] The MTD treated cells also downregulated

a substantial number of genes associated with cell adhesion, which is a common sign of EMT. CDH1 or E-Cadherin is the most common EMT associated adhesion gene and is almost always downregulated during EMT.[15,16,17,20,21] Our MTD treated cells reduced CDH1 expression by 68.5-fold relative to control compared to a 3.6-fold decrease by EE treated cells. The MTD treated cells also downregulated a number of other adhesion genes such as EpCAM[30,31], CEA cell adhesion molecule 5 (**CEACAM5**)[32], gap junction protein beta 3 (**GJB3**)[33], tight junction protein 3 (**TJP3**)[34], ladinin 1 (**LAD1**)[35], myelin protein zero like 2 (**MPZL2**)[36], and lipolysis stimulated lipoprotein receptor (**LSR**)[37].

Additionally, other genes associated with epithelial cells were significantly perturbed by the MTD treated cells. For instance, the EPH receptor A1 (**EPHA1**) gene is associated with ephrin signaling, which helps regulate the actin cytoskeleton, and is localized to epithelial junctions by E-cadherin. The loss of E-cadherin by the MTD treated cells caused downregulation of the EPHA1 gene, further supporting the loss of an epithelial phenotype.[38] ERB-B2 receptor tyrosine kinase 3 (**ERBB3**), a well-known growth factor receptor in cancer was also significantly down regulated.[39] Myosin VB (**MYO5B**), a gene associated with apical-basolateral polarization, is downregulated.[40] Similarly, PATJ, a gene that regulates tight junction formation and polarization, is downregulated.[41] serine protease 8 (**PRSS8**), a glycosylphosphatidylinositol anchored epithelial extracellular membrane serine protease prostasin, is expressed abundantly in normal epithelial cells and is essential for terminal epithelial differentiation, but is downregulated by MTD treated cells. Downregulation has been associated with EMT in human bladder carcinomas[42] and is associated with increased growth and metastasis in hepatocellular

carcinoma.[43] Lipocalin 2 (**LCN2**) is a member of the lipocalin superfamily and has been found to be highly expressed in early-stage colorectal cancer, but significantly downregulated in metastatic or advanced stage colorectal cancer, which may suggest that the MTD treated cells are not only transitioning into a more mesenchymal phenotype, but also are significantly more aggressive.[44] The loss of any single epithelial gene would not support an EMT hypothesis, however, the consistent downregulation of many epithelial genes simultaneously indicates that the MTD treated cells are most likely undergoing EMT, while the EE treated cells appear to remain relatively stable.

We also analyzed the known EMT regulatory genes in **figure 8**. Snail, slug, TWIST1, TWIST2, ZEB1, and ZEB2 are the most well-known EMT regulatory genes, however, many of these factors do not appear to play a significant role in the EMT transition of the MTD treated cells based on our RNAseq expression data.[15,16,17,20,21] Although CXCL8 is not strictly a regulatory gene in EMT and is more accurately classified as an EMT trigger, we included its expression profile in this figure to highlight its initial burst of expression during the first day of exposure and consistent decline in expression during the remainder of the experiment. In addition to CXCL1 to a lesser extent (**Figure 6**), CXCL8 is one of the few genes (3 total using our criteria) with significant early altered expression relative to control. CXCL8 is known to promote proliferation, inhibit apoptosis, increase heterogeneity, and stimulate EMT.[53] Additionally, elevated CXCL8 expression is correlated with high Gleason scores and elevated PSA.[54] Based on our data and CXCL8's known role in EMT, it's likely that elevated CXCL8 expression is an important early trigger of MTD topotecan induced EMT and drug resistance. ZEB1 was

not originally identified based on the selection criteria, however, after further

evaluation, it appears to be significantly altered in the MTD treated cells and is not

consistently altered in the EE treated cells. Further supporting ZEB1's role, Tripartite

motif-containing protein 29 (**TRIM29**) was found to be downregulated in MTD treated

cells and is associated with increased ZEB1 expression and EMT in cervical cancer cells.[45]

Additionally, MTD treated cells downregulated FXYD domain containing ion transport

regulator 3 (**FXYD3**), which was found to be downregulated in mammary epithelial cells

because of TGFβ and ZEB1 signaling, further supporting ZEB1's role in the EMT of MTD

treated cells.[46] Notch3 is another important regulator that has been associated with

chemotherapy resistance in esophageal cancer cells when downregulated. In this study,

silencing Notch3 resulted in increased production of VIM and resulted in increased

chemotherapy resistance.[47] In another study, Notch3 was found to inhibit EMT in breast

cancer by activating downstream transcriptional complexes.[48] Our results also highlight

the important role of Notch3 in regulating EMT as it was one of the first regulatory

genes to become significantly downregulated (41.15-fold by week 3) by the MTD treated

cells. ESRP1 and ESRP2 are epithelial splicing regulatory proteins that regulate

alternative splicing events associated with epithelial phenotypes and are significantly

downregulated during EMT.[49] Further supporting this finding, OVOL1 was significantly

downregulated in MTD treated cells and induces MET by upregulating ESRP1. OVOL1 is

also a part of a regulatory feedback loop with ZEB1. Thus, its downregulation correlates

with a downregulation of ESRP1 and an upregulation of ZEB1.[50] Lastly, an interesting

article by Chung et al. highlights the EMT suppressor role of GRHL2 in ovarian cancer

cells. GRHL2 was significantly downregulated by the MTD treated cells (279.19-fold by week 5) and many of the genes identified in the article were also altered by the MTD treated cells (KRTs, GRHL2, ESRP1/2, EpCAM, CDH1, CDH3, ERBB3, ZEB1, CLDNs, prominin2 (**PROM2**), S100A14, serine peptidase inhibitor kunitz type 1 (**SPINT1**), LAD1, and ST14 transmembrane serine protease matriptase (**ST14**)). GRHL2 knockdown was found to result in genome-wide epigenetic remodeling through increased methylation of CpG sites and through nucleosomal remodeling. It was found that GRHL2 most likely regulated the CpG methylation of epithelial genes at its binding sites. It was also found the GRHL2 knockdown would most likely cause an intermediate form of EMT.[35] Our results echo their findings with widespread knockdown of epithelial genes in response to a significant knockdown of GRHL2. The MTD treated cells are also most likely in an intermediate stage of EMT as significant loss of epithelial markers is evident, but significant gains in mesenchymal markers is not (**Figure 9**).

The EE treated cells did not lose OVOL1, ESRP1, GRHL2, or Notch3 expression and did not significantly upregulate ZEB1 expression consistently. These cells did not display significantly increased mesenchymal markers and did not significantly downregulate their epithelial markers. The long-term dosing of topotecan appeared to prevent EMT within these cells while still maintaining efficacy, which prevented EMT induced drug resistance. These results are further supported in **figures 10 and 11**, which show that EE treated cells maintain a similar expression level of efflux pumps and topoisomerase genes to control cells. On the other hand, MTD treated cells express a significantly greater number of efflux pumps and express a high quantity of alternative

topoisomerase genes. Each of these mechanisms could drastically reduce the exposure or efficacy of topotecan and likely contribute to the reduction of IC50 potency shown in **figure 4**.

Overall, in this article, we have demonstrated that alternative dosing strategies can have a substantial impact on the underlying cell population, which can directly affect treatment outcomes. These results also support the need for frequent genetic testing when administering oncologic therapeutics to quickly identify failed therapies and to avoid harming patients. Finally, these results call into question the use of short-term efficacy models as drug-screening tools and support the need to better understand the impact of oncologic medications on surviving cell populations.

1. Browder T, Butterfield CE, Kraling BM, Marshall B, O'Reilly MS, Folkman J (2000) Antiangiogenic scheduling of chemotherapy improves effi cacy against experimental drugresistant cancer. Cancer Res 60:1878–1886

2. Klement G, Baruchel S, Rak J, Man S, Clark K, Hicklin D, Bohlen P, Kerbel RS (2000) Continuous low-dose therapy with vinblastine and VEGF receptor-2 antibody induces sustained tumor regression without overt toxicity. J Clin Invest 105:R15–R24

3. Bocci, G., & Francia, G. (Eds.). (2014). Metronomic Chemotherapy (Vol. 5). Berlin, Heidelberg: Springer Berlin Heidelberg. https://doi.org/10.1007/978-3-662-43604-2

4. Mpekris, F., Baish, J. W., Stylianopoulos, T., & Jain, R. K. (2017). Role of vascular normalization in benefit from metronomic chemotherapy. Proceedings of the National Academy of Sciences, 114(8), 1994–1999. https://doi.org/10.1073/pnas.1700340114

5. Cazzaniga, M. E., Cordani, N., Capici, S., Cogliati, V., Riva, F., & Cerrito, M. G. (2021). Metronomic chemotherapy. Cancers, 13(9), 1–27. https://doi.org/10.3390/cancers13092236

6. Kerbel, R. S., & Kamen, B. A. (2004). The anti-angiogenic basis of metronomic chemotherapy. Nature Reviews Cancer, 4(6), 423–436. https://doi.org/10.1038/nrc1369

7. Albertsson, P., Lennernäs, B., & Norrby, K. (2012). Low-dosage metronomic chemotherapy and angiogenesis: Topoisomerase inhibitors irinotecan and mitoxantrone stimulate VEGF-A-mediated angiogenesis. Apmis, 120(2), 147–156. https://doi.org/10.1111/j.1600-0463.2011.02830.x

8. Mpekris, F., Baish, J. W., Stylianopoulos, T., & Jain, R. K. (2017). Role of vascular normalization in benefit from metronomic chemotherapy. Proceedings of the National Academy of Sciences of the United States of America, 114(8), 1994–1999. https://doi.org/10.1073/pnas.1700340114

9. Maiti, R. (2014). Metronomic chemotherapy. Journal of Pharmacology and Pharmacotherapeutics, 5(3), 186. https://doi.org/10.4103/0976-500X.136098

10. Simsek, C., Esin, E., & Yalcin, S. (2019). Metronomic Chemotherapy: A Systematic Review of the Literature and Clinical Experience. Journal of Oncology, 2019(November 2017). https://doi.org/10.1155/2019/5483791

11. Aljuffali, I. A., Mock, J. N., Costyn, L. J., Nguyen, H., Nagy, T., Cummings, B. S., & Arnold, R. D. (2011). Enhanced antitumor activity of low-dose continuous administration schedules of topotecan in prostate cancer. Cancer Biology and Therapy, 12(5), 407–420. https://doi.org/10.4161/cbt.12.5.15950

12. Metzger, W., Sossong, D., & Chle, A. B. Ä. (2011). The liquid overlay technique is the key to formation of co-culture spheroids consisting of primary osteoblasts , fibroblasts and endothelial cells, (August 2010), 1000–1012. https://doi.org/10.3109/14653249.2011.583233

13. Sasha Babicki, David Arndt, Ana Marcu, Yongjie Liang, Jason R. Grant, Adam Maciejewski, and David S. Wishart. Heatmapper: web-enabled heat mapping for all. Nucleic Acids Res. 2016 May 17 (epub ahead of print). doi:10.1093/nar/gkw419

14. Levine, H., Jolly, M. 2021. EMT resistance in cancer cells and two potential causes. Oncotarget. EMT Resistance in Cancer Cells and Two Potential Causes | Oncotarget.

15. Dongre, A., Weinberg, R.A. New insights into the mechanisms of epithelial–mesenchymal transition and implications for cancer. Nat Rev Mol Cell Biol 20, 69–84 (2019). https://doi.org/10.1038/s41580-018-0080-4

16. 2016. Epithelial-Mesenchymal transition (EMT) markers. Epithelial-Mesenchymal Transition (EMT) Markers (novusbio.com)

17. Kalluri, R., & Weinberg, R. A. (2009). The basics of epithelial-mesenchymal transition. Journal of Clinical Investigation, 119(6), 1420–1428. https://doi.org/10.1172/JCI39104

18. Lambert, A. W., & Weinberg, R. A. (2021). Linking EMT programmes to normal and neoplastic epithelial stem cells. Nature Reviews Cancer, 21(5), 325–338. https://doi.org/10.1038/s41568-021-00332-6

19. Shih, J. Y., & Yang, P. C. (2011). The EMT regulator slug and lung carcinogenesis. Carcinogenesis, 32(9), 1299–1304. https://doi.org/10.1093/carcin/bgr110

20. Ribatti, D., Tamma, R., & Annese, T. (2020). Epithelial-Mesenchymal Transition in Cancer: A Historical Overview. Translational Oncology, 13(6), 100773. https://doi.org/10.1016/j.tranon.2020.100773

21. Yang, J., Antin, P., Berx, G., Blanpain, C., Brabletz, T., Bronner, M., … Sheng, G. (2020). Guidelines and definitions for research on epithelial–mesenchymal transition. Nature Reviews Molecular Cell Biology, 21(6), 341–352. https://doi.org/10.1038/s41580-020-0237-9

22. Dagogo-Jack, I., Shaw, A. Tumour heterogeneity and resistance to cancer therapies. Nat Rev Clin Oncol 15, 81–94 (2018). https://doi.org/10.1038/nrclinonc.2017.166

23. Lim, Z. F., & Ma, P. C. (2019). Emerging insights of tumor heterogeneity and drug resistance mechanisms in lung cancer targeted therapy. Journal of Hematology and Oncology, 12(1), 1–18. https://doi.org/10.1186/s13045-019-0818-2

24. Saunders, N. A., Simpson, F., Thompson, E. W., Hill, M. M., Endo-Munoz, L., Leggatt, G., … Guminski, A. (2012). Role of intratumoural heterogeneity in cancer drug resistance: Molecular and clinical perspectives. EMBO Molecular Medicine, 4(8), 675–684. https://doi.org/10.1002/emmm.201101131

25. Safran M, Rosen N, Twik M, BarShir R, Iny Stein T, Dahary D, Fishilevich S, and Lancet D. The GeneCards Suite Chapter, Practical Guide to Life Science Databases (2022) pp 27-56 [PDF]

26. Shin, K., Straight, S., & Margolis, B. (2005). PATJ regulates tight junction formation and polarity in mammalian epithelial cells. Journal of Cell Biology, 168(5), 705–711. https://doi.org/10.1083/jcb.200408064

27. Kobak, D., & Berens, P. (2019). The art of using t-SNE for single-cell transcriptomics. Nature Communications, 10(1). https://doi.org/10.1038/s41467-019-13056-x

28. Bragulla, H. H., & Homberger, D. G. (2009). Structure and functions of keratin proteins in simple, stratified, keratinized and cornified epithelia. Journal of anatomy, 214(4), 516–559. https://doi.org/10.1111/j.1469-7580.2009.01066.x

29. Kufe, D. (2009). Mucins in cancer: function, prognosis and therapy. Nat Rev Cancer 9, 874–885 https://doi.org/10.1038/nrc2761

30. Hyun, K. A., Koo, G. B., Han, H., Sohn, J., Choi, W., Kim, S. I., Jung, H. I., & Kim, Y. S. (2016). Epithelial-to-mesenchymal transition leads to loss of EpCAM and different

physical properties in circulating tumor cells from metastatic breast

cancer. Oncotarget, 7(17), 24677–24687. https://doi.org/10.18632/oncotarget.8250

31. Gires, O., Pan, M., Schinke, H., Canis, M., & Baeuerle, P. A. (2020). Expression and

function of epithelial cell adhesion molecule EpCAM: where are we after 40

years?. Cancer metastasis reviews, 39(3), 969–987. https://doi.org/10.1007/s10555-020-09898-3

32. Zhang, X., Han, X., Zuo, P., Zhang, X., & Xu, H. (2020). CEACAM5 stimulates the

progression of non-small-cell lung cancer by promoting cell proliferation and

migration. The Journal of international medical research, 48(9), 300060520959478.

https://doi.org/10.1177/0300060520959478

33. Wu, J. I., & Wang, L. H. (2019). Emerging roles of gap junction proteins connexins in

cancer metastasis, chemoresistance and clinical application. Journal of biomedical

science, 26(1), 8. https://doi.org/10.1186/s12929-019-0497-x

34. Megan B. Salt, Sourav Bandyopadhyay, Frank McCormick; Epithelial-to-

Mesenchymal Transition Rewires the Molecular Path to PI3K-Dependent

Proliferation. Cancer Discov 1 February 2014; 4 (2): 186–

199. https://doi.org/10.1158/2159-8290.CD-13-0520

35. Chung, V.Y., Tan, T.Z., Ye, J. et al. The role of GRHL2 and epigenetic remodeling in

epithelial–mesenchymal plasticity in ovarian cancer cells. Commun Biol 2, 272

(2019). https://doi.org/10.1038/s42003-019-0506-3

36. Wesdorp, M., Murillo-Cuesta, S., Peters, T., Celaya, A. M., Oonk, A., Schraders, M.,

Oostrik, J., Gomez-Rosas, E., Beynon, A. J., Hartel, B. P., Okkersen, K., Koenen, H.,

Weeda, J., Lelieveld, S., Voermans, N. C., Joosten, I., Hoyng, C. B., Lichtner, P., Kunst, H., Feenstra, I., … Kremer, H. (2018). MPZL2, Encoding the Epithelial Junctional Protein Myelin Protein Zero-like 2, Is Essential for Hearing in Man and Mouse. American journal of human genetics, 103(1), 74–88. https://doi.org/10.1016/j.ajhg.2018.05.011

37. Parsana, P., Amend, S.R., Hernandez, J. et al. Identifying global expression patterns and key regulators in epithelial to mesenchymal transition through multi-study integration. BMC Cancer 17, 447 (2017). https://doi.org/10.1186/s12885-017-3413-3

38. Pasquale E. B. (2010). Eph receptors and ephrins in cancer: bidirectional signalling and beyond. Nature reviews. Cancer, 10(3), 165–180. https://doi.org/10.1038/nrc2806

39. Salt, M. B., Bandyopadhyay, S., & McCormick, F. (2014). Epithelial-to-mesenchymal transition rewires the molecular path to PI3K-dependent proliferation. Cancer discovery, 4(2), 186–199. https://doi.org/10.1158/2159-8290.CD-13-0520

40. Roland, J. T., Bryant, D. M., Datta, A., Itzen, A., Mostov, K. E., & Goldenring, J. R. (2011). Rab GTPase-Myo5B complexes control membrane recycling and epithelial polarization. Proceedings of the National Academy of Sciences of the United States of America, 108(7), 2789–2794. https://doi.org/10.1073/pnas.1010754108

41. Shin, K., Straight, S., & Margolis, B. (2005). PATJ regulates tight junction formation and polarity in mammalian epithelial cells. The Journal of cell biology, 168(5), 705–711. https://doi.org/10.1083/jcb.200408064
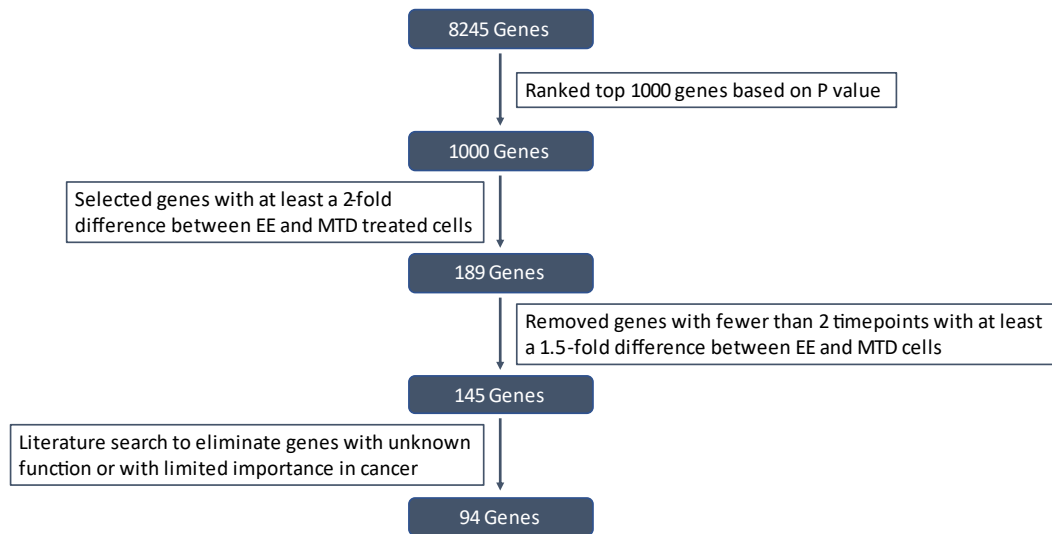
42. Chen, LM., Verity, N.J. & Chai, K.X. Loss of prostasin (PRSS8) in human bladder transitional cell carcinoma cell lines is associated with epithelial-mesenchymal transition (EMT). BMC Cancer 9, 377 (2009). https://doi.org/10.1186/1471-2407-9-377

43. Zhang L, Jia G, Shi B, Ge G, Duan H, Yang Y: PRSS8 is Downregulated and Suppresses Tumour Growth and Metastases in Hepatocellular Carcinoma. Cell Physiol Biochem 2016;40:757-769. doi: 10.1159/000453136

44. Kim, S. L., Lee, S. T., Min, I. S., Park, Y. R., Lee, J. H., Kim, D. G., & Kim, S. W. (2017). Lipocalin 2 negatively regulates cell proliferation and epithelial to mesenchymal transition through changing metabolic gene expression in colorectal cancer. Cancer science, 108(11), 2176–2186. https://doi.org/10.1111/cas.13389

45. Masuda, Y., Takahashi, H., & Hatakeyama, S. (2015). TRIM29 regulates the p63-mediated pathway in cervical cancer cells. Biochimica et biophysica acta, 1853(10 Pt A), 2296–2305. https://doi.org/10.1016/j.bbamcr.2015.05.035

46. Yamamoto, H., Mukaisho, K., Sugihara, H., Hattori, T., & Asano, S. (2011). Down-regulation of FXYD3 is induced by transforming growth factor-β signaling via ZEB1/δEF1 in human mammary epithelial cells. Biological & pharmaceutical bulletin, 34(3), 324–329. https://doi.org/10.1248/bpb.34.324

47. Matsuura, N., Tanaka, K., Yamasaki, M., Yamashita, K., Saito, T., Makino, T., Yamamoto, K., Takahashi, T., Kurokawa, Y., Nakajima, K., Eguchi, H., Nakagawa, H., & Doki, Y. (2021). NOTCH3 limits the epithelial-mesenchymal transition and predicts a

favorable clinical outcome in esophageal cancer. Cancer medicine, 10(12), 3986–3996. https://doi.org/10.1002/cam4.3933

48. Lin, HY., Liang, YK., Dou, XW. et al. Notch3 inhibits epithelial–mesenchymal transition in breast cancer via a novel mechanism, upregulation of GATA-3 expression. Oncogenesis 7, 59 (2018). https://doi.org/10.1038/s41389-018-0069-z

49. Ishii, H., Saitoh, M., Sakamoto, K., Kondo, T., Katoh, R., Tanaka, S., Motizuki, M., Masuyama, K., & Miyazawa, K. (2014). Epithelial splicing regulatory proteins 1 (ESRP1) and 2 (ESRP2) suppress cancer cell motility via different mechanisms. The Journal of biological chemistry, 289(40), 27386–27399. https://doi.org/10.1074/jbc.M114.589432

50. Roca, H., Hernandez, J., Weidner, S., McEachin, R. C., Fuller, D., Sud, S., Schumann, T., Wilkinson, J. E., Zaslavsky, A., Li, H., Maher, C. A., Daignault-Newton, S., Healy, P. N., & Pienta, K. J. (2013). Transcription factors OVOL1 and OVOL2 induce the mesenchymal to epithelial transition in human cancer. PloS one, 8(10), e76773. https://doi.org/10.1371/journal.pone.0076773

51. Ritchie, M. E., Phipson, B., Wu, D., Hu, Y., Law, C. W., Shi, W., & Smyth, G. K. (2015). limma powers differential expression analyses for RNA-sequencing and microarray studies. Nucleic acids research, 43(7), e47. https://doi.org/10.1093/nar/gkv007

52. Krämer A, Green J, Pollard J Jr, Tugendreich S. (2014). Causal analysis approaches in Ingenuity Pathway Analysis. Bioinformatics. 30(4), 523-530. doi:10.1093/bioinformatics/btt703

53. Xiong, X.; Liao, X.; Qiu, S.; Xu, H.; Zhang, S.; Wang, S.; Ai, J.; Yang, L. (2022). CXCL8 in Tumor Biology and Its Implications for Clinical Translation. Front. Mol. Biosci. 1–13. https://doi.org/10.3389/fmolb.2022.723846.

54. Liu, Q.; Li, A.; Tian, Y.; Wu, J. D.; Liu, Y.; Li, T.; Chen, Y.; Han, X.; Wu, K. (2016). The CXCL8-CXCR1/2 Pathways in Cancer. Cytokine Growth Factor. 31, 61–71. https://doi.org/10.1016/j.cytogfr.2016.08.002.

Appendix

Illustration of the gene selection process and exclusion criteria.

8245 Genes

Ranked top 1000 genes based on P value

1000 Genes

Selected genes with at least a 2-fold difference between EE and MTD treated cells

189 Genes

Removed genes with fewer than 2 timepoints with at least a 1.5-fold difference between EE and MTD cells

145 Genes

Literature search to eliminate genes with unknown function or with limited importance in cancer

94 Genes

Determining the Impact of Extended Exposure Topotecan on DNA Repair and on Docetaxel Resistance

1. **Introduction**

During a typical day, on average, each human cell weathers an estimated 90,000 insults to its DNA. These insults are caused by many different types of DNA damaging events such as oxidation, deamination, depurination, depyrimidination, bulky adducts, methylation, alkylation, single-strand breaks (**SSBs**), and double-strand breaks (**DDBs**).[1,2] Unrepaired DNA from these DNA damaging events can cause erroneous permanent mutations. For instance, oxidation of guanine to 8-hydroxyguanine can alter the natural base pairing from G-C to 8OHdG-A. If this damage is not repaired prior to replication, a single nucleotide polymorphism (**SNP**) can occur in the newly formed sister chromatid.[3] Alternatively, the DNA base can lose an amine through deamination, which can convert adenine to hypoxanthine, guanine to xanthine, or cytosine to uracil. Thymine lacks an amine and thus cannot be deaminated. In general, deamination converts a hydrogen donor into a hydrogen acceptor, which can alter the base pairing of the unnatural base. Similar to oxidation, unrepaired deaminated bases can cause mutations during replication.[4] Furthermore, depurination and depyrimidination events cause DNA nucleotides to lose their nitrogen bases. These abasic sites are usually repaired through base excision repair (**BER**) or nucleotide excision repair (**NER**), but may also be repaired through translesion synthesis, which can be mutagenic because translesion synthesis polymerases are usually lower in fidelity.[5] DNA adducts, methylation, and alkylation each cause damage through covalent bonding. Common DNA adducts include

polyaromatic hydrocarbons, methylating agents, alkylating agents, mustards, and aromatic amines. DNA adducts can cause distortions in the helical structure of the DNA, which can interfere with DNA transcription and replication. DNA adducts can also induce mutations that are unique to the particular type of DNA adduct.[6] Highly reactive methyl donors can create adducts that lead to depurination, that block replicative DNA polymerases and require more error prone translesion polymerases, and that are frequently mispaired during replication. Also, larger alkyl adducts can induce DNA helix distortion, which can inhibit replication and translation.[7]

SSBs are common and occur roughly 10,000 times per day for the average cell. Alone, these insults are relatively innocuous since the damage is contained within the DNA backbone without any loss of genetic material. These nicks in the DNA backbone can compromise DNA replication and transcription but are usually less mutagenic than other forms of DNA damage.[8,9] Topotecan causes many SSBs by interacting with topoisomerase I (**TOP1**), which is an enzyme that functions to relieve supercoiling during DNA replication by creating nicks in the phosphodiester backbone to facilitate controlled rotation.[10] Topotecan stabilizes the TOP1 enzyme, prevents ligation, and causes the SSBs to persist. The replication fork then collides with the SSB, which causes a DSB to form. This form of DNA damage is much more deleterious. A double strand break causes the cell to lose complementary binding between the sense and non-sense strands. This makes it difficult for the cell to determine if the backbone was simply severed and requires ligation or if loss of genetic material occurred, which requires addition of nucleotides. DSBs can lead to mutations, loss of heterozygosity, and

chromosome rearrangements.[12] Out of all the different types of DNA damage, DSBs are the most dangerous. DSB repair occurs using four main mechanisms: non-homologous end joining (**NHEJ**), homologous repair (**HR**), single strand annealing (**SSA**), and alternate end joining (**Alt-EJ**). Of these, NHEJ and HR are preferred and are utilized most often. Alt-EJ and SSA are more error prone repair mechanisms. NHEJ assumes no loss of genetic material and simply reconnects each strand together. This can achieve an accurate repair but may also result in loss of genetic material if nucleotides were lost during the DSB. HR can achieve complete accuracy, even for damage that causes loss of genetic material because it uses the sister chromatid as a template. The main drawback of HR is that it usually requires cells to be in S phase as sister chromatids are not present during other phases of the cell cycle. HR sometimes occurs during other phases of the cell cycle but uses the homologous chromosome instead of the sister chromatid. HR is usually suppressed outside of S phase because the use of the paternal chromosome to repair the maternal chromosome (or vice versa) can result in the loss of heterozygosity, which can be extremely dangerous for the cell, especially if the paternal gene is defective.[13,14]

Based on the mechanism of repair, NHEJ is the simpler, faster, but less accurate repair mechanism and HR is the more complex and more accurate repair mechanism. Based on these characteristics, we hypothesized that large amounts of DNA damage would require greater utilization of NHEJ, the quicker damage repair pathway. Alternatively, utilization of HR for frequent DSBs would prove difficult as the machinery required to accurately pair the damaged DNA with its sister chromatid is complex and

relatively energy intensive. Therefore, we hypothesized that maximum tolerable dosing (**MTD**) of topotecan would significantly increase the utilization of NHEJ relative to extended exposure (**EE**) dosing of topotecan. MTD dosing results in much higher peak topotecan levels and therefore would expose cells to a greater number of DSBs in a shorter period of time relative to EE topotecan. Because NHEJ is much more error prone relative to HR, surviving MTD treated cells would possess a greater number of mutations relative to surviving EE treated cells. Finally, the higher mutation rate of MTD treated cells would decrease the time to drug resistance. Taken further, if the underlying mutation rate of the cell is altered based on treatment A, then this would subsequently reduce the time to resistance of treatment B. To evaluate this, we assessed the long-term efficacy of docetaxel after combination treatment using MTD docetaxel with MTD topotecan and MTD docetaxel with EE topotecan. MTD docetaxel was also chosen because it is the standard of care for prostate cancer and would help determine if EE topotecan would be an appropriate add on therapy for clinical patients.

2. Materials and Methods

2.1. Cell line and cell culture

The human prostate cancer (**PC3**) cell line was obtained from ATCC and was maintained as monolayers in complete medium using F12K (Corning) and 10% (v/v) FBS (Hyclone) at 37C in a 5% CO_2 atmosphere using a Heracell bios 160i incubator (Thermoscientific). Cells were kept at lower passage numbers (<10 PC3) throughout the experiment to maintain genotypic and phenotypic consistency. Cells were passaged using 0.25% (w/v) trypsin (Hyclone) for 2-3 minutes every 2-4 days according to

confluency, which was determined using a Primovert microscope (Zeiss). During the experiment, the PC3 cell line was forked into multiple sub cell lines according to the treatment group, which will be described in greater detail below. Each of these sub cell lines was treated as a unique cell line (separate flasks, no mixing, ect.) throughout the experiment using the same methods described above.

2.2. Spheroid formation

Our spheroid protocol was largely adapted from a high-throughput liquid overlay technique developed by Metzger, et al.[15] This technique rapidly generates many spheroids with minimal incubation time (24 hr). Briefly, 96 well U bottom plates (Grenier bio-one) are coated with a 1.2% w/v poly-HEMA (Sigma Aldrich) solution in 95% v/v ethanol. This solution was produced by incubating poly-HEMA crystals overnight with a magnetic stir rod at 80°C to ensure full dissolution. The poly-HEMA solution is kept warm throughout the coating process to prevent precipitation during the evaporation step. 60 μL of the poly-HEMA solution is added to each well and the plates are heated using a 10x10 hot plate (VWR). Plates are then left on the hot plate for approximately 1 hour with the lid raised to evaporate the ethanol. Plates are then sealed using Parafilm (Bemis) for future use. After cells have been passaged and placed into a separate conical tube, they are mixed thoroughly, and a small sample is counted using a TC10 automated cell counter (Biorad). A minimum of two counts are taken per cell line to ensure accurate counts for cell seeding. Cells are diluted to achieve a concentration of 50,000 cells per mL and placed on ice. 2.5% v/v of Matrigel (Corning) is added to the cell suspension using an ice-cold syringe and needle. The cells are then plated using 100 μL

of the cell suspension to attain 5,000 cells per well. The plates are then centrifuged at 400 g for 5 to 10 minutes at 4°C. This protocol rapidly generates fully formed spheroids within 24 hours for the PC3 cell line.

2.3. Dosing and spheroid handling

Two days after initial seeding and spheroid formation, spheroids received an additional 100 µL of media +/- drug, reaching a total volume 200 µL for the remainder of the experiment. On days 3 and 5, media was exchanged by removing 100 µL of media per well and replacing it with 100 µL of fresh media +/- drug. Limiting the media exchanges and leaving some residual, old media prevented spheroid loss throughout the experiment. During days without media exchange, 10 µL of media was removed and replaced with 10 µL of media or treatment solution according to the treatment group. Dosing of topotecan (Chempac) and docetaxel (Fluka) occurred using 20x concentrated solutions which could be directly spiked into the wells at 10 µL in 190 µL of media. The conventional or MTD treatment was given as a bolus dose on day 0. Metronomic or EE treatment was given daily as a fractionated dose at $1/7^{th}$ the MTD. The cumulative dose for the MTD and EE treatments were equal throughout the experiment. In total, there were 4 treatment groups: control, MTD docetaxel, MTD docetaxel with MTD topotecan, and MTD docetaxel with EE topotecan. Topotecan dosing occurred at 10 nM (cumulative) and docetaxel dosing occurred at 2.5nM during each week of therapy. For IC50 analysis, MTD docetaxel was given at doses between 0.01nM and 100 nM.

2.4. Synergism study

The plate design to assess for synergism between topotecan and docetaxel is shown in **figure 1**. Cells were plated at 2,500 cells/well in a 96 well clear bottom plate (Grenier bio-one). Plates were grown for 24 hours prior to initial dosing. MTD dosing was given at time 0H and EE dosing was given at time 0H, 24H, and 48H. Plates were exposed to a total of 72 hours of therapy before the mitochondrial activity was assessed using resazurin. In this study, we compared the synergism between EE topotecan and MTD topotecan with docetaxel. Thus, 3 total treatment groups were assessed in this study: control, EE topotecan with MTD docetaxel and MTD topotecan with MTD docetaxel. **Importantly, in this study, the EE topotecan dose was not given at the same cumulative dose as MTD topotecan, but instead was given at 3/7th the cumulative dose or 1/7th daily for 3 total doses.** Synergism was assessed using Synergy Finder 3.0 to calculate a ZIP score.[18] A score less than -10 is considered antagonistic, a score between -10 and 10 is considered additive, and a score greater than 10 is considered synergistic.

Figure 1. Synergism plate design. Topotecan doses are depicted in blue and docetaxel doses are depicted in green. Topotecan doses are given as shown in column 2 for the remainder of columns 3-12 and docetaxel is given as shown in row H for the remainder of rows A-G. Control wells are depicted in column 1.

2.5. Long-term docetaxel resistance study protocol

Spheroids were generated according to the protocol described in Section 2.2 and were grown for approximately 2-3 days to allow size-dependent drug barriers to form. Spheroids were then dosed according to the protocol in Section 2.3 for a total of 7 days. During the first week of exposure, samples were taken for genomic and proteomic analysis on days 0, 1, 3, and 7. The remaining spheroids were saved for future weeks by digestion using Accumax (Innovative cell technologies) for approximately 1 hour until a single cell suspension was achieved. At this point, a total of 4 treatment groups generated 4 unique cell-lines that were maintained throughout the experiment: PC3-Control, PC3-MTD-Docetaxel, PC3-EE-Topotecan-MTD-Docetaxel, and PC3-MTD-Topotecan-MTD-Docetaxel. The digested spheroids were grown in 2D for approximately 1-2 weeks until the cell population was replenished sufficiently to plate additional spheroids. Each cell population was then used to generate two groups of spheroids. One group (3D) was exposed to an additional week of treatment and one group (3D) was used to assess the resulting sensitivity of the drug (Docetaxel) from the previous week(s) of drug exposure. After another full week of exposure, some spheroids were harvested for genomic and proteomic analysis, and some were digested to prepare for another week of exposure and analysis. This cycle was repeated throughout the experiment. A schematic is depicted below (**Fig. 2 and Fig. 3.**) to help better orient readers to the study protocol. **The RNAseq data shown in 3.1 was generated using a study protocol similar to the one depicted in figures 2 and 3 but used different treatment groups. These were Control, EE topotecan, and MTD topotecan.**
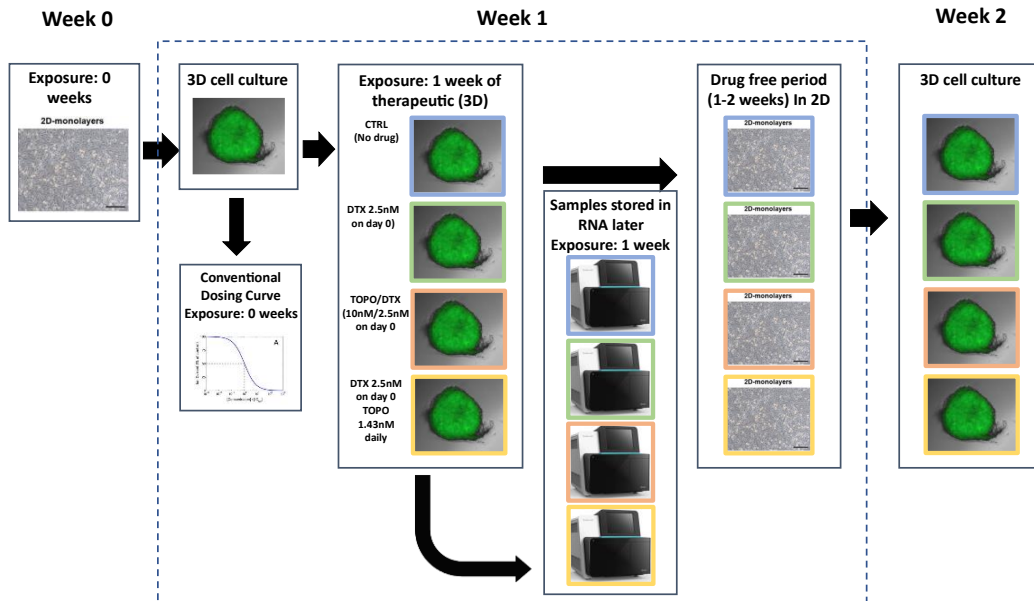
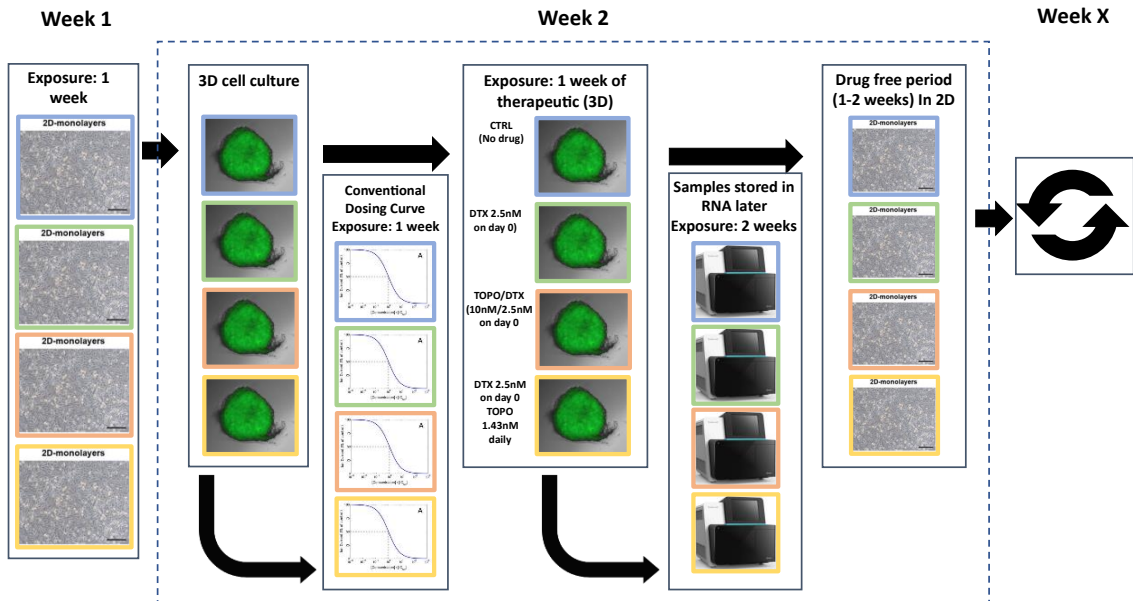**Figure 2.** Schematic depicting the first week of the study protocol, starting from the base cell line (PC3).

Figure 3. Schematic depicting the second week of the study protocol, starting from the treatment exposed cell lines.

2.6. Resazurin assay (Cytotoxicity)

Resazurin was used to measure the mitochondrial activity of the cells as a surrogate for cell viability because the reductive conversion of resazurin to resorufin creates a water-soluble end-product. This prevents the need for a solubilizing step, which would be untenable in a 3D format. Resazurin (Alfa Aesar) was made fresh for each assay at a 0.015% w/v concentration in PBS and was sterilized using a 0.22 μm filter. Before resazurin was added to the spheroids, the spheroids were moved from U bottom 96 well plates to flat bottom black, fluorescent plates (Grenier bio-one). This was accomplished using a 1 mL pipette tip to move the spheroid and 100 μL media. Moving the spheroids increased the accuracy of the imaging and spectrophotometry. This also ensured that well volume variability from inconsistent evaporation dynamics that occur over the duration of the experiment would not alter the resorufin concentrations. Resazurin was added at a ratio of 10 μL per 100 μL of media and was incubated for 4 to 12 hours with readings taken over time (2, 4, 6, 8, 12). Generally, 4-6 hours was the most appropriate time point for spheroids and achieved the lowest CV values with the greatest sensitivity and limited assay saturation. For 2D analysis, 4 hours achieved the lowest CV values. Fluorescent measurements for each plate were read using a Cytation 5 plate reader (BioTek) with excitation set at 560 nm and emission set at 590 nm.

2.7. RNA storage protocol

Cells and spheroids are separated into individual microfuge tubes at approximately 1,000,000 cells/mL and washed 2x using PBS (Wards science) and the Heraeus Fresco 21 microcentrifuge (Thermoscientific) set at 400g and 4°C for 10 minutes. Samples are maintained on ice for the duration of the protocol. PBS is aspirated and replaced with 300µL of RNA later (Qiagen). Samples are stored overnight (24H) at 4°C before moving to -80°C for long-term storage.

RNA Isolation

Total RNA was isolated from cultured cells and 3D spheroid model using standard RNA extraction kits (RNeasy Kits–QIAGEN). RNA concentration and integrity were estimated by a NanoDrop 2000 UV-Vis spectrophotometer (Thermo Scientific, United States), Qubit® 2.0 Fluorometer (Invitrogen, Carlsbad, CA, United States), and Agilent 2,100 Bioanalyzer (Applied Biosystems, Carlsbad, CA, United States). RNA integrity number threshold of eight was used for RNAseq analysis.

2.8. RNAseq

RNAseq libraries were constructed using Illumina TruSeq RNA Sample Preparation Kit v2. Libraries were then size selected to generate inserts of approximately 200 bp. RNA sequencing was performed on llumina's NovaSeq next-generation highthroughput sequencing system using 150 bp paired-end protocol with a depth of more than 20 million reads per sample. The average quality scores were above Q30 for all libraries in both R1 and R2.

RNAseq Data Processing

RNAseq data were normalized, and fragments per kilobase million values were used in further analysis using Partek Genomics Suite and Galaxy data analysis software, an open source, web-based platform that provides tools necessary to create and execute RNA-seq analysis. In brief, RNA-seq data analysis pipeline was developed using Galaxy software workflow. Quality control (QC) check on the RNAseq raw reads was performed using the FastQC tool, followed by read trimming to remove base positions with a low median (or bottom quartile) score. Tophat2 Aligner tool mapped processed RNAseq reads to the hg19 human genome build. Picard's CollectInsertSizeMetrics tool was applied on the initial tophat2 run to obtain estimated insert sizes, which was then used to calculate mean inner distance between mate pairs (mean = estimated_insert-size−2×read_length). Tophat2 was re-run using corrected mean value and Cufflinks tool was to assemble the reads into transcripts.

Bioinformatics Analysis.

Gene expression data were filtered using the following criteria: genes with mean FPKM < 1 were removed. Global gene expression profile (GEP) data were analyzed further using a combination of R and Partek Flow to perform differential expression testing to identify GEP signatures of drug response. Mean fold-change > j1j and P < 0.05 were considered thresholds for reporting significant differential gene expression. Differentially expressed gene analysis was performed between two groups of gene expression datasets (e.g., treated vs. untreated). Heatmaps were generated using unsupervised hierarchical clustering analysis based on the DEGs. Owing to the small sample size, Limma, an empirical Bayesian method, was used to detect DEGs, obtain P

values, and further provided a false discovery rate based on the P value using the

Benjamini-Hochberg procedure to detect the DEGs.[20] The advantage of Limma

compared with a traditional t test is that it provides a moderated t test statistic by

shrinking the variance statistics and therefore improves the statistical power.

All samples were initially normalized to control day 0. Then, each timepoint for

the MTD and EE samples was normalized to the corresponding control timepoint. E.g.

day 7 MTD and EE samples were normalized to day 7 control. After normalization, MTD

and EE samples were compared, and top 1000 genes were selected based on a p-value,

which were further screened using a relative fold change (MTD/EE) > 2. Additionally,

genes that were upregulated in one treatment and downregulated in the other

treatment were added to the initial gene list. The gene list was then inspected manually

to remove genes that did not trend throughout the experiment. This was done to

remove genes that were initially identified in the screen based on one off gene changes

that occurred during a single week. Each gene was then manually investigated to

determine its role and function using databases such as GeneCards as well as literature

searches using Pubmed.[16] Genes without a well-defined function or genes without a

clear role were labeled as unknown. Heatmaps were generated using heatmapper, a

web-based tool.[17]

Statistical Analysis

All statistical analyses were performed using R for statistical computing and

graphics, v3.4.2, and GraphPad Prism v7.0. We used parametric methods to analyze

differences between two groups of cells. If the assumption appeared violated, appropriate nonparametric procedures were used. All tests were two-sided, and differences with a P < 0.05 were considered statistically significant.

2.9. Statistics

The curve fitting and statistical analysis of the IC50 data were performed using Graphpad Prism (Dotmatics, Boston MA, USA). The IC50 was determined at ½ of fitted maximal activity. Usually, an extra sum-of-squares F test was used to compare IC50 values between treated and control samples.

3. Results

3.1. Determining the effect of treatment scheduling on DNA repair genes.

To better understand the effects of EE topotecan on DNA repair, RNA was isolated and analyzed from a similar experiment shown in 3.3, but with different treatment groups (Control, EE topotecan, MTD topotecan). In **Figure 4**, we present a heatmap of the long-term gene expression of NHEJ genes (Blue) and HR genes (Orange) from EE and MTD treated spheroids over a 5-week exposure timeframe. These results were normalized to control each week. Grey boxes represent genes there were not significantly different from control, green boxes represent genes that were significantly downregulated from control, and red boxes represent genes that were significantly upregulated from control. We also included a number of other DNA repair genes in the analysis that did not have any statistically significant alterations from control, which are shown at the bottom of **figure 4**. In this experiment, we found that most DNA repair

genes associated with NHEJ and HR were not significantly altered by either treatment throughout the entire experiment. Even genes such as XRCC6, which were significantly different from control for most of the experiment were directionally similar between each treatment group.
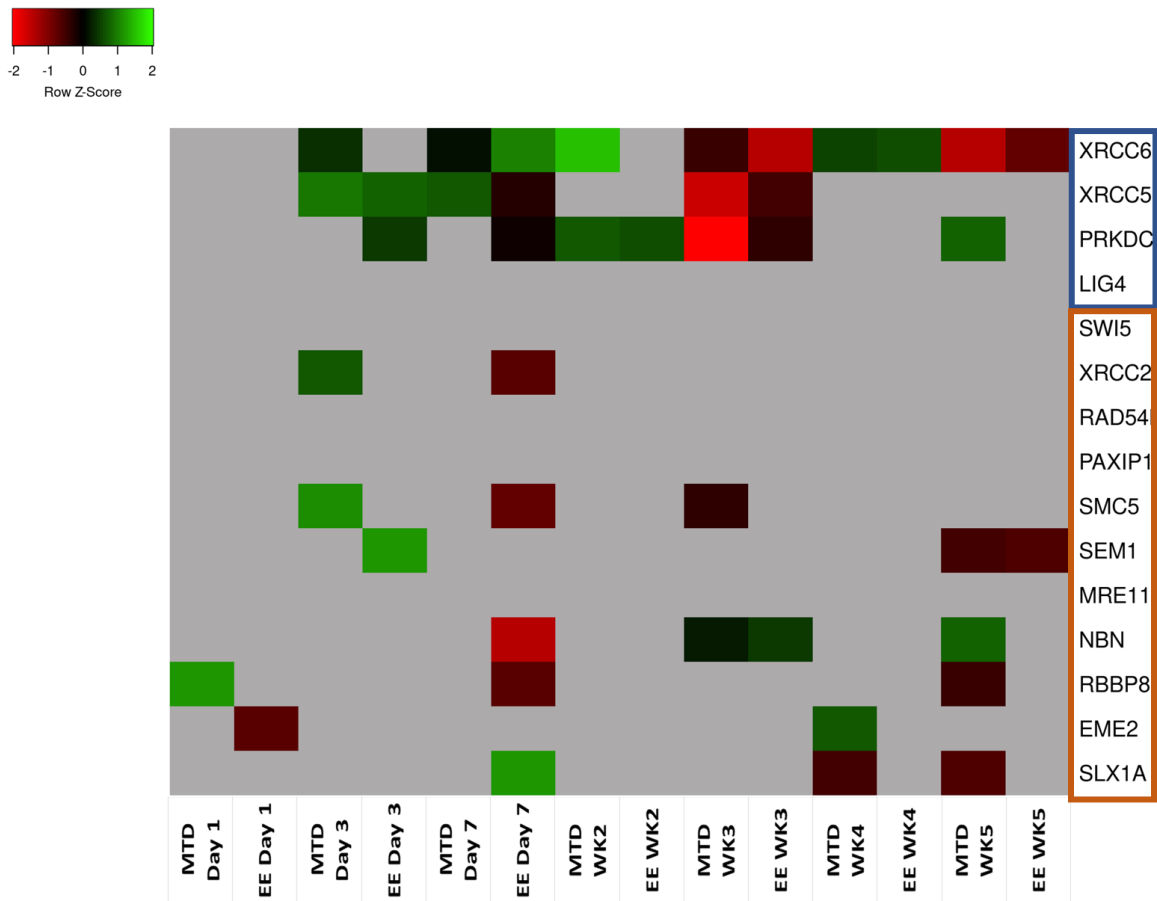
Figure 4. Heatmap of the DNA repair genes with at least one statistically significant timepoint from either MTD or EE treated cells. Genes associated with non-homologous end joining are identified using a blue square and genes associated with homologous recombination are identified using an orange square.

Genes without statistically significant changes:

NHEJ: XRCC4, DCLRE1C, NHEJ1)

HR: RAD51, RAD51B, RAD51D, HELQ, SWSAP1, SPIDR, PDS5B, DMC1, XRCC3, RAD52, RAD54B, BRCA1, BARD1, ABRAXAS1, SMC6, SHLD1, SHLD2, SHLD3, RAD50, MUS81, EME1, SLX1B, GEN1

3.2. Comparing the efficacy of EE topotecan and MTD docetaxel with MTD topotecan

and MTD docetaxel.

In this experiment, we determined whether EE topotecan could be used in combination with MTD docetaxel and whether it would be more effective than MTD topotecan. The results of this study are shown in **figure 5**. Topotecan dosing is arranged from bottom to top, and docetaxel dosing is arranged from left to right with the highest dose for each agent in the top right corner. MTD topotecan is shown in graph A and EE topotecan is in graph B. On the left is a 2D representation of the synergistic activity of both agents with red representing synergism and green representing antagonism. The same information is also presented as a 3D mountain plot (right) with higher peaks representing increased synergism and lower valleys representing increased antagonism. A Zero interaction potency (**ZIP**) model was then applied to the treatment response data to evaluate each treatment as a whole. Based on this model, MTD topotecan was found to be additive to MTD docetaxel with a ZIP score of 3.486 and EE topotecan was found to be synergistic to MTD docetaxel with a ZIP score of 10.386.
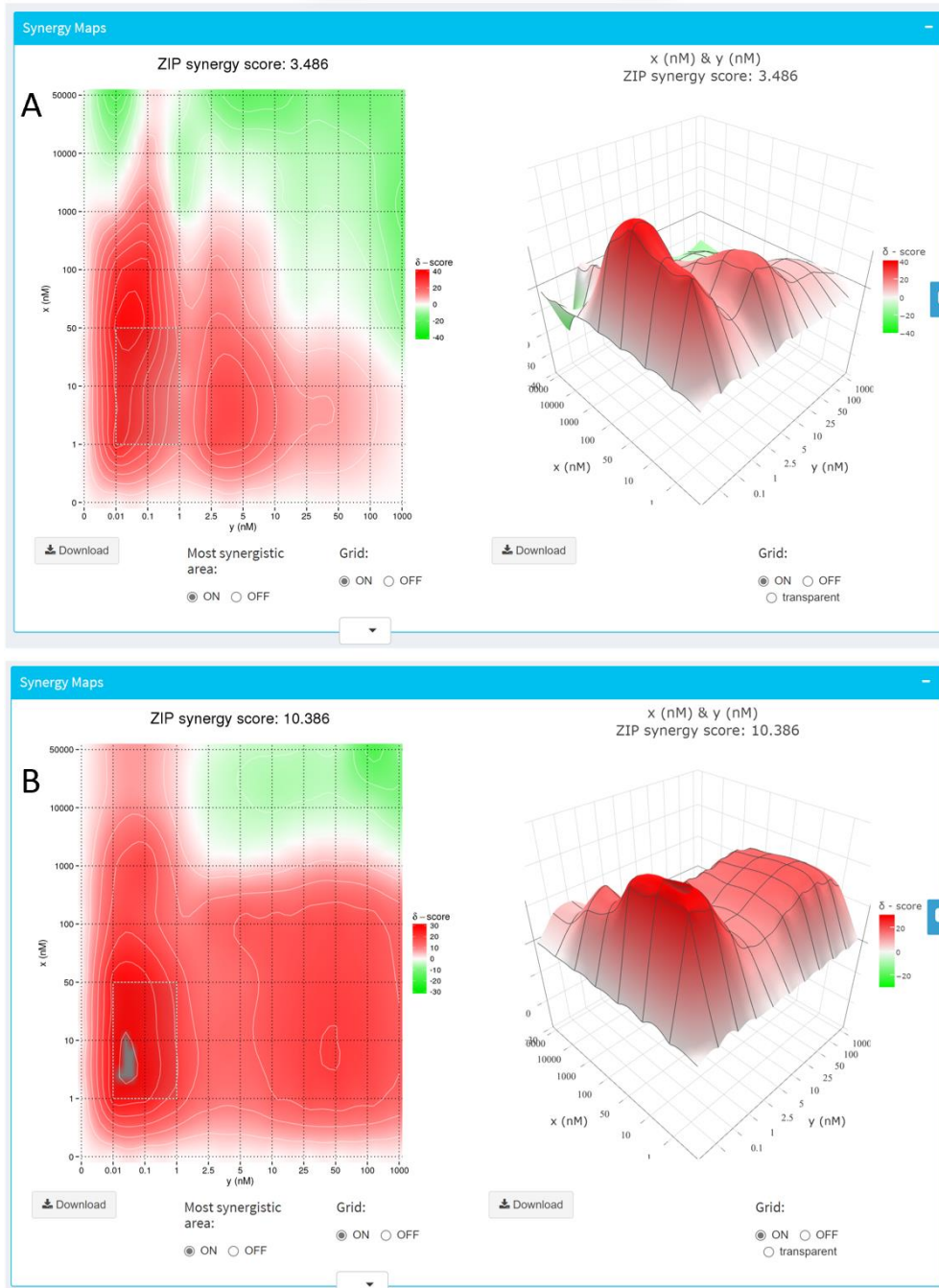
Figure 5. Synergism scores after 72H exposure with MTD (A) and EE (B) dosed topotecan in combination with conventionally dosed docetaxel. EE topotecan was given at 1/7th the MTD topotecan dose for a total of 3 doses to achieve a cumulative dose equal to 3/7th the MTD dose. Scores between -10 and 10 are considered additive and scores > 10 are considered synergistic.

3.3. Determining the effect of EE topotecan on long-term docetaxel potency.

EE topotecan was given in combination with MTD docetaxel using a long-term spheroid model of PC3 cells (**figure 6**). We also included an untreated control group as well as a docetaxel only treatment for comparison. The EE topotecan with docetaxel treatment was also directly compared to the MTD topotecan with docetaxel treatment to identify schedule dependent differences in docetaxel resistance. Overall, docetaxel did not change drastically from weeks 0 to weeks 5 in any treatment group. The docetaxel only group demonstrated the highest IC50 values in most weeks with statistical differences in weeks 2 and weeks 4. The IC50 value of the control group increased from 2.18nM to 4.002nM over 5 weeks of treatment, indicating a fold change of 1.84. The IC50 value of the docetaxel only treatment increased from 2.18nM to 5.045nM, indicating a fold change of 2.31. The IC50 value of EE topotecan with docetaxel increased from 2.18nM to 3.339nM, indicating a fold change of 1.53. The IC50 value of MTD topotecan with docetaxel increased from 2.18nM to 4.166nM, indicating a fold change of 1.911. Although most IC50s drifted throughout the experiment, no treatment demonstrated a significant difference from control at the end of the 5-week experiment.

Docetaxel IC50 after Multiple Weeks of Exposure to Each Treatment Group

Docetaxel IC50 after Multiple Weeks of Exposure to Each Treatment Group
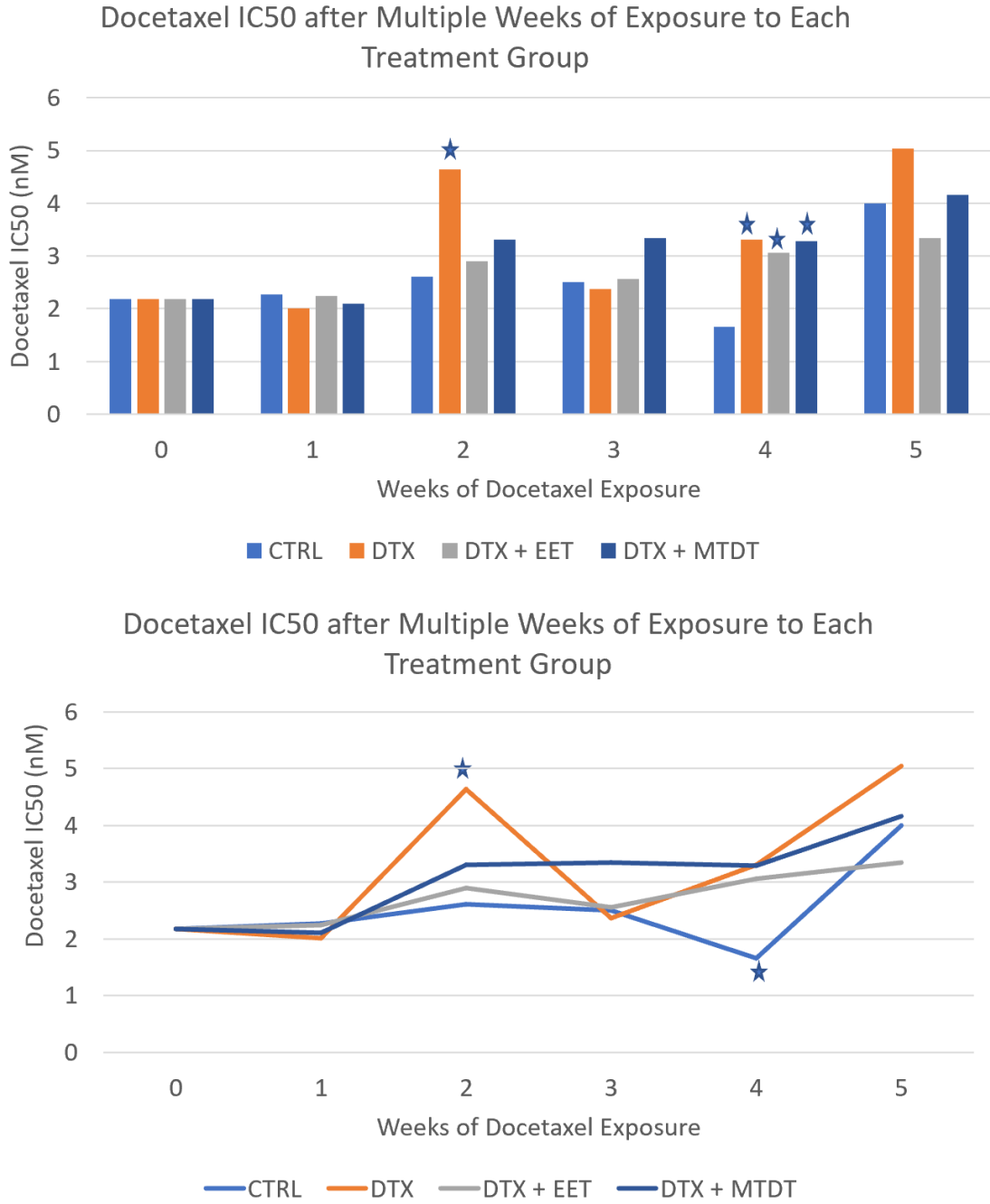

Figure 6. Effect of MTD and EE dosed topotecan on docetaxel resistance over time. Stars identify samples with statistical difference relative to control.

4. Discussion

In this study, we wanted to determine whether EE topotecan could reduce the mutation rate of surviving cancer cells relative MTD topotecan. We also wanted to determine if EE topotecan could be used in combination with MTD docetaxel, the treatment standard for prostate cancer, and finally, we wanted to determine if EE topotecan altered the resistance profile of MTD docetaxel over time. In **figure 4**, we analyzed the expression of DNA repair genes following treatments with EE and MTD topotecan. This data did not demonstrate significant alterations to DNA repair genes, regardless of treatment. It's possible that the sample timing did not appropriately reflect the expression profile of DNA repair genes, however, Yang et al. found that most transcribed genes are repaired within 48H and it takes weeks to repair non-transcribed genes.[19] Therefore, if DNA repair enzymes were upregulated within 48H to repair the transcribed genes, then this should have been identified in the Day 1 data and if DNA repair enzymes were upregulated during the weeks for non-transcribed genes, then this should have been reflected in weeks 1-5. It's possible that most cells with significant DNA damage simply died off, however, it's surprising that DNA repair wasn't significantly upregulated at any point in the study. However, despite this, EE topotecan was still able to outperform MTD topotecan in combination with MTD docetaxel, which was shown in the synergism study in **figure 5**. In this study, EE topotecan achieved synergism, while MTD topotecan was only modestly additive. Importantly, EE topotecan achieved this at 3/7th the cumulative dose of MTD topotecan. EE topotecan was more effective in combination with MTD docetaxel at less than ½ the dose of MTD topotecan.

These results highlight the clinical possibilities for EE topotecan for prostate cancer as a less toxic and more effective treatment relative to MTD topotecan. Importantly, we evaluated the long-term efficacy of MTD and EE topotecan in combination with MTD docetaxel in **figure 6** to determine if EE topotecan could increase the time to resistance for docetaxel or could be given with docetaxel without altering docetaxel resistance. After 5 weeks of therapy, no treatment group experienced a significant increase in resistance to docetaxel relative to control. One potential explanation for this is that docetaxel has a high barrier to drug resistance in PC3 cells, which would explain its use clinically. It's also possible that a higher dose of topotecan was necessary to be more impactful as the normal IC50 of topotecan in PC3 cells is ~100 nM. 10nM was chosen in addition to 2.5nM of docetaxel based on a combination IC50. We also wanted docetaxel to exert relatively more selective pressure on the cells to encourage a resistance mechanism to docetaxel instead of topotecan. Additionally, EE topotecan with MTD docetaxel treated cells were consistently more sensitive to docetaxel than MTD topotecan with MTD docetaxel treated cells, however, this did not achieve statistical significance. Out of all treatments, the docetaxel only treatment appeared to demonstrate the worst efficacy with statistically worse efficacy in weeks 2 and 4 and non-statistically worse efficacy in week 5. Based on this information, the addition of topotecan might be somewhat protective against docetaxel resistance with EE topotecan appearing relatively better than MTD topotecan, however, EE topotecan was only directionally more effective and was not statistically more effective than MTD topotecan. Although not shown, EE topotecan in combination with docetaxel was

statistically more effective than the docetaxel only treatment in week 5 (P = 0.0031).

Importantly, although EE topotecan was not drastically more protective against

docetaxel resistance, it also did not significantly increase docetaxel resistance.

Therefore, combination therapy using EE topotecan with MTD docetaxel appears to be

synergistic in PC3 cells without the threat of increased docetaxel resistance and with

some potential to improve docetaxel resistance.

References

1. Bernstein, C., Prasad, A. R. , Nfonsam, V., & Harris Bernstein, H. (2013). DNA Damage, DNA Repair and Cancer. In (Ed.), New Research Directions in DNA Repair. IntechOpen. https://doi.org/10.5772/53919

2. Tasaki, E., Mitaka, Y., Nozaki, T., Kobayashi, K., Matsuura, K., & Iuchi, Y. (2018). High expression of the breast cancer susceptibility gene BRCA1 in long-lived termite kings. Aging, 10(10), 2668–2683. https://doi.org/10.18632/aging.101578

3. Cooke, M. S., Evans, M. D., Dizdaroglu, M., & Lunec, J. (2003). Oxidative DNA damage: mechanisms, mutation, and disease. FASEB journal : official publication of the Federation of American Societies for Experimental Biology, 17(10), 1195–1214. https://doi.org/10.1096/fj.02-0752rev

4. Kow Y. W. (2002). Repair of deaminated bases in DNA. Free radical biology & medicine, 33(7), 886–893. https://doi.org/10.1016/s0891-5849(02)00902-4

5. Boiteux, S., & Guillet, M. (2004). Abasic sites in DNA: repair and biological consequences in Saccharomyces cerevisiae. DNA Repair, 3(1), 1–12. https://doi.org/10.1016/j.dnarep.2003.10.002

6. Hwa Yun, B., Guo, J., Bellamri, M., & Turesky, R. J. (2020). DNA adducts: Formation, biological effects, and new biospecimens for mass spectrometric measurements in humans. Mass spectrometry reviews, 39(1-2), 55–82. https://doi.org/10.1002/mas.21570

7. Soll, J. M., Sobol, R. W., & Mosammaparast, N. (2017). Regulation of DNA Alkylation Damage Repair: Lessons and Therapeutic Opportunities. Trends in biochemical sciences, 42(3), 206–218. https://doi.org/10.1016/j.tibs.2016.10.001

8. Caldecott, K. W. (2003). DNA single-strand break repair and spinocerebellar ataxia. Cell, 112(1), 7–10. https://doi.org/10.1016/S0092-8674(02)01247-3

9. Hossain, M. A., Lin, Y., & Yan, S. (2018). Single-strand break end resection in genome integrity: Mechanism and regulation by APE2. International Journal of Molecular Sciences, 19(8), 1–13. https://doi.org/10.3390/ijms19082389

10. Pommier, Y. (2006). Topoisomerase I inhibitors: Camptothecins and beyond. Nature Reviews Cancer, 6(10), 789–802. https://doi.org/10.1038/nrc1977

11. Staker, B. L., Hjerrild, K., Feese, M. D., Behnke, C. A., Burgin, A. B., & Stewart, L. (2002). The mechanism of topoisomerase I poisoning by a camptothecin analog. Proceedings of the National Academy of Sciences of the United States of America, 99(24), 15387–15392. https://doi.org/10.1073/pnas.242259599

12. Cannan, W. J., & Pederson, D. S. (2016). Mechanisms and Consequences of Double-Strand DNA Break Formation in Chromatin. Journal of cellular physiology, 231(1), 3–14. https://doi.org/10.1002/jcp.25048

13. Trenner, A., & Sartori, A. A. (2019). Harnessing DNA Double-Strand Break Repair for Cancer Treatment. Frontiers in Oncology, 9(December), 1–10. https://doi.org/10.3389/fonc.2019.01388

14. Ceccaldi, R., Rondinelli, B., & D'Andrea, A. D. (2016). Repair Pathway Choices and Consequences at the Double-Strand Break. Trends in Cell Biology, 26(1), 52–64. https://doi.org/10.1016/j.tcb.2015.07.009

15. Metzger, W., Sossong, D., & Chle, A. B. Ä. (2011). The liquid overlay technique is the key to formation of co-culture spheroids consisting of primary osteoblasts , fibroblasts and endothelial cells, (August 2010), 1000–1012. https://doi.org/10.3109/14653249.2011.583233

16. Safran M, Rosen N, Twik M, BarShir R, Iny Stein T, Dahary D, Fishilevich S, and Lancet D. The GeneCards Suite Chapter, Practical Guide to Life Science Databases (2022) pp 27-56 [PDF]

17. Sasha Babicki, David Arndt, Ana Marcu, Yongjie Liang, Jason R. Grant, Adam Maciejewski, and David S. Wishart. Heatmapper: web-enabled heat mapping for all. Nucleic Acids Res. 2016 May 17 (epub ahead of print). doi:10.1093/nar/gkw419

18. Ianevski, A., Giri, K. A., Aittokallio, T., 2022. SynergyFinder 3.0: an interactive analysis and consensus interpretation of multi-drug synergies across multiple samples. Nucleic Acids Research. gkac382, https://doi.org/10.1093/nar/gkac382

19. Yang, Y., Liu, Z., Selby, C. P., & Sancar, A. (2019). Long-term, genome-wide kinetic analysis of the effect of the circadian clock and transcription on the repair of cisplatin-DNA adducts in the mouse liver. Journal of Biological Chemistry, 294(32), 11960–11968. https://doi.org/10.1074/jbc.RA119.009579

20. Ritchie, M. E., Phipson, B., Wu, D., Hu, Y., Law, C. W., Shi, W., & Smyth, G. K. (2015). limma powers differential expression analyses for RNA-sequencing and microarray studies. Nucleic acids research, *43*(7), e47. https://doi.org/10.1093/nar/gkv007

Conclusion

Over the past century, thousands of novel therapeutics were brought to market for a variety of ailments such as heart disease, diabetes, psychopathy, and asthma. Many of these diseases were highly responsive to drug therapy due to the relatively stable genetics of the target cell population. For instance, hypertension can be controlled by drugs such as beta blockers, which target the beta-adrenergic receptors on heart muscle cells. Importantly, although some cellular changes can take place such as a reflexive increase in beta receptor production by cells exposed to beta blockers, these changes usually occur within a relatively narrow range. Thus, exposure to beta blockers elicits a predictable and stable response in most patients.

Unfortunately, oncology does not share the same genetic stability as other diseases. Although we have brought hundreds of drugs to market over the past century, few have generated a true breakthrough. Instead, most drugs extend the life of a patient a few months and carry many unwanted side effects. In comparison to oncology, hypertension is quite simple. Excessive adrenergic stimulation is blunted by an inhibitor. If a cancer cell was the target of a beta blocker, it could nullify the drug in many ways such as generating its own adrenaline, creating excessive beta receptors, producing constitutively active blunt beta receptors, or producing another type of receptor with similar downstream effects. Inhibiting a single receptor on a cardiac muscle cell can achieve a desired reduction in blood pressure, however, inhibiting cancer growth is far more complex. It's estimated that 1% to 3.5% of human genes are mutated in cancer.[1] This translates to roughly 200 to 1200 potential oncogenes. This means that cancer cells

have many different pathways to maintain growth and are unlikely to maintain efficacy over time to a drug targeting a single pathway. Normal cells on the other hand cannot adapt, causing toxicity. Inhibiting an oncogene can inhibit tumor growth substantially if the cancer cell population depends heavily on that specific gene to drive growth. However, many cancer populations are heterogeneous and possess many different varieties of the same cancer cell, which leads to more rapid evasion of the drug mechanism. Cancer cell heterogeneity is increased by exposure to unique microenvironments present in many metastatic sites, further reducing the odds that an oncologic drug will be successful in eliminating all cancer cells. Cancer's unique characteristics create an environment that is prone to drug resistance.

The failure of many unique medications with sufficient *in vitro* and *in vivo* efficacy to prolong survival has not altered the methods of drug selection and criteria for approval of oncologic medications. The reliance on short-term potency *in vitro* and tumor shrinkage *in vivo* has lured researchers and clinicians away from the most important determinant of clinical outcomes: resistance. Typically, the drug development process begins with a wide screen of molecules that are efficacious for a particular cancer or that are able to inhibit a molecule of proven importance to cancer. Unfortunately, this screening method does not appropriately select for drugs with high barriers to drug resistance or for drugs with limited toxicity. A drug with a 10% tumor reduction with limited resistance and toxicity is far more valuable than a drug with 90% tumor reduction with rapid resistance and excessive toxicity.

A major reason for omitting early resistance screening in the drug development process is the absence of model systems with the necessary attributes to adequately assess resistance changes over time. One of the main focuses of this project was the development and assessment of a novel spheroidal model system to address these shortcomings. In particular, we developed a high-throughput long-term model that could be rapidly generated and displayed adequate characteristics to assess drug resistance such as increased heterogeneity, increased barriers to drug delivery, and potential for co-culture. This model system was then used to assess the efficacy of EE topotecan and docetaxel. Importantly, when controlling for the total drug exposure, EE topotecan showed similar efficacy to MTD topotecan *in vitro*. However, EE topotecan was highly efficacious *in vivo* relative to MTD topotecan. Thus, this treatment epitomized many of the concepts described above. Relying on short-term potency would have screened out EE topotecan and would have selected MTD topotecan based on ease of administration. However, MTD topotecan had limited success clinically in metastatic prostate cancer, and while EE topotecan has not yet been evaluated clinically, it has shown promise in an *in vivo* mouse model.

Applying the novel spheroidal model system to our seemingly paradoxical *in vitro* and *in vivo* data allowed us to evaluate whether alternative screening markers such as long-term potency could potentially provide more reliable predictions of success downstream in the drug approval process. Our results showed that MTD topotecan rapidly evoked an aggressive and resistant phenotype from the PC3 cell line. These changes started as quickly as the second week of dosing and flourished during the 5th

and 6th week of dosing. Overall, MTD topotecan resulted in upwards of a 40-fold reduction in potency relative to EE topotecan. In contrast, EE topotecan maintained potency throughout our study duration. Surprisingly, EE topotecan potency increased even relative to our control group by the end of the 6th week of exposure, though this was not statistically significant.

Based on these results, we further explored the underlying transcriptomic changes of our treatment populations to understand how the MTD topotecan generated such a resistant cell line in such a short period of time. We hypothesized that MTD topotecan might increase the mutation rate of surviving cancer cells by forcing these cells to utilize lower fidelity repair mechanisms due to the sheer volume of double strand breaks from the high topotecan concentration. However, we did not find evidence to substantiate this hypothesis. Our scRNAseq data showed that our model system generated increased heterogeneity relative to a 2D model of PC3 cells and that MTD treated cells were highly heterogenous relative to EE treated cells. Increased heterogeneity increases the probability that a resistant subtype is present during treatment and decreases the time to resistance. Using RNAseq, we analyzed the phenotypic changes of each population of cells and determined that MTD treatment with topotecan caused the PC3 cells to rapidly undergo EMT, which created a much more resistant cell line with increased MDR pump expression and altered topoisomerase expression. EE and CTRL cells did not undergo this shift. Additionally, these changes were tracked over time and early transcriptomic changes could be seen as soon as the second week with weeks 4 and 5 changing most prominently.

Finally, we wanted to determine whether EE topotecan could be used concurrently with docetaxel (treatment standard for prostate cancer) and whether our model system could appropriately predict that docetaxel is clinically meaningful using long-term potency as a surrogate marker for clinical efficacy. We found that EE topotecan was highly synergistic with docetaxel while MTD topotecan was not and in some cases was antagonistic. EE and MTD topotecan also did not significantly alter docetaxel resistance, however, MTD topotecan treated cells did have lower (not significantly) potency relative to EE topotecan treated cells in all weeks of exposure. The long-term potency of docetaxel did not significantly change throughout the study duration using our model system, further validating the use of long-term potency as a more appropriate drug evaluation tool for initial drug screening protocols.

This project calls into question the use of short-term efficacy models to evaluate drug candidates for oncologic diseases and supports the use of long-term efficacy models as a more reliable means of identifying drug candidates and treatment protocols with higher potential for clinical success. It also supports the need to revaluate the approval criteria for oncologic drugs with a greater focus on resistance. Lastly, the use of long-term potency models not only improves drug selection, but also opens the door to identifying low to no potency drugs that improve the durability of treatments without inhibiting or killing cancer cells

References

1. Marc Tollis, Aika K Schneider-Utaka, Carlo C Maley, The Evolution of Human

   Cancer Gene Duplications across Mammals, Molecular Biology and Evolution,

   Volume 37, Issue 10, October 2020, Pages 2875–2886,

   https://doi.org/10.1093/molbev/msaa125